LRP-1-mediated Blood Brain Barrier Transcytosis: Mechanisms and Therapeutic Applications

Sophie Ebba Linnéa Nyberg

Thesis submitted to University College London for the Degree of Doctor in Philosophy

University College London

Faculty of Mathematics and Physical Sciences

Department of Chemistry

2016

Abstract

The endothelial cells lining the brain microvasculature make up the blood-brain barrier (BBB) of the central nervous system (CNS), physically restricting access of blood-borne compounds to the brain. Very few drugs possess the narrow set of physicochemical characteristics required to cross the BBB, causing a hurdle in delivering therapeutics to the CNS without using invasive methods or disrupting the BBB. However, several transporters at the BBB mediate import and export of macromolecules in a process called transcytosis. The work presented in this thesis explores the use of polymeric nanoparticles or 'polymersomes' as drug delivery vehicles to the brain. Through attaching a peptide ligand to LRP-1 receptor expressed at the BBB, polymersomes were provided with a targeting mechanism to achieve transportation across the blood-brain barrier in a non-disruptive manner. It is shown herein that Angiopep-2-POEGMA-PDPA (A-EP) polymersomes are able to transverse brain endothelial cells through transcytosis upon interaction with the LRP-1 receptor. However, transcytosis at the BBB is a poorly characterised process. Efforts to elucidate the mechanism by which LRP-1 mediates A-EP transcytosis at the BBB were undertaken through 3D or 4D confocal microscopy in conjunction with immunocytochemistry or small molecule inhibitors of various endocytic processes. This work was completed in parallel with fluorescence quantification of A-EP fluorescence in the rat brain, confirming that A-EP polymersomes enter the brain *in vivo*. Finally, applications for delivery of macromolecular therapeutics to the CNS *in vivo* were explored with the chief aim to achieve clinical translation.

Declaration of Authorship

I, Sophie Nyberg, hereby declare that the work presented in this thesis is my own. Where information has been derived from other sources, I confirm that this has been clearly indicated in the thesis.

Sophie Nyberg

University College London
London, 21/1/2016

“I may not have gone where I intended to go, but I think I ended up where I needed to be.”

- Douglas Adams

Acknowledgements

First and foremost I deeply thank Prof Giuseppe Battaglia for the supervision, for giving me the freedom to pursue this project according to my own hunches but always making sure I didn't lose track of the big picture, or as he likes to call it - "the engineering point of view". I also thank Dr Alethea Tabor for being my secondary supervisor. Many thanks to the UCL Department of Chemistry for sponsoring my PhD.

I am very grateful to Dr Jens Gaitzsch, Dr Alessandro Poma and Dr Jeppe Madsen, who made my project possible by synthesising the polymers and performing most of the polymer conjugations. I also thank Dr Gavin Fullstone for providing some of his computer modelling data and calculations that were highly relevant to my project; Dr Xiaohe Tian for both providing some 4D confocal data and passing on some of his confocal expertise to me; Dr Loris Rizzello for providing much valued general feedback to my data; Dr Lea Messager and Ms Claudia Contini for providing electron microscopy images; and also Dr Mark Turmaine at the UCL Anatomy facility for the electron microscopy sample preparation for transwell EM.

I wish to thank the rest of the Battaglia lab group, past and present, with special mention to Ms Silvia Bianco for providing some of the polymersome illustrations.

I am indebted to Prof Joan Abbott and Dr Jane Preston for a very fruitful collaboration along with providing plenty of invaluable scientific insight and discussion, and for helping me integrate into the blood-brain barrier community. I am also grateful for other collaborators of the project: Dr Sarah Salvage, Prof Arshad Majid, Dr Ok-Nam Bae, Dr Sean Davidson, and Dr Lucia Delogu. Special thanks to Mr Juzaili Azizi for performing the numerous hours of *in vivo* work with me, and Dr Atsuko Hikima for expertly helping out with the immunohistochemistry.

Thank you to Dr Irene Canton for the encouragement and the scientific mentorship, and for being one of my role models. Thanks to all the staff in the department of Biomedical Science at the University of Sheffield for my early postgraduate time. Also, a big thank you to Dr Rob Piggott for your sage advice - it had more of an impact than you might have imagined. Thank you to Dr Svetomir Tsokov at the University of Sheffield Electron Microscopy facility for the EM training. Thanks to all of my friends for the good times, and for the support when I needed it - even if I just needed a good laugh - especially Jess, Serena, Christine, Mark, Will, Sam, Max, Victoria, Matt, Ludovica, and Niels. Also I can't forget to mention Gavin, Eloise and James.

Last but not least, a huge thank you my parents for all the support and encouragement. Special thanks to my father, Dr Svante Nyberg, who made some indirect contributions to my research through constantly providing interesting scientific discussion, teaching me scientific writing, and even providing the occasional proofreading; but most of all, for sparking my scientific curiosity.

Table of Contents

List of Publications and Presentations

Publications

CNS-targeting Polymersomes with Carnosine as Neuroprotectant Treatment in a Rat Model of Stroke
Nyberg, S., Bae, O., Battaglia, G., Majid, A.
In preparation

A Proposed Mechanism for LRP1-mediated Transcytosis in Brain Endothelial Cells
Nyberg, S., Tian, X., Battaglia, G.
E-Life, in preparation (2016)

Glucose Chemotactic Synthetic Vesicles
Contini, C., Joseph, A., Cecchin, D., Nyberg, S., Ruiz-Perez, L., Gaitzsch, J., Fullstone, G., Gill, A., Madsen, J., Azizi, J., Preston, J., Golestanian, R., Volpe, G., Battaglia, G.
Nature Nanotechnology, submitted (2016)

LRP-1-mediated Intracellular Antibody Delivery to the Central Nervous System
Tian, X.*, Nyberg, S.*, Sharp, P., Madsen, J., Daneshpour, N., Armes, S.P., Berwick, J., Azzouz, M., Shaw, P., Abbott, N.J., Battaglia, G.
Scientific Reports (2015) 5:11990
*These authors have contributed equally.

Physicochemical Properties of pH-sensitive Polymersomes Targeting the Central Nervous System (2016), in preparation. Nyberg, S., Gaitzsch, J., Madsen, J., Chierico, L., Battaglia, G.
In preparation

Book Chapter: 'From the Blood to the Central Nervous System, a Nanoparticle's Journey through the Blood-Brain Barrier by Transcytosis'. In preparation. Fullstone, G., Nyberg, S., Tian, X., Battaglia, G. International Review of Neurobiology: Nanotechnology and the Brain, Elsevier.

Book Chapter: Smart Materials for Drug Delivery: Volume 1 (2013) 1, 179-207. Pearson, R., Avila-Olias, M., Joseph, A., Nyberg, S., Battaglia, G, RSC publishing.

Presentations

Materials Research Society Fall 2015 Conference, Boston, Massachusetts, November 2015
Poster presentation

University College London Neuroscience Symposium, 2014 and 2015
Poster presentation

London Polymer Group Meeting 2015, University College London, 24/3 2015.
Poster presentation

4th UK & Ireland Early Career Blood Brain Barrier Symposium, University College London, 21/11 2014.
Oral presentation
Event co-organiser.

'Proteins and Nanoparticles at Membrane 2014' technical conference, Julich Forschungszentrum, Germany, 19-23/9 2014
Oral + poster presentation
Awarded travel grant.

10th International Symposium on Polymer Therapeutics, Principe Felipe Centro del Investigacion, Valencia, 19-21/5 2014
Poster presentation

IUPAC MACRO World Polymer Congress, Virginia Tech, Blacksburg, Virginia, 2012
Oral presentation

List of Figures and Tables

List of Abbreviations

%ID	% injected dose / gram
A	Apical
AD	Alzheimer's Disease
A-EP	Angiopep-2-POEGMA-PDPA
AgNP	Silver Nanoparticle
AP2	Adaptor Protein 2
ApoE	Apolipoprotein E
ATRP	Atom Transfer Radical Polymerisation
AUC	Area Under Curve
AuNP	Gold Nanoparticle
AZT	Azidothymidine
β-FGF	β-fibroblast Growth Factor
BBB	Blood Brain Barrier
BCRP	Breast Cancer Resistance Protein
BCSFB	Blood-Cerebrospinal Fluid Barrier
BDNF	Brain Derived Neurotrophic Factor
BEC	Brain Endothelial Cell
bEnd.3	Mouse Brain Endothelioma
BL	Basolateral
Cav-1	Caveolin-1
CCV	Clathrin Coated Vesicle
CD	methyl-β-cyclodextrin
CP	Choroid Plexus
CME	Clathrin-Mediated Endocytosis
CMT	Carrier-Mediated Transport
CNS	Central Nervous System
CSF	Cerebrospinal Fluid
Cy3	Cyanine-3
Da	Dalton
DLS	Dynamic Light Scattering
DMEM	Dulbecco's Modified Eagle Medium
DNA	Deoxyribonucleic Acid
EM	Electron Microscopy
EP	POEGMA-PDPA
FACS	Fluorescence Activated Cell Sorting
FBS	Foetal Bovine Serum
FDA	Food and Drug Administration
Fe-Tf	Iron-transferrin
GDNF	Glial Derived Neurotrophic Factor
GLUT-1	Glucose Transporter 1

GM1	Monosialotetrahexosylganglioside
GPC	Gel Permeation Chromatography
GTP	Guanosine Triphosphate
HER2	Humanised Anti-epidermal Growth Factor Receptor 2
HIR	Human Insulin Receptor
HIV	Human Immunodeficiency Virus
HPLC	High Performance Liquid Chromatography
HSA	Human Serum Albumin
I-CAM	Intercellular Cellular Adhesion Molecule
IC	Intracerebral
ICV	Intracerebroventricular
IF	Immunofluorescence
IGF-II	Insulin Growth Factor II
IgG	Immunoglobulin G
IHC	Immunohistochemistry
IL-1β	Interleukin 1β
iPS	induced Pluripotent stem cells
IR	Insulin Receptor
ISF	Interstitial Fluid
ISP	*In Situ* Perfusion
kDa	kiloDalton
LAMP1	Lysosomal Associated Membrane Protein 1
LAT-1	L-type Amino Acid Transporter 1
LCMV	Lymphocytoic Choriomeningitis Virus
LDL	Low Density Lipoprotein
LDL-R	Low Density Lipoprotein Receptor
LRP-1	Low Density Lipoprotein Receptor Related Protein 1
MAb	Monoclonal Antibody
MDCK	Madin-Darby Canine Kidney
MPS	Mononuclear Phagocyte System
MRI	Magnetic Resonance Imaging
mRNA	microRNA
MRP-1	Multidrug Resistance Protein 1
MTT	3-(4,5-dimethylthiazol-2-yl)-2,5-diphenyltetrazolium bromide
Mw	Molecular weight
NEM	N-ethylmaleimide
NGF	Nerve Growth Factor
NSF	N-ethylmaleimide Soluble Factor
NVU	Neurovascular Unit
PBEC	Porcine Brain Endothelial Cells
PBS	Phosphate Buffered Saline
PDPA	poly((diisopropylamino)ethyl methacrylate)

PEG	Poly(ethylene) glycol
Pgp	P-glycoprotein
PI	Phosphatide Inositol
PLA	Polylactic Acid
PMPC	poly[2-(methacryloyloxy)ethyl phosphorylcholine]
POEGMA	poly[oligo(ethylene glycol) methyl ether methacrylate]
PTA	Phosphotungstic Acid
RAGE	Receptor For Advanced Glycation End Products
RCF	Rotational Centrifugal Force
Rr	Pearson's Correlation Coefficient
rtPA	Recombinant Tissue Plasminogen Activator
RT	Room Temperature
RVG	Rabies Virus Glycoprotein
S.D.	Standard Deviation
S.E.M.	Standard Error of Mean
sdAb	single domain Antibody
SEC	Size Exclusion Chromatography
siRNA	short interfering RNA
SLC	Solute Carrier
sLRP-1	Soluble LRP-1
SM	Sec1/Munc1
SNAP	Synaptosomal Associated Protein
SNARE	SNAP Receptor
SR-B1	Scavenger Receptor B1
TEER	Trans-Endothelial Electrical Resistance
TEM	Transmission Electron Microscopy
Tf	Transferrin
TFA	Trifluoroacetic Acid
TIRF	Total Internal Reflective Fluorescence microscopy
TfR	Transferrin Receptor
tMCAO	Transient Middle Cerebral Artery Occlusion
t-SNARE	Target SNARE
UV	Ultraviolet
VAMP	Vesicle Associated Membrane Protein
v-SNARE	Vesicular SNARE
WBC	White Blood Cell
ZO-1	Zonula Occludens 1

Chapter 1.
The Central Nervous System and its Barriers

1.1. Clinical Motivation

1.1.1. Introduction to the Central Nervous System

The brain and spinal cord together comprise the central nervous system (CNS). Neurons of the CNS transmit electrical impulses in the form of action potentials to control complex conscious functions, as well as essential unconscious functions such as respiration and temperature regulation. Neuron-neuron communication via synapses is essential for these roles, which is reflected in the high extensive vascularisation and metabolic demand of the brain compared to the rest of the body. Synapses require a specialised environment to function, with precise ionic gradients and neurotransmitters controlling the function of synapses. Glial cells (from Greek γλοία meaning 'glue') assist with the maintenance of the specialised extracellular conditions of the brain. These cells regulate the local environment in the brain by releasing signalling molecules, supplying nutrients, and removing neurotransmitter metabolites which can be harmful if allowed to accumulate. Figure 1.1 shows a brief summary of the different cells found in the CNS.

The CNS is able to carry out its highly specialised functions due to the separation of the brain and spinal cord from the rest of the body by several barriers. The molecular 'microenvironments' present within the brain are maintained through orchestrated efforts of the brain barriers, glia, and fluids bathing the CNS. Malfunction of any of these regulatory systems can cause a range of pathologies that are often difficult to treat.

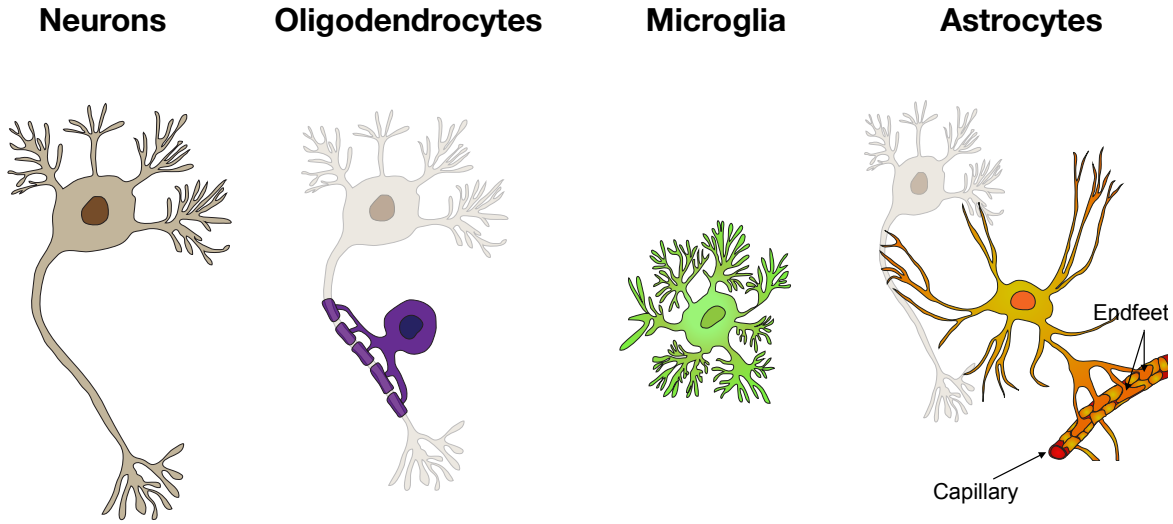

- Transmit information via action potentials
- Communicate with each other by releasing neurotransmitters into synapses

- Insulate neurons with a lipid enriched myelin sheath, which enhances neurotransmission

- Specialised immune cells of the CNS, remove pathogens via phagocytosis (non-selective internalisation)

- Provide nutrients to neurons
- Remove metabolites from the extracellular environment
- Help maintain brain barriers

Figure 1.1. Cells of the central nervous system: a summary of structure and function.

1.1.2. Diseases of the Central Nervous System

A distinct number of CNS diseases lack adequate treatment. This is true for pathologies ranging from stroke and spinal cord injuries to neurodegenerative disorders such as Alzheimer's disease or Parkinson's disease. One of the deadliest CNS diseases is stroke, i.e. the deprivation of oxygen (ischaemia) to the brain due to arterial occlusion. The 10-year cumulative mortality rate is around 32% (Prencipe, Culasso et al. 1998). Treatment is often performed during the acute stage of stroke, which entails regaining circulation to the ischaemic area before widespread damage such as cell death and oedema occurs. The only drug on the market for the acute phase of stroke is recombinant tissue plasmogen activator (rtPA, generic name *alteplase*), which breaks down blood clots. This drug is administered to less than 2% of patients, and was furthermore found to have an associated mortality rate of approximately 10% (Reed, Cramer et al. 2001). There is currently no treatment available for the long-term damage associated with ischaemic stroke.

Dementia is another example highlighting the lack of CNS targeted therapeutics on the market. Dementia is the progressive decline in cognitive function caused by widespread neurodegeneration. In 2005 the World Health Organisation estimated nearly 25 million people worldwide to suffer from dementia, a number set to rise to double every 20 years until 2040 (Ferri, Prince et al. 2005). Nearly 50% of elderly patients in the U.K. live in institutions due to cognitive impairments, costing £4.6 billion a year (Comas-Herrera, Wittenberg et al. 2007). Alzheimer's disease (AD) constitutes approximately 50% of all dementia cases, with vascular dementia or mixed cases making up the remainder. AD is characterised by the hallmark presence of amyloid β protein aggregates. There are five FDA-approved drugs on the market for AD, four of which belong to the group of anticholinesterase agents which primarily improve cognitive function in mild to moderate cases. There are no drugs on the market treating the underlying cause of dementia, i.e. extensive neurodegeneration. Between 2002 and 2012 there were 413 clinical trials in the U.S. for novel Alzheimer's disease therapeutics, 99.6% of which failed (Cummings, Morstorf et al. 2014).

1.1.3. Bottleneck in CNS Drug Development

The significant lack of drugs on the market to treat CNS disorders is due to a combination of factors. Firstly, our knowledge of many CNS diseases is incomplete. Many neurodegenerative diseases are highly complex, manifesting in a range of malfunctions at the cellular level such as oxidative stress and protein aggregation which results in death of entire cell populations in specific areas of the brain. Many drugs are focused on a specific mechanism of aspect of the pathology, for example focused efforts to develop anti-amyloid agents for AD. Secondly, the clinical manifestation of symptoms in neurodegenerative diseases often occur decades after cell death has begun (Rosen, Hansson et al. 2013). Thirdly, the current animal models of CNS disorders are inadequate with major discrepancies between pre-clinical and clinical results (Markou, Chiamulera et al. 2009). Finally, perhaps most importantly, the

highly restrictive barriers isolating the CNS from the rest of the body are a significant obstacle in achieving clinical efficacy due to keeping most drugs from entering the brain. A review of >7500 small molecule drugs found that <5% are active in the CNS, of which most are for affective disorders such as schizophrenia and depression (Ghose, Viswanadhan et al. 1999). Drugs must in order enter the CNS be <500Da, lipophilic, and form <8 hydrogen bonds with solvent water (Ajay, Bemis et al. 1999). 100% of macromolecules cannot enter the brain, unless they are nutrients imported by transporters at the brain. The barriers of the CNS have evolved over millions of years, and are extremely efficient in protecting the CNS from exogenous compounds (Abbott 2005). Expanding current knowledge of these barriers is essential to develop strategies in targeting putative therapeutics to the CNS.

1.2. Anatomy of the Central Nervous System

1.2.1. Fluids

The brain and spinal cord are immersed in and surrounded by fluids functionally and physiologically distinct from blood. The brain parenchyma is bathing in brain interstitial fluid (ISF), a low-protein solution similar to plasma. The different ion composition compared to plasma must be maintained for homeostasis in neurotransmission. The physiological differences in composition of the blood and the brain interstitial fluid are highlighted in table 1.1.

The other major fluid of the CNS is cerebrospinal fluid (CSF). It surrounds the outer membranes of the brain, where it reduces the effective weight and provides cushioning. CSF is continuously secreted by choroid plexus (CP) epithelial cells lining the cavernous ventricles of the brain. The choroid plexus is also a source of secreted nutrients such as insulin growth factor II (IGF-II) and transthyretrin, which are distributed throughout the brain via CSF (Dickson, Aldred et al. 1986, Stylianopoulou, Herbert et al. 1988). CSF is secreted at a rate of approximately 600 ml per 24 hours, or

the equivalent to replacing the entire CSF volume of the human brain 4 times a day (Brown, Davies et al. 2004). Efficient fluid drainage from the skull is thus essential to eliminate waste and to avoid dangerous pressure build-up due to fluid retention. Secreted CSF moves in bulk flow along the ventricles and out to the perivascular space (also called the Virchow-Robin space), which is located underneath the pial membrane. In the perivascular space CSF flows along the outside of blood vessels in the subarachnoid space, before it drains via arachnoid villi into sinuses leading into the venous blood of the systemic circulation.

Nutrient	Blood conc.	Brain conc.	Notes
K^+	4.6 mM	2.9 mM	High [K^+] in brain can cause seizures
pH **[K^+]**	7.4 39 pM	7.3 57 pM	Higher [H^+] causes faster neuronal repolarisation after action potential firing
Albumin	6 g/dl	0.02 g/dl	
Free [Ca^{2+}]	2.4 mM	1.2 mM	Low calcium and glutamate reduces risk for neuronal damage due to overexcitation
Glutamate	40 µm	0.05 µm	

Table 1.1. Differences in solute and protein concentrations in blood plasma and brain interstitial fluid. (Janigro 2012)

1.2.2. Barriers

The highly specialised environment of the CNS is maintained through the separation from the rest of the body by several physical and metabolic barriers. The concept of a brain barrier crystallised following two critical experiments performed by Edwin Goldmann (1909;1913): in the first experiment he confirmed an earlier observation by Paul Ehrlich that trypan blue, when injected intravenously, stained an animals tissues generally but not the central nervous system (Goldmann 1909, Goldmann 1913). The crucial second experiment demonstrated that when the trypan blue was injected into CSF via the cerebral ventricles, the brain became stained. Thus access of the dye to the nervous tissue was a crucial factor. In 1969 Brightman and Reese further noted that injected contrast agent peroxidase accumulated along the borders of brain capillaries,

unable to enter the CNS due to the presence of intercellular physical barriers or 'tight junctions' which inhibit the paracellular movement of solutes (Brightman and Reese 1969). The efficiency of this barrier is further illustrated in an experiment by Pardridge et al., in which injections of the radiolabelled small molecule histamine (~100 Da) in mice penetrated every tissue except the brain and spinal cord (figure 1.2) (Pardridge 2005).

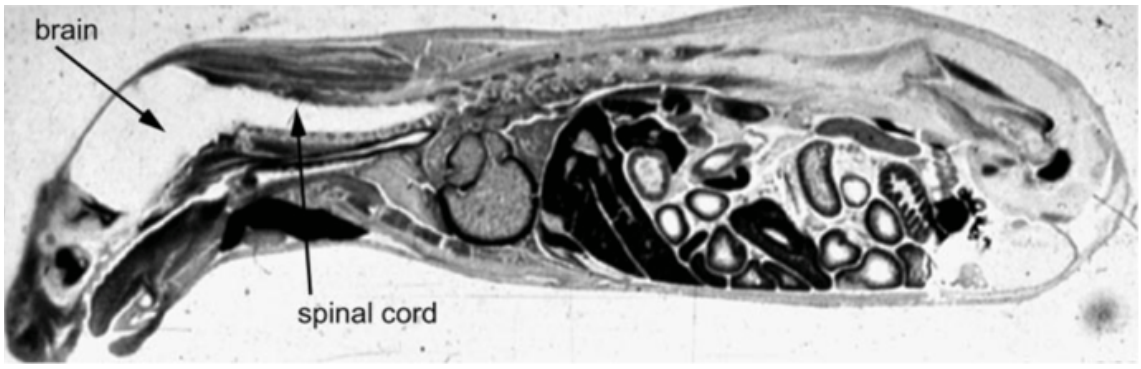

Figure 1.2. The CNS is protected by barriers. Radiolabelled histamine in the mouse systemic circulation, illustrating the presence of a barrier separating the CNS from the rest of the body (Pardridge 2005).

The barriers control all molecular traffic to and from the CNS. They facilitate import of nutrients from blood to brain and export of metabolites into the blood, while keeping the CNS inaccessible to the majority of blood-borne compounds. Barriers are classified according to their anatomical location and function, as illustrated in figure 1.3 and described in the following sections.

1.2.1.1. Arachnoid Epithelium

The arachnoid membrane is an avascular membrane that extends along the subdural space and encloses CSF and ISF in the skull. Secreted CSF is ultimately drained through the arachnoid epithelium, which is equipped with tight junctions to separate CSF from the venous blood in the sagittal sinus (see figure 1.3). Villi on the arachnoid epithelial cells increase the surface area efficiently to facilitate the drainage of CSF into venous blood. Drug delivery through the arachnoid epithelium would be impractical, as

it would grant limited access to the brain. Additionally, the drug would have to diffuse against the bulk flow of CSF being drained into the veins (Abbott, Patabendige et al. 2010).

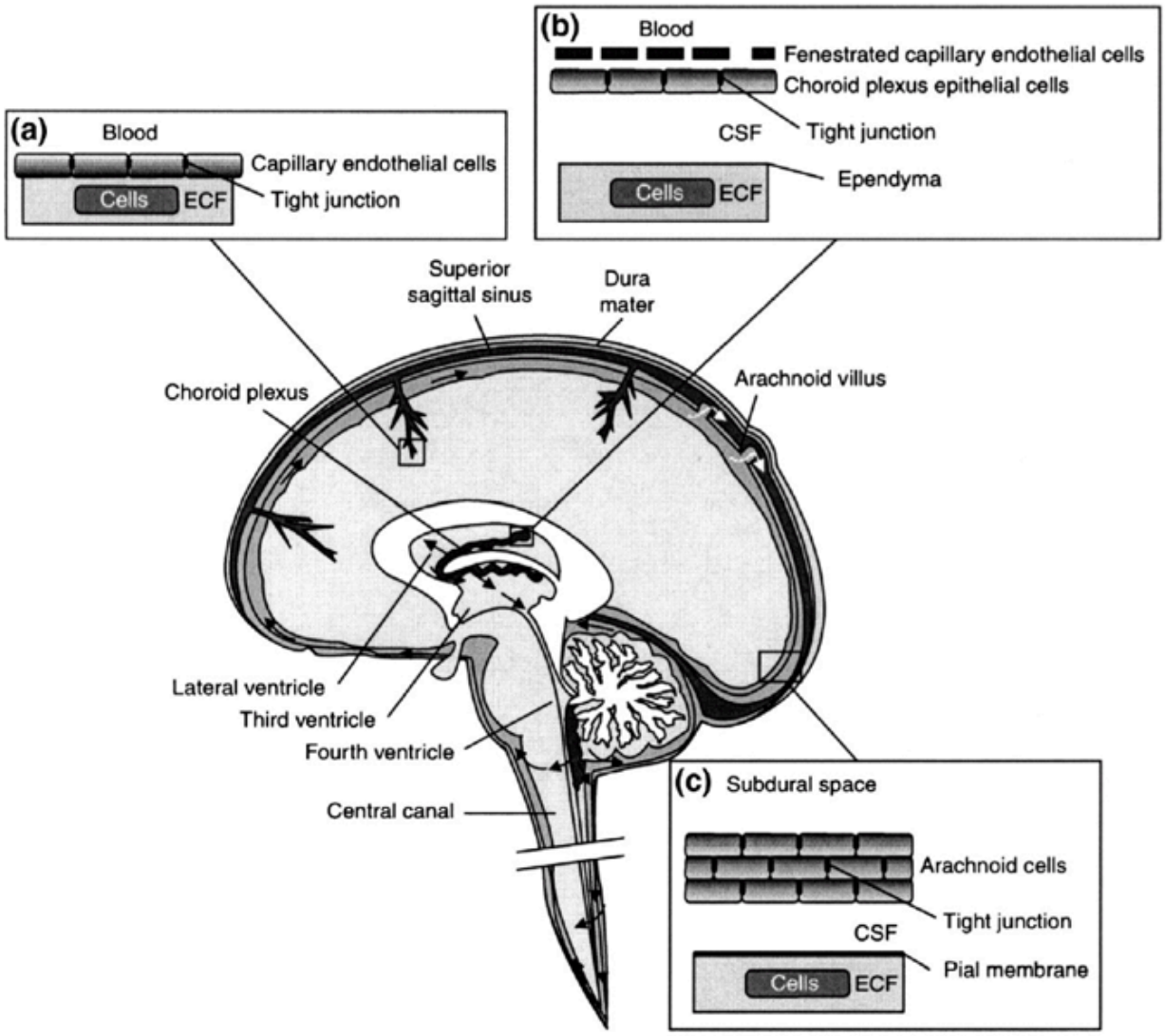

Figure 1.3. Anatomy of the brain barriers and properties of barrier capillaries. (Kandel, Schwartz et al. 2012)

1.2.1.2. Blood-Cerebrospinal Fluid Barrier

The choroid plexus epithelium is highly vascularised to accommodate for the high secretion rate of CSF. Microvilli on the basolateral side of the epithelium facing the ventricles maximises the surface area available for secretion (Keep and Jones 1990). Furthermore, the epithelium is supplied by fenestrated or 'leaky' capillaries. To maintain

a barrier between the blood and the CSF, tight junctions are present at the apical side of the epithelium which prevents the paracellular movement of most large water-soluble molecules into the CSF.

The blood-cerebrospinal fluid barrier (BCSFB) is considered distinct from the blood-brain barrier (BBB), which separates blood from brain interstitial fluid. Indeed, some drugs can affect the CNS without entering the brain parenchyma. For example, systemic administration of radiolabelled anti-HIV drug azidothymidine (AZT) has neurological effects despite its absence from the parenchyma and inability to cross the BBB. Instead, AZT enters CSF through the BCSFB (Wu, Clement et al. 1998). However, research suggests that exchange between CSF and ISF occurs across the barriers. Rhesus monkeys that had their choroid plexuses removed only had a 30% reduction in CSF production, suggesting that the majority of the CSF is produced by other means than the choroid plexus (Milhorat, Hammock et al. 1971). Recent evidence using *in vivo* two-photon microscopy in mice showed that CSF and ISF can mix along several points of the perivascular space (Iliff, Wang et al. 2012). The ability for the fluids of the brain to mix explains the high turnover rate of CSF.

Further work is required to investigate the efficiency of delivering therapeutics via the BCSFB. The high turnover rate of CSF makes it a ‘sink’, efficiently eliminating metabolites and also therapeutics from the brain. For example, intracerebroventricular injections of brain-derived neurotrophic factor (BDNF) results in very little uptake into the brain parenchyma, limited to the ipsilateral site of injection (Yan, Matheson et al. 1994). On the other hand, the ependyma lining the ventricles are exposed to very high doses of the drug, with detrimental consequences such as astrogliosis (Cho, Lee et al. 2002). An alternative strategy for drug delivery would be to gain access via the vast capillary network supplying the CNS, forming the interface of the blood-brain barrier (BBB). With a total surface area of 21 m^2, the need to maintain the CNS

microenvironment separate arises at the capillary level (Pardridge 2001). Specialised brain endothelial cells (BECs) line the brain capillaries, serving as the 'gatekeepers' of the CNS. The blood-brain barrier will be discussed further in section 1.4.

1.3. The Neurovascular Unit

The blood-brain barrier is induced and maintained through constant communication between brain endothelial cells and their neighbouring CNS resident cells. Figure 1.4 depicts the extended network of cells surrounding the blood-brain barrier. The brain endothelial cells adhere to a basal lamina (BL1), a sheet of collagenous extracellular matrix. A second basal lamina (BL2) separates the endothelial basal lamina and the brain parenchyma, forming a 'perivascular space'. In this space, support cells such as pericytes and smooth muscle cells wrap around the endothelial cells. Finally, on the brain side of the second basal lamina astrocyte end-feet processes cover almost all of the capillary endothelial cells.

Although brain endothelial cells inherently have a different phenotype from peripheral endothelial cells, induction of the BBB phenotype requires interactions with adjacent neural tissue during embryogenesis (Stewart and Wiley 1981). Pericytes are essential for the embryonic induction of the BBB, as mice deficient in the *Pdgfr* pericyte gene formed abnormal blood brain barriers with leakier vessels compared to wildtype mice (Daneman, Zhou et al. 2010).

The phenotype of brain endothelial cells in the adult brain is regulated by CNS resident astrocytes and pericytes in the vicinity, which has led to the term 'neurovascular unit' (NVU) to reflect the local synergy of the cells (Hawkins and Davis 2005). Astrocyte end-feet can release soluble factors such as glial-derived neurotrophic factor (GDNF) and β-fibroblast growth factor (β-FGF) which locally increase or decrease endothelial cell permeability (Abbott, Rönnbäck et al. 2006). Every neuron is surrounded by

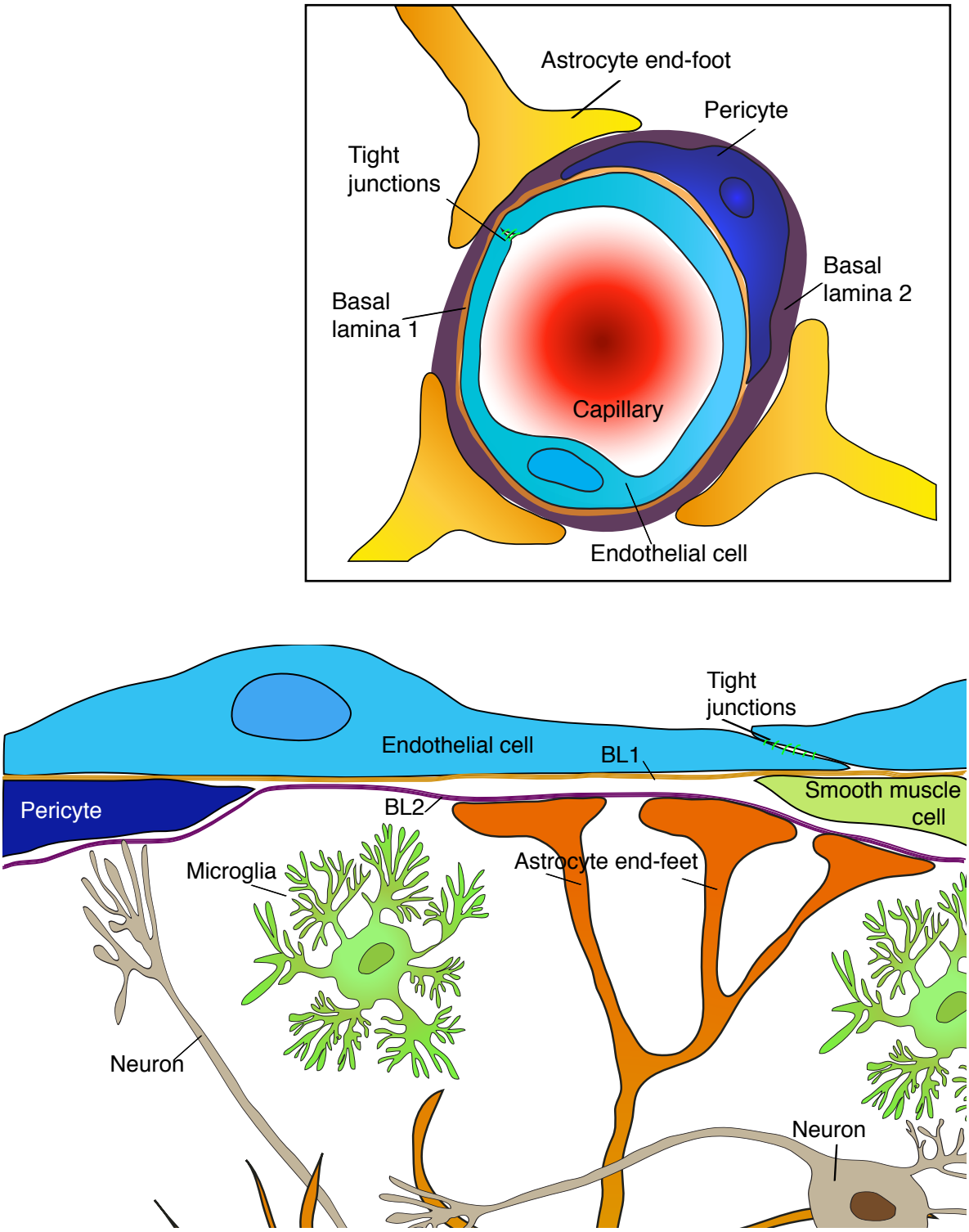

Figure 1.4. The cells of the neurovascular unit. Cross-section on the top. Adapted from Abbott et al. (2010).

approximately 6 astrocytes, and together they function as the relay between neurons and vasculature as a separate unit (Gabbott and Stewart 1987). *In vivo* imaging has shown that cortical astrocytes are able to rapidly cause vasodilation in response to stimuli such as increased neural activity (Takano, Tian et al. 2006). Pericytes can also

directly modulate the function of endothelial cells, constricting or relaxing in order to regulate brain capillary diameter and thus blood flow (Peppiatt, Howarth et al. 2006). There is also evidence for a passive pericyte impact on brain endothelial permeability. Pericyte-deficient mice had an increased BBB permeability to water and tracers of a range of molecular weights (Armulik, Genove et al. 2010). Pericytes may therefore enhance the BBB phenotype of brain endothelial cells by decreasing the transportation occurring across the BBB, possibly through the regulation of gene expression pattern in brain endothelial cells.

In summary, pericytes and astrocytes help establish the BBB phenotype of brain endothelial cells in the embryo and help maintain this phenotype in the adult brain. The neurovascular unit provides bidirectional communication between the brain endothelial cells and other cells in the vicinity, and modulate the barrier properties as necessary. The NVU interactions in the developing nervous system and in the adult brain make brain endothelial cells take on a different, more impermeable phenotype compared to peripheral endothelial cells.

1.4. The Blood-Brain Barrier

1.4.1. Properties of the Vasculature

All blood vessels are lined by a monolayer of endothelial cells, which have different properties depending on location. Endothelia can be classified into two relevant types: fenstrated (‘leaky’) or continuous. Fenestrated endothelia are found in tissues such as the kidney and intestine, and have pores spanning 50-60 nm in diameter which allows for the diffusion of many proteins. Continuous endothelia are a continuous sheet held together by intercellular junctions, found in tissues such as skin and muscle. The endothelial cells at the blood-brain barrier are also continuous. This type of endothelia has tight junctions preventing paracellular transportation. Instead these cells perform a highly regulated process of intracellular cargo transport. Endothelial protein expression

is polarised to maintain different environments at the apical and basolateral side. An essential component of these polarised cells are tight junctions, physical links between adjacent cells which prevent the paracellular movement of polar molecules and macromolecules. All CNS barriers express tight junctions to maintain a separate environment, but the brain endothelial cells have a number of specialised and enhanced barrier properties compared to any other barrier.

1.4.2. Barrier Properties

Brain endothelial cells (BECs) are polarised cells with the apical layer facing the blood vessel lumen and the basolateral side facing the basement membrane they adhere to. The polarity helps maintain separate environments at the apical ('blood') side and basolateral ('lumen') side, but requires strict regulation of all molecular traffic between the environments. Brain endothelial cells differ from peripheral endothelial cells in a number of ways: firstly, the composition of tight junctions is different even to other continuous endothelia. The combined expression of tight junction proteins claudin-5, occludin and zonula occludens 1 (ZO-1) contribute to a 'tighter' tight junction phenotype (Wolburg and Lippoldt 2002). Secondly, endothelial cells in peripheral tissues transfer nutrients across constitutively and non-selectively via a process called micropinocytosis. Tracing injections of peroxidase, Reese and Karnovsky noted a lack of micropinocytic vesicles at the BBB (Reese and Karnovsky 1967). Instead, certain molecules are shuttled intracellularly across the brain endothelium. This occurs passively for a narrow set of small lipophilic molecules, or actively via intracellular vesicular transport upon interaction of a ligand with specific receptors or transport proteins.

The 'tightness' of a polarised cell layer can be quantified by transendothelial electrical resistance (TEER), a measure of resistance to electrical charge moving across a polarised membrane such as endothelial or epithelial monolayers. In all effect TEER

measures ion transport across the monolayer. Resistance increases with barrier tightness, corresponding to a decrease in permeability of the cell layer. Brain capillary endothelial cells are by far the tightest continuous layer in the body with values up to 2000 Ω/cm^2, compared to <200 Ω/cm^2 in the choroid plexus epithelium and <40 Ω/cm^2 in muscle capillary endothelium (Olesen and Crone 1983)(Crone and Olesen 1982) (Saito and Wright 1983).

In addition to the enhanced physical barrier properties, the BBB is also a metabolic barrier. BECs express drug efflux transporters more than any other barrier cells (Loscher and Potschka 2005). Efflux transporters include Breast Cancer Resistance Protein (BCRP), P-glycoprotein (Pgp) and Multidrug Resistance Protein 1 (MRP-1). The efflux transporters can have a significant impact on the half-life of a drug entering the CNS, with a wide range of substrates including anticancer drugs, antibiotics, antihistamines and human immunovirus (HIV) suppressants (Schinkel and Jonker 2012). Additionally, BECs express enzymes for intracellular degradation of compounds. The cytochrome P450 group of enzymes metabolise a wide range of compounds including neurotransmitters and centrally acting drugs, and its mRNA is expressed at the human BBB (Dauchy, Dutheil et al. 2008)(Dutheil, Jacob et al. 2010).

Brain endothelial cells thus possess physical and metabolic properties which make them the ‘first frontier’ of the BBB. The neurovascular unit significantly influences the local permeability of the BBB. Regulation of molecular transport occurring across the BBB will be discussed in the following section.

1.4.3. Transport Across the Blood-Brain Barrier

Many nutrients that the brain requires are synthesised peripherally and must pass through the BBB. There are a number of routes for molecules to be transported across

the brain endothelium, as explained in the following sections. The routes are summarised in figure 1.5.

1.4.3.1. Passive Diffusion

At the BBB, tight junctions restrict the paracellular diffusion of all molecules except water and oxygen. Furthermore, only highly lipophilic small molecules of <500 Da and with less than 8 hydrogen bonds can passively diffuse through the endothelium (Pardridge 2001). Active transcellular transport is therefore a highly important mechanism to import and export compounds to the CNS.

1.4.3.2. Carrier-Mediated Transport

Some small (<5nm) hydrophilic molecules are shuttled across BECs by transport proteins in carrier-mediated transport (CMT). Export of compounds from the brain to the blood by ABC efflux transporters has been covered in section 1.4.2. The second group of transporter expressed at the brain microvasculature falls under the gene classification of Solute Carrier (SLC), of which 53 genes have been identified (Hediger, Clemencon et al. 2013). These transporters mediate import of nutrients from the blood to the brain, the most commonly characterised transporters including L-type amino acid transporter 1 (LAT-1) for import of amino acids and glucose transporter 1 (GLUT-1) for import of glucose. CMT operates on the millisecond scale through the formation of stereospecific pores by the transmembrane regions of the transport proteins, and has a high ligand-transporter specificity.

1.4.3.3. Macromolecules

Macromolecular nutrients gain access to the brain from the blood by interacting with receptors expressed at the brain endothelial cell surface. Ligand-receptor interaction results in internalisation of cargo by the cell, intracellular shuttling and finally export to the other side of the cell. Receptors at the BBB involved in macromolecular

transendothelial transport include the insulin receptor (IR) which imports insulin; transferrin receptor (TfR) for the import of iron-transferrin (Fe-Tf) complexes; and low density lipoprotein receptor related protein 1 (LRP-1) for LDL-cholesterol. These transporters are expressed on the apical and basolateral sides of the endothelium, allowing bi-directional movement across the BBB via a transcellular route.

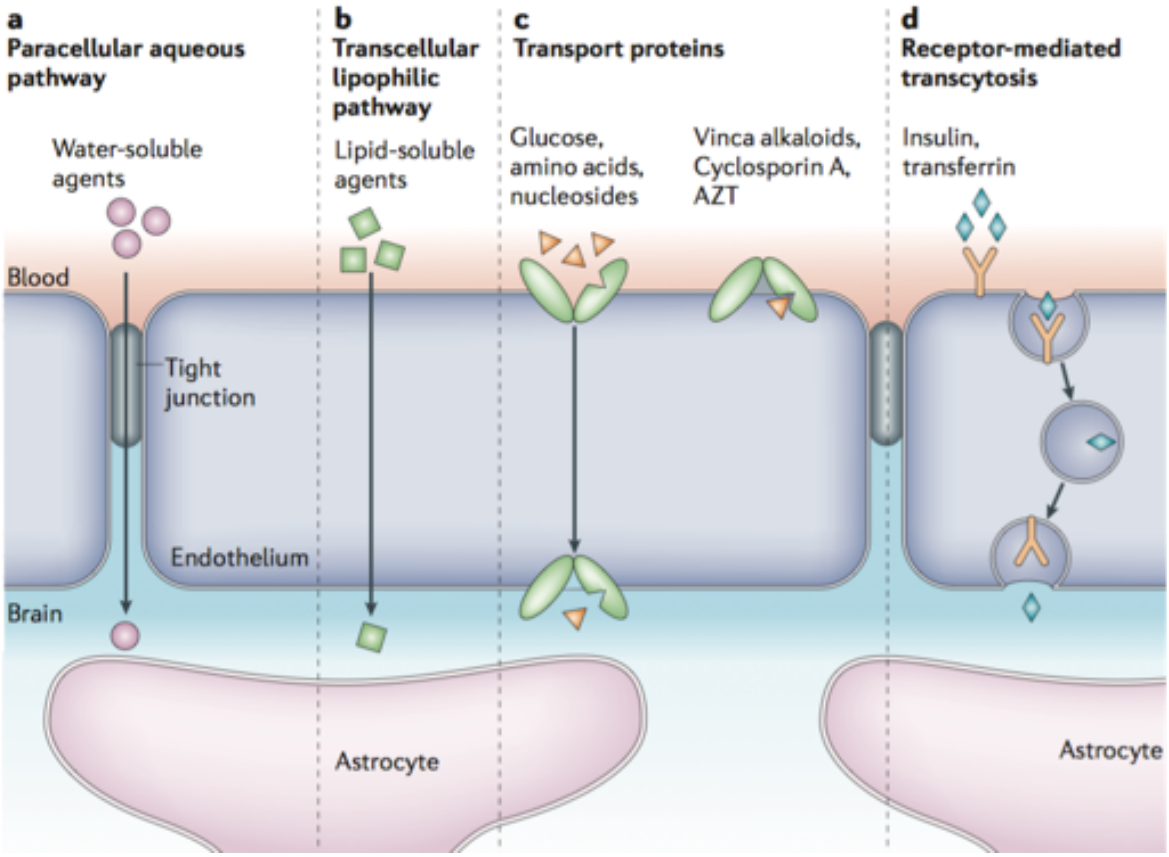

Figure 1.5. Transport pathways across brain endothelial cells. Tight junctions stop the paracellular movement of all molecules except water and oxygen. Transcellular lipophilic pathways and transport proteins shuttle smaller molecules across the endothelium. Transport of macromolecules occurs by receptor-mediated transcytosis. (Abbott, Rönnbäck et al. 2006)

1.5. Transcytosis

The process of active, receptor-mediated transcellular transport in a polarised cell is called transcytosis. In continuous endothelia in which paracellular transport is severely limited, transcytosis is an important and highly regulated means to transport polar molecules or macromolecules which are unable to passively diffuse across the membrane. Transcytosis can be divided into three distinct sequential parts: i) extensive

plasma membrane remodelling and internalisation of ligand as cargo in endocytosis, ii) intracellular trafficking to the opposing plasma membrane, and iii) membrane remodelling and externalisation of cargo in exocytosis. In endocytosis, part of the plasma membrane folds inwards together with lipids and proteins and pinches off into discrete vesicles inside the cell together with the cargo. Endocytosis is essential to cells for uptake of nutrients, but also for purposes such as regulation of signalling at the plasma membrane (Shibata, Yamada et al. 2000) and remodelling of the plasma membrane lipid composition (Bu, Maksymovitch et al. 1994). The mirror event of endocytosis is exocytosis, where intracellular membrane vesicles fuse with the plasma membrane to secrete cargo from the cell interior. Endocytosis and exocytosis are highly energy-dependent processes, as plasma membrane remodelling is energetically unfavourable. The exact cellular machinery operating under the different stages of transcytosis may differ between cells with different phenotypes expressed by the polarised cell. The processes of endocytosis, intracellular trafficking and exocytosis are outlined in the following sections.

1.5.1. Endocytosis

Endocytosis occurs when a ligand binds and activates its target receptor, resulting in internalisation of the ligand-receptor complex through intracellular vesicles. The protein and lipid composition of these intracellular vesicles varies, and the different pathways of endocytosis have been well characterised in model organisms such as yeast as well as different kinds of mammalian cells. Some pathways involve uptake of molecules of the micrometre scale, such as phagocytosis and micropinocytosis. These processes are absent at the blood-brain barrier, and will therefore not be discussed herein (Brightman and Reese 1969).

There are several mechanisms of internalisation upon ligand-receptor interaction. The major pathway of uptake is clathrin-mediated endocytosis (CME). In CME, ligand-

receptor interaction triggers the formation of pits in the plasma membrane adjacent to the binding site. The pits are surrounded by the protein clathrin, which self-assemble into triskelia or 'cage-like' structures, and clathrin supporting adaptor proteins. Many types of clathrin adaptor proteins have been identified and maintain specific subcellular localisations, and only adaptor protein 2 (AP2) associates with clathrin at the plasma membrane to mediate endocytosis. Clathrin and AP2 surround the pits, forming clathrin-coated vesicles (CCVs) as they fold inwards (Brodsky, Chen et al. 2001). The deformation of the plasma membrane into clathrin-coated vesicles is completed by fission into complete intracellular vesicles. This is commonly mediated by the GTPase dynamin, which assembles around the thin phospholipid neck of the vesicle and severs it in an energy-dependent manner (Tuma, Stachniak et al. 1993). Additionally, the cytoskeleton helps in vesicular biogenesis and actin is essential for the invagination process of endocytosis. The lifetime of a clathrin-coated vesicle is around 20-120 seconds, and can be up to 200 nm depending on cargo size (Ehrlich, Boll et al. 2004) (Canton and Battaglia 2012).

The most studied clathrin-independent mechanism is caveolae-mediated endocytosis. There is also a clathrin- and caveolae-independent endocytosis pathway mediated by Arf6, but this will not be discussed here. Caveolae are plasma membrane-resident 50-70 nm diameter flask-shaped pits, coated with the protein caveolin-1. They are present in many cell types and often abundant in vascular endothelial cells, with the exception of at the BBB where they are sparse (Frank, Woodman et al. 2003). Upon stimulation they can undergo endocytosis after dynamin pinches off the necks of the infolded vesicles (Henley, Krueger et al. 1998, Oh, McIntosh et al. 1998).

1.5.2. Intracellular Trafficking

The cell is compartmentalised into several subcellular organelles specialised for certain tasks. Once cargo is internalised through the endocytic pathway, it can have one of the

following fates: recycling to the plasma membrane, targeting to a specific organelle, or degradation. All cargo must therefore come with an 'address label' which directs its fate once inside the cell. This destination information often comes in specific sequences of amino acids. For example, nuclear localisation signals often consist of a stretch of basic amino acids, whereas proteins resident at the endoplasmic reticulum have a KDEL or KKXX amino acid sequence. Some ligands are targeted for lysosomal degradation. This endo-lysosomal pathway follows a pH gradient and becomes increasingly acidic along the pathway, from pH 7.4 to approximately pH 5 in lysosomes. It is unclear to what extent this pathway is utilised in cells capable of transcytosis, as cargo must avoid lysosomal degradation. Cargo can be recycled from endosomes to the plasma membrane, common for receptors which have undergone endocytosis together with their cargo. Indeed, recycling endosomes are frequently implicated in epithelial cell transcytosis (Tuma and Hubbard 2003). A simplified summary of the common endocytosis pathways is outlined in figure 1.6, though their relative contributions to transcytosis are likely to differ as discussed in section 1.6.

All organelles of the endosomal pathway are distinguished by their unique plasma membrane domains, containing different combinations of phosphatide inositols (PIs) and Rab GTPases (Sönnichsen, De Renzis et al. 2000). The Rabs are a group of proteins which use energy from guanosine triphosphate (GTP) hydrolysis to exert regulatory roles in various stages of membrane trafficking, from vesicle docking to fusion (Stenmark 2009). Some Rabs implicated in endocytosis include Rab5 in early endosomes, Rab4 and 11 in 'recycling' endosomes returning to the plasma membrane, and Rab7 in late endosomes (Bucci, Parton et al. 1992, Vitelli, Santillo et al. 1997, Sönnichsen, De Renzis et al. 2000, Stow and Jennifer 2005). More than 70 Rabs have been identified in humans, and 75% or more are believed to have roles in endocytic trafficking (Wandinger-Ness and Zerial 2014).

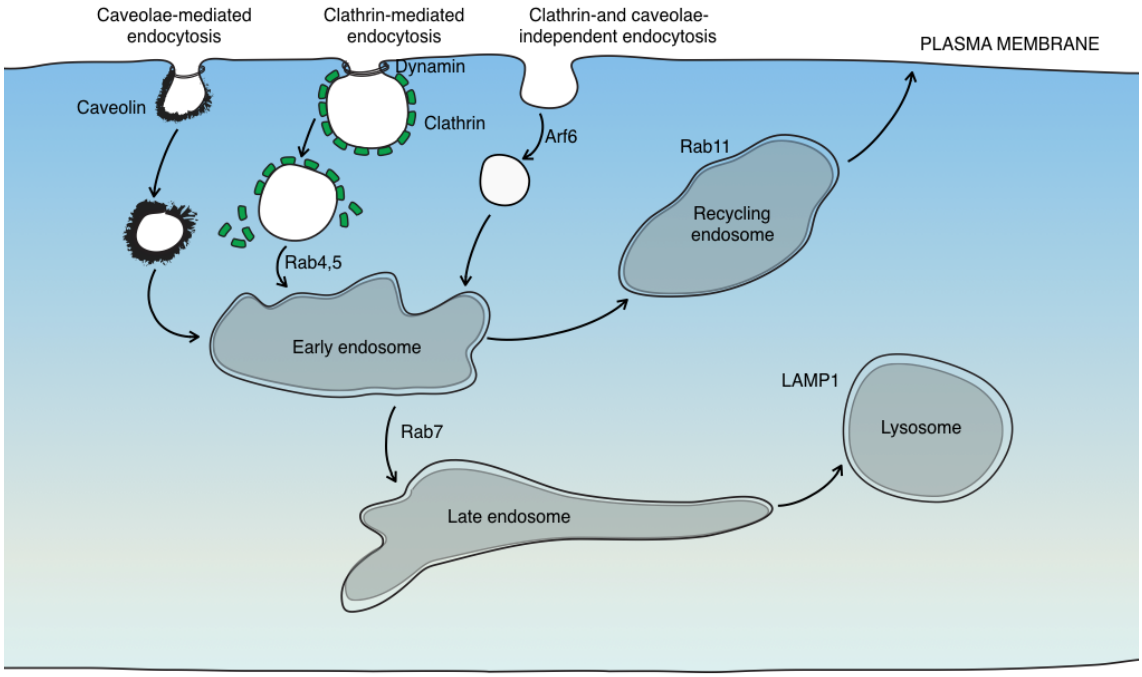

Figure 1.6. The endosomal sorting pathway (simplified). Adapted from (Gould and Lippincott-Schwartz 2009).

1.5.3. Exocytosis

Exocytosis is the fusion of an intracellular vesicle with the plasma membrane. Constitutive exocytosis occurs in all cell types as a means for cells to recycle lipids and proteins to the plasma membrane, and is very slow. In specialised cells such as neurons, there is additionally a highly regulated form of exocytosis which synchronously releases many vesicles of intracellular contents into the extracellular environment on a millisecond scale. Here, the final steps of fusion between the vesicular and target plasma membrane is under tight temporal control by specialised proteins which also provide the energy for fast fusion.

The protein machinery regulating exocytosis has been identified mostly through studying neuron transmission of synaptic vesicles. In neurons, vesicles containing the neurotransmitters fuse with the plasma membrane at the synapse and release all cargo. Using affinity chromatography, Rothman and colleagues initially identified three

main components essential for membrane fusion in synaptic vesicle exocytosis: N-ethylmaleimide Soluble Factor (NSF), Synaptosomal Associated Proteins (SNAPs), and SNAREs (SNAP-Receptors) (Söllner, Whiteheart et al. 1993). He subsequently coined the SNARE hypothesis, which states that membrane fusion is dependent on the association of SNARE proteins on the vesicular and target membranes. Experimental evidence in support for this hypothesis is strong: knockout of SNARE proteins vesicle-associated membrane protein (VAMP) and SNAP-25 in mice is lethal (Schoch, Deak et al. 2001). Furthermore, exocytosis and synaptic transmission is inhibited by botulinum toxins and clostridium neurotoxins, which target SNAPs or SNAREs for proteolysis (Xu, Binz et al. 1998).

The essential step of membrane fusion involves the association of SNARE proteins expressed on the intracellular vesicle (v-SNARE) and the opposing target membrane (t-SNARE). All SNAREs have the same SNARE motif of 60-70 amino acids, which in their monomeric state lacks structure. However, the appropriate combination of 4 SNAREs on the vesicle and target membrane intertwine into stable core complexes of 4 α helices (sometimes referred to as a SNARE-pin). As this transmembrane trans-SNARE complex assembles or ‘zips up’, it docks the vesicle to the membrane. When both bilayers of lipids have merged, a pore opens throughout the membranes to form a channel. This pore collapses eventually, releasing cargo and trapping all proteins in the target membrane. After fusion has occurred, the membrane fusion ATPase NSF disassembles the SNARE complexes via SNAP, its adaptor protein. This ‘recycling’ of cis-SNARE complexes is essential for membrane fusion to occur again.

Although SNARE complexes are critical for membrane fusion, they are too slow to mediate it alone. SNARE regulatory proteins assist with the fusion process, and are especially significant in quick regulated exocytosis such as neurotransmission. A range of both positive and negative regulators of secretion have been identified, and fine-tune

the exocytosis process. Knockout studies have identified the protein family of Sec1/Munc18 (SM) as regulators essential to every fusion step in neuronal exocytosis (Dulubova, Khvotchev et al. 2007). SM proteins bind to the syntaxin family of t-SNAREs in the plasma membrane, and can take on open or closed conformations to negatively regulate secretion. Total Internal Reflection Fluorescence (TIRF) microscopy of fluorescently labelled cargo in Munc18 knockout adrenal chromaffin cells showed that Munc18 is required for stable vesicle docking, causing average a vesicular membrane residency of >10 seconds (Toonen, Kochubey et al. 2006). The regulatory role of SM proteins appears to be conserved in cell types other than neurons. For example, expression of the isoform Munc18c was detected in human microvascular endothelial cells. Furthermore, exocytosis was inhibited upon treating cells with siRNA to syntaxin 4 which directly interacts with Munc18c (Fu, Naren et al. 2005).

1.6. Transcytosis in Brain Endothelial Cells

Transcytosis occurs *in situ* in the microvasculature of several tissue types, including intestinal epithelial cells, lung, brain, and liver (Brightman and Reese 1969). It has frequently been studied in epithelial cell lines such as liver or kidney cell lines MDCK and Caco-2, and the fate of cargo such as immunoglobin complexes has been well characterised in epithelia (Kaetzel, Robinson et al. 1991). However, epithelial cells have a largely different phenotype to brain endothelial cells. A particular discrepancy is size: epithelial cells span 10 µm across, compared to 0.2 µm across the thinnest parts of brain endothelial cells (Keep and Jones 1990). Endothelial cell transcytosis has mostly been studied in pulmonary endothelial cells, which are more permeable and have a higher occurrence of transcytosis than brain endothelial cells (Brightman and Reese 1969, Abbott, Patabendige et al. 2010). Because of the specialised structure and function of BECs, the cellular machinery of BEC transcytosis might differ from that in peripheral transcytosis.

Studying transcytosis by the endothelial cells at the BBB is complicated, as transportation may be bi-directional from blood to brain and *vice versa*. Also, it is unclear what signalling cues endothelial cells receive which determines when to direct the cargo to the opposite side of the plasma membrane and when to target it to intracellular organelles or lysosomal degradation. There are many questions that need to be answered about transcytosis in general, but especially at the BBB. Current knowledge of the stages of transcytosis are outlined below.

1.6.1. Endocytosis

Endothelial cells often have a number of intracellular vesicles with openings facing the capillary lumen, as displayed in figure 1.7. Many morphological studies performed in peripheral tissues such as the myocardium or pulmonary microvasculature have identified these vesicles as caveolae. However, evidence supporting a role for caveolae in brain endothelial cell transcytosis is lacking, not least because very few studies examining vesicular transcytosis have been performed in the brain endothelium. Indeed, the role of caveolae in transcytosis is controversial. A paper reported that caveolae are completely static at the plasma membrane and do not transport cargo whatsoever (Thomsen, Roepstorff et al. 2002). On the other hand, work by Predescu et al. provides plenty of electron microscopy data supporting a role for caveolae in transcytosis. Specifically, this group concluded that 95% of the vesicular population in endothelial cells are caveolae, and subsequently stated that ubiquitously, 95% of vesicles mediating endothelial cell transcytosis are caveolae (Predescu, Predescu et al. 2007). This claim remains unsupported. Furthermore, a significant caveat to notice is the extrapolation of findings in murine microvascular pulmonary tissue to apply to ‘all’ endothelia (Oh, Borgström et al. 2007). Although caveolin-1 is expressed by human BECs, endothelial cell transcytosis has mainly been studied in peripheral endothelia (Frank, Woodman et al. 2003)(Virgintino, Robertson et al. 2002). Further data is required on transcytosis in brain endothelial cells, but there is some evidence against

the hypothesis of caveolae being the intracellular vesicles mediating transcytosis at the brain endothelium. A study reported deficient *in vivo* internalisation of caveolar ligand albumin by mouse endothelial cells devoid of caveolae (Schubert, Frank et al. 2001). However, brain endothelial cells do not express the albumin receptor (Pardridge, Eisenberg et al. 1985). Although caveolar proteins are expressed by brain endothelial cells, these cells are known to contain by far the lowest vesicular population with <100 vesicles per μm^3 (Henley, Krueger et al. 1998). Perhaps the most important evidence against a role for caveolae in BBB transcytosis is that mice devoid of caveolar coat protein caveolin-1 are viable, suggesting that removing these structures does not disturb the essential process of import and export of compounds across the BBB (Drab, Verkade et al. 2001).

Figure 1.7. Morphology of endothelial cell intracellular vesicles. Electron micrograph of cat myocardium. (Fawcett 1965)

The role of caveolae in transcytosis remains controversial. The vast majority of endocytosis occurs through clathrin-mediated vesicles, and evidence exists for an important role of these structures in transcytosis. A recent study using TIRF microscopy and siRNA gene knockdown of CCVs in adipose microvasculature endothelial cells showed that transcytosis of insulin was mediated by CCVs (Azizi, Zyla et al. 2015). In brain endothelial cells, transcytosis of iron-transferrin complexes occurs via clathrin-coated vesicle internalisation *in vivo* (Roberts, Sandra et al. 1992). However, there is a lack of studies following the complete steps of transcytosis, from apical to basolateral or *vice versa*.

1.6.2. Intracellular Trafficking

The intracellular trafficking events in endothelial cell transcytosis are not well known. At the BBB, it is uncertain whether cargo is trafficked through endosomes at all. Experiments tracking cargo with tracer dyes in clathrin-mediated endocytosis showed up in early endosomes within 1-5 minutes of incubation, late endosomes after 10-15 minutes and lysosomes after 30 minutes (Pfeffer 2001). Internalisation by caveolae can take as long as 1-2 hours (Schnitzer, Oh et al. 1994, Pelkmans, Kartenbeck et al. 2001). In both cases the timing is inconsistent with the rapid transcytosis rates observed *in vivo*, which has been observed using live imaging to occur in <60 seconds in the lung endothelium (Oh, Borgström et al. 2007). Another discrepancy is the mechanism of Fe-Tf transcytosis across the brain endothelium. One theory is that after internalisation in clathrin-coated vesicles, Tf shuttles iron across to the opposing plasma membrane, and then recycles in an unbound state (Moos and Morgan 2000). Normally in the case of ligand-receptor interactions, dissociation occurs as a result of encountering the acidic pH of endosomes. This raises question whether Fe-Tf undergoes transcytosis at the brain endothelium through a pathway independent of acidifying endosomes.

It would be energetically favourable for cargo to be shuttled from membrane to membrane by travelling the shortest distance possible. Brain capillary endothelial cells are approximately 40% thinner than peripheral endothelial cells (Coomber and Stewart 1986), and the non-nuclear area can be as thin as 0.2-0.5 μm. As a result, cargo requires shorter transportation distances from one membrane leaflet to the other, which facilitates rapid transcytosis. Interestingly, there is ultrastructural evidence for a network of endothelial intracellular vesicles which have merged into ‘tubes’ or pores. Transendothelial channels can be defined as chains of fused intracellular vesicles which are simultaneously open on the endothelial cell apical and basolateral sides.

Bundgaard and colleagues performed electron microscopy of frog mesenteric capillaries to investigate transcytosis, where the addition of electron dense tannic acid seemed to fill out intracellular clusters of 2-5 vesicles which had fused (Bundgaard, Frøkjaer-Jensen et al. 1979). Repeating these studies in hagfish brain endothelium, they found through 3D reconstructions of serial EM sections that many of the vesicles traditionally observed in 2D electron micrographs appeared to be part of a larger branching network when reconstructed in the *z* plane. An illustration of the network of tubes observed in the hagfish brain is displayed in figure 1.8. These branching networks of intracellular vesicles were also observed in the EM work of Simionescu et al, investigating caveolar transcytosis of gold-labelled albumin in the mouse lung, heart and diaphragm (Simionescu, Popov et al. 2009). An example of a single transendothelial channel can be seen in figure 1.9. However, this section was obtained from a choroid plexus, which have leaky capillaries without tight junctions. Instead, the branching networks of vesicles seem a more plausible hypothesis for the blood-brain barrier as these networks are more frequent at the BBB; a study used 3D reconstructions of serial ~20nm electron micrographs to compare the number of transendothelial channels in microvasculature from different origins, and found an average of 8 channels per μm^2 in mouse BECs, compared to 4 in choroid plexus. These channels were located at the thinnest area of the cell, and were approximately the size of a single vesicle rather than a network of fused vesicles, although the latter were also present (Coomber and Stewart 1986).

A caveat of the channel hypothesis is that evidence is predominantly electron microscopy based. Electron microscopy of cell or tissue samples requires the fixation and processing with harsh lipid removal techniques, which undoubtedly affect membrane structures including intracellular vesicles. Further evidence for transendothelial channels should ideally be obtained through alternative methods which do not require processing with fixatives.

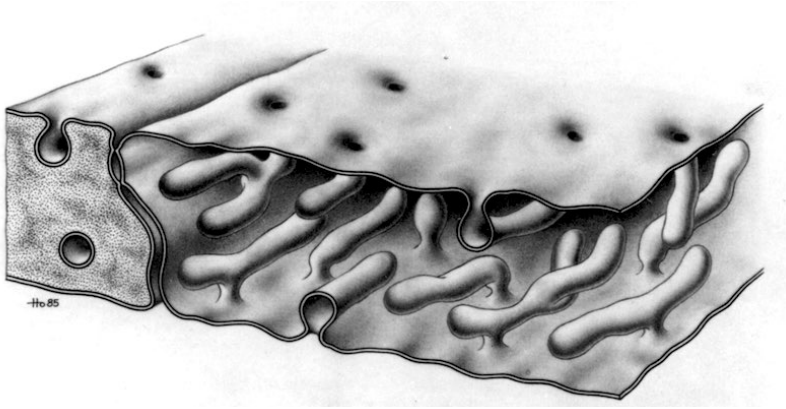

Figure 1.8. Tubular networks in the brain endothelium. Illustration of 3D serial EM reconstructions of hagfish brain endothelium. From Bundgaard et al (1987).

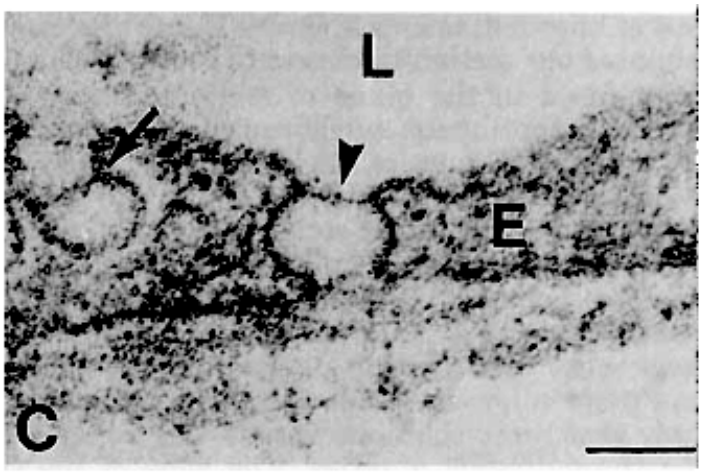

Figure 1.9. Electron micrograph of a transendothelial channel. Mouse choroid plexus, L: lumen, E: endothelial cell. Arrows point to a fused multivesicular channel as well as a single transendothelial channel. (Coomber and Stewart 1986)

In summary, knowledge of the intracellular transportation stages of transcytosis is lacking. It is possible that brain endothelial cell transcytosis is a system completely independent of the endosomal pathway, and instead potentially consists of tubulation of intracellular vesicles into a fused network to facilitate rapid transcytosis. However, more evidence must be obtained regarding the existence of these tubes and their involvement in transcytosis.

1.6.3. Exocytosis

Although SNAREs have been well characterised in neurons, the roles of SNAREs and their regulatory proteins in transcytosis is far less understood. There have been several reports of inhibition of myocardial vasculature transcytosis *in vivo* transcytosis through the use of NSF inhibitor N-Ethylmaleimide (NEM) (Predescu, Horvat et al. 1994). The addition of recombinant NSF rescued NEM-inhibited transcytosis in hepatic cell-free systems (Sztul, Colombo et al. 1993). However, implicating certain SNAREs important for brain endothelial cell transcytosis is proving complicated. More than 100 SNARE proteins have been identified in mammalian cells, with 36 members in humans (Hong 2005). Only certain combinations out of the hundreds available fuse, meaning that SNAREs provide specificity to membrane fusion (Südhof and Rothman 2009). This targeting mechanism may indeed be conserved in transcytosis. However, a combination of SNAREs specific to transcytosis have not been identified. In polarised cells there may be some asymmetrical distribution of SNAREs in the apical and basolateral leaflets, as reviewed by Tuma and Hubbard (Tuma and Hubbard 2003). Also, co-immunoprecipitation of lung microvasculature identified a few molecular mediators of transcytosis in a complex containing syntaxin, cellubrevin, SNAP-23, Rab5, NSF, and α- and γ-SNAP (Predescu, Predescu et al. 2001). However, further work needs to be done in order to elucidate the role of SNAREs and their associated proteins in transcytosis. Interestingly, the SNARE components identified in lung microvasculature by Predescu et al. were associated with lipids in supramolecular protein-lipid complexes, highlighting the role of lipids as protein segregating platforms in advanced membrane signalling and remodelling events such as exocytosis.

1.6.4. Cholesterol in Endothelial Cell Transcytosis

It is a widely accepted hypothesis that the plasma membrane is organised into lipid rafts, i.e. dynamic assemblies of sphingolipids and cholesterols which form functional

domains on the nanometre scale (Simons and Ikonen 1997). The selective incorporation or exclusion of specific proteins into lipid rafts is a protein sorting mechanism, and facilitates cell-cell signalling, endocytosis and exocytosis (Simons and Vaz 2004). Predescu et al. identified an essential role for cholesterol in the organisation of t-SNAREs syntaxin-4 and SNAP-23 in endothelial cells, which was required for transcytosis (Predescu, Predescu et al. 2005). Although their study was performed in a cell-free system with t-SNAREs they had previously identified in lung microvascular endothelial cells, the findings are still interesting in terms of cholesterol dependence (Predescu, Predescu et al. 2001). It is possible that SNAREs are also organised into cholesterol-enriched lipid rafts to mediate exocytosis in brain endothelial cells.

1.7. Low Density Lipoprotein Receptor Related Protein 1

Receptors with reported roles for transcytosis across the BBB include the insulin receptor, transferrin receptor, and low density lipoprotein related protein 1 (LRP-1). LRP-1 was first identified as receptor involved in lipoprotein metabolism, due to its high structural similarity to the low density lipoprotein receptor (LDL-R) and also because of its binding to Apolipoprotein E (ApoE) (Herz, Hamann et al. 1988)(Beisiegel, Weber et al. 1989). LRP-1 has since been reported to bind more than 30 different ligands, in contrast to TfR and insulin receptors which are single-ligand receptors at the BBB (Lillis, Van Duyn et al. 2008). LRP-1 is expressed in several tissues including the liver, kidneys and gastrointestinal tract, as well as the central and peripheral nervous systems. However, expression is enriched approximately 100-fold in the CNS compared to the liver (Moestrup, Gliemann et al. 1992). The enriched CNS expression combined with the number of different ligands makes LRP-1 a highly interesting receptor mediating transcytosis at the BBB.

1.7.1. Structure of LRP-1

The structure of LRP-1 is shown in figure 1.10. It is present on the cell surface as a two-chain molecule: a 585kDa α chain which consists of several ligand binding domains, and a 85kDa β chain transmembrane domain (Beisiegel, Weber et al. 1989). The two chains are non-covalently associated: the extracellular α chain is subject to shedding by proteolysis, and can be found circulating in human plasma and serum (Herz, Hamann et al. 1988, Quinn, Grimsley et al. 1997). The β chain contains intracellular sorting motifs, including a YXXL motif essential for receptor endocytosis, and a binding motif for Sortin Nexin 17 which is required for receptor recycling from the early endosome (Li, Marzolo et al. 2000, van Kerkhof, Lee et al. 2005). The extracellular domain has four different ligand binding clusters (I-IV), where specific ligand binding has been identified partially through screening with 'mini-receptors' expressing one of the four clusters(Goto and Tanzi 2002, Ranganathan, Cao et al. 2011). Ligands with a particularly high binding affinity to LRP-1 have very diverse roles, and include the serine protease tissue plasminogen activator (tPA) (Tooyama, Kawamata et al. 1995); lipoprotein lipase (Chappell, Fry et al. 1992); and the chylomicron endocytosis inhibitor lactoferrin (Huettinger, Retzek et al. 1992, Willnow, Goldstein et al. 1992).

1.7.2. LRP-1 in the Central Nervous System

Through immunohistochemistry, LRP-1 expression in the human brain has been strongly localised to the cerebral cortex, cerebellum, hippocampus and midbrain (Bu, Maksymovitch et al. 1994). On the cellular level, LRP-1 expression is high in neurons, and moderate in astrocytes, glia, and pericytes (Moestrup, Gliemann et al. 1992, Wolf, Lopes et al. 1992, Tooyama, Kawamata et al. 1995). Electron microscopy combined with immunolabelling of LRP-1 in glioblastoma cells located the receptor confined to clathrin-coated pits at the plasma membrane, but also has a minor intracellular

association with the endoplasmic reticulum and Golgi complex (Bu, Maksymovitch et al. 1994).

LRP-1 has been implicated in the pathogenesis of Alzheimer's disease, but the roles and contributions are not entirely clear. LRP-1 mediates bidirectional transport of amyloid-β aggregates across the BBB through the association with clathrin-coated pits (Pflanzner, Janko et al. 2011). Knockdown of clathrin or removal of the cytoplasmic tail of LRP-1 inhibited its ability to undergo endocytosis, which also decreased uptake of Amyloid β-42 plaques (Fuentealba, Liu et al. 2010). Isoforms of amyloid plaques bind with differential affinity to LRP-1. 'Normal' amyloid β-40 bind with high affinity to ligand clusters II and IV and are subsequently transported out of the brain. By contrast, AD isoform amyloid β-42 transcytosis is significantly reduced, resulting in accumulation of plaques in the mouse brain (Deane, Wu et al. 2004). Furthermore, the soluble extracellular α chain (soluble LRP-1 or sLRP-1) may act as a "peripheral sink" of plaques, as administering sLRP-1 increased learning in mice and reduced plaque presence in the brain (Zlokovic, Deane et al. 2010).

Li and colleagues found that out of the lipoprotein receptors, LRP-1 has the fastest endocytosis rate, with a half life of 30 seconds to recycle to the membrane (Li, Lu et al. 2001). This makes it a superior receptor to target for drug delivery in terms of kinetics ,compared to the TfR with a half life of 3 minutes (Iacopetta and Morgan 1983), and 18 minutes for the insulin receptor (Bottaro, Bonner-Weir et al. 1989). Once internalised, it is unclear whether LRP-1 shuttles with its ligand to the opposing plasma membrane, or is recycled back to its original membrane. Further work utilising *in vitro* models of the blood-brain barrier may prove useful in elucidating the physiological roles of LRP-1 in transcytosis, and applications for drug delivery.

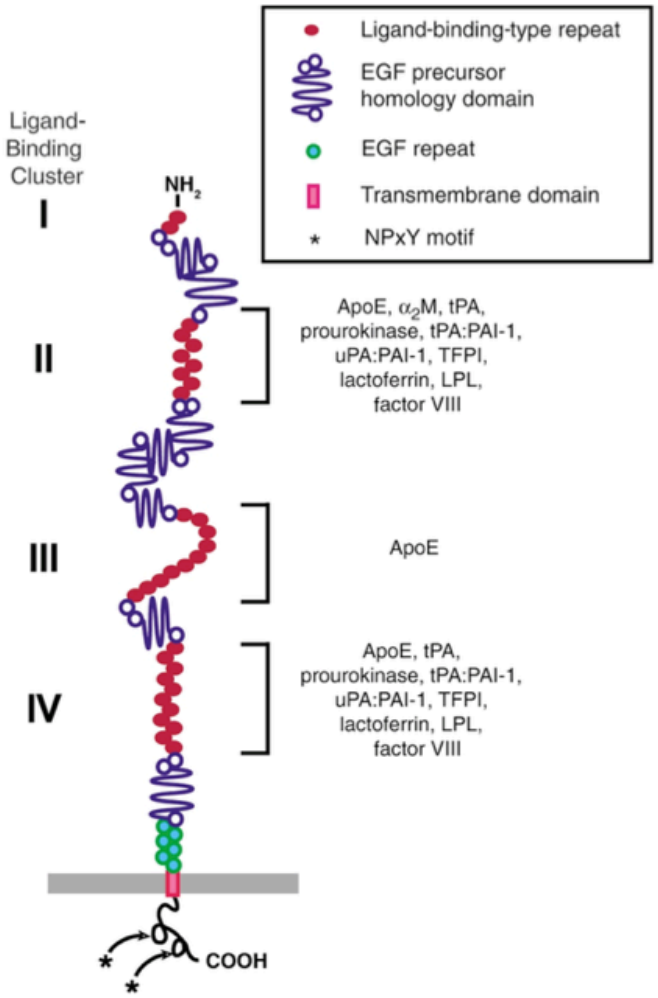

Figure 1.10. Structure of the LRP-1 receptor. The extracellular domain contains four ligand binding clusters, with example ligands for each as indicated.(Herz and Strickland 2001)

1.8. *In Vitro* Models for Studying the Blood Brain Barrier

In vivo, the blood-brain barrier is a synchronised effort of more than the endothelial cells lining brain capillaries. However, simplistic *in vitro* models of the BBB may be applied in order to enable the use of a range of molecular biology methods for the elucidation of BBB characteristics. The cell models of the BBB are centred around brain endothelial cells differentiated in a three-dimensional environment similar to the extracellular matrices present at the BBB. A common 3D model of the BBB utilises a transwell setup, in which brain endothelial cells are coated onto a porous layer of collagen-coated thin filter membrane which is analogous to the basal lamina. The

transwell is inserted into a regular wellplate, separating into two compartments analogous to the ‘apical’ and ‘basolateral’ sides of the endothelial cells.

The *in vitro* transwell BBB models have gained merit in the last couple of decades, though with widely varying parameters. For example, in the 1990s it was the norm to conduct studies with bovine endothelial cells, which changed as a result of stricter regulations after the discovery of bovine encephalitis virus. Bovine BBB cultures were replaced with murine cultures, and recently porcine cells have become an alternative. Porcine brain endothelial cells (PBECs) display some of the highest TEERs achieved *in vitro* to date, averaging 800 Ω/cm^2 (Patabendige, Skinner et al. 2013). Recent efforts have also yielded human models. Lippman et al. generated a human BBB model by directing human induced pluripotent stem (iPS) cells into endothelial cells and astrocytes, yielding a TEER of approximately 1450 Ω/cm^2 (Lippmann, Azarin et al. 2012). However, both iPS and PBEC cells are laboursome to obtain and maintain compared to established murine cell lines.

As one might expect from the need for pericytes to induce BBB properties *in vivo* (Daneman, Zhou et al. 2010), brain endothelial cells *in vitro* may not intrinsically show full blood-brain barrier properties. It is unclear precisely which soluble factors are released by pericytes and other adjacent cells during development to direct differentiation of endothelial cells into a blood-brain barrier phenotype. The addition of soluble factors such as adenosine antagonists is known to improve barrier-like properties *in vitro* (Gao, Qian et al. 2014). Although soluble factors or cells could be added to cell culture in order to enhance barrier-like properties, there is a balance to be struck between mimicking the BBB without overly complicating the system and also maintaining reproducibility.

Choosing the appropriate *in vitro* BBB model should depend on the research questions and aims. Firstly, the species origin of cells is particularly useful to consider when comparing data to previously obtained *in vivo* data. Genetic variance should be taken into account, e.g. whether the receptor expression is the same between rats and humans for a particular gene of interest. Cells with an origin of larger mammals such as bovine and porcine cells may be more relevant in terms of *in vitro* to i*n vivo* translation, but porcine cells generally lack commercially available antibodies established to identify the proteins transcribed by relevant genes, complicating common research methodologies such as immunohistochemistry. Secondly, whether the cells are primary (i.e. directly extracted from tissue) or immortalised also makes a difference: cells which have been transformed into cell lines via expression of tumour cell genes may show a differing phenotype to primary cells, but are on the other hand homogeneous and already characterised. It should also be noted that the use of 'surrogate' cells of a different nature in the assessment of barrier properties, such as epithelial MDCK and Caco-2 cells, is outdated for BBB studies as many better alternatives exist. Finally, protocols between labs inevitably differ, and as does physically quantifiable properties *of in vitro* BBB models such as TEERs.

Chapter 2.
Drug Delivery to the Central Nervous System

2.1. Drug Delivery

Because the majority of cell-surface receptors are expressed ubiquitously in the body, drugs targeting a specific receptor inevitably bind and affect tissues in addition to the target tissue. Paul Ehrlich coined the notion of a ‘magic bullet’, referring to an ideal therapeutic able to destroy its target but leave all other cells unharmed. (Ehrlich 1908) Developing smart drug delivery vehicles through manipulation of materials at the nanoscale may be essential in accomplishing this concept.

The drug must be present systemically to obtain the desired concentration at the target tissue, which means that the drug will potentially cause off target binding and adverse effects in addition to undesired target related effects. A frequently discussed example of off-target effects concerns cancer chemotherapy, which is highly toxic to healthy cells in addition to cancer cells. If chemotherapeutics would selectively bind to receptors expressed by cancer cells in addition to having high affinity and potency, the undesired target and off-target related effects would decrease.

2.2. Hurdles to Overcome in Drug Delivery

There are a number of hurdles which therapeutics must overcome in order to reach and exert effects at the target.

2.2.1. Solubility

Regardless of the route of administration, drugs must be soluble in plasma at the target site in order to become absorbed by the target tissue. Poor aqueous solubility results in poor uptake of the drug at the target. More than 40% of new agents developed in the

pharmaceutical industry are insoluble in water, requiring further physicochemical modification before they can be used (Savjani, Gajjar et al. 2012).

2.2.2. Protein Fouling

Drugs or nanoparticles dispersed in the circulation are susceptible to become coated by opsonin proteins present in plasma. Due to attractive intermolecular interactions, proteins in the plasma interact with the particles. The adsorption of proteins onto the particle surface is called protein fouling. This process results in the formation of a protein corona on the particle surface, which can be classified as ‘soft’ or ‘hard’. Proteins are continuously attaching and detaching in a soft corona due to weak intermolecular interactions, whereas adsorption and detachment in hard coronas occurs with much slower kinetics (Lynch, Salvati et al. 2009). The proteins involved in adsorption are referred to as ‘opsonins’, and include immunoglobulins, albumin, fibronectin among other plasma proteins. As particles become opsonised they become recognisable by the mononuclear phagocyte system (MPS), which recognises the adsorbed opsonins as a phagocytosis signal. Opsonisation can be quick, as elimination of nanoparticles by macrophages can occur just seconds after intravenous administration (Gref, Minamitake et al. 1994).

2.2.3. The Physiological Barrier

Protein fouling results in the detection and subsequent elimination by the macrophages and monocytes of the MPS. Another potential issue is excretion. The glomeruli of the kidneys are the porous filtration units, acting as molecular sieves with pores spanning approximately 12 nm (Gagliardini, Conti et al. 2010). Unbound drugs eventually become excreted by the kidney. By contrast, drugs bound to plasma proteins are poorly filtered through the glomeruli, and remain in circulation.

2.2.4. The Cell Membrane

Drug candidates aiming for intracellular targets must pass through the plasma membrane (i.e. possess permeability). One strategy is to target receptors at the plasma membrane to gain access via endocytosis. However, crossing lipid membranes can occur passively, depending on the lipid solubility of the drug. For passive diffusion to occur, the drug be hydrophilic enough to dissolve in plasma and lipophilic to penetrate cell membranes. One measure of this is the partition coefficient (Log_P), giving the ratio of distribution of a compound in octanol and water in equilibrium. Log_P can be measured experimentally ($_MLog_P$) or calculated computationally ($_CLog_P$). Attempting to make rules for pharmaceuticals, Lipinski's rule of five was formulated in 2001 as an experimental and computational approach to estimate drug solubility and permeability (Lipinski, Lombardo et al. 2001). These rules state that poor drug absorption and permeation is more likely to occur when the drug has:

>5 H-bond donors

>10 H-bond acceptors

>Mw of 500 Da

>5 $_CLog_P$ or >4.15 $_MLog_P$.

Lipinski's rules have been under debate for potentially being misleading, as many new drugs do not fit the set of rules. A new method of 'drug-likeness' has been formed by Hopkins and colleagues, which also takes into account the drug potency at the target (Bickerton, Paolini et al. 2012).

2.3. Approaches to Crossing CNS Barriers

In addition to the obstacles discussed in section 2.2, CNS targeting drugs are faced with additional barriers. Two different types of approach can be adapted: the disruptive approach involves bypassing these barriers through invasive surgery or to break the

barriers temporarily or permanently. Here, 'disruptive' is defined as any mechanism compromising the integrity of the CNS barriers, whether temporary or permanent. The alternative is to design drugs or drug delivery vehicles to use the transport mechanisms in place at the barriers, e.g. transcytosis.

2.3.1. Invasive Surgery

Gaining access to the brain via surgery is a highly invasive and risky procedure. The main goal is frequently intracerebral (IC) or intracerebroventricular (ICV) injections of a drug, or to place an implant for extended drug release. The latter often involves implanting a biodegradable hydrogel matrix into the ventricles to slowly emit a drug. Controlled release over time is essential for these materials, but can be difficult to achieve. Nevertheless, IC or ICV injections have produced therapeutic results in some instances. One group implanted 'microspheres' which released nerve growth factor (NGF) into the rat striatum as a protectant against neuron cell death, and observed neuroprotectant effects in the striatum 2.5 months after the surgery (Menei, Pean et al. 2000). Biodegradable polymers have also been used to deliver macromolecules over time to treat glioblastomas (Guerin, Olivi et al. 2004). In addition to the inherent risks of surgery and risk of inflammation, a major limiting factor of invasive CNS drug delivery is the limited spread of the drug. This is because once in the brain parenchyma, the distribution of the drug depends largely on diffusion. The time taken for a drug to diffuse can be expressed in equation [1],

$$t = \frac{x^2}{D} \qquad [1]$$

where x is the diffusion distance of the molecule, D is the diffusion coefficient (cm^2/s), and t is time (s). The diffusion coefficient is inversely related to molecular weight and size, and diffusion times for some example molecules present in the brain are given in table 2.1. The equation shows that the efficacy of diffusion decreases with the square

of the distance. Indeed, the radial spread of chemotherapeutics from intracerebral implants in rats decreased by 90% just 0.5 mm^2 after the origin (Fung, Shin et al. 1996). Additionally, the implantation procedure is not readily repeatable. Consequentially, drugs injected IC or ICV have to carry high initial concentrations of a drug in order account for this effect. These high concentrations far exceed physiological values, and can result in adverse affects such as astrogliosis and Schwann cell hyperplasia (Winkler, Ramirez et al. 1997) as has been observed in rodents (Yamada, Kinoshita et al. 1991, Winkler, Ramirez et al. 1997). Similar results have been observed in clinical trials: in 1999, ICV infusions of GDNF into a patient with Parkinson's disease was discontinued due to extensive neurotoxicity (Kordower, Palfi et al. 1999).

Molecule	M_w (Da)	D (cm^2/s)	Time taken to diffuse 5 mm
Na^{2+}	23	20×10^{-6}	3.5 hours
Myoglobin	17500	1.1×10^{-6}	2.7 days
Albumin	68000	0.7×10^{-6}	4.2 days
Glucose	180	6×10^{-6}	11.7 hours

Table 2.1. Diffusion times for some molecules in the brain. (Pardridge 2001)

Another strategy for bypassing the barrier obstacle involves disruption of the BBB. This can be achieved through the injection of hyperosmolar agents such as mannitol, which disrupts brain endothelial tight junctions by shrinking the endothelial cells (Rapoport 1970). Several clinical trials have been completed using mannitol in conjunction with chemotherapeutics to treat aggressive gliomas (Boockvar, Tsiouris et al. 2011)(Hall, Doolittle et al. 2006). Nevertheless, mannitol injections require direct access to the carotid artery, which must be exposed through surgery under general anaesthesia.

A recently established technique involves the focal use of ultrasound in gas microbubbles to disrupt the BBB. Magnetic resonance imaging (MRI)-guided focused

ultrasound has also been used to deliver chemotherapeutic monoclonal antibody Herceptin to the mouse brain (Kinoshita, McDannold et al. 2006), with clinical trials currently being prepared for similar applications (Ellens, Kobelevskiy et al. 2015). Ultrasound can be focused on areas as small as a few millimetres, and the combination with MRI allows for real-time target planning, making this method advantageous for achieving localised drug delivery e.g. to a tumour lesion. Thus far this is the only CNS delivery method simultaneously achieving localised delivery and also incorporating an element of personalised medicine where treatment is tailored to the patient. Although the ultrasound method does not require surgery, it does disrupt the blood-brain barrier which results in exposing the CNS to other compounds in the bloodstream that would normally be excluded. Even ubiquitous plasma proteins such as albumin can have adverse effects in the CNS such as neuroinflammation as a direct result of activating microglia and initiating BBB breakdown (Hooper, Pinteaux-Jones et al. 2009). The long-term safety issues of this method are a high priority area to investigate.

In summary, invasive or disruptive CNS targeting often provide limited efficacy and high risk. Instead, targeting the BBB in CNS drug delivery in a non-invasive manner is desirable for several reasons: i) not requiring surgery, ii) not disrupting homeostasis, iii) gaining access to the entire capillary network supplying the brain, leading to widespread delivery of the therapeutic rather than relying on diffusion from the origin of an implant.

2.3.2. Stealthing Through the CNS Barriers

Exploiting the transport mechanisms present at the blood-brain barrier provides the putative therapeutic with access to virtually the entire CNS without disrupting homeostasis. Drugs can cross the BBB via endogenous transporters in carrier-mediated transport or transcytosis. CMTs expressed at the BBB include GLUT1 glucose transporter, and large amino transporter LAT1. Targeting CMTs for drug

delivery is a viable option for low molecular weight drugs. For example, the dopamine pro-drug L-dopa is imported across the BBB via LAT-1, and is enzymatically converted into dopamine in the parenchyma (Kageyama, Nakamura et al. 2000). By contrast, targeting the transcytosis receptors opens the possibility of delivering macromolecular therapeutics. Receptors mediating transcytosis at the BBB include the insulin receptor (IR), transferrin receptor (TfR) and Low Density Lipoprotein Receptor Protein 1 (LRP-1). Of these, IR and TfR are highly specific to their ligands. There is no insulin mRNA expressed in the brain, therefore the IR on the BBB imports all of the brain insulin supply (Coker, Studelska et al. 1990). Similarly, the only endogenous ligand of TfR is the iron binding protein transferrin (Fishman, Rubin et al. 1987). Receptor for advanced glycation end products (RAGE) transports some glycated ligands across the blood-brain barrier, including amyloid-β peptides which thus implicates the receptor as a therapeutic target for Alzheimer's disease (Deane, Du Yan et al. 2003). LRP-1 is by far the most diverse receptor expressed at the BBB, with over 30 different ligands reported such as lipoproteins, proteases, viruses and toxins (Herz and Strickland 2001).

2.4. Drawing Inspiration from Nature: Biological Agents Crossing the Barriers

Nutrients, immune cells and many pathogens are all capable of crossing CNS barriers. Understanding the process by which these biological agents enter the brain is a step towards engineering smart materials for CNS drug delivery. Viruses are of special interest because they are unlike bacteria reliant on host cells to replicate and survive, and have therefore evolved advanced ways to enter mammalian cells. Commonly, viruses interact with membrane receptors to gain entry to the cell interior, thus avoiding detection by the immune system. They can be internalised by clathrin-mediated endocytosis, caveolae, macropinocytosis, or other mechanisms (Mercer, Schelhaas et al. 2010).

2.4.1. Immune cells

The barriers protect the CNS from pathogens. Inflammation is normally a useful immune system response to pathogens, and serves to limit cell and tissue damage as it typically culminates in the death of the pathogen-carrying cell followed by replacement by a new identical cell. However, unlike most cells of the body, neurons are not mitogenic, i.e. do not divide in the adult organism. The nervous system thus has a highly limited capacity for regeneration and repair. Inflammation is mostly considered to be detrimental to the CNS, and is indeed often present in CNS pathologies. For example, one of the hallmarks of multiple sclerosis is increased leukocyte trafficking to the CNS, and postmortem examinations often look for the presence of leukocytes in the perivascular space (Stolp and Dziegielewska 2009). Similarly, increased leukocyte presence in the CNS has been linked to other CNS pathologies such as stroke (Frijns, Kappelle et al. 1997), neurodegeneration (Cifelli, Arridge et al. 2002), and infection (Liu, Lossinsky et al. 2002).

Leukocytes can migrate across the BBB in a paracellular manner (paracellular diapedesis), but also through a phagocytosis-like transcellular mechanism (transcellular diapedesis). Both pathways start with leukocyte communication with the brain endothelial cells, and binding to I-CAMs expressed by the BECs (Adamson, Etienne et al. 1999). The paracellular mechanism involves the release of soluble factors by both leukocytes and endothelial cells to disrupt endothelial cell tight junctions, opening a gap between two or more endothelial cells. Transcellular leukocyte migration is more complex, involving extensive endothelial cell remodelling into large transient transcellular pores (Carman and Springer 2004). When leukocytes adhere to BECs, they extend their long cell protrusions (invadosomes) into BECs to probe for areas to migrate through (Carman 2009). In areas of low physical resistance (i.e.

remote from the basal lamina of the nucleus), the leukocyte extends the invadosomes deeper until the endothelial cell is breached. Upon breaching endothelial cells or their tight junctions, leukocytes use matrix metalloproteases MMP2 and MMP9 to cleave the basement membrane anchorage of astrocyte end-feet via a dystroglycan receptor (Agrawal, Anderson et al. 2006). Leukocyte infiltration is accompanied by an increase in BBB permeability due to partial breakdown of the BBB tight junctions (Bolton, Anthony et al. 1998).

Immune cell presence in the healthy brain is low, but there is constant interaction between brain endothelial cells and leukocytes to maintain a basal immune system surveillance in the CNS (Greenwood, Heasman et al. 2011). An estimated 2-5% of BBB tight junctions may show signs of opening at any time, which facilitates immune cell patrolling (Plumb, McQuaid et al. 2002). However, the reduced immune system presence in the CNS relative to the rest of the body reduces the propensity for a pathogen or foreign body to be eliminated. As a result, pathogens have evolved a range of strategies for entering the CNS.

2.4.2. Pathogens

Pathogens in the bloodstream can enter the CNS via the BBB. One strategy involves disrupting the tight junctions. For example, anthrax toxin (*Bacillus anthracis*) downregulates ZO-1 at the BBB (Ebrahimi, Kern et al. 2009). Pathogen disruption of the BBB can result in haemorrhagic encephalitis, as occurs in infection with anthrax or Nipah virus in humans (Maisner, Neufeld et al. 2009). Other pathogens enter through exploiting the barrier transporters: *C. neoformans* may enter the BBB via caveolae-mediated transcytosis, as knockdown of Cav1 in a human *in vitro* BBB model reduced transcytosis of the pathogen (Long, Huang et al. 2012). Furthermore, HIV is able to traverse brain endothelial cells via macropinocytosis (Liu, Lossinsky et al. 2002). *Neisseria meningitides*, *Streptococcus pneumoniae* and *Cryptococcus neoformans* can

cause meningitis by propagating in CSF of the subarachnoid spaces. *In vitro*, *C. neoformans* pathogens can cross the BBB via transcytosis, providing a mechanism for entry through meningeal vessels.(Vu, Weksler et al. 2009)

Some pathogens use leukocytes as 'Trojan horses' to infect the CNS. Pathogens such as *Herpes simplex*, *Listeria monocytogenes* and *Toxoplasma gondii* replicate within white blood cells and "hitchhike" across the BBB in this way (Kristensson 2011). Other pathogens use white blood cells in more opportunistic but indirect ways. The parasite *Trypanosoma brucei* is able to cross the CNS without white blood cells in the more advanced stages of the disease, when cells have already disrupted the BBB through opening tight junctions and basement membranes (Kristensson, Nygard et al. 2010). Malaria carried by red blood cells causes cerebral malaria through an association with the cerebral vessel walls, but without entering the CNS. Cells infected with malaria release 'microparticles' which stimulate macrophages to secrete pro-inflammatory cytokines, causing disruption of the BBB and neurovascular units (Couper, Barnes et al. 2010).

There are other ways for pathogens to enter the central nervous system without going through the blood brain barrier. Microbes can exploit weaknesses in peripheral nerve fibres to enter, often travelling a long way before reaching the cell bodies located within the CNS. Neurons in the peripheral nervous system are shielded by the perineurium, a sheet of connective tissue surrounding a bundle of nerves. However, unshielded nerve endings are potential entry routes for pathogens, which can exploit endosomal retrograde axon transport to infect the cell (Kristensson and Olsson 1973). Rabies virus replicates in skeletal muscle, and enters neuromuscular junctions to advance into the spinal cord via retrograde transport (Klingen, Conzelmann et al. 2008)(Lafon 2004). Finally, the olfactory system is directly exposed to the external environment and provides entry routes for viruses such as rhabdoviruses and paroxymaviruses.

Pathogens are transported along axons through the cribriform plate and to the olfactory bulb, where they can spread further by retrograde axon transport or by anterograde axon transport in the monoaminergic neurons of the brainstem (Mohammed, Norrby et al. 1993). Evidence for bacterial entry through the olfactory system can be seen through the presence of bacteria in the brain but absence from the blood, as is observed in cases of Pneumococcal bacteria (van Ginkel, McGhee et al. 2003).

Some of the aforementioned pathways are being explored for drug delivery; intranasal delivery is a conventional method, and as an example several formulations of opioids have been approved on the market for intranasal delivery (Grassin-Delyle, Buenestado et al. 2012). However, as discussed in previous sections, to maximise the spread of the drug it should enter through the dense capillary network supplying the brain parenchyma. The blood-brain barrier may therefore be the most profitable barrier to target for drug delivery. The use of 'Trojan horse' nanoparticles targeting the blood brain barrier has been reported (Pardridge 2006). The advantages of using nanocarriers to exploit endogenous transportation mechanisms are explored in the following sections.

2.5. Nanocarrier Requirements

The manipulation of materials on the nanoscale has given rise to a multitude of 'smart' nanomaterials able to carry drugs, or 'nanocarriers'. Nanocarriers engineered to enter the central nervous system via the blood-brain barrier must fulfil a number of criteria, which can be considered as part of the nanoparticle's journey from injection to entering the brain parenchyma:

i) Solubility in blood plasma

Nanocarriers must be able to disperse homogeneously in water in order to achieve optimal uptake at the target. Note that the commonly used method of dispersion of nanoparticles in a surfactant may compromise the integrity of the blood-brain barrier.

ii) Avoidance of protein fouling and immune system

The nanocarrier should be biologically compatible. Furthermore, the ability to avoid the immune system ('immune stealth') is essential in order to avoid detection as a foreign agent and subsequent elimination (unless the target is the immune system). Poly(ethylene) glycol (PEG) is a FDA-approved polymer used heavily in the medical field which is both biocompatible and confers immune stealth. PEG forms hydrogen bonds with water, making the particle it is attached to prefer water to protein and therefore avoid protein fouling. PEGylation (i.e. the addition of PEG chains) to a range of drugs, peptides and proteins has been reported to prolong the blood circulation half-life through decreasing immunogenicity and degradation (Veronese and Pasut 2005).

iii) Getting out of the bloodstream, i.e. equipped with CNS targeting

An increasingly used strategy to gain access to the cell interior is to exploit the active process of endocytosis by designing ligands which bind to specific receptors. In doing so, the 'drug-likeness' rules for passive diffusion across plasma membranes no longer apply. To exploit endocytosis, a different set of rules apply: first and foremost, size of the therapeutic determines the extent and kinetics of internalisation. Mammalian cells actively and selectively endocytose a range of ligands in the size range of 10-300 nm (Ehrlich, Boll et al. 2004). Therefore, nanocarriers are highly suitable for combination with targeting ligands inducing endocytosis. However, there are a number of factors to consider when choosing the receptor to target, especially as cargo entry into the cell is highly regulated at the plasma membrane. Important considerations include receptor

expression, i.e. whether it is ubiquitous in the body or enriched at the target tissue; endogenous ligands to the receptor, and whether they compete with the ligand; efficacy of ligand-receptor interactions; and receptor half-life or rate of recycling to the plasma membrane after endocytosis.

To achieve delivery to the CNS via the blood-brain barrier, carriers need a targeting sequence which not only targets BBB receptors but also induces complete transcytosis of the drug. Targeting moieties can include antibodies or a short peptide targeting sequence. Once in the parenchyma, the nanocarrier must additionally target receptors for endocytosis.

iv) Delivery of cargo at the target site

The main purpose of a drug delivery vehicle is to carry cargo to a specific location and release it selectively at the target. Vehicles must thus be able to efficiently carry cargo, and also ideally have a controlled release mechanism.

2.6. Types of Nanocarriers

A number of nanocarriers have been used as strategies to deliver therapeutics to the brain. Nanoparticles created for biomedical purposes come in many shapes, sizes and materials. They can be categorised into ‘soft’ or ‘hard’ systems on the basis of the intramolecular bonds they form: ‘hard’ nanoparticles consist of strong bonds such as metallic, covalent or ionic bonds. Weaker interactions make up ‘soft’ nanoparticles, and include hydrogen bonds, Coulombic forces, the hydrophobic effect, and combinations of them all. The use of hard or soft systems for drug delivery has been extensively reported, as reviewed by Akinc and Battaglia (Akinc and Battaglia 2013). The following sections summarise the properties of these carriers as well as their suitability for CNS drug delivery.

2.6.1. Antibodies

Antibodies are proteins produced by the immune system as a response to foreign molecules in the body. Monoclonal antibodies (MAbs) respond to a single epitope or sequence of amino acids, whereas polyclonal antibodies recognise several similar sequences. Because of the specificity of MAbs and the techniques available to produce antibodies in batches, MAbs are of high therapeutic value in diseases where a single protein target can be defined. This is reflected in the pharmaceutical industry, where there is currently a range of approved therapeutic antibodies. For example, the humanised anti-epidermal growth factor receptor 2 (HER2) MAb Herceptin (*trastuzumab*) has been largely successful in treating breast cancer patients overexpressing the HER2 protein (Vogel, Cobleigh et al. 2002). However, clinically approved antibodies for targets within the CNS are lacking, as they cannot penetrate the BBB unless they are engineered specifically to target a BBB receptor.

Approaches for using antibodies for CNS delivery have included the antibody itself as a treatment, or when fused to a delivery construct. A MAb against the human insulin receptor (HIR) was pioneered for the use of radiolabelled brain imaging probes. Furthermore, the 83-14 antibody complexed with a radiolabelled amyloid β 1-40 complex entered the rhesus monkey brain *in vivo* via transcytosis (Pardridge, Kang et al. 1995, Wu, Yang et al. 1997). Another example is the engineered llama-derived single domain antibody (sdAbs) FC5, which crosses a human model of the BBB via clathrin-mediated transcytosis. Upon interaction with the α(2,3)-sialoglycoprotein receptor, FC5 entered early endosomes but bypassed later stages of the endosomal pathway, and was exocytosed in an intact state (Abulrob, Sprong et al. 2005). The use of sdAbs over conventional antibodies is advantageous, as their immunogenicity is reduced due to the absence of the light chain from the antibody (Muyldermans, Atarhouch et al. 1994). Nevertheless, antibodies developed in different species require

chimerisation or humanisation before they can be used in a clinical setting. Furthermore, the short plasma half-life and high production costs are limitations to consider for therapeutic antibodies (Chames, Van Regenmortel et al. 2009).

2.6.1.1. Affinity

Targeting transcytosis at the BBB relies on ligand-receptor interactions. The engineered ligand needs to bind and activate its target receptor, induce complete transcytosis, and then release the cargo. Ligand-receptor interactions are quantified in affinity: the strength of interaction between the antibody's antigen binding site and the epitope. In practical terms, affinity refers to the number of ligand-receptor complexes in equilibrium. The cumulative intermolecular interactions between the complex is quantified in avidity, measuring the overall stability of the complex. Avidity is influenced by several components: intrinsic affinity; valency, i.e. the number of arms in an antibody to bind the antigen; and the spatial orientation of the interacting components.

Paradoxically, higher affinity does not guarantee more effective delivery. At the BBB, the efficiency of the monoclonal TfR-targeting antibody OX26 was questioned after reported findings in the rat that OX26 predominantly accumulates inside brain capillaries instead of entering the brain parenchyma (Moos and Morgan 2001). Similar studies tracking OX26 and OX26-conjugated liposomes showed that neither was present in the choroid plexus epithelium, neurons or glia despite using *in situ* perfusion, a method to increase uptake to the brain by bypassing the systemic circulation (Gosk, Vermehren et al. 2004). It was concluded that OX26 with or without liposomes had previously yielded false positives and does not cross the BBB. In 2011, further clarification was provided by Yu et al. who showed that if the antibody affinity is too high, the cargo is never released and consequently shuttles back and forth at the BBB remaining complexed with the antibody. They were able to boost uptake into the parenchyma through reducing the affinity of the antibody to its transcytosis target (Yu,

Zhang et al. 2011). There is thus an inverse correlation between affinity and brain uptake, which must be taken into consideration when using antibodies for targeting the BBB.

2.6.2. Hard Nanoparticles

The 'hard' nanomaterials include metals such as gold and silver nanoparticles, quantum dots, and carbon nanotubes. A number of *in vivo* applications have been reported for hard nanoparticles: quantum dots are 2-10 nm fluorescent semiconductor crystals particularly useful for *in vivo* imaging and diagnostics (Gao, Cui et al. 2004, Michalet, Pinaud et al. 2005); silver nanoparticles (AgNPs) have been engineered with potential applications for antibiotics-resistant bacteria (Siddhartha, Tanmay et al. 2007); gold nanoparticles (AuNPs) can be used as a non-invasive imaging agent in gliomas (Cheng, Dai et al. 2014); and glucose-coated gold nanoparticles are able to cross the BBB *in vitro* and enter astrocytes (Gromnicova, Davies et al. 2013). Although there are merits to these nanoparticles, they tend to contain heavy metals such as cadmium and mercury and therefore pose a considerable toxicity concern to biological systems (Longmire, Choyke et al. 2008). Quantum dots accumulate in the liver, where their cadmium core causes acute liver toxicity due to oxidative stress (Derfus, Chan et al. 2004). Inhaled silver nanoparticles are internalised by alveolar macrophages, which within 24 hours produce inflammatory responses (Carlson, Hussain et al. 2008). Furthermore, gold nanoparticles were recently reported to enter the CNS through opening BBB endothelial cell tight junctions (Li, Jhan et al. 2015).

'Hard' nanoparticles have solid cores and can therefore only carry drugs through surface conjugation. Attaching drugs to the surface of the nanoparticle exposes the drug to premature degradation by the extracellular environment, e.g. by proteases. The engineering of nanoparticles with hollow cores provides the possibility to carry the drug

within the vehicle, protected from the extracellular environment. Designing nanoparticles with hollow cores is possible in the case of 'soft' nanoparticles.

2.6.3. Amphiphiles

'Soft' materials are more biologically compatible than hard nanoparticles, partially because the intermolecular interactions holding soft nanoparticles together are on a similar level to those in living systems. Amphiphiles are a major category of 'soft' drug delivery vehicles, and are a class of molecules with a hydrophobic and a hydrophilic component linked together. Common amphiphilic materials include lipids and polymers. In water, only the hydrophilic part of the amphiphile dissolves, and the hydrophobic parts prefer to pack together as it is more energetically favourable. This hydrophobic effect causes the rearrangement of amphiphiles into ordered structures, with a hydrophilic corona and a hydrophobic core.

The resulting structure of the assembled amphiphile depends on the dimensionless packing parameter *p*, the calculation of which is given in equation 2*:*

$$p = \frac{v}{a_0 lc} \qquad [2]$$

Where *v* is hydrophobic block volume, *lc* is hydrophobic chain length and a_0 is the optimal surface area of the assembled polymer. A low packing parameter $p < 1/3$ causes high membrane curvatures and favours the formation of micelles, *p* between 1/3 and 1/2 creates micellar filostructures or 'tubes', and $p > 1/2$ causes low membrane curvatures and the formation of bilayer membrane vesicles with an aqueous core (Smart, Lomas et al. 2008). The different structures formed by different packing parameters in the case of a polymer are shown in figure 2.1.

Micelles of either lipid or polymer compositions have been used for drug delivery applications. However, vesicles offer a number of advantages to micelles: the encapsulation of hydrophobic compounds in addition to hydrophilic; higher drug release kinetics (Chen, Meng et al. 2010); and protection of cargo from degradation by the extracellular environment (Simone, Dziubla et al. 2008). Furthermore, the vesicular nature of liposomes and polymersomes confers better cargo carrying capacities than antibodies. The ability to encapsulate drugs into amphiphilic nanocarriers such as liposomes or polymersomes, which can be chemically modified to display targeting moieties on the surface, is a major advantage. Antibodies targeting the BBB can carry 1-4 individual drug molecules per antibody, compared to >10,000 drug molecules per individual ~100nm liposome or polymersome. (Huwyler, Wu et al. 1996, Pegoraro, Cecchin et al. 2013)

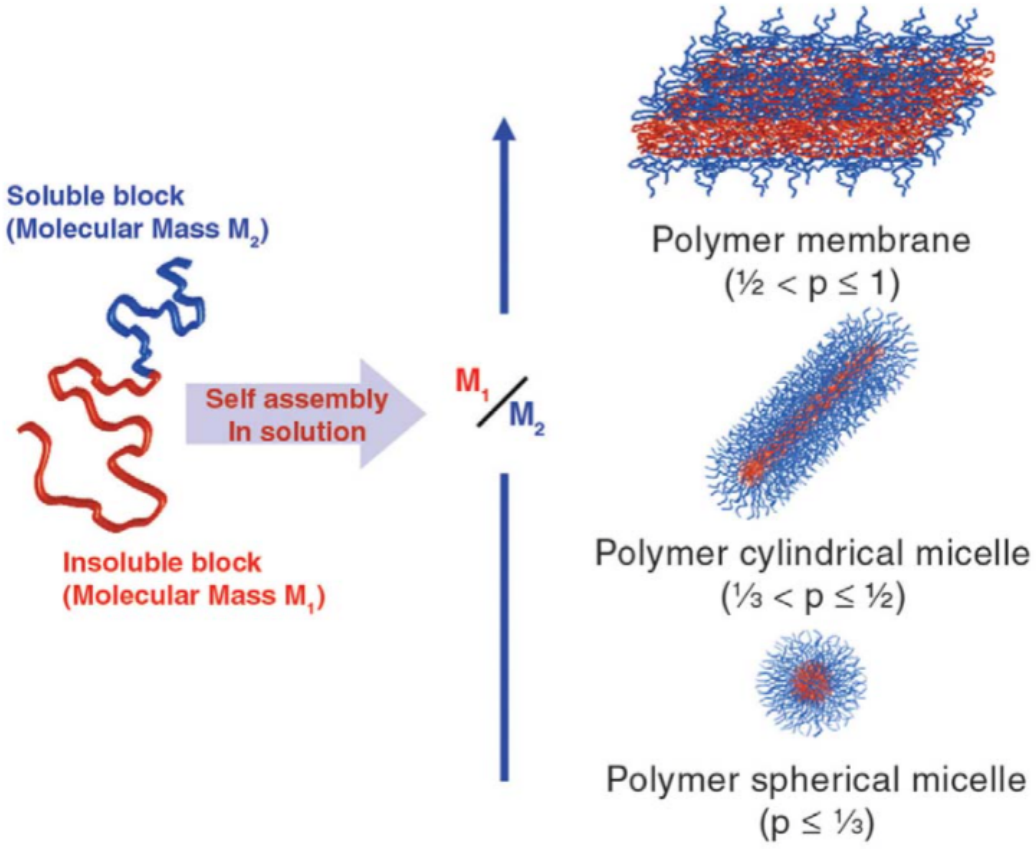

Figure 2.1. Amphiphilic block copolymer self-assembly into different structures.(Smart, Lomas et al. 2008)

2.6.3.1. Liposomes

The pioneering amphiphiles used for drug delivery are liposomes, i.e. lipids self-assembled into a vesicular membrane. The hollow nature of these vesicles confers the ability to encapsulate hydrophobic or hydrophilic drugs, and liposomes are furthermore biocompatible due to their phospholipid composition. Because different lipids can be used to create liposomes, there is some versatility in physicochemical properties such as size and surface charge. These nanocarriers have been used since the 1960s for targeted delivery of antiretrovirals (Hostetler, Stuhmiller et al. 1990), genes (Gao and Huang 1995), chemotherapeutics (Yang, Cui et al. 2007), and many other agents. However, liposomes are rapidly recognised in the body and cleared by the MPS. This problem can be addressed through PEGylation, which prolongs plasma circulation in by decreasing opsonisation and therefore 'stealthing' from macrophages. However, there are some issues with PEGylation. For instance, PEGylated liposomes with conjugated mAbs can lose their tumour targeting selectivity due to steric hindrance between the mAb and the targeted receptor (Klibanov, Maruyama et al. 1991). Additionally, only a small total surface area of liposomes can be PEGylated as addition of PEG chains destabilises the vesicle. This is due to a change in the packing factor with the addition of long hydrophilic PEG chains, and the hydrophilic/hydrophobic ratio essential for vesicle formation is destabilised if PEG is added above a certain amount. Indeed, liposome stability is a common issue and they are prone to leakage upon encountering serum (Allen and Cleland 1980).

PEGylated liposomes have been used in conjunction with antibodies for targeting transcytosis at the BBB. Immune-evading liposomes are sometimes referred to as 'Trojan horses' due to their ability to stealth through the blood-brain barrier. The OX26 monoclonal anti-TfR antibody fused to PEGylated immunoliposomes has extensively been reported to cross the BBB in rats (Huwyler, Wu et al. 1996). Attempts to translate

OX26 delivery into mice were complicated by the transferrin sequence differing between mice and rats, but was achieved eventually after re-engineering the sequence (Lee, Engelhardt et al. 2000). Further reports have also highlighted that OX26 may give a false positive of CNS entry but in fact accumulates inside the endothelial cells, indicating restricted transport to the brain (Moos and Morgan 2001, Paris-Robidas, Emond et al. 2011).

Liposomes have been used as a non-invasive alternative for CNS delivery. Despite equipping liposomes BBB endogenous transporter targeting moieties, many liposome preparations require stabilisation in surfactants. The BBB is like other lipid membranes disrupted by surfactants and organic solvents such as ethanol and dimethyl sulphoxide. (Hanig, Morrison et al. 1972, Saija, Princi et al. 1997). It is not clear whether liposomes can cross the BBB without the co-injection of surfactants (Pardridge 2001). Furthermore, the above putative therapies have thus far achieved limited efficacy in delivery. The brain uptake, as quantified in injected dose/g (%ID), is 0.2-0.3% for OX26 liposomes (Friden, Olson et al. 1996). In comparison, a human insulin receptor HIR monoclonal antibody achieved corresponding injected dose values of 3-4% (Pardridge, Kang et al. 1995).

2.7. Polymersomes

More recently, amphiphilic block copolymers have been used to obtain polymer vesicles, or polymersomes (Discher and Eisenberg 2002). The structure of a polymersome is depicted in figure 2.2. A diverse range of applications have been reported for polymersomes, such as carriers for imaging agents, nano-reactors, and theranostics in addition to their uses for drug delivery.

2.7.1. Physical Chemistry

Polymersomes offer a number of improved physicochemical advantages to liposomes. Firstly, the polymersome membrane is 20x less permeable than their liposome counterparts, which provides improved stability and more efficient protection of cargo from degradation (Battaglia, Ryan et al. 2006). Secondly, the use of polymers approved by governmental regulatory bodies such as FDA also creates potential for quick translation into the clinic. Thirdly, polymersome physicochemical properties such as size and surface topology can be precisely controlled via altering block copolymer architecture and chain length. The virtually inexhaustible resources of polymers created through polymerisation methods allows for the creation of sophisticated controlled-release vehicles with more options than lipid counterparts can offer, as summarised in figure 2.3.

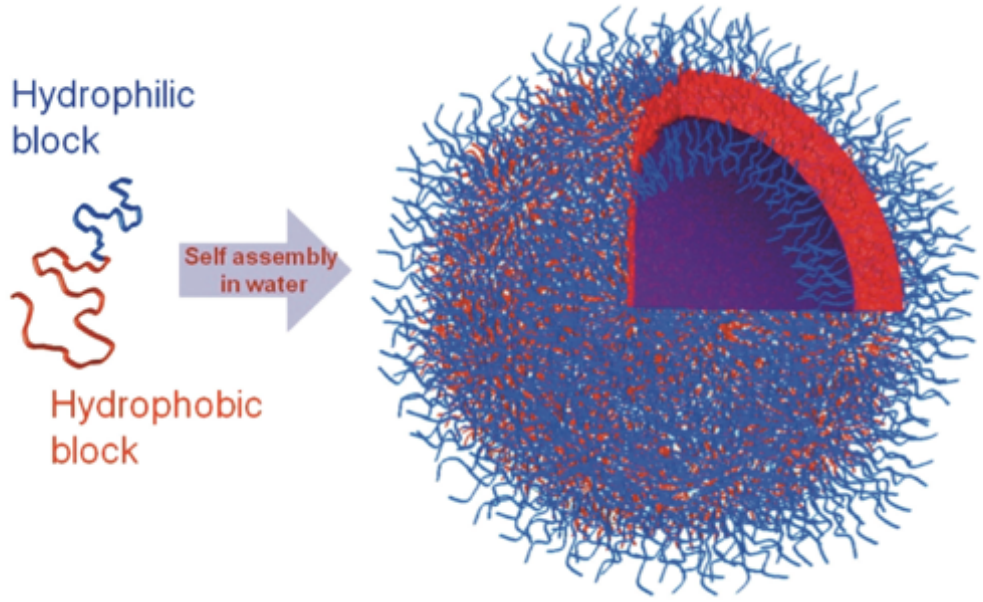

Figure 2.2. Schematic of a polymersome.(Smart, Lomas et al. 2008)

Polymersome membrane topology can be precisely engineered. Polymersomes formed from a diblock copolymer in which the two blocks differ significantly in molecular weight undergo phase separation in the polymersome membrane over time. Effectively, phase

separation creates segregated nano-domains in the polymersome (LoPresti, Massignani et al. 2011). The membrane of viruses is often arranged into such nano-scale domains, which are essential to their endocytosis by mammalian cells (Canton and Battaglia 2012). Indeed, phase-separated polymersomes with “patches” on their membrane have faster internalisation kinetics than pristine polymersomes, making polymersomes akin to ‘synthetic viruses’ (Massignani, Lopresti et al. 2009). The ability to fine tune physical properties combined with amphiphilic cargo loading and controlled release capabilities makes polymersomes optimal vehicles for drug delivery.

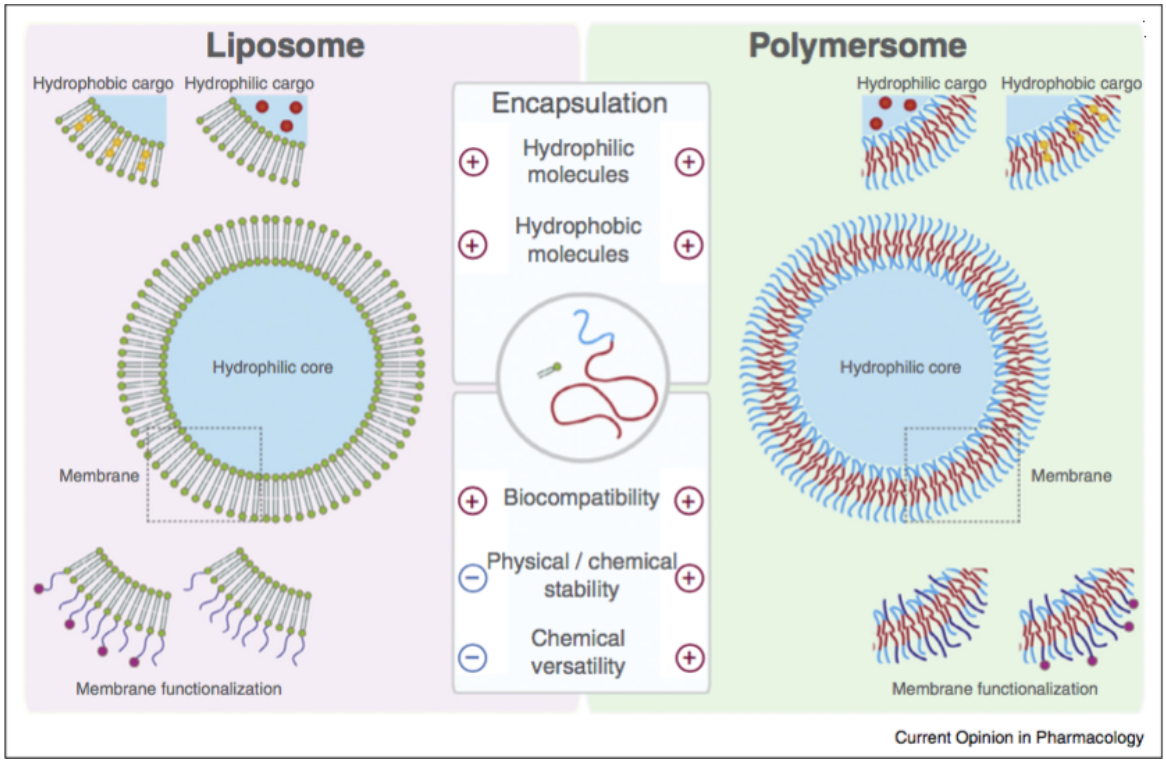

Figure 2.3. Comparison between liposomes and polymersomes. (Messager, Gaitzsch et al. 2014).

2.7.2. Stealth

Liposomes require PEGylation to obtain stealth properties, but the hydrophilic character of PEG destabilises the lipid head group in liposomes which can result in drug leakage (Tirosh, Barenholz et al. 1998). Conversely, polymersomes can be formed in a stable manner from PEG-based block copolymers, with improved stability as PEG molecular weight increases (Lee, Bermudez et al. 2001). Polymersomes can

be 100% PEGylated in the brush as long as hydrophobic chain length is increased to compensate for it.

2.7.3. Stimulus Responsiveness

The design of polymersomes responsive to various triggers such as UV, pH or calcium has been reported (Li and Keller 2009). Work by the Battaglia group has established the use of poly[2-(methacryloyloxy)ethyl phosphorylcholine]-*block*-poly((diisopropylamino)ethyl methacrylate) (PMPC-PDPA) polymersomes for drug delivery (Lomas, Canton et al. 2007). The PMPC block is non-protein fouling, and polymersomes are internalised by a wide range of cells with no signs of toxicity (Lomas, Massignani et al. 2008). The PMPC block can be substituted for other polymers with similar properties. For example, the Poly(ethylene) Glycol (PEG) derivative Poly[oligo(ethylene glycol) methyl ether methacrylate] (POEGMA) is both stable and non- protein fouling *in vitro* (Tugulu and Klok 2008). The PDPA block confers pH sensitivity to the polymersomes: above its pKa of approximately 6.4 the block is hydrophobic. Below this pKa, de-protonation of the tertiary amine groups causes the normally hydrophobic PDPA block to become hydrophilic and thus causes rapid disassembly of polymersomes due to a change in intermolecular forces, as depicted in figure 2.4. When polymersomes are internalised by cells, they are sorted into the endo-lysosomal trafficking pathway. The acidic pH of endosomes (5.5-6.1) causes a drop in pKa, prompting a quick disassembly of pH sensitive polymersomes. The major increase in the concentration of unimers in the endosomal compartment causes an osmotic shock, temporarily lysing the endosomal membrane and allowing the unimers and the cargo to escape into the cell cytosol (Lomas, Massignani et al. 2008). pH sensitive polymersomes have been used for delivery of a range of therapeutics, including anti-cancer drugs, imaging agents and antivirals (LoPresti, Lomas et al. 2009).

2.7.4. Conjugation of Peptides Targeting the Blood-Brain Barrier

A major advantage of polymersomes is the ability to chemically incorporate targeting moieties such as peptides or antibodies. Indeed, the 83-14 antibody against HIR has recently been combined with a polymersome delivery vector to obtain an efficient drug delivery system targeting the BBB (Dieu, Wu et al. 2014). Furthermore, peptide sequences can be derived synthetically to target transcytosis at the BBB and are less immunogenic than antibodies. A peptide which has been used for CNS entry is Rabies Virus Glycoprotein (RVG), which was used as a targeting mechanism to deliver siRNA to the mouse CNS through transvascular delivery (Kumar, Wu et al. 2007). RVG is a 29 amino acid peptide which binds specifically to nicotinic acetylcholine receptors expressed by neurons. However, attempts to combine the RVG peptide with pH-sensitive polymersomes failed to induce transcytosis *in vitro* (Tian, Nyberg et al. 2015). *In vivo* CNS entry of a RVG-mannitol-PEI polymer siRNA drug delivery system was reported, although no endeavours to confirm receptor colocalisation were undertaken (Park, Singh et al. 2015).

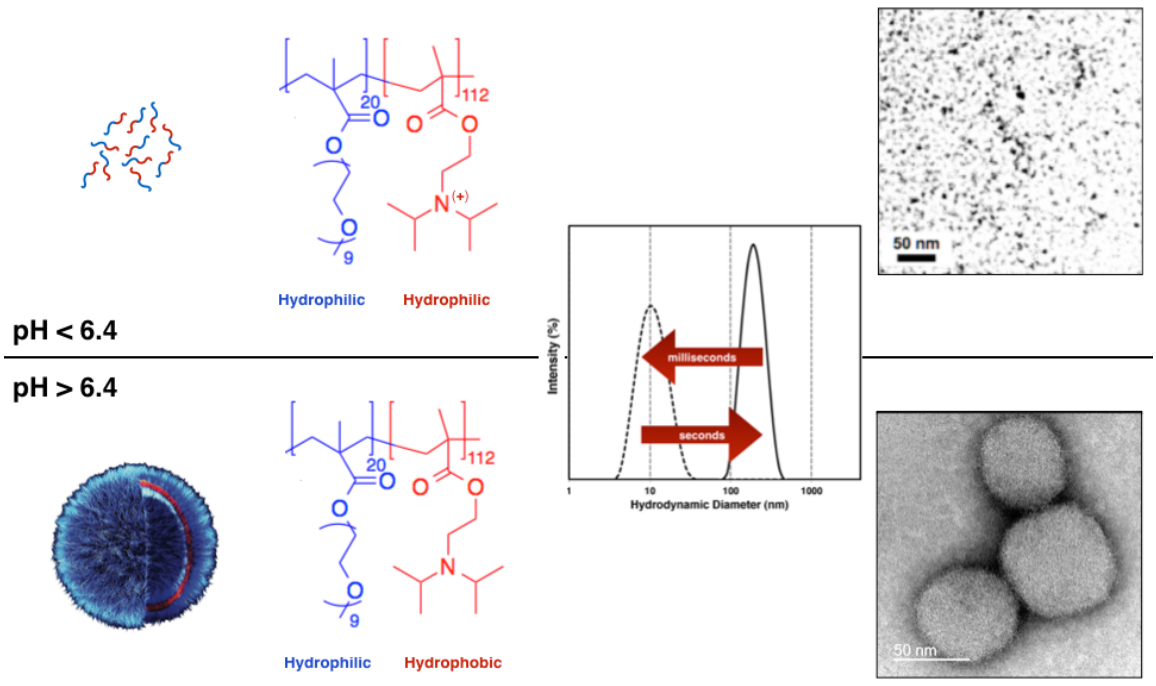

Figure 2.4. pH sensitivity mechanism of POEGMA-PDPA polymersomes. Adapted from ref (Lomas, Massignani et al. 2008).

Conjugation of the GM1-targeting peptide G23 to polymersomes resulted in a small amount of accumulation in the mouse brain *in vivo* via transcytosis. The transcytosis efficiency was comparable to that of polymersomes with a transferrin receptor targeting moiety (Stojanov, Georgieva et al. 2012). GM1 is a ganglioside strongly concentrated in caveolae (Parton 1994). However, GM1 is not recycled to the membrane with caveolae, which indicates that GM1 only enters caveolae in endocytosis but not complete transcytosis (Balasubramanian, Scott et al. 2007). Further work is required to elucidate the mechanism by which GM1 induces transcytosis at the BBB.

A Kunitz protease inhibitor domain was identified as the essential domain required by amyloid precursor protein to enter the brain via LRP-1-mediated transcytosis (Kounnas, Moir et al. 1995). Based on this discovery, Demeule et al. developed a series of peptides derived from the Kunitz domain and screened the peptide transcytosis ability in a blood-brain barrier model. Subsequently the synthetic 19 amino acid peptide Angiopep-2 was identified to have a high transcytosis capacity *in vitro*, and furthermore confirmed to enter the parenchyma *in vivo* via a vascular route (Demeule, Regina et al. 2008). It does so through transcytosis mediated by the LRP-1 receptor at the BBB (Demeule, Currie et al. 2008). Data suggests that the transcytosis of Angiopep-2 is only partially inhibited by other LRP-1 ligands (Demeule, Regina et al. 2008), and uptake is not affected by Pgp inhibition.(Demeule, Currie et al. 2008) Furthermore, human serum albumin (HSA) nanoparticles coated with ApoE cross the blood brain barrier *in vitro* and *in vivo* via transcytosis (Zensi, Begley et al. 2009) which may also be mediated by LRP-1 as ApoE is a LRP-1 ligand. LRP-1 is thus a promising receptor to target for drug delivery across the BBB.

Aims and Objectives

There are several aims and objectives for this thesis project, entitled 'LRP-1-Mediated Blood Brain Barrier Transcytosis: Mechanisms and Therapeutic Applications'.

Previously, several peptides were conjugated to the diblock copolymer poly[oligo(ethylene glycol) methyl methacrylate]-block- poly((diisopropylamino)ethyl methacrylate) (POEGMA-PDPA). Polymersomes with peptide targeting systems (RVG and Angiopep-2) were subsequently screened *in vitro* for their transcytosis capabilities, and Angiopep-2-POEGMA-PDPA (A-EP) were shown to have a high capacity for transcytosis whereas RVG-POEGMA-PDPA or non-targeting POEGMA-PDPA (EP) polymersomes did not undergo transcytosis at all. Furthermore, A-EP polymersomes were successfully delivered into the mouse CNS after intravenous injections (Tian, Nyberg et al. 2015). Subsequently, A-EP polymersomes were chosen for further investigation as CNS drug delivery vehicles. However, characterisation of A-EP transcytosis *in vitro* and *in vivo* is required.

i) Aim:

To elucidate the kinetics of A-EP transcytosis across the blood-brain barrier, using an *in vitro b*rain endothelial cell transwell model.

Hypothesis:

A transwell model of the BBB can be used to probe A-EP transcytosis kinetics. LRP-1 induces transcytosis of A-EP polymersomes in a saturable manner, and the optimum density of number of Angiopep-2 molecules on the polymersome membrane can be found through using transcytosis assays with varying number of ligands conjugated.

ii) Aim:

To elucidate the mechanisms of A-EP transport across the blood-brain barrier.

Hypothesis:

Because LRP-1 mediates transcytosis of the peptide Angiopep-2 *in vivo*, it is hypothesised that LRP-1 induces transcytosis of A-EP polymersomes across the brain endothelium. This is followed by transportation through membrane-bound organelles which may or may not form a tubular network, and is caused by clathrin-mediated endocytosis and not caveolae as frequently implicated in peripheral endothelia. Importantly, it is hypothesised that transcytosis by brain endothelial cells does not occur through acidifying endosomal trafficking pathway, but may go through a tubular network instead. It is further hypothesised that the protein machinery involved in exocytosis is likely to be somewhat conserved between regulated exocytosis machinery in neurons, with non-neuronal isoforms of the SNARE proteins having an essential role.

iii) Aim:

To confirm CNS uptake of polymersomes in a living system, and to quantify uptake of fluorescently labelled polymersomes *in vivo*.

Hypothesis:

In situ perfusion can be used as a delivery method of polymersomes to the rat brain. Because this method increases uptake into the brain, polymersome fluorescence may be sufficient for quantification through methods such as fluorescence spectroscopy or high-performance liquid chromatography.

iv) Aim:

Deliver macromolecular therapeutics to the CNS using A-EP polymersomes as a drug delivery vehicle.

Hypothesis:

Because LRP-1 is expressed in neurons and glia in addition to brain endothelial cells, it is hypothesised that A-EP polymersomes can be used to deliver macromolecular cargo intracellularly within the CNS. The use of pH sensitive polymersomes provides the adequate controlled release mechanism upon internalisation through acidifying endosomal compartments in non-transcytosing cells. LRP-1 transcytosis is non-acidifying, keeping cargo-carrying polymersomes intact. By contrast LRP-1 endocytosis by glia or neurons operates through a canonical endocytosis pathway, resulting in cargo release into the cytosol upon encountering the acidic endosomal environment.

The chief hypothesis of the project can be summarised as follows: A-EP polymersomes can be used as a CNS macromolecular drug delivery vehicle through targeting LRP-1 transcytosis at the BBB.

Chapter 3.
Materials and Methods

3.1. Block Copolymer Synthesis

All polymers were synthesised by Steven Armes' group (Department of Chemistry, The University of Sheffield, U.K.). Poly (ethylene glycol) methyl ether methacrylate ($P(OEG_{10}MA)_{25}$) *block* poly- (diisopropylamino)ethyl methacrylate $(PDPA)_{114}$ or abbreviated as EP was synthesised by atom transfer radical polymerisation (ATRP) (Madsen, Warren et al. 2011). The structure of EP (M_w = 33000) is depicted in figure 3.1. The POEGMA block is hydrophilic, and PDPA is hydrophobic at a pH above its pKa of ~6.4.

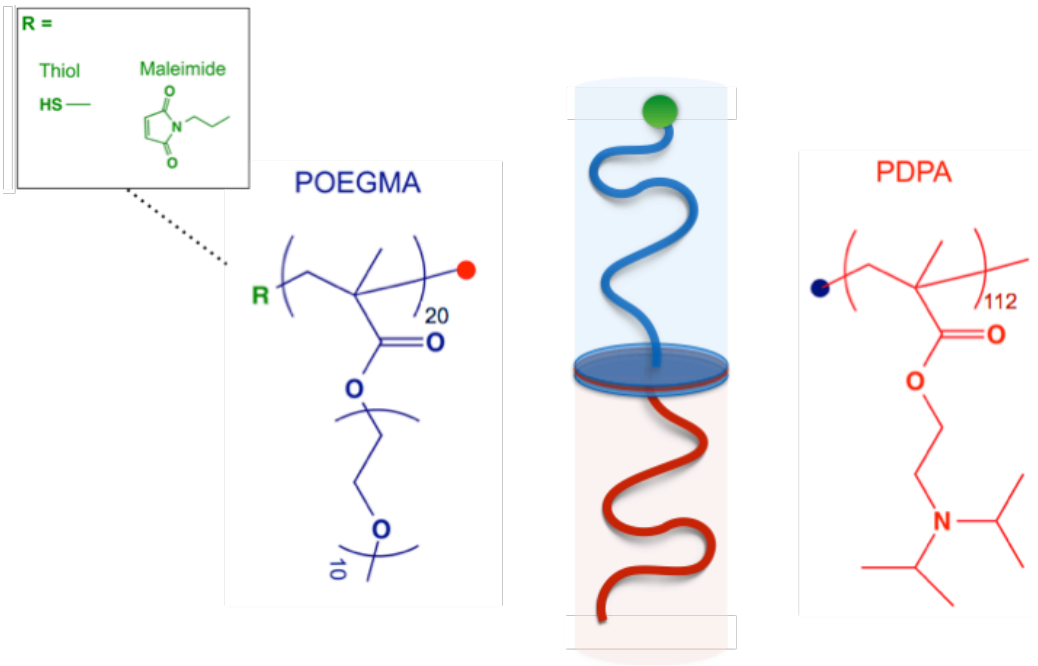

Figure 3.1. Chemical structure of POEGMA-PDPA. Blue denotes hydrophobic blocks and red hydrophilic, functional group R (here R = maleimide).

It is possible to add a functional group (R) onto the POEGMA chain via chemical cross-linking. A maleimide linker was used as the strategy for addition of functional R groups onto the backbone of POEGMA. Angiopep-2 was ordered from Pepceuticals

(Nottingham, England), with an additional cysteine added to the N terminus of the amino acid sequence, as specified below:

CTFFYGGSRGKRNNFKTEEY

Angiopep-2 was conjugated onto POEGMA-PDPA (A-EP) via a maleimide, and conjugation measured by HPLC. Approximately 40% of the polymer was successfully functionalised (Tian, Nyberg et al. 2015). The resulting structure is displayed in figure 3.2.

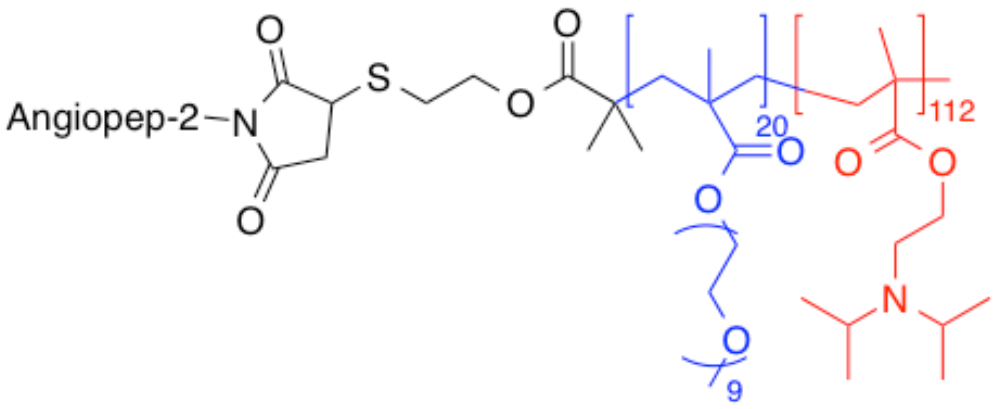

Figure 3.2. Chemical structure of Angiopep-2-POEGMA-PDPA (A-EP). M_w: 33000.

3.1.1. Functionalisation of POEGMA-PDPA with Cy3

Cy3-maleimide from Lumiprobe (Germany) (m_w = 615.20 g/mol, λ_{ex} 555nm, λ_{em} 570nm) and $PDPA_{100}$-$POEGMA_{20}$-SS-$POEGMA_{20}$-$PDPA_{100}$ (m_w = 45000 g/mol) were weighed out in a 2:1 molar ratio and dissolved in 2:1 $ChCl_3$ and MeOH mixture. The solution was N_2 purged for 20 minutes in room temperature (21°C). 1.2 equivalents of PPh_3 was added, and N_2 purged for 1 minute. After 48 hours, the solution was run through a 1000 Da MWCO dialysis membrane against EtOH, left in RT for 6h before changing to fresh EtOH and leaving it overnight. EtOH was changed to milli-QH_2O

(Millipore, U.S.), left for 8 hours, followed by flash freezing in liquid N_2 and freeze dried in -50°C.

3.2. Polymersome Preparation

All polymersomes for *in vitro* experiments were labelled with 10% (mol) Cy3-POEGMA-PDPA polymer. All polymersomes for *in vivo* experiments were labelled with 20% (mol) Cy3-POEGMA-PDPA. Where polymersomes were functionalised with Angiopep-2-POEGMA-PDPA, the final Angiopep-2 functionalisation was 1.2% (mol) unless otherwise specified.

Polymersomes were prepared via a bottom-up pH switch approach. Polymers were dissolved at a total concentration of 10 mg/ml in pH 2 PBS, sterilised with a 0.2 μm filter and gradually brought up to pH 7.4 using 0.5M NaOH under magnetic stirring. In cases where Angiopep-2-POEGMA-PDPA was part of the polymer mixture, it was added at pH 6.0 in order to avoid peptide denaturation, and left to stir for approximately 10 minutes to disperse into the polymer mixture. The solution was subsequently filter sterilised. Once pH 7.4 was reached, polymersome size was assessed with dynamic light scattering (DLS) and if necessary, polymersomes were sonicated on ice for 20 minutes to decrease the presence of aggregates formed in the pH switch process. Polymersomes were stored in 4°C until use.

3.2.1. Purification via Gel Permeation Chromatography

Polymersomes produced via pH switch were purified using gel permeation chromatography (GPC). GPC is a form of size exclusion chromatography (SEC), in which particles are eluted through a column in a size-dependent manner. Here, a column filled with sepharose 4B (Sigma-Aldrich, U.K.) was used as the substrate. Polymersome samples containing larger polymersomes (e.g. tubes) or micelles are

suitable for purification via GPC, but this method is often limited to a few millilitres per column to allow adequate column length for sample separation.

3.2.2. Purification via Centrifugation

Centrifugation causes particles of different sizes in a sample to sediment at different rates, with large particles sedimenting first. It is a technique commonly used to purify different subcellular organelles, and has recently been shown to work in the separation of PMPC-PDPA polymersome tubes from spheres (Robertson, Yealland et al. 2014). 100 mL of Angiopep-2-POEGMA-PDPA polymersomes were produced as a single batch via the pH switch method, and measured into centrifugation tubes at 25 mL each. Samples were centrifuged at 1000 RCF (rotational centrifugal force) for 20 minutes, resulting in a pellet and a supernatant. The pellet was resuspended in PBS, and samples were characterised with DLS and TEM before and after centrifugation.

3.3. Physicochemical Characterisation of Polymersomes

3.3.1. Dynamic Light Scattering

Dynamic Light Scattering (DLS) is a frequently used method to determine the size of particles in solution. Essentially, the method derives size from measuring the Brownian motion of particles. The speed of particle diffusion is measured by measuring the rate at which the intensity of scattered light fluctuates. Two assumptions are made in order to calculate size from light scattered in the solution: i) that the particle is spherical, and ii) that particles in solution undergo Brownian motion. Scattered light is fitted to a correlation function, which is useful in assessing the quality of the sample (e.g. whether concentration is in range and detecting whether there are aggregates present in the sample, which indicates polymersomes have precipitated). The correlation function compares the similarity between two signals, or one signal with itself at different time intervals ($t+\delta t$). If signals at $t+2\delta t$, $t+3\delta t$ etc are compared with t then correlation will slowly decrease from 1 to 0. If particles are large, the signal will change slowly and

correlation will persist for a long time. The correlation reduces quickly if particles are small and moving rapidly. The time at which correlation starts to significantly decay is an indication of the mean size of the sample, and is illustrated in figure 3.3.

DLS was used to assess the size of polymersomes in PBS, using a Malvern Zetasizer Nano ZS laser light scatterer equipped with a He-Ne 4mW 633 nm laser. Polymersomes were diluted in filtered PBS in 1 ml disposable cuvettes, and experiments were an average of n=3 runs at a set angle of 173°.

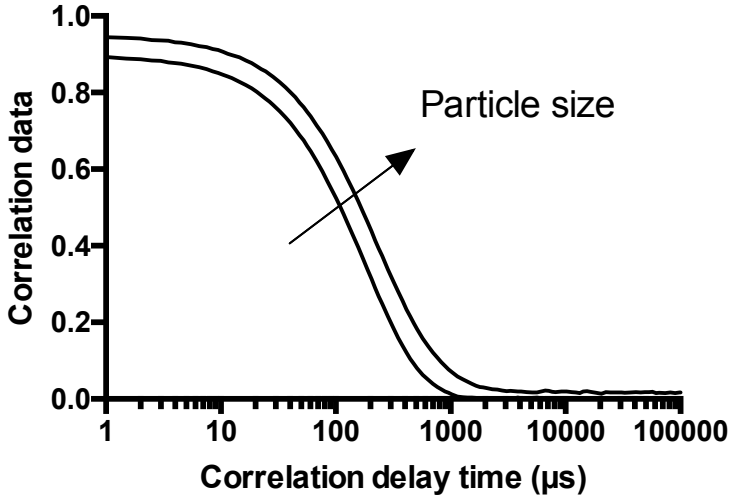

Figure 3.3. Correlation function of dynamic light scattering.

3.3.2. Transmission Electron Microscopy

Polymersomes in filtered PBS were also assessed for morphology using transmission electron microscopy (TEM). Samples were mounted on glow-discharged copper grids by submerging the grids into the polymersome solution for 60 seconds, followed by blotting and staining for 5 seconds with 0.75% (w/w) phosphotungstic acid (PTA). Grids were then washed with PBS, dried under vacuum and assessed via a JEOL microscope using 100 kV voltage tension.

3.4 GPC-HPLC for Quantification of Polymer-Protein Interactions

To evaluate the potential interactions between POEGMA-PDPA or Angiopep-2-POEGMA-PDPA and model protein IgG, GPC was used in conjunction with HPLC for detection. Samples were run through a 1.5 x 30 cm column with Sepharose 4B (Sigma-Aldrich) connected to HPLC (Dionex Ultimate 3000). 150 µl of samples of either polymer, protein, or both were injected into the GPC and eluted with PBS at a flow rate of 260 µl/min, with a total elution time of 180 minutes. HPLC detection was set to UV/Vis absorbance at 220 nm for POEGMA-PDPA and IgG. Areas under the detected peaks were measured using Chromeleon software.

3.5. Electroporation for Cargo Encapsulation Within Polymersomes

To encapsulate cargo into polymersomes, cargo was electroporated into purified polymersomes as previously reported (Wang, Chierico et al. 2012). In general, stock solutions of 3 mg/ml polymersomes were loaded together with protein stock solutions dissolved in PBS into 800 µl electroporation cuvettes (BioRad). For the encapsulation of carnosine (Sigma-Aldrich), a stock of protein stock was dissolved in PBS at 10 mg/ml and filter sterilised before use. For IgG-FITC or IgG-Gold, 0.1 µg/ml was loaded with polymersomes into the cuvettes. Electroporation was performed with an Eppendorf 2510 electroporator, with a total of 10 pulses applied at a voltage of 2500 kV. Electroporated polymersomes were left in room temperature for 30-60 minutes before purification, to allow the pores to re-seal. Finally, samples were purified by GPC with sepharose 4B as a substrate to remove residual free protein. Purified samples were assessed for size via DLS, and the protein encapsulation was determined via HPLC.

3.5.1. Quantification of Polymer and Cargo Content with HPLC

High Performance Liquid Chromatography (HPLC) was performed using a Dionex Ultimate 3000 instrument. To detect total polymer and protein content, polymersomes were disrupted in 0.05% trifluoroacetic acid (TFA) (Sigma-Aldrich). This step was

performed to obtain a pH below 6.4, causing polymersomes to disassemble and thus allowing for quantification of polymer and cargo content. A multi-step gradient of HPLC grade methanol (Sigma-Aldrich) as eluent A and milliQ water (Millipore) in 0.05% trifluoroacetic acid as eluent B was used to elute samples over 30 minutes with a C18 column (Phenomenex® Jupiter C18 300Å, 150 x 4.60 mm, 5 µm) as reported previously (Wang, Chierico et al. 2012). The gradient profile used was as follows: (1) 20 to 40% B in 6 min; (2) 40 to 45% B in 10 min; (3) 45 to 50% B in 3 min; (4) 50% B for 1 min; (5) 50 to 70% B in 3 min; (6) 70 to 100% B in 1 min; (7) 100% B for 1 min; (8) 100 to 20% B in 2 min; (9) 20% B for 3 min.

Cy3-labelled polymersomes were detected with an excitation wavelength of 540 nm and emission at 565 nm. Using the conditions specified, Cy3-labelled POEGMA-PDPA polymer can be detected within the UV/Vis channel (220 nm) or in the fluorescence emission channel of 565 nm. To quantify protein content of electroporated polymersomes, a standard curve for the protein was created under the same conditions for polymer elution, but with detection at an additional channel excitation at 274 nm and emission at 303 nm due to the presence of tyrosine residues in the peptide sequence. Areas under the detected peaks were measured using Chromeleon software.

3.6. Transwell Cell Culture

3.6.1. Maintenance culture

For maintenance and expanding cells, bEnd.3 cells (ATCC® CRL-2299) were cultured in Dulbecco's Modified Eagle Medium (DMEM) supplemented with 2 mM L-glutamine, 10% foetal bovine serum (FBS), 100 U/ml streptomycin, 100 U/ml penicillin, and 1 µg/ml Fungizone. Mouse C8-D1A astrocytes (ATCC® CRL-2541) were cultured in DMEM supplemented with L-glutamine and 10% FBS. Mesenchymal stem cells (MSCs, Gibco® Mouse C57BL/6) previously shown to have pericyte properties (Tian 2014), henceforth referred to as pericytes, were cultured in DMEM F12 media supplemented

with 10% FBS, gluta-max-I and 5 µg/ml gentamicin. In the case of BEnd.3, flasks or well-plates were pre-coated with 0.4 mg/ml collagen type I from rat tail (Sigma-Aldrich), incubated in room temperature for 2 hours and washed with PBS before seeding cells. Cultures were kept in 37°C and 5% CO_2. Sub-culture was performed by incubating with 0.25% trypsin-EDTA for 5 minutes at 37°C, followed by centrifugation and re-suspension in new media.

3.6.2. bEnd.3 monoculture

For the purposes of mimicking the blood-brain barrier *in vitro*, immortalised CNS cells were seeded in a transwell setup. 12-well transwell filter inserts (Corning) have a cell growth area of 1.12 cm^2 and contain a transparent polystyrene membrane with 0.4 µm diameter pores (membrane thickness 10 µm, 4 x 10^6 pores per cm^2). The inserts were coated with rat tail collagen type I 0.4 mg/ml on both sides, and left in room temperature to polymerise for 2 hours before rinsing with PBS and media. bEnd.3 cells were seeded on the upper side of the transwell membrane at a density of 20 000 – 40 000 cells per well, in a total of 0.5 ml of media in the top compartment and 1.5 ml in the bottom compartment. Transwell cultures were kept in 37°C and 5% CO_2 for approximately 7 days until fully confluent, after which TEER was measured and experiments were performed. Media was changed every 2-3 days.

3.6.3. bEnd.3 co-culture

For co-culture, bEnd.3 cells were seeded on the top of 12-well transwell filter membranes as specified in section 3.6.2. bEnd.3 monocultures were incubated in 37°C and 5% CO_2 to grow for 3-4 days. After this time, astrocytes or pericytes seeded on the bottom of the well (non-contact co-culture) at a density of 10 000 cells. After seeding with a second cell type, transwell cultures were kept in 37°C and 5% CO_2 for approximately 3-4 days until the bEnd.3 monolayer reached full confluency, after which TEER values were measured and experiments were performed. Media used for co-

culture was DMEM F12 media supplemented with 10% FBS, gluta-max-I and 5 µg/ml gentamicin. Media was changed every 2-3 days, and was added at a volume of 0.5 ml in the upper compartment and 1.5 ml in the lower compartment.

3.6.4. Transendothelial Electrical Resistance (TEER) Measurements

In order to measure barrier-like properties of the cells, trans-endothelial electrical resistance (TEER) was assessed using an EVOM2 Epithelial Voltohmmeter with STX3 electrodes (World Precision Instruments). TEER values were obtained from an average of n=5 wells and by subtracting the values from a cell-free transwell from the obtained value. TEER values were measured at day 6-7 after seeding bEnd.3, and before each experiment.

3.7. MTT Viability Assay

Cell viability was quantified by assessing the mitochondrial dehydrogenase reduction of 3-(4,5- dimethylthiazol-2-yl)-2,5-diphenyl tetrasodium bromide (MTT) into purple formazan crystals. Cells grown in 96-well plates were treated with the sample for 24 or 48 hours or PBS for the control. At the end of the incubation time, solutions were aspirated from the plate and rinsed 2x with PBS, followed by addition of 5 mg/ml of MTT to each well and incubated at 37°C for 60 minutes. The MTT solution was aspirated carefully, and the formazan was solubilised using acidified isopropanol. Absorbance was read with a spectrophotometer plate reader at 570 nm with a reference at 630 nm. Readings were obtained for n=3 samples per well, n=3 per treatment in n=3 independent experiments.

MTT was also assessed after incubation with pharmacological inhibitors used in sections 6.4, 6.5 and 6.8, as some inhibitors can be cause cell stress. bEnd.3 cells in 96 well plates were incubated with the inhibitor, followed by rinsing in PBS and adding new media to the cells. Cells were returned to the incubator for 24 hours to recover,

and were incubated with MTT solution at the end of the recovery period. The following concentrations of inhibitor were used for the specified incubation times before washing the cells: 10 mM cyclodextrin 1h, Dynasore 80 µM 10 min, N-ethylmaleimide 500 µM 1h. The MTT results for the inhibitors can be seen in figure 3.4.

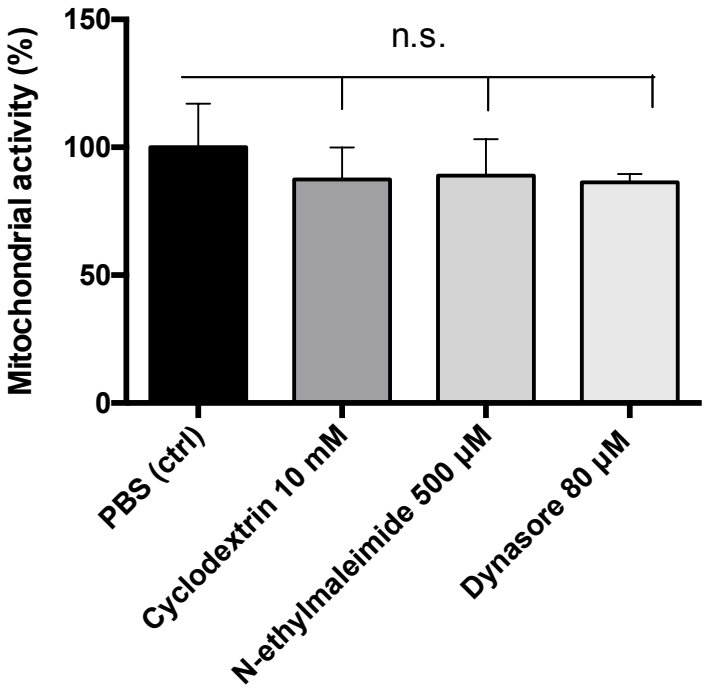

Figure 3.4. MTT of pharmacological inhibitors in bEnd.3. Error: st.dev., student's t-test, n=9 readings in n=3 experiments, *p<0.05.

3.8. FITC-Dextran Permeability Assay

A working solution of 1 mg/ml Cy3-labelled Angiopep-2-POEGMA-PDPA, Cy3-POEGMA-PDPA, or FITC-Dextran (m_w = 70kDa, Sigma) was prepared in DMEM imaging media (Gibco), supplemented with 10% FBS, 100 U/ml penicillin and 100 µg/ml streptamycin, 1 µg/ml fungizone and 2 mM L-glutamine. bEnd.3 monolayers in 12-well transwells were aspirated from media and rinsed with PBS at the start of the experiment. 0.5 ml of 1 mg/ml FITC-dextran or polymersomes in medium was applied to the bEnd.3 monolayer at the top transwell compartment (n=6), and 1.5 ml of media was added to the bottom compartment. A transwell insert without cells was used as a control (n=3). After the FITC-dextran had been added, transwells were incubated at

37°C in 5% CO_2 for up to 24 hours. At each timepoint, 50 µl samples were transferred from the bottom chambers to a black 96-well plate and read in a fluorimeter with excitation set to 495 nm and emission to 518 nm for FITC-Dextran or excitation 540 nm and emission 565 nm for Cy3-polymersomes. Concentration was converted to cumulative apical to basolateral flux of fluorescence, accounting for the gradual dilutions of the basolateral compartment media over time due to sampling 50 µl per time point.

3.9. Fluorescence Quantification of Polymersome Transcytosis *In Vitro*

bEnd.3 cells were seeded on collagen-coated 12-well transwell filters and allowed to grow to a confluent monolayer. TEER values were measured in order to ensure confluence. At the beginning of each experiment, media was changed to supplemented DMEM imaging media and added to the transwells at a volume of 500 µl to the upper and 500 µl to the lower compartment. Cy3-labelled polymersomes were added at a concentration of 1 mg/ml to the upper compartment, incubated at 37°C and 5% CO_2 for time points between 0-24 hours, followed by collection of media from both compartments. 100 µl of collected media was transferred to black fluorescence 96-wellplates, n=3 wells per compartment and timepoint, and fluorescence was measured with a fluorescence spectrometer (Varian CaryEclipse) with excitation set to 540 nm and emission of 565 nm.

3.10. Calculation of Angiopep-2 Density in Polymersome Membrane

In order to calculate the number of Angiopep-2 ligands per vesicle, the number of polymers ($\mathbf{N_{agg}}$) in a vesicle of radius **r** must be calculated first (figure 3.5). First, the membrane volume was calculated by subtracting the volume of the sphere of the inner edge of the membrane from the volume of the sphere of the outer edge of the membrane. To do so, the radius of the inner and outer spheres must be calculated from particle radius **r**, brush length **b** and membrane thickness **t.** For POEGMA, the brush

length scales with hydrophilic chain length (see ref (Battaglia and Ryan 2005)) and is equal to:

$$b = 0.247 N_{POEGMA} \quad [1]$$

Thus, for $POEGMA_{25}$-$PDPA_{114}$ the brush length is

b = 0.247 x 25 = 6.187 nm.

Membrane thickness **t** scales to the length of hydrophobic repeating units ($\mathbf{N_{PDPA}}$) according to a power law of 2/3(Battaglia and Ryan 2005, Smart, Mykhaylyk et al. 2009, Pearson, Warren et al. 2013):

$$t = 0.359 (N_{PDPA})^{\frac{2}{3}} \quad [2]$$

Thus, for $POEGMA_{25}$-$PDPA_{114}$ the membrane thickness is

t = 0.359 x $(114)^{2/3}$ = 8.44 nm.

The average diameter of polymersomes was determined to be 80 nm by dynamic light scattering. Using the values of **r** = 40 nm, **b** = 6.187 nm and **t** = 8.44 nm, the membrane volume (**V**) can be calculated as:

$$V = (\frac{4}{3}\pi(r-b)^3) - (\frac{4}{3}\pi(r-b-t)^3) \quad [3]$$

Which gives a membrane volume **v** of 93511.3 nm^3.

The molecular volume of each PDPA polymer (**Mv_{PDPA}**) was then calculated from molecular weight of DPA (**Mw_{DPA}**), number of repeating units (**N_{PDPA}**), polymer density (**p**) and Avogadro's number (**N_A**). The MwPDPA was calculated first:

$$Mw_{PDPA} = N_{PDPA} \times Mw_{DPA} \quad [4]$$

Equal to 24516.2 g/mol for a PDPA length of 114.

Molecular volume was then calculated:

$$v_{PDPA} = \frac{Mw_{PDPA}}{p\rho_{PDPA}N_A} \quad [5]$$

The density of POEGMA-PDPA is estimated to be the same as water, 1 g/cm^3. Therefore, for a PDPA length of 114, Mv_{PDPA} = 40.37 nm^3.

To calculate N_{agg}, the whole membrane volume [equation 3] was divided by the molecular volume of each PDPA chain [equation 5]:

$$N_{agg} = \frac{v}{Mv_{PDPA}} \quad [6]$$

To calculate the number of ligands, the total number of polymers were distributed according to the ratio of the outer versus inner membrane surface area **$R_{O/I}$**.

$$R_{\frac{O}{I}} = \frac{4\pi(r-b)^2}{4\pi(r-b-t)^2} \quad [7]$$

And finally, the number of ligand (N_{Ligand}) per vesicle is obtained from the molar percentage functionalisation of ligand ($F_{\%}$):

$$N_{Ligand} = \frac{F_{\%}}{100} \times R_{\frac{O}{I}} \frac{N_{agg}}{(R_{\frac{O}{I}} + 1)} \quad [8]$$

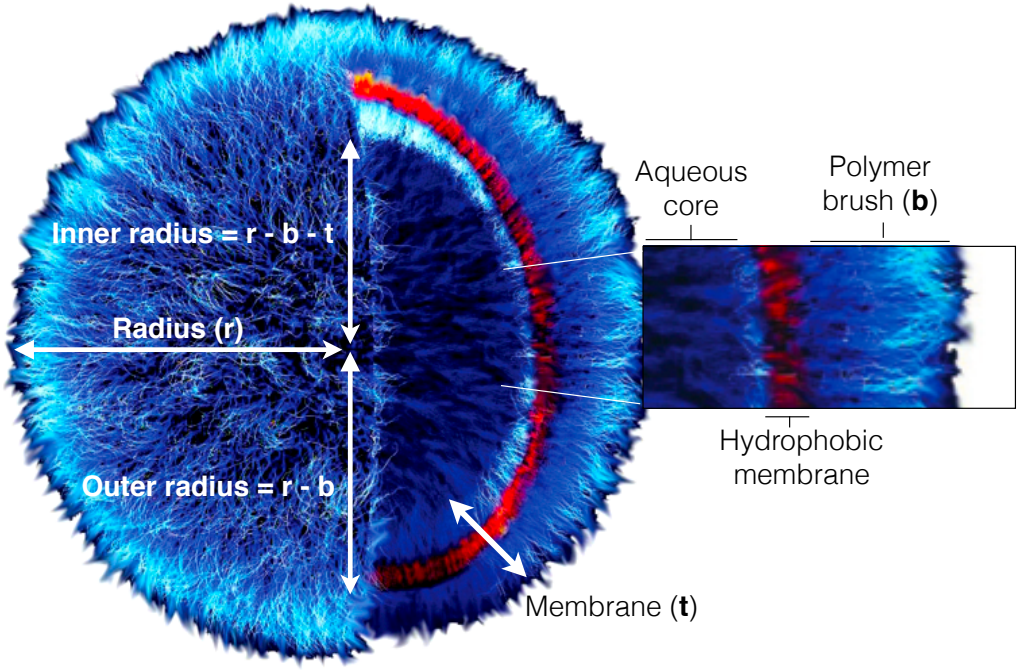

Figure 3.5. Schematic of calculations for N_{agg}. and N_{Ligand}.

3.10.1. Calculation of Transcytosis Efficiency

Polymersome fluorescence in transwell compartments was converted to % transcytosis efficiency by obtaining the fluorescence (***F***) of polymersomes shifted over from the apical to basolateral compartment:

$$\%transcytosis = \frac{F_{Basolateral}}{F_{Total}(\frac{F_{Apical}}{F_{Basolateral}})}$$

3.11. FACS For Quantification of Polymersome Uptake

For Fluorescence Activated Cell Sorting (FACS) quantification of polymersome uptake, bEnd.3 cells were seeded in collagen-coated 6-wellplates. Poly-L-lysine (Sigma-Aldrich) was prepared at 300 µM in PBS and lactoferrin (Sigma-Aldrich) was prepared in PBS at a concentration of 250 nM. Cy3-labelled Angiopep-2-POEGMA-PDPA polymersomes were prepared via pH switch and purified. When cells had reached confluency, they were pre-incubated with poly-L-lysine, lactoferrin or PBS (control) for 30 minutes, followed by incubation with A-EP for 60 minutes in 37°C and 5% CO_2. At the end of the incubation time, cells were rinsed 2x with PBS and treated with 0.25% trypsin-EDTA at 37°C for 5 minutes to detach the cells. Detached cells were centrifuged at 1000 RCF for 5 minutes, and the pellets were resuspended in 4°C PBS to 500 µl. 150 µl of cells in suspension were pipetted into 96-wellplate for FACS. FACS was performed with a BD FACSArray instrument with a flow rate set to 0.5 µl/s. For the detection of Cy3-labelled polymersomes, excitation wavelength was set to 545 nm and emission to 560-600 nm.

3.12. Angiopep-2 and A-EP Ligand Competition

FITC-Angiopep-2 (ProteoGenix, France) was dissolved in diH_2O at 1.75 pM, the equivalent of ligand functionalisation in 1.2% (mol) Angiopep-2-POEGMA-PDPA. Angiopep-2 or A-EP were added separately or together to the apical transwell compartment, and transwells were returned to the incubator. After 10 or 60 minutes, transwells were washed 2x with PBS and fixed with 3.7% PFA. Filters were excised with a scalpel and mounted on coverslips with VectaShield-DAPI (Vector Labs, U.K.) for confocal imaging. Quantification of intracellular fluorescence of A-EP (Cy3 channel) or FITC was performed via ImageJ, normalising fluorescence to DAPI.

3.13. Pharmacological Small Molecule Modulation of Endocytic Processes

For the inhibition of dynamin, 40 μM Dynasore (Sigma-Aldrich) was prepared in PBS and filter sterilised. Cells were pre-incubated with CellMask Deep Red (ThermoFisher Scientific) (exc. 649 em. 666 nm) for 10 minutes and washed, replacing with new media. Dynasore was added to the cell medium and pre-incubated for 10 minutes at 37°C, followed by the addition of Cy3-labelled A-EP. Cells were incubated with polymersomes for 10 or 60 minutes before live confocal imaging. After images were acquired, cells were washed with pH 5 PBS before imaging again.

For the inhibition of NSF, 0.5 mM N-ethylmaleimide (Sigma-Aldrich) was prepared in PBS, added to bEnd.3 and incubated at 37°C for 60 minutes. Before the start of imaging, cells were incubated with CellMask Deep Red (ThermoFisher Scientific) for 10 minutes before rinsing 2x with PBS and replacing full media. Cells were incubated with Cy3-labelled A-EP with FITC-IgG cargo for a further 5 minutes before live confocal imaging.

3.14. Cholesterol Depletion and Quantification

To deplete bEnd.3 cells of membrane cholesterol, 10 mM methyl-β-cyclodextrin (CD) (Sigma-Aldrich) was applied to either the apical or basolateral side of cells grown in transwells according to a previously established method.(Tugizov, Herrera et al. 2013) Transwells were washed 2x with PBS and media was replaced with serum free media, and TEER values were measured. CD was added to bEnd.3 transwell monolayers either to the basolateral or apical side, and incubated in 37°C for 15 minutes. After incubation, media from both compartments was collected and saved for later quantification of cholesterol content. Transwells were rinsed 2x in PBS and serum free media was replaced, and TEER values were obtained for all transwells and untreated controls (n=3). Cells were incubated with Cy3-labelled A-EP for 60 minutes, before rinsing with PBS and fixating transwell filters in 3.7% PFA and permeabilising for 30

minutes with 0.1% Triton X-100. Cells were stained for Caveolin-1 by incubating with Rb Cav-1 1:250 in room temperature for 2 hours, washed 3x, and incubated with goat anti-Rb488 1:200 for 2 hours in room temperature. Filters were washed, excised with a scalp and mounted on coverslips with VectaShield-DAPI and assessed under a confocal microscope.

Free cholesterol shed into the collected media after CD treatment was measured with a cholesterol quantitation kit (Sigma-Aldrich) according to instructions, and compared to a serum free media control. Briefly, after the enzymatic assay, sample fluorescence was measured against a cholesterol standard curve from the kit in a fluorimeter with excitation at 535 nm and emission at 570 nm. Concentration of cholesterol shed into the apical and basolateral media was calculated according to the standard.

3.15. Confocal Microscopy

Confocal micrographs were acquired using a Leica TCS SP8 confocal microscope equipped with Diode 405, Argon, DPSS 561 and HeNe633 lasers. In all cases where more than one fluorophore was used, channel images were obtained by a sequential scan to minimise bleed-through. 3D projections of z-stacks were created with the Leica Application Suite (LAS X) software.

3.15.1. Real Time 4D Imaging of Live Cells

An incubator with 37°C and 5% CO_2 connected to the unit was used and allowed to stabilise for 60 minutes before imaging. Cells were immersed in DMEM imaging medium (no phenol red) before imaging unless stated otherwise. CellMask Deep Red (ThermoFisher Scientific) was applied to cells to stain the plasma membrane, incubated at 37°C for 10 minutes before rinsing with PBS. Images were acquired with a 10X 0.3NA objective in resonant scanning mode with a speed of 700Hz and a resolution of 128x512 pixels.

3.15.2. Immunocytochemistry

For a typical immunofluorescence labelling experiment, cells were fixed with 3.7% paraformaldehyde for 10 minutes and washed 3 times with PBS for 5 minutes each time. Cells were incubated in 10% BSA and 0.1% Triton X-100 for 30 minutes to reduce non-specific antibody binding. Antibodies were diluted in 1% BSA and 0.1% Triton X-100 (see table 3.1 for antibody specifics*)*. Following blocking and permeabilisation, cells were incubated with primary antibodies for 2 hours in room temperature, washed with PBS, followed by incubation with secondary antibodies in room temperature for 2 hours. Samples were kept in the dark during antibody incubation to avoid photobleaching. Cell nuclei were stained using 1 µg/ml Hoechst 33542 with a 10-minute incubation, alternatively with VectaShield-DAPI when mounted. Cells grown on transwell membranes were further processed by using a scalpel to cut out the membrane filter, and mounting excised filters onto glass coverslips with Vectashield mounting media before imaging. Images were acquired with a 63x xNA oil immersion objective at 400Hz and 512x512 pixels.

Target	**Host**	**Supplier**	**Application (+dilution)**
Primary antibodies			
LAMP-1	Rabbit	Abcam	IF (1:200)
Rab5	Rabbit	Abcam	IF (1:200)
Rab7	Rabbit	Abcam	IF (1:200)
Rab11	Rabbit	Abcam	IF (1:200)
Claudin 5	Rabbit	Abcam	IF (1:200)
Occludin	Rabbit	Abcam	IF (1:200)
ZO-1	Rabbit	Abcam	IF (1:200)
LRP-1	Mouse	Abcam	IF (1:250)
Caveolin-1	Rabbit	Sigma-Aldrich	IF (1:250)
CD34	Rabbit	Abcam	IHC (1:200)

Target	Host	Supplier	Application (+dilution)
Secondary antibodies / conjugates			
Anti-Goat IgG H&L (6nm gold)	Rabbit	Abcam	TEM (0.1 µg/ml)
Anti Rabbit-Alexa488	Goat	Sigma-Aldrich	IF (1:250)
Anti Rabbit IgG-Alexa488	Donkey	Abcam	IF (1:250)
Anti mouse-647	Donkey	Santa Cruz	IF (1:200)

Table 3.1. List of antibodies used.

For staining with phalloidin, a stock solution of phalloidin-Atto647N (Invitrogen) was prepared in methanol. Cells were fixed for 10 minutes in 3.7% paraformaldehyde, permeabilised with 0.1% Triton X-100 for 30 minutes, and incubated with 50 µg/ml Phalloidin-Atto647N at 4°C for 20 minutes before washing with PBS, excising filters and mounting filters on microscopy slides with VectaShield-DAPI.

3.15.3. Image Z-stack Processing and Colocalisation Analysis

Acquired micrographs were analysed with ImageJ (nih.gov). To obtain red/green channel localisation, the plug-in 'Colocalization Finder' was used (authors: Laummonerie, C., Mutterer, J., Institut de Biologie Moleculaire des Plantes, Strasbourg, France). Colocalisation analysis is based on pixel intensity, determining how much pixels from two channels (e.g. red and green) overlap. Images were converted to 8-bit grayscale and analysed for Pearson's correlation coefficient *Rr*, to analyse pixel *i* in the images:

$$R_r = \frac{\Sigma(R_i - \bar{R}) - (G_i - \bar{G})}{\sqrt{\Sigma(R_i - \bar{R})^2 \times \Sigma(G_i - \bar{G})^2}}$$

where *R* is red channel intensity and *G* is green channel intensity. Sum values can be between -1 and 1, with -1 meaning perfect exclusion, 0 for random localisation, and 1

for perfect colocalisation. An example of colocalisation with the plugin is shown in figure 3.6.

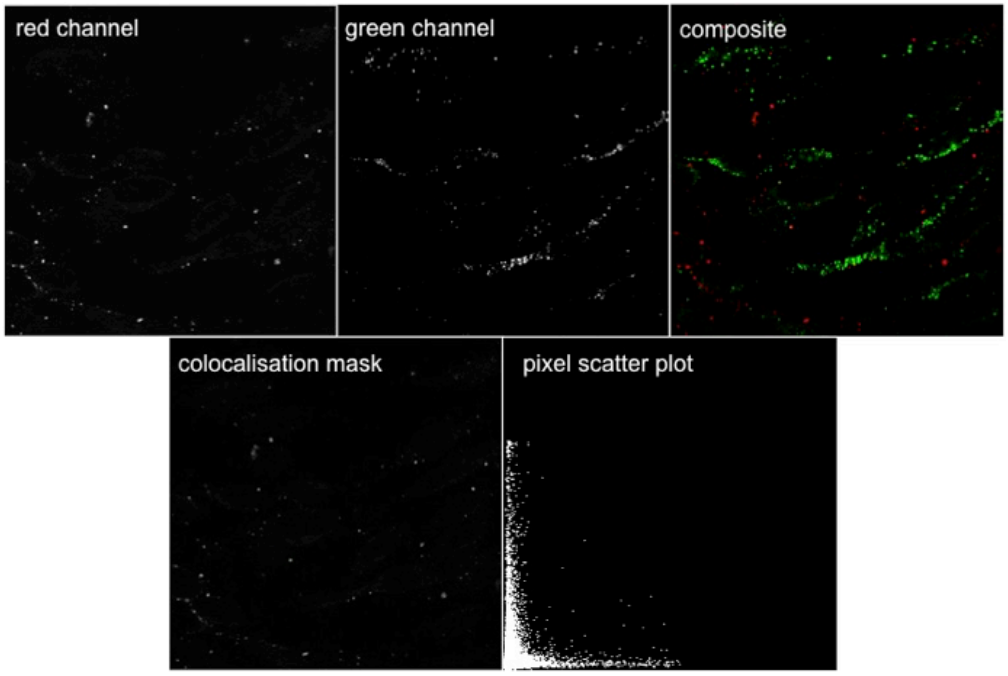

Figure 3.6. Example of colocalisation via Pearson's correlation coefficient.

3.15.4. Quantitative Fluorescence Analysis of Confocal Images

To quantify channel fluorescence of confocal images acquired in the *xy*, ImageJ was used with the plugin 'ROI Manager'. Cell outlines were chosen as regions of interest (ROI), and fluorescence intensity was measured within the ROIs. Cell fluorescence intensity from the ROIs were normalised per nuclei, i.e. the Hoescht/DAPI channel. n=3 images were used to obtain standard errors. To quantify channel fluorescence of confocal images acquired in the *xyz* dimensions, the Leica SP8 Confocal LAS X software was used to automatically measure fluorescence intensity across the z-stacks per individual channel. This method was applied to figures 6.16 and 6.26, where data is represented across the transwell as 0 where the transwell filter begins, +10 µm at the end of the filter and -10 µm to be 10 µm above the filter (where cells are located).

3.16. Transwell Electron Microscopy of A-EP-Gold

Rabbit 6nm anti-goat IgG-Gold (Abcam) was encapsulated into A-EP via electroporation and polymersomes were purified via GPC. bEnd.3 monolayers grown in 12-well transwells were grown until confluency, and incubated with A-EP-gold for 1 hour or 3 hours at 37°C and 5% CO_2 before washing cells with PBS and fixing in 3% glutaraldehyde in 0.1M phosphate buffer, and left in 4°C overnight. Secondary fixation was carried out by washing transwell filters 2x with 0.1M phosphate buffer and incubating with 1% aqueous osmium in 0.1M phosphate buffer for 20 minutes in 4°C. The solution was aspirated and transwells washed 1x in PBS, and gradually dehydrated with increasing concentrations of EtOH for 10 minutes each: 25%, 50%, 70%, 90% and 100%. Resin components Agar-100, DDSA and MNA were weighed out, DBMA was added and the mixture was stirred up. The resin was transferred to a Corning tube, and the following percentages of EtOH were added for 30 minutes each to get 25% resin, 50% resin, 75% resin, and 100% resin. Resin in transwells was incubated in room temperature overnight, and removed from the transwells the following day. The filters were excised with a scalpel and cut into 2x2mm slivers. Transwell filter slivers were placed in the resin in the oven at 60°C for >24h. Ultra-thin (50-70nm) sections were obtained with a diatome. Samples were assessed under a Jeol 1010 transmission electron microscope.

3.17. *In situ* rat brain perfusion

Empty A-EP or control EP polymersomes were prepared with a 20% (mol) Cy3 label, 2x the Cy3 molarity used for *in vitro* studies. Polymersomes were purified via GPC and characterised via DLS and TEM. DLS showed a normal size distribution, with EP averaging approximately 80 nm and A-EP 70 nm. TEM showed slight polydispersity in the vesicle size obtained, with some smaller vesicles of ~50 nm present in A-EP and EP samples. Physicochemical characterisation of polymersomes used for the *in vivo* quantification pilot study is shown in figure 3.7.

All animal experiments were performed in accordance with the Animals (Scientific Procedures) Act 1986 (U.K.) Male adult Wistar rats were anaesthetised with 100 mg/kg ketamine and 1 mg/ml medetomidine via intraperitoneal injection. The right and left external carotid arteries were isolated from the carotid sheaths and cannulated according to a previously established procedure.(Takasato, Rapoport et al. 1984) The perfusion fluid was modified Ringer's solution (6.896 g/L NaCl, 0.350 g/L KCl, 0.368 g/L $CaCl_2$, 0.296 g/L $MgSO_4$, 2.1 g/L $NaHCO_3$, 0.163 g/L KH_2SO_4, 2.383 g/L HEPES, additionally 0.5005 g/L glucose (5.5 mM) and 11.1 g/L BSA). The perfusion fluid was bubbled with 5% CO_2 and heated to 37°C for 20 minutes prior to perfusion. For the injection of polymersomes, 20% (mol) Cy3-labelled polymersomes in PBS with our without protein encapsulated were diluted to 1 mg/ml in Krebs buffer (pH 7.4, 188 mM NaCl, 4.7 mM KCl, 2.5 mM $CaCl_2$, 1.2 mM $MgSO_4$, 1.2 mM KH_2PO_4, 25 mM $NaHCO_3$, 10 mM D-glucose, 3 g/dl bovine serum albumin). The polymersome solution was supplied via an additional syringe pump connected to the perfusion system via two tubes feeding into the system at a rate of 0.16 ml/min, making the overall perfusion rate 1.5 ml/min. The perfusion time was 10 minutes. At the end of the perfusion time, the syringe pump was stopped and the system was flushed for 60 seconds with modified Ringer's perfusate in order to remove unbound polymersomes. After 60 seconds, cerebrospinal fluid was extracted via cisternal puncture followed by decapitation and removal of the brain.

3.18. Capillary Depletion and Fluorescence Quantification

After decapitation, brains were removed and washed in ice cold 9 g/L NaCl, followed immediately by homogenisation on ice to initiate the capillary depletion method (Triguero, Buciak et al. 1990). A flowchart of the procedure is illustrated in figure 3.8. Briefly, the cerebellum was removed and the cerebrum was weighed, adding 2x brain weight in PBS followed by 3x dilution in 30% (w/v) dextran (average mw 64-74k).

Centrifugation of homogenates at 8000g for 20 minutes in 4°C resulted in several fractions that were carefully separated: capillary depleted fraction (i.e. parenchyma), dextran, and the capillary enriched fraction (pellet). The capillary enriched pellet was re-suspended in PBS, and 100 µl samples were added to a black 96-wellplate and read in a fluorimeter at an excitation wavelength of 540 nm and emission at 565 nm.

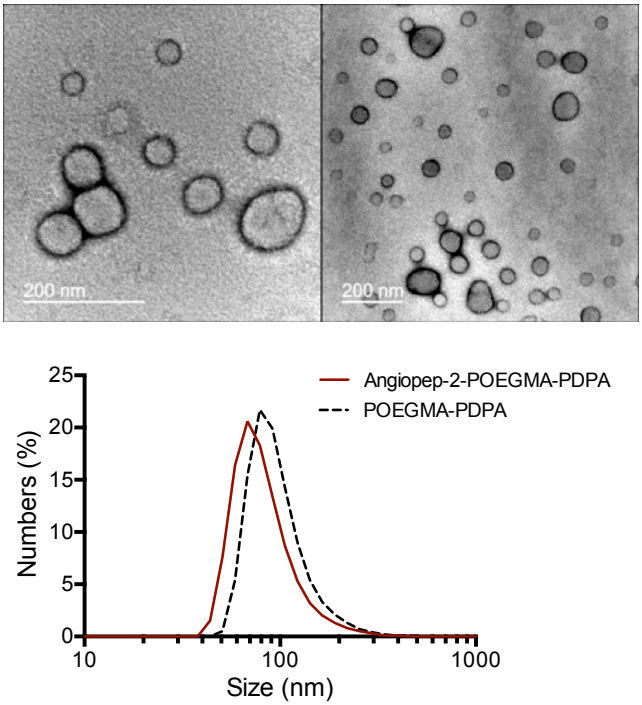

Figure 3.7. Characterisation of polymersomes used for *in vivo* studies.

All sample fluorescence readings were normalised to readings obtained from sham perfused rats (n=3) for each sample type, i.e. CD, dextran or capillaries. Figure 3.9 shows the fluorescence obtained for some controls, demonstrating that fluorescence is sufficient in order to quantify polymersome fluorescence in homogenates. Homogenates from a sham perfused rat was used as a negative control, in order to obtain the background fluorescence from the respective fractions resulting from capillary depletion. Some background fluorescence was measured from the sham homogenate. Normalised fluorescence readings were converted to polymersome (Cy3) amount was converted into % injected dose *%id* of the positive control value for that

experiment, where %id = [normalised sample value (mg) ÷ mean positive control value (mg)] * 100. This was further converted into fluorescence per whole brain. All statistical analysis was one-way ANOVA, *p <0.05.

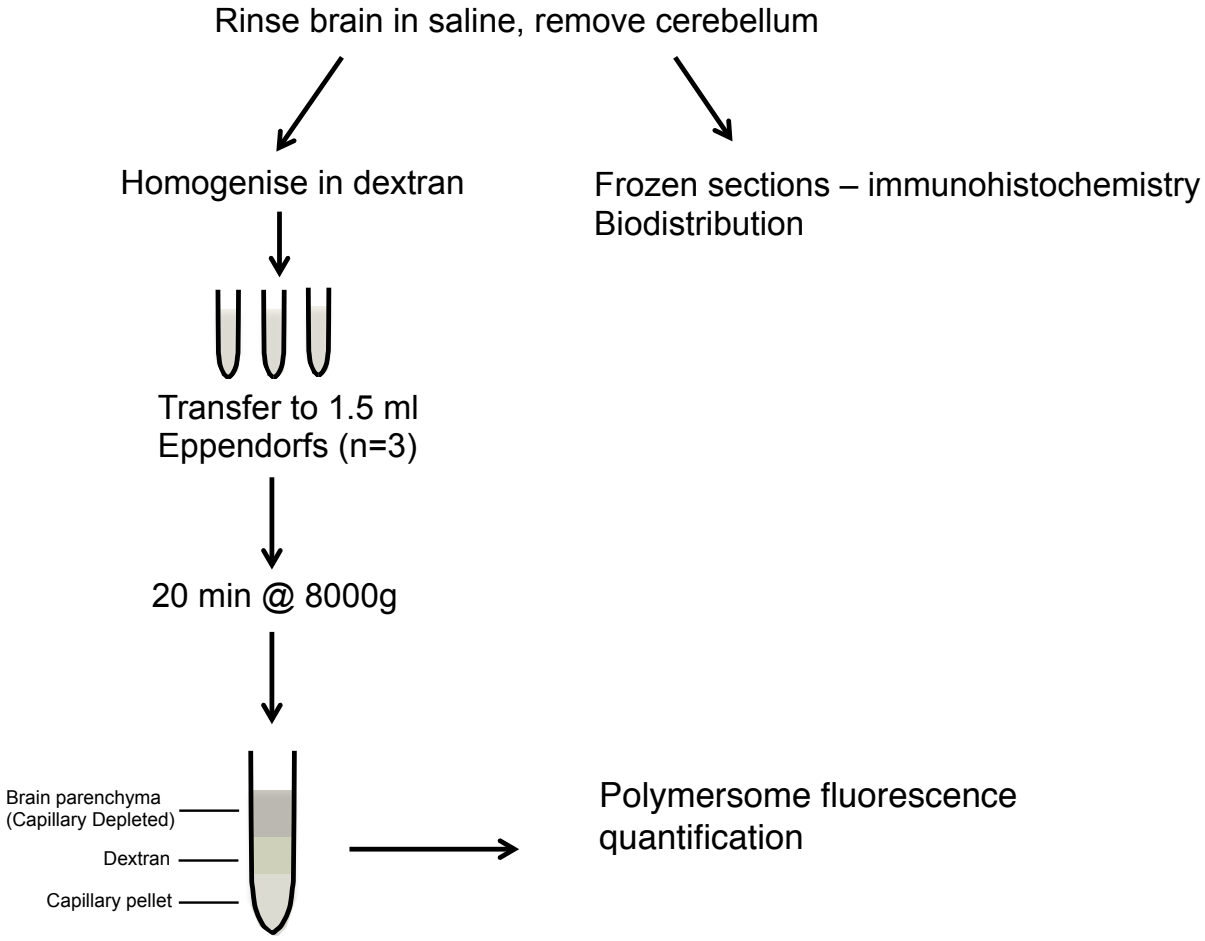

Figure 3.8. Schematic of *in vivo* sample processing.

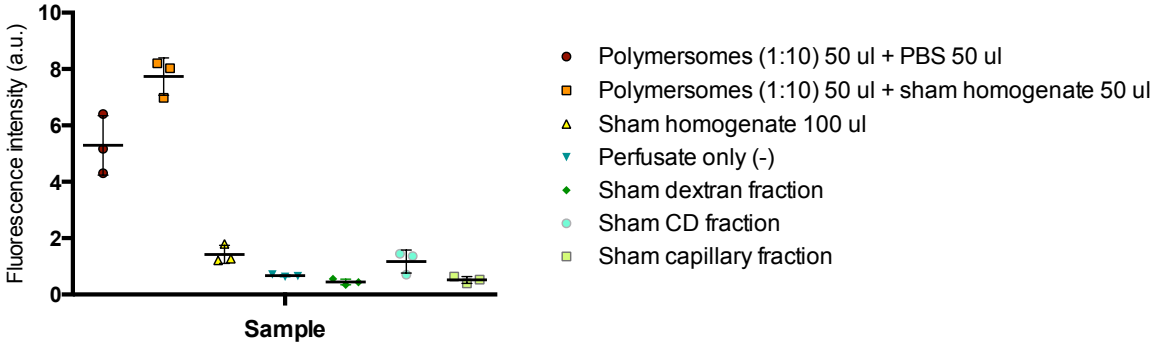

Figure 3.9. Raw fluorescence data obtained from *in situ* perfusion controls

3.19. Cryosectioning and Immunohistochemistry

Rats were perfused as described in section 3.17. At the end of the perfusion time, whole animal perfusion fixation with 4% PFA was performed for 3 minutes at 1.47 ml/min according to a previously established method (Gage, Kipke et al. 2012). The brain was extracted and rinsed with PBS, followed by incubation in 4% PFA at 21°C for 5 days. This was followed by incubation in 30% sucrose (w/v) in 0.1M PBS with 0.05% sodium azide at 21°C for 7 days. Sectioning was performed with a Leica SM2000R freezing microtome. 30 μm transverse sections were cut after freezing rat brains in -40°C and mounting with Bright Cryo M-Bed media. Sections were stored in PBS with 0.05% sodium azide in 4°C after cutting.

Anti-rabbit CD34 (Abcam) concentration was determined through titration. Sections were washed in 0.1M PBS for 10 minutes, and incubated for 30 minutes at room temperature while shaken with 0.3% H_2O_2 in 0.1M PBS. Sections were incubated for 1 hour in 1% BSA/0.05% Triton X-100/0.1M PBS to prevent non-specific binding, followed by incubation with CD34 at 1:200 overnight while shaking. Sections were washed with 0.05% Triton X-100/0.1M PBS, and incubated for 1 hour with 1:200 goat anti-rabbit-Alexa488. Samples were washed 2x in 0.1M PBS for 30 minutes each to reduce background staining, and mounted with VectaShield-DAPI on coverslips before assessing fluorescence using a fluorescence microscope, acquiring each channel in sequence.

3.20. Statistical Analysis

Statistical analysis was performed as indicated at each experiment. For analysis of two groups of data, student's t-test was performed with *$p<0.05$. For three or more groups

of data, one-way ANOVA was performed with *$p<0.05$. For all experiments, errors are given for n=3 independent experiments unless otherwise indicated.

Chapter 4.

RESULTS AND DISCUSSION I

Polymersome Physicochemical Properties

4.1. Introduction

This section is dedicated to work undertaken to synthesise and characterise polymersomes conjugated with peptide Angiopep-2 designed to target the blood-brain barrier.

4.1.1. Polymersome Preparation Methods

The directed self-assembly of amphiphilic block copolymers in a solvent results in a range of morphologies in addition to spherical polymersomes, such as micelles and tubular polymersomes (see section 2.6.3 of Chapter 2). This is due to several factors, such as the hydrophilic/hydrophobic ratio, the block copolymer chain length typically measured by its degree of polymerisation, *N,* and method of self-assembly i.e. bottom-up or top-down.

Polymersomes can be prepared via two different approaches: from polymers in bulk (top-down approach), or from single block copolymer chains (bottom-up approach). The top-down approach consists of gradually hydrating a thin film of polymer in solution while applying a source of energy, such as shear stress or ultrasound. The energy source causes parts of the film to gradually detach into the solution. As this occurs, different phases or structures start to arrange themselves according to the hydrophobic effect. These structures are variable, but are often long and ‘worm-like’ as a result of the lamellar shape of the polymer film as it becomes hydrated. Given enough time, the energy source applied starts to break down the long worms into vesicles.

The bottom-up approach triggers self-assembly of dissolved polymer unimers into structures. This involves immersing the polymer in a solvent which dissolves both the hydrophobic and hydrophilic part of the polymer, and then changing the solvent conditions into one which only dissolves the hydrophilic block. This 'switch' can be changing the solvent, or changing conditions such as pH or temperature (Lomas, Canton et al. 2007). Applying the switch causes unimers to progressively add on to each other, re-arranging into structures in which the hydrophobic block of the polymer avoids the solvent. The vast majority of structures formed by this process are vesicular, because vesicles have a packing factor of 1 and are thus the most stable structures in equilibrium. However, the extent of unimer addition is difficult to control, and as a result yields some structures with asymmetric membranes (Pearson, Warren et al. 2013).

Because both the top-down and bottom-up approaches yield structures other than vesicles, it is essential to separate the desired spherical polymersomes from other structures. Purification of polymersome populations can be done by size exclusion chromatography (SEC), in which the sample is passed through a substrate with porous beads, creating longer column retention times for particles of smaller due to interactions with the bead interior. An alternative to SEC is centrifugation, which separates tubular polymersomes from spherical as a result of differing relative polymer mass of the different structures (Robertson, Yealland et al. 2014).

4.1.2. Encapsulation of Cargo into Polymersomes via Electroporation

An advantage of using polymersomes as drug delivery vehicles is the ability to encapsulate cargo, protecting it from interaction or degradation with the external environment. Polymersomes can carry hydrophobic cargo integrated into the membrane, and hydrophilic cargo in the lumen of the polymersome. One strategy of cargo encapsulation is including cargo in the polymer mixture prior to polymersome formation. However, this approach must often occur in the presence of organic solvents

or at a pH harmful to the cargo. Another way to encapsulate cargo is through electroporation, a method often applied in biology to load exogenous genes into embryos through creating temporary membrane destabilisation. Electroporation involves the application of an external electric field to polymersomes, temporarily permeabilising the polymersome membrane and allowing the diffusion of materials to the vesicle interior. Permeabilisation occurs through the formation of pores in the membrane due to electrically induced rearrangement of membrane phospholipids. Pore formation occurs on a millisecond scale and resealing within minutes, trapping cargo within the membrane (Kotulska, Basalyga et al. 2010). Electroporation has been used to load biological macromolecular cargo such as antibodies, proteins and even nucleic acids into pH-sensitive polymersomes (Wang, Chierico et al. 2012). Encapsulation of cargo into polymersomes via electroporation is a crucial step for enabling delivery of macromolecular cargo into the central nervous system. The ability to load fluorescently labelled cargo also provides a useful tool for tracking the fate of the cargo, and its therapeutic effects where applicable.

RESULTS

4.2. Physicochemical Characterisation of Polymersomes

Polymersomes were produced via the pH switch method of directed self-assembly, in which raising the pH above the pKa of the PDPA block (~pH 6.4) causes the dissolved block copolymer mixture to spontaneously self-assemble into vesicles. Size measurements via Dynamic Light Scattering (DLS) showed POEGMA-PDPA formed via pH switch had an average diameter of around 60 nm, as shown in figure 4.1. The average diameter of Angiopep-2-POEGMA-PDPA polymersomes was 80 nm.

Transmission Electron Microscopy (TEM) was used to assess polymersome morphology, with the electron dense agent phosphotungstic acid (PTA) as a staining

agent. Micrographs in figure 4.2 illustrate the heterogeneity of self-assembled shapes present in a polymersome sample prepared via pH switch, before purification. Micelles in particular are markedly present, averaging <40 nm in diameter and with slightly less contrast in the membrane. A few non-spherical polymersomes can also be seen.

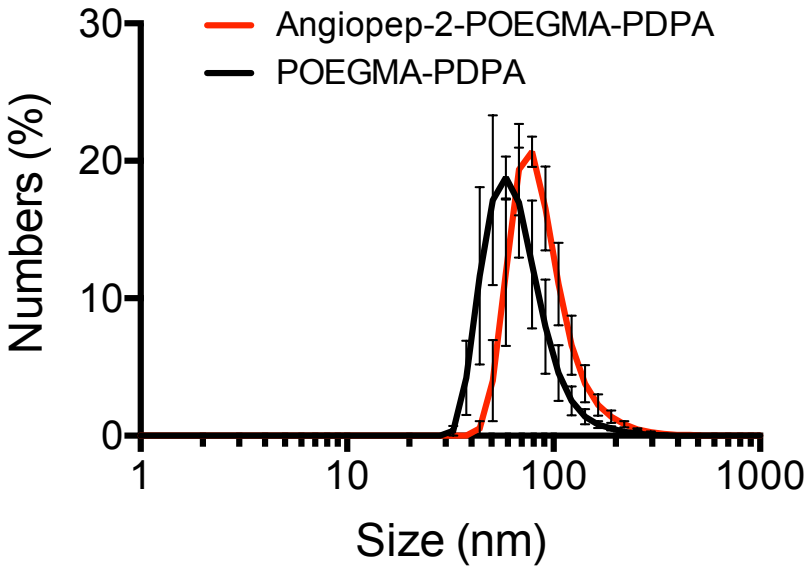

Figure 4.1. Typical size distribution of A-EP and EP polymersomes obtained via pH switch. Peaks are an average of n=3 independent experiments, error bars: S.E.M.

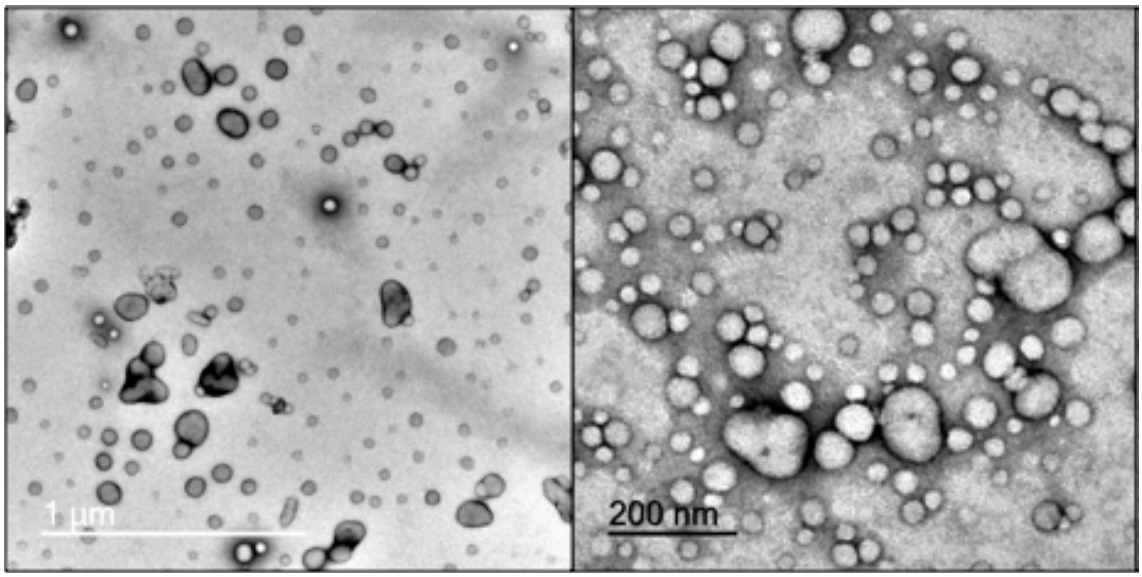

Figure 4.2. Transmission electron micrographs of A-EP. The sample was made via pH switch, and shows a distribution of shapes and sizes.

4.3. Separation of Polymersomes From Other Nanostructures

4.3.1. Gel Permeation Chromatography

Gel permeation chromatography (GPC) with sepharose 4B as a substrate was used to purify polymersome-enriched fractions from the initial heterogeneous samples obtained via pH switch. In this approach, 1 ml of 6 mg/ml polymersomes was added to the top of the sepharose and all fractions exiting the column were collected drop by drop (~50 µl). Polymersome size and total polymer amount as a function of elution volume was quantified via DLS and fluorescence spectroscopy.

DLS sizing and correlation data was obtained in increments of 0.1 ml, but have been merged into a few significant groups for coherence. Figure 4.3 shows the DLS correlation data as a function of elution volume. Correlation values for samples 0-3.6 ml and 6-9 ml indicated impure samples, or a concentration out of range for measurement. Furthermore, these two samples display a slow decay at later delay times, indicating that large structures are present in the sample (likely dust). Overall, the reliability of sizing data obtained from these two samples is therefore low. Sizing data by numbers is displayed in figure 4.4. Sample volumes up to 3.6 ml show the presence of large structures, although a low correlation function indicates impurities in these fractions. Polymersomes in elution volumes above approximately 5 ml mainly contain micelles. The fractions in between 3.7-5 ml contained polymersomes.

Figure 4.5 summarises the cumulative polymer eluted, concentration, and average size of all samples collected, and also representative electron microscopy images obtained from different stages of the separation. The cumulative polymer mass present in eluted samples increased rapidly between 3.5-6 ml, indicating this range as the elution volume containing the majority of polymer and thus narrowing down the range of interest for further characterisation by DLS. The measured polymersome concentration

peaked around 4-4.5 ml, indicating that the average size obtained for these elution volumes may represent the majority of polymersomes in solution. DLS showed a decreasing trend in average diameter consistent with GPC separation.The purified fraction containing polymersomes is contained in the 4 to 5 ml elution range via sepharose-based GPC. All subsequent work using GPC-purified polymersomes consequently involved harvesting polymersomes in this elution range.

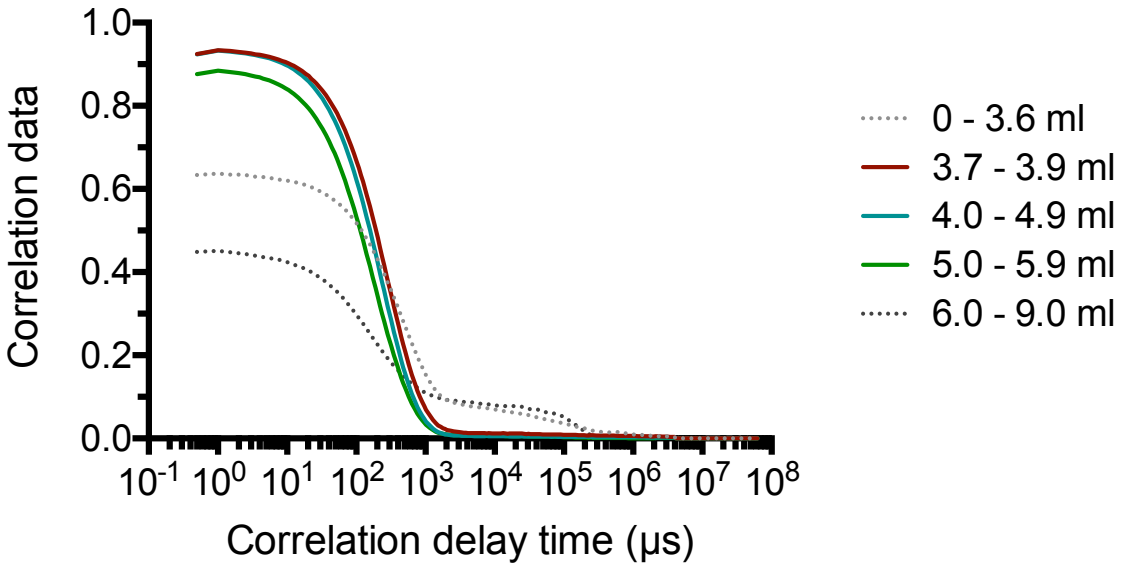

Figure 4.3. Correlation function of A-EP polymersomes as a function of elution volume.

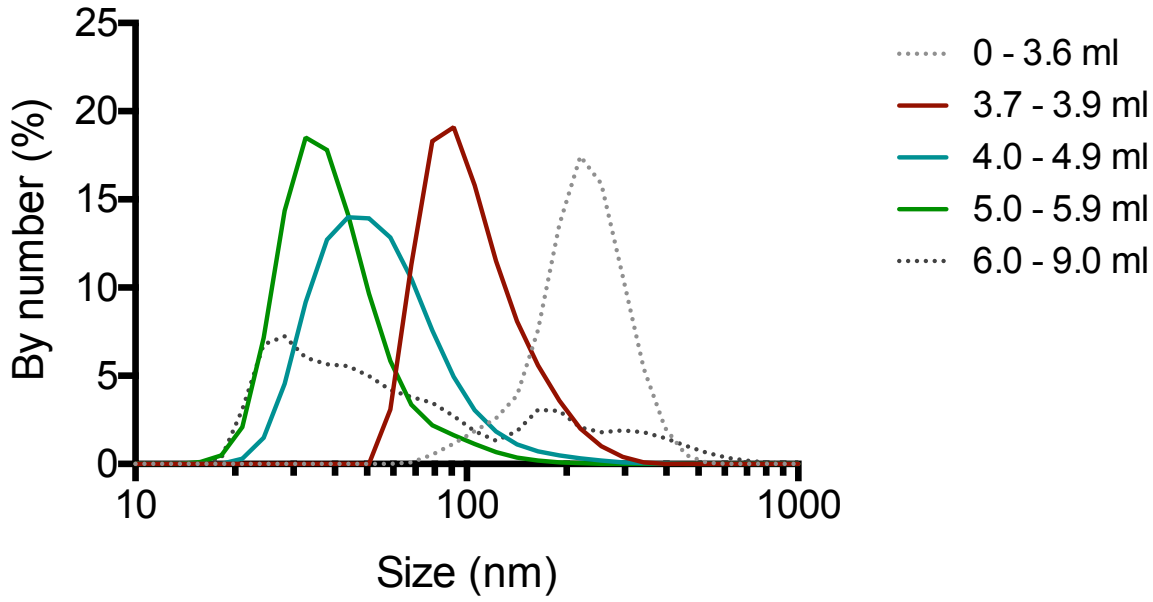

Figure 4.4. Average size of A-EP polymersomes as a function of elution volume.

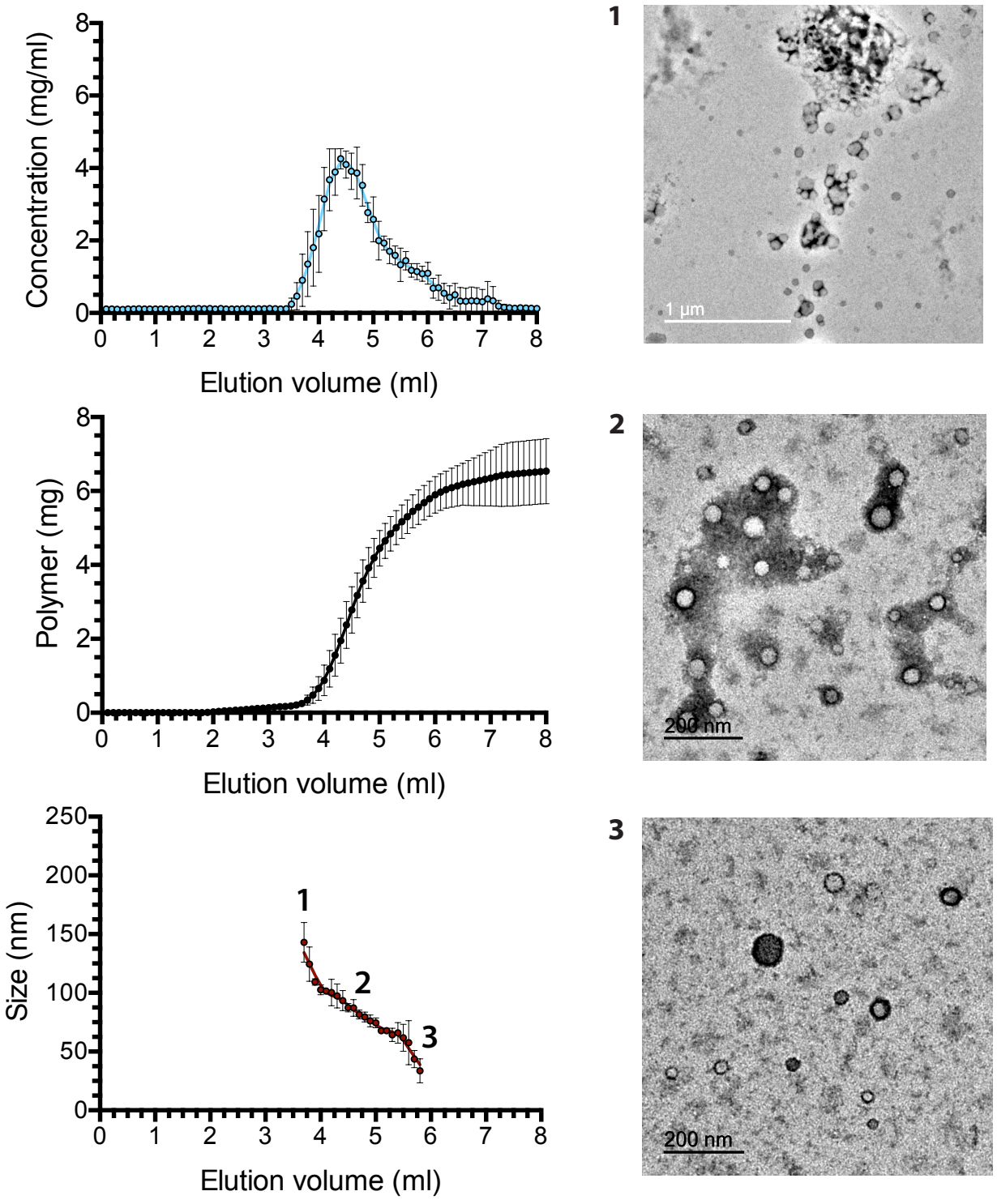

Figure 4.5. Characterisation of A-EP polymersome fractions obtained from GPC. Representative TEM pictures from different elution volumes. n=3 experiments. Error bars: S.E.M.

4.3.2. Centrifugation

GPC is feasibly limited to separation of small volumes (~<2ml) of polymersomes in solution, as the length of the column must increase with sample volume in order to

adequately separate structures of different sizes. Robertson et al. reported the separation of tubular from spherical polymersomes via centrifugation, where the tubular polymersomes pellet due to their higher mass (Robertson, Yealland et al. 2014). A method of high-volume size separation is useful for making larger batches of polymersomes, e.g. for *in vivo* work. Centrifugation was hypothesised to be able to separate the two populations of polymersomes and micelles akin to the separation of polymersomes from tubes. Centrifugation of Angiopep-2-POEGMA-PDPA polymersomes resulted in a supernatant and a pellet, the latter of which was resuspended in PBS. Figure 4.6 shows DLS size distributions of the pellet and supernatant, indicating a predominantly micellar population present in the supernatant. The average size of the resuspended pellet population was 78 nm, comparable to previously obtained values of POEGMA-PDPA polymersomes purified via GPC separation (figures 4.1 and 4.5). Figure 4.7 shows electron micrographs of polymersomes before and after centrifugation. The micrographs confirm the pellet population as mostly containing polymersomes with a few micelles. By contrast, micelles predominate the supernatant with the presence of a few polymersomes.

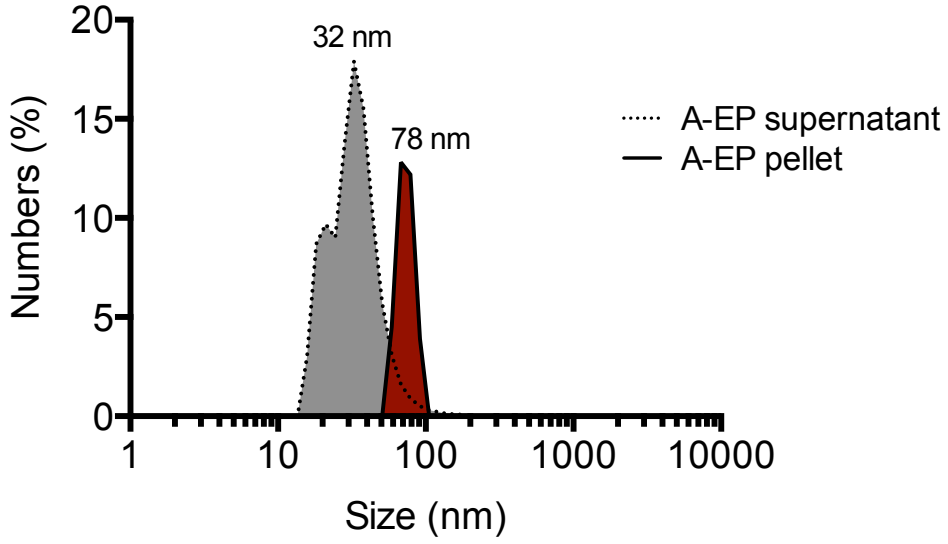

Figure 4.6. DLS of A-EP separated via centrifugation.

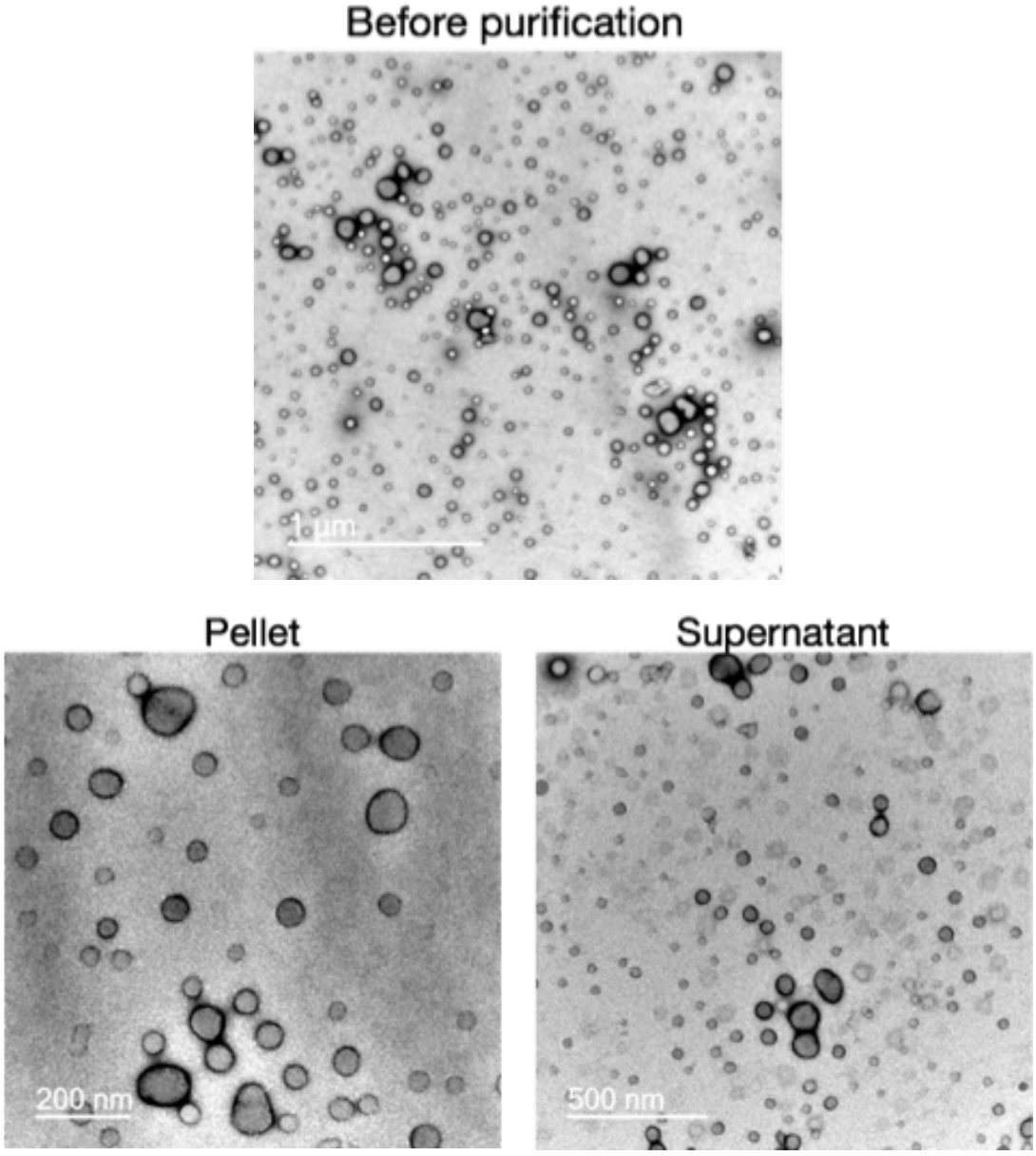

Figure 4.7. Electron micrographs of polymersomes before and after centrifugation.

4.4. MTT Viability Test of Polymersome Toxicity

The reduction of 3-(4,5-dimethylthiazol-2-yl)-2,5-diphenyltetrazolium bromide (MTT) into a purple formazan salt by mitochondria can be used to quantify cellular metabolic respiration. An increase in formazan reduction implies cellular stress, and a decrease corresponds to lower metabolic activity due to cell death. MTT was used to assess the effect of POEGMA-PDPA or Angiopep-2-POEGMA-PDPA polymersomes on bEnd.3 metabolic activity. After 24 hours, no significant changes in formazan production were

observed in the polymersome-treated groups compared to the PBS-treated controls (figure 4.8). This indicates that polymersomes can be used at a concentration of up to 1 mg/ml in bEnd.3 cells without any changes in cellular metabolism at the time examined. Furthermore, the presence of Angiopep-2 in the polymersome membrane does not impact mitochondrial activity compared to POEGMA-PDPA alone.

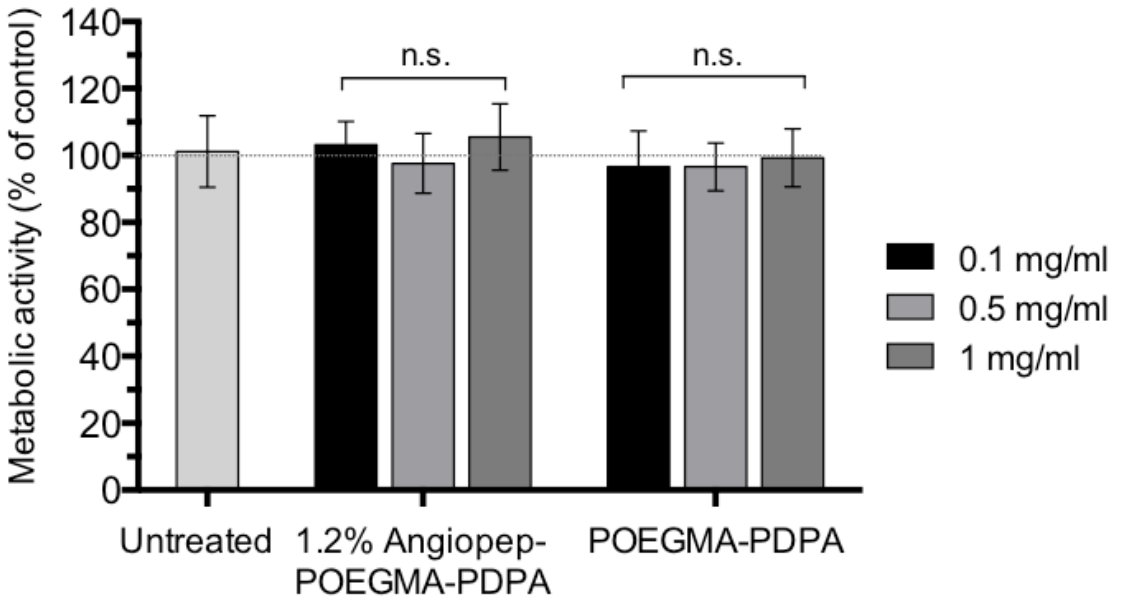

Figure 4.8. MTT test of A-EP or EP in bEnd.3 cells. 24 hours after incubation. n=3; error bars = S.D, *p <0.05.

4.5. Assessing Non-Fouling Properties of Polymersomes

An important characteristic of drug delivery vehicles is to avoid protein fouling, i.e. the gradual adsorption of proteins onto the vehicle surface, as this effect can reduce plasma circulation half-life. POEGMA is a PEG derivative and has been shown to be non-fouling (Alswieleh, Cheng et al. 2014). However, the presence of Angiopep-2 peptide might create a hot spot for protein adsorption. While the formation of 'soft' protein coronas is more difficult to assess due to their dynamic nature, 'hard' corona formation of A-EP and EP polymers can be assessed through GPC coupled with HPLC for detection. Through using conditions to obtain clearly separate polymer and protein elution times, it is possible to assess potential hard polymer/protein interactions if there

are shifts in the elution times when polymer and proteins are run through the column together.

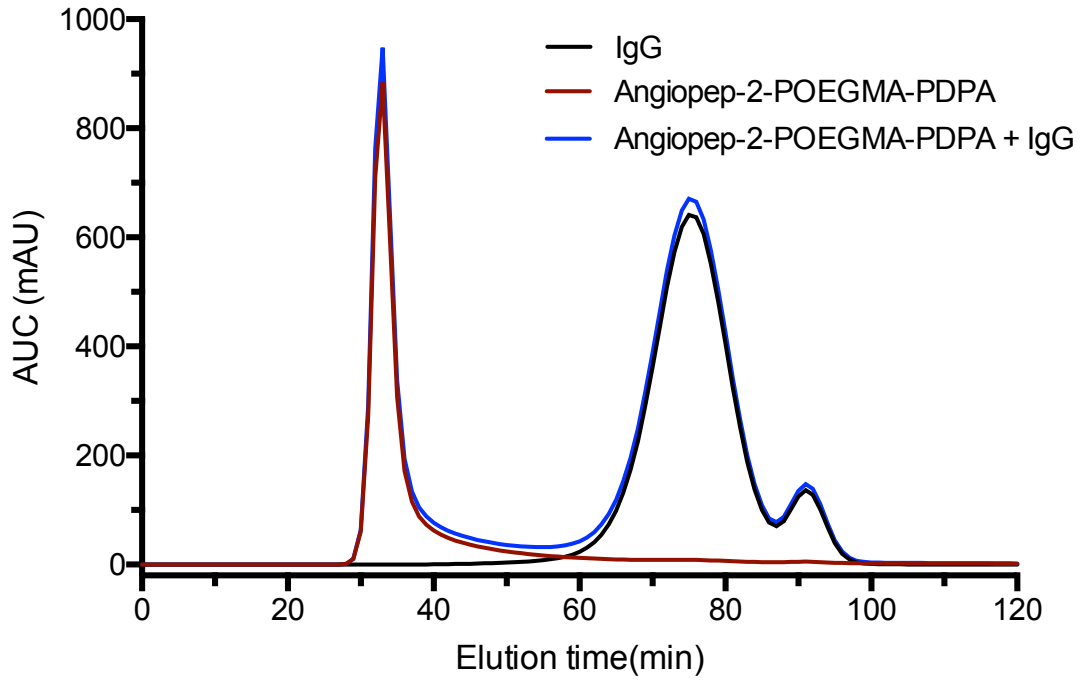

Figure 4.9. GPC-HPLC assessment of EP interactions with IgG.

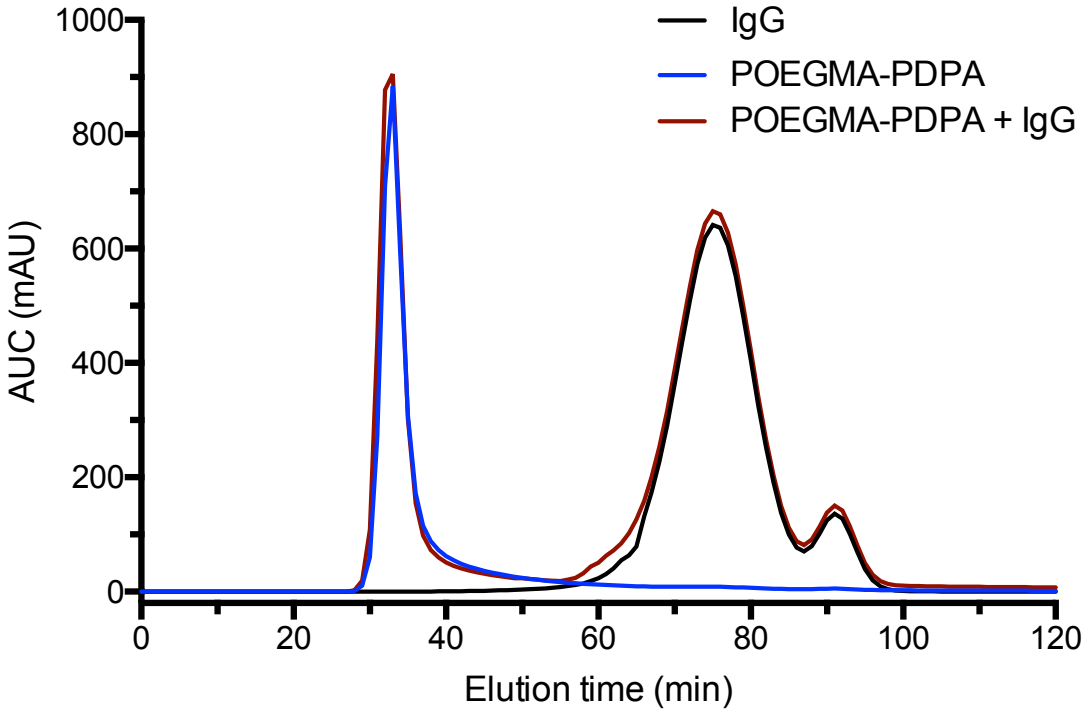

Figure 4.10. GPC-HPLC assessment of A-EP interactions with IgG.

The non-fouling properties of Angiopep-2-POEGMA-PDPA and POEGMA-PDPA against a model protein IgG were assessed via GPC-HPLC. Under the separation conditions used, IgG emits a trace with a wide peak at 60-80 minutes followed by a smaller peak at 90-100 minutes. Figure 4.9 shows the elution times of POEGMA-PDPA, IgG, and POEGMA-PDPA mixed with IgG. The polymer is eluted between 30 minutes and 40 minutes, with a slight shoulder until ~60 minutes. In the absence of IgG, the shoulder of POEGMA-PDPA is negligible and there is no overlap between the polymer peak compared to the control protein peak. Mixing of polymer and protein showed no shift in the peak sizes or retention times, indicating that no interaction is occurring between POEGMA-PDPA and IgG. Similar results were observed for Angiopep-2-POEGMA-PDPA, as displayed in figure 4.10. Mixing polymer and protein in the same sample resulted in a minor continuation of the polymer shoulder, and where it vanishes around 60 minutes in the case of free polymer it instead merges into the protein peak. However, this convergence of peaks is occurring at a negligible scale and there is no evidence for 'hard' corona formation. Nevertheless, experiments are required to determine whether 'soft' corona formation and protein fouling occurs in the case of Angiopep-2-POEGMA-PDPA.

4.6. Encapsulation of Cargo into Polymersomes Via Electroporation

4.6.1. Gold-labelled Polymersomes

An experiment described in section 6.9 of chapter 6 was performed to localise polymersomes within brain endothelial cells with electron microscopy. The harsh sample fixation processing techniques used in electron microscopy preparation are problematic as they destroy the polymersome membrane. By contrast, gold is unaffected by fixation and is frequently used as a label in EM studies. IgG with 6 nm gold was thus encapsulated into A-EP via electroporation. Figure 4.11 shows the DLS and TEM characterisation of polymersomes with gold encapsulated, where electron dense gold particles can be seen within the polymersomes.

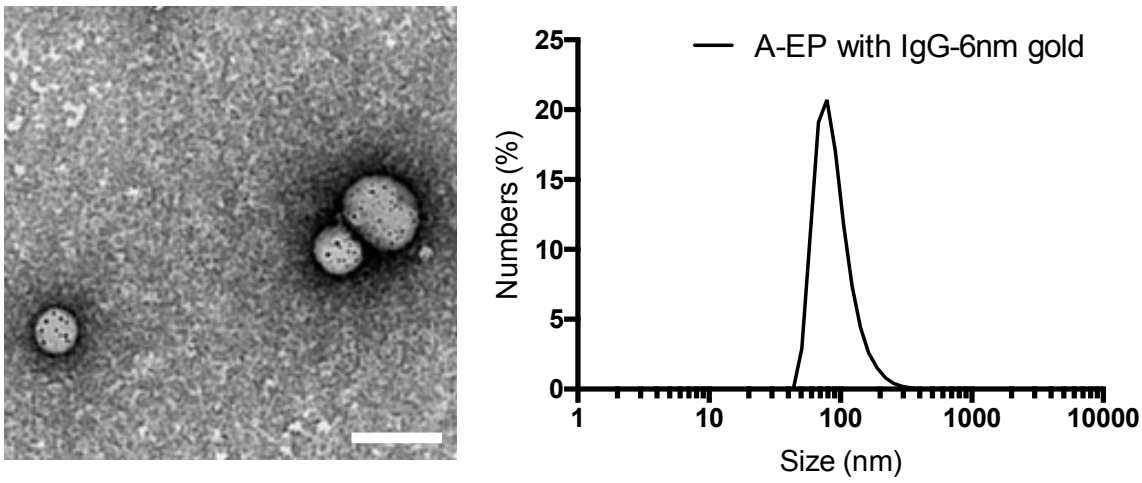

Figure 4.11. Morphology and size of A-EP with 6nm IgG-gold encapsulated. Scale bar: 200 nm.

4.6.2. Encapsulation of Carnosine

For experiments described in section 7.5 of chapter 7, carnosine was encapsulated into A-EP polymersomes via electroporation, followed by purification via GPC to remove residual unencapsulated protein. Protein content of polymersomes was analysed via HPLC after a standard curve of free carnosine had been established. The elution trace of carnosine in HPLC detected in the UV Vis channel of 280 nm can be seen in figure 4.12. Subsequently, area under curve (AUC) integration analyses to obtain concentration were used between 1.5-2.5 minutes, with the standard curve displayed in figure 4.13.

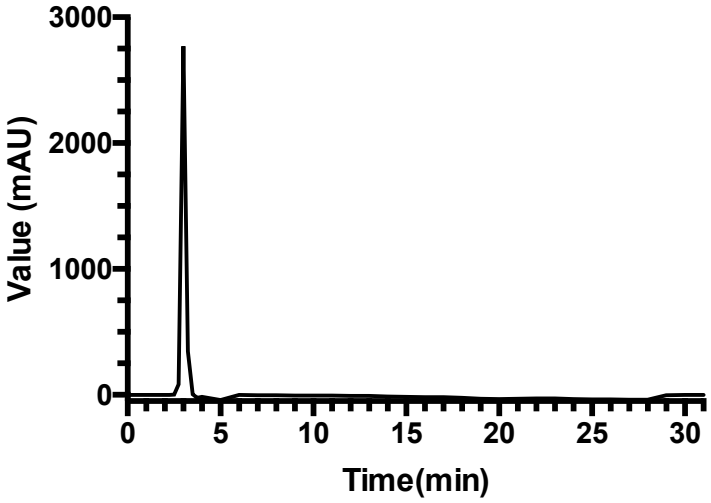

Figure 4.12. HPLC elution trace of carnosine. Detection at 280 nm.

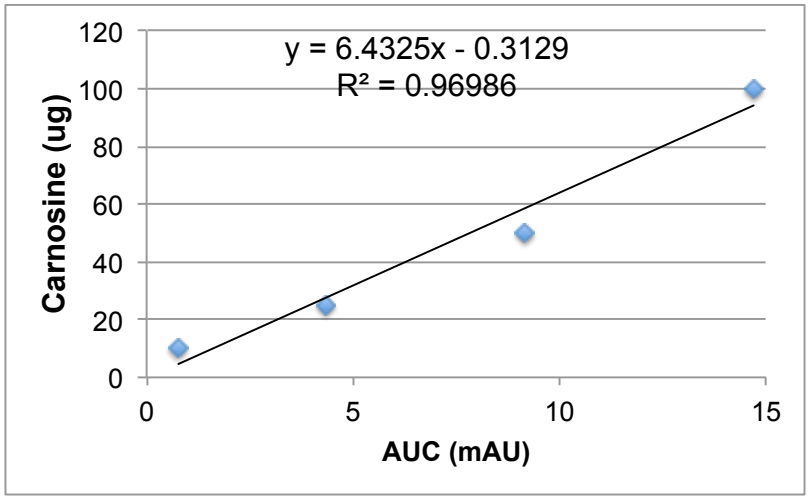

Figure 4.13. Standard curve of carnosine protein concentration at emission of 280 nm. Obtained from AUC integration of HPLC traces.

The encapsulation of carnosine was performed with an initial protein concentration of 1.5 mg/ml. The protein content of GPC-purified polymersomes was determined to be approximately 1 mg/ml (table 4.1). The encapsulation efficiency was much higher compared to other reports of polymersome encapsulation of macromolecular cargo, ranging between 15-40% (O'Neil, Suzuki et al. 2009). However, through changing the number of pulses or voltage it may be possible to further increase encapsulation efficiency.

[Carnosine] before purification mg/ml	[Carnosine] after purification mg/ml	Encapsulation efficiency %
1.45	0.95	66

Table 4.1. Carnosine content of purified A-EP as determined by HPLC.

4.7. Discussion

The ability to characterise polymersome transcytosis at the blood-brain barrier depends on a reliable method of separating polymersomes from micelles and other structures formed in the self-assembly process. Neither gel permeation chromatography nor centrifugation provided fully separated populations of vesicles, but make up the

majority of the purified fractions as evidenced by sizing data and electron microscopy. Separation by GPC yielded purer populations of vesicles as the eluted fractions were collected on the scale of microlitres. By contrast, centrifugation is useful when preparing large volumes of sample for e.g. *in vivo* studies. Ideally, the centrifugation method can be further refined to separate micelles (<50 nm) from small polymersomes (50-100 nm). Another method to investigate in future work could be hollowfibre filtration for the purification of polymersomes to obtain more precise size ranges.(Robertson, Yealland et al. 2014)

A-EP and EP polymersomes showed no cell stress in bEnd.3 cells, showing that they are suitable for use *in vitro* for concentrations of up to 1 mg/ml. Furthermore, through GPC-HPLC it was shown that EP polymersomes do not interact with the model protein IgG to form a 'hard' protein corona. A-EP and IgG may interact on a minuscule level, possibly due to the peptide sticking out of the polymersome corona. However, overall A-EP appears to be a suitable vector for drug delivery to the CNS in terms of physicochemical properties.

Chapter 5.

RESULTS AND DISCUSSION II

Polymersome Interactions With an *In Vitro* Blood-Brain Barrier Model

5.1. Introduction

This section is dedicated to work undertaken to establish a simplistic *in vitro* model of the blood-brain barrier, formed by brain endothelial cells. Subsequent characterisation of the model was performed to ensure the model possessed the phenotype of brain endothelial cells, such as TEER values and expression of BBB-specific tight junction proteins. The section is concluded with characterisation of polymersome transcytosis in the transwell model, including kinetics of transcytosis on the macroscale and efficiency of transcytosis as a function of variation of the number of targeting ligands.

5.1.1. The *In Vitro* Model of the Blood Brain Barrier

There are a variety of established *in vitro* models of the blood brain barrier, and choosing the appropriate model depends on research aims and applications (for a comparison between common *in vitro* models, refer to section 1.8 of chapter 1). The immortalised mouse brain microvasculature endothelial cell line bEnd.3 has been used extensively as a BBB model, with average TEER values around 100-140 Ω/cm^2 (Neumann, Schaefer-Ridder et al. 1982, Brown, Morris et al. 2007). These cells have been used for the purpose of investigating transcytosis (Bien-Ly, Yu et al. 2014), making it a good cell line for the work undertaken in this project. Use of a mouse cell line gives the advantage of quick translation into *in vivo* murine studies used later in this project. Moreover, the co-culture of additional neurovascular unit cell types with brain endothelial cells has been reported to enhance barrier-like properties and bridge the gap between *in vitro* and *in vivo* TEER values (Zysk, Schneider-Wald et al. 2001)

(Lippmann, Weidenfeller et al. 2011). The addition of astrocytes or pericytes to the transwell setup is a quick and easy way to expand the model and examine the effects of neurovascular unit interactions as an element of transcytosis.

5.1.2. Fluorescence Colocalisation by Pearson's Correlation Coefficient

There are a number of ways to assess protein-protein colocalisation from fluorescence microscopy, either directly measuring physical proximity of the target proteins (e.g. via Forster Resonant Energy Transfer), or indirectly through calculating overlap of fluorescence of two targets acquired in separate channels. Pearson's correlation coefficient (***Rr***) gives the linear correlation between X and Y values from fluorescence channels, with resulting output values between -1 and +1. The formula can be applied to protein-protein colocalisation through immunocytochemical labelling the targets of interest with fluorophores, detecting emission in the red and green channels to provide X and Y values of fluorescence intensity. The fluorescence overlap is calculated according to the coefficient, where values +1 equates to full colocalisation and -1 complete exclusion of targets from one another. See Chapter 3 (Materials and Methods) for further details of Pearson's correlation coefficient calculations applied to work presented in this section and in chapter 6.

RESULTS

5.2. bEnd.3 Properties

To obtain a three-dimensional BBB mimicking environment, immortalised mouse bEnd. 3 brain endothelioma cells were seeded on top of a porous transwell filter membrane (pore diameter = 400 nm), which separates the well into two compartments (figure 5.1). The transwell membrane was coated with collagen to mimic the basal lamina onto which brain endothelial cells (BECs) adhere to *in vivo*. Seeding brain endothelial cells on the top side of the membrane corresponds to the 'blood' side of the BBB, and the bottom compartment to the 'brain' side.

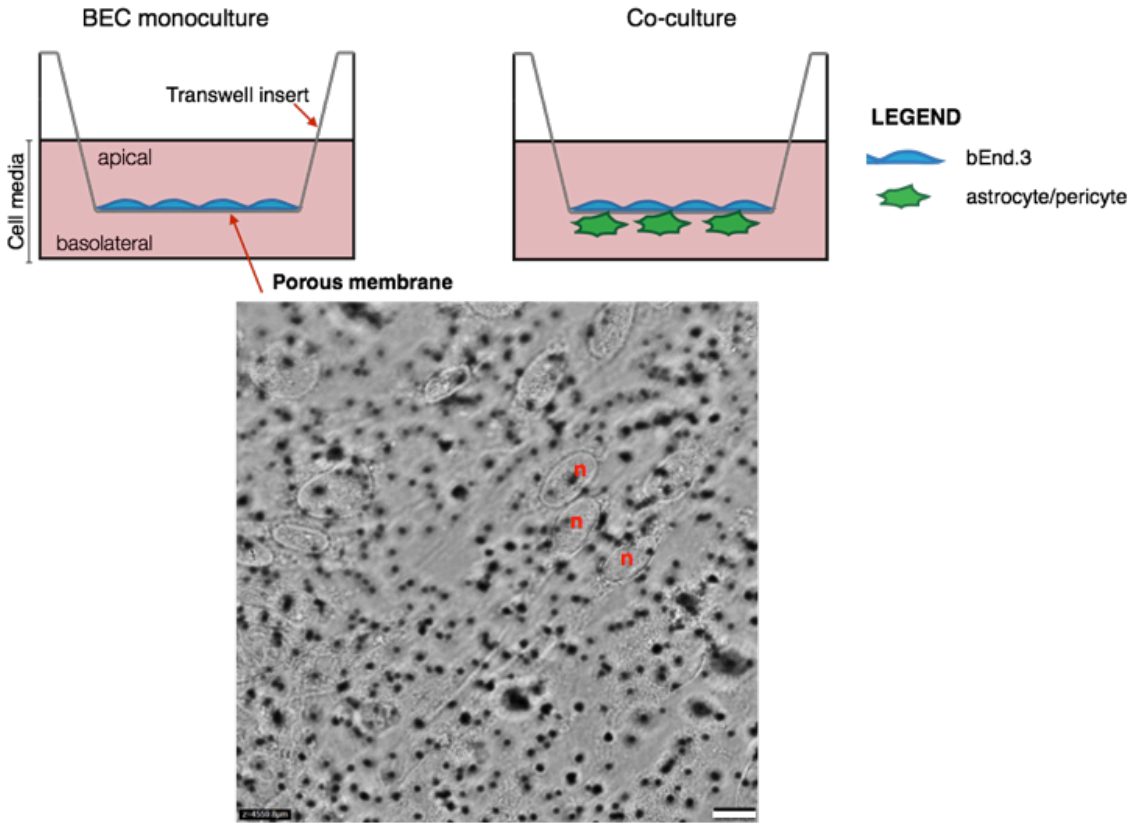

Figure 5.1. Transwell BBB model of BEC monoculture and co-culture configurations. Insert: Transmitted light micrograph of bEnd.3 monolayer seeded on top of the porous transwell filter. n: nucleus. Scale bar: 10 µm.

The transwell model was used in two different configurations, as shown in figure 5.1. A setup containing a bEnd.3 monolayer only was used to characterise polymersome interactions with endothelial cells, in which the presence of other cells could have interfered e.g. by internalising the polymersomes. A second setup in which mouse astrocytes or pericytes were cultured on the opposing side of the transwell membrane was also utilised in order to more closely mimic the BBB, and to enable investigating the fate of polymersomes after transcytosis.

5.2.1. Expression of Brain Endothelium Tight Junction Proteins

To ensure confluent bEnd.3 monolayers grown in a transwell setting expressed the appropriate brain barrier-like properties, immunocytochemistry was performed for tight junction markers specific to the blood brain barrier: zonula occludens-1 (ZO-1), occludin and claudin-5. Claudin-5 and occludin immunoreactivity was present in

confluent bEnd.3 monolayers cultured in a transwell setup, with some claudin-5 localisation along the plasma membrane (figure 5.2). ZO-1 expression was also present, although weaker than occludin and claudin-5 and more localised to the cytoplasm. The presence of all three proteins is consistent with a blood brain barrier phenotype.

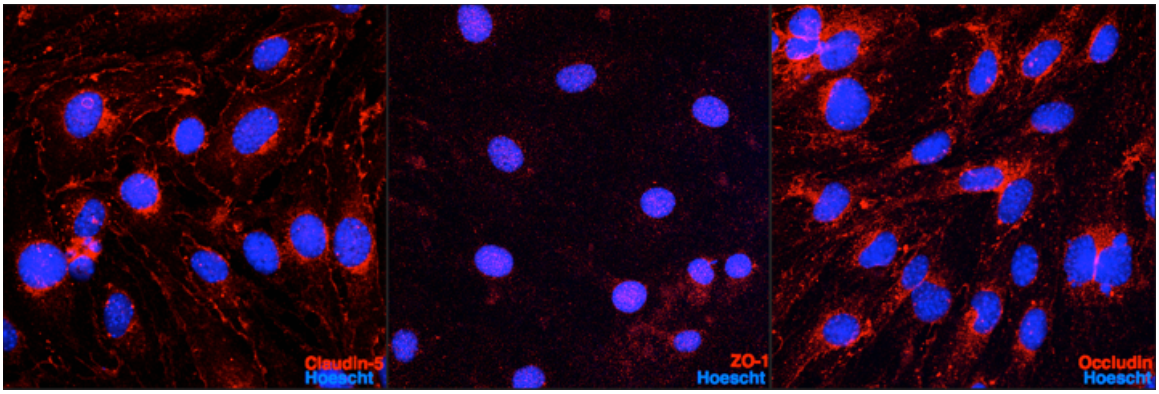

Figure 5.2. Tight junction markers in bEnd.3 grown in transwells. Expression of brain endothelial phenotype specific tight junction markers (red) in the cell line bEnd.3 grown in transwells as monoculture. Cell nuclei counterstained with Hoescht (blue).

5.2.2. TEER Values of bEnd.3 in Monoculture or Co-culture

Further to tight junction protein expression, trans-endothelial electrical resistance (TEER) measurements were measured an indicator of *in vitro* barrier tightness. TEER values of fully confluent bEnd.3 monolayers were assessed for 7 days after seeding, shown in figure 5.3. BECs grown as a monoculture started at values of 150 Ω/cm^2 on day 1, rising to an average of 176±18 Ω/cm^2 at day 7 (n=5 wells per n=3 experiments). Culturing endothelial cells with pericytes in non-contact co-culture on the basolateral membrane side resulted in a rapid increase in TEER values from day 2. At day 7, the measured co-culture TEER values were 217±27 Ω/cm^2 (n=5 wells per n=3 experiments), significantly higher than the values obtained from bEnd.3 cells alone (student's independent t-test, *$p<0.05$). bEnd.3 cells alone had TEER values higher than previously reported in literature, indicating these cells show sufficient barrier properties when used as a monoculture (Brown, Morris et al. 2007).

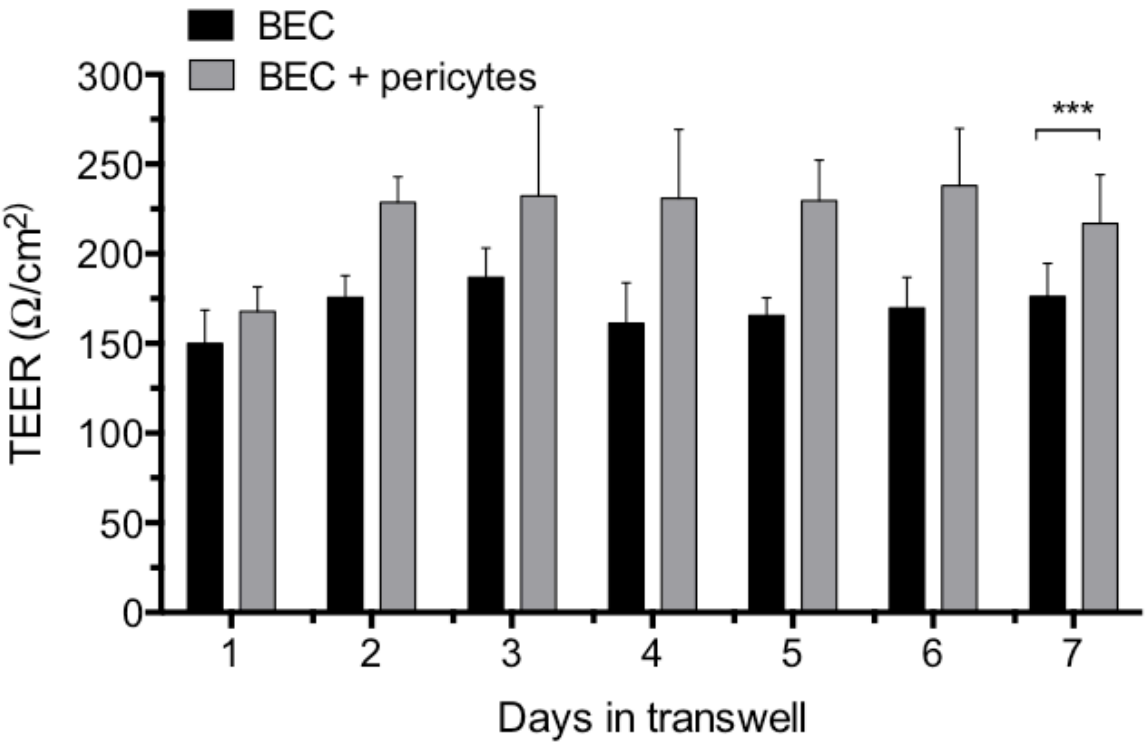

Figure 5.3. TEER values of bEnd.3 in mono- or co-culture. The addition of pericytes to the transwell culture caused a significant increase in barrier tightness at day 7 of co-culture compared to bEnd.3 alone. Error bars: S.D., $p < 0.05$.

5.2.3. bEnd.3 Expression of LRP-1

LRP-1 expression by bEnd.3 cells is essential to probe transcytosis of Angiopep-2. Unfortunately, few antibodies against the large (585kDa) ligand-binding extracellular domain of LRP-1 are currently commercially available. The expression of LRP-1 was thus probed with an antibody against the 85 kDa intracellular domain of the receptor ($LRP\text{-}1_{ICD}$). Figure 5.4 shows the expression of LRP-1 in bEnd.3 cells in the absence of A-EP as a ligand. Fluorescence is mostly diffuse throughout the cytoplasm, somewhat demarcating the elongated shape of the cell in some cases. Nevertheless, it was confirmed that bEnd.3 cells express LRP-1.

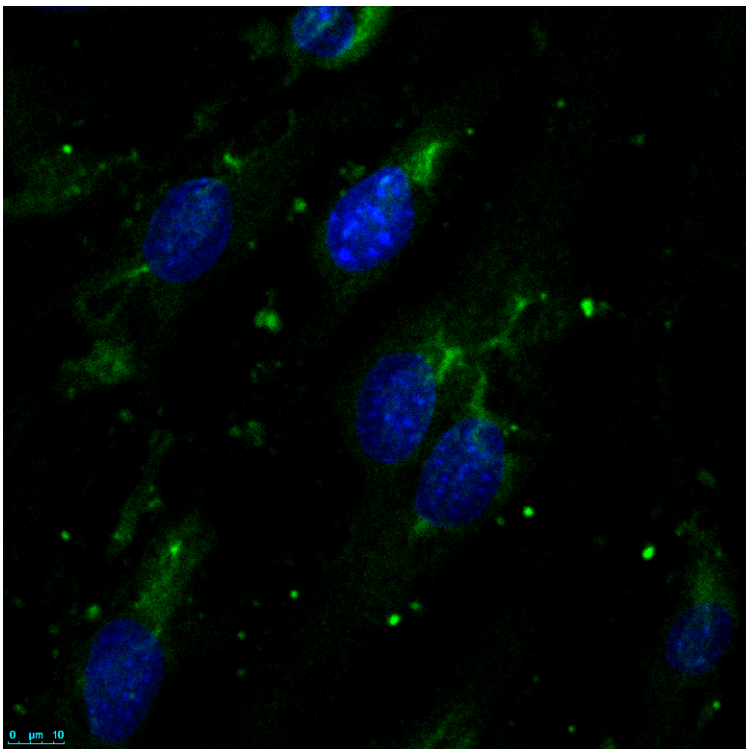

Figure 5.4. LRP-1 expression by bEnd.3. Immunofluorescence of LRP-1 (green), nuclei stained with DAPI (blue). Scale bar: 10 µm.

5.3. *In Vitro* Transcytosis of Polymersomes

Having established a cell culture setup expressing a blood brain barrier phenotype with the appropriate tight junction markers and TEERs comparable to reports in literature, the next step was to investigate polymersome transcytosis across the transwell model.

5.3.1. Polymersome Colocalisation with LRP-1

In order to confirm that Angiopep-2-POEGMA-PDPA polymersomes (A-EP) interact with the LRP-1 receptor in brain endothelial cells, immunocytochemistry of LRP-1_{ICD} was performed after incubation with A-EP for 10, 60 or 120 minutes. Figure 5.5 shows the association of A-EP with LRP-1_{ICD} after 60 minutes.

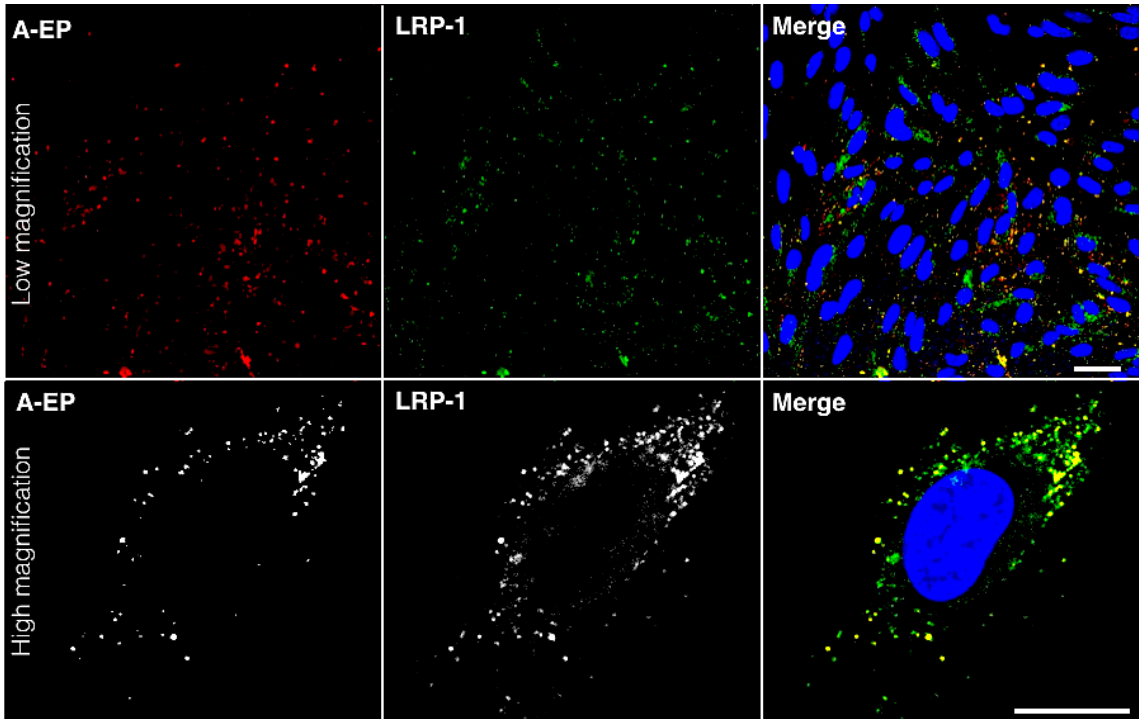

Figure 5.5. A-EP uptake by LRP-1 in bEnd.3. LRP-1_{ICD} (green) and A-EP (red) colocalisation in bEnd.3 after 60 minutes. Cell nuclei stained with DAPI (blue). Scale bar: 20 µm.

At 60 minutes, the A-EP signal is seen in many different areas of the transwell and is observed in cytoplasmic puncta. At higher magnification, many puncta of LRP-1_{ICD} and A-EP are visibly colocalising within the cell. This is in contrast to the diffuse LRP-1_{ICD} pattern observed in unstimulated bEnd.3 cells.

To elucidate the extent and time that A-EP associates with LRP-1_{ICD}, red/green fluorescence was quantified with Pearson's correlation coefficient (Rr). After 10 minutes of incubation Rr was 0.78 for A-EP and LRP-1_{ICD} colocalisation, and remained high at 0.75 after 120 minutes (figure 5.6). The continuously high Rr values indicate that A-EP remains associated with the intracellular domain of LRP-1 in the intracellular trafficking stages of transcytosis.

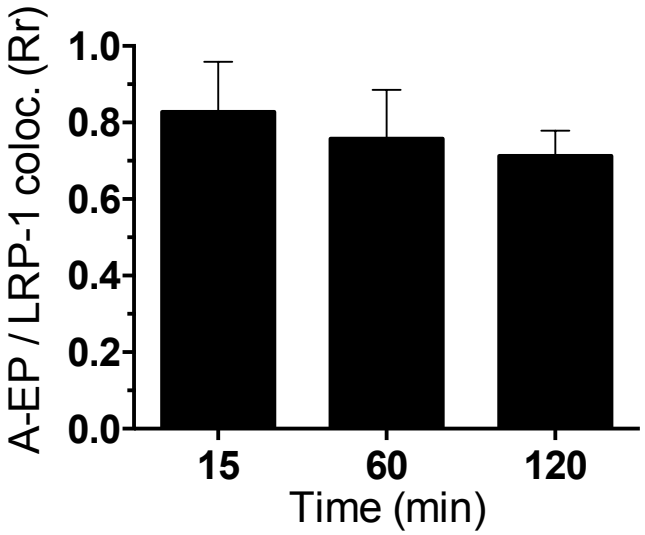

Figure 5.6. LRP-1_{ICD} and A-EP colocalisation in bEnd.3 cells over time. Calculated with Pearson's correlation coefficient (Rr) of red/green fluorescence intensity overlap. n=3 experiments, error bars: S.D.

5.3.2. LRP-1 Transcytosis Ligand Competition Assay

To confirm that Angiopep-POEGMA-PDPA polymersomes are internalised by bEnd.3 cells via LRP-1-mediated transcytosis, cells positive for polymersomes in the presence of transcytosis ligands was quantified via fluorescence activated cell sorting (FACS). Lactoferrin is a LRP-1 antagonist (Mantuano, Lam et al. 2013). Poly-L-lysine has been reported to inhibit transcytosis of cationic macromolecules, and should not have an effect on A-EP transcytosis (Herve, Ghinea et al. 2008). Figure 5.7. shows bEnd.3 uptake in the presence of transcytosis inhibitors. After 60 minutes, 37±11% of cells were positive for A-EP. Uptake of polymersomes in cells incubated in 4C was non-existent after 60 minutes, confirming that internalisation is an active process. Furthermore, incubation with poly-l-lysine yielded 37±2% of cells positive for polymersome fluorescence. Incubation with lactoferrin resulted in an uptake of 23±4%. Neither of the pharmacological agent treatments significantly inhibited A-EP internalisation (one-way ANOVA, $p < 0.05$, n=3). However, this may be due to the larger standard deviation obtained for the polymersome control group. Furthermore, it is possible that lactoferrin antagonises a different ligand binding domain of LRP-1 than the A-EP binding domain.

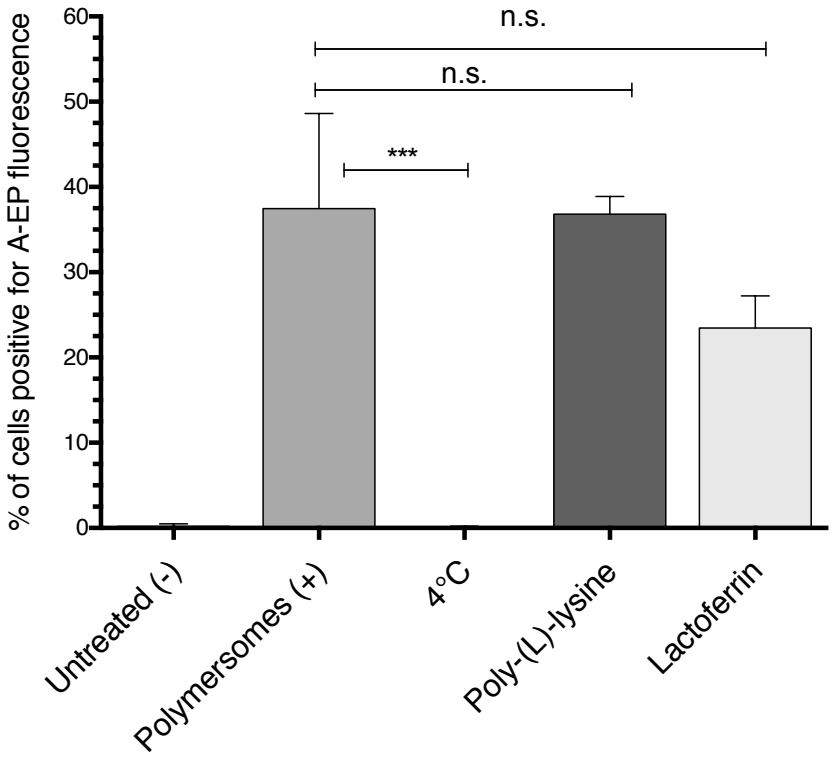

Figure 5.7. bEnd.3 internalisation of A-EP after 60 minutes in the presence of transcytosis inhibitors. error bars: S.D., one-way ANOVA, $p<0.05$.

5.4. Transcytosis Kinetics

5.4.1. Permeability of bEnd.3 Monolayers to Polymersomes

To assess the permeability of bEnd.3 monolayers in transwells and simultaneously obtain polymersome flux kinetics, quantification of apical-to-basolateral flux of polymersomes was compared to a fluorescently labelled dextran. FITC-Dextran does not interact with transcytosis receptors and is frequently used as an indicator of barrier tightness in transwell permeability assays (Sanders, Madara et al. 1995). After addition of 1 mg of polymersomes or FITC-dextran to the apical compartment, fluorescence over time was quantified in the basolateral compartment. Flux behaviour of polymersomes in the presence of bEnd.3 monolayers were compared to controls without any cells, where apical-to-basolateral transport occurs by gradual diffusion through the porous transwell membrane. Furthermore, A-EP flux was compared to non-targeting POEGMA-PDPA (EP) polymersomes. Polymersome and FITC-dextran apical-

to-basolateral flux over time is shown in figure 5.8. FITC-dextran fluorescence was steadily increasing over time in the no-cell control. This indicates that 70 kDa FITC-dextran is able to move across the porous membrane provided that it is allowed to diffuse freely. In a bEnd.3 monolayer, basolateral fluorescence increase of FITC-Dextran over time was markedly lower, although not completely absent. The apical-to-basolateral movement of POEGMA-PDPA polymersomes across bEnd.3 over time was higher than that of FITC-Dextran, but lower than any of the free diffusion controls. Finally, the pattern of cell-free A-EP diffusion is similar to that of FITC-dextran, but increases drastically in the presence of bEnd.3 cells. After 12 hours, the full initial apical concentration of A-EP has shifted to the basolateral compartment. This behaviour indicates that the bEnd.3 monolayer is not impairing but rather enhancing the apical-to-basolateral flux of A-EP polymersomes, strongly reinforcing that A-EP crosses bEnd.3 monolayers via active transcellular transportation or transcytosis.

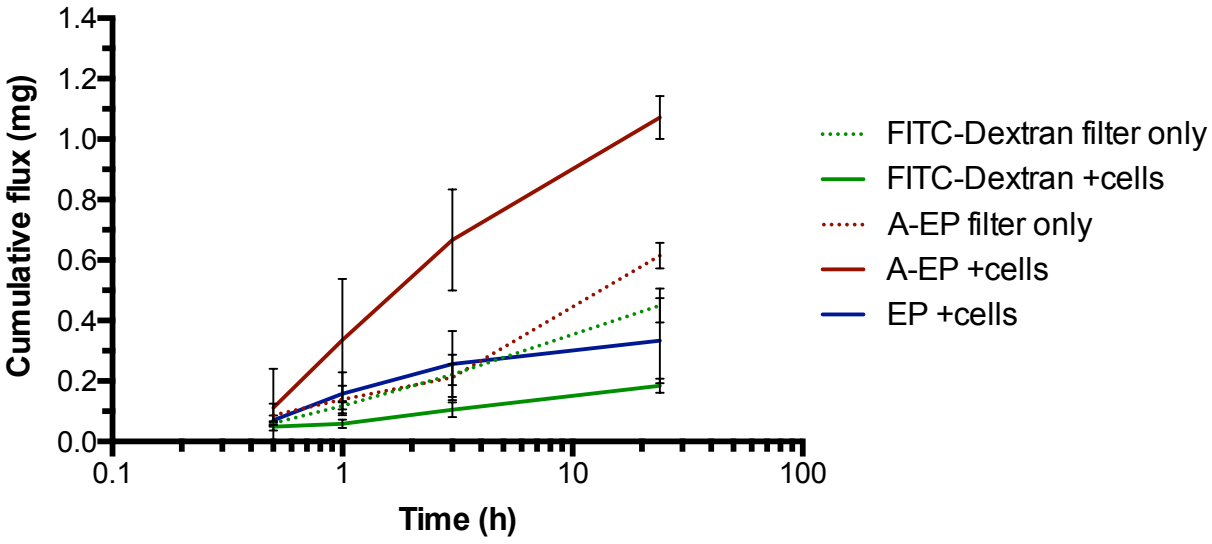

Figure 5.8. Cumulative apical-to-basolateral flux of A-EP or EP over time. Compared to a 70 kDa FITC-dextran control. n=3, error bars: S.D.

5.4.2. Kinetics of Polymersome Transcytosis *In Vitro*

Quantification of fluorescence in basolateral media is useful for assessing monolayer permeability, but may give inaccurate results when measuring transcytosis over time as

it does not account for reverse (basolateral to apical) transport. To quantify polymersome transcytosis over time, media was collected from both compartments after incubation with 1 mg/ml polymersomes, and fluorescence was measured at different collection time points. Figure 5.9 shows polymersome fluorescence over time in the apical and basolateral compartments, and the different experimental conditions are depicted in the insets (top right corner). Non-targeting EP does not shift to the basolateral compartment, indicating an intact monolayer (figure 5.9a). A-EP polymersomes added to filter-only transwells (figure 5.9b) showed a linear and gradual decrease in apical compartment fluorescence, with a corresponding basolateral increase. This is consistent with passive diffusion of polymersomes through the transwell pores into the opposing compartment, with apical-basolateral and basolateral-apical exchange reaching equilibrium after 24 hours.

By contrast, A-EP polymersomes added to the apical compartment of bEnd.3 monolayer (figure 5.9c) resulted in the transfer of the majority of A-EP to the basolateral side within 60 minutes. This basolateral fluorescence was accompanied by a corresponding decrease in fluorescence in the apical compartment. Finally, in a transwell setup with astrocytes seeded on the basolateral side of the membrane (figure 5.9d), the decrease in apical fluorescence corresponding to transcytosis ceased after 3 hours. However, a corresponding increase in the basolateral compartment was low compared to the endothelial-only setup. This is likely due to the endocytosis of polymersomes by astrocytes, reducing the polymersomes available in media.

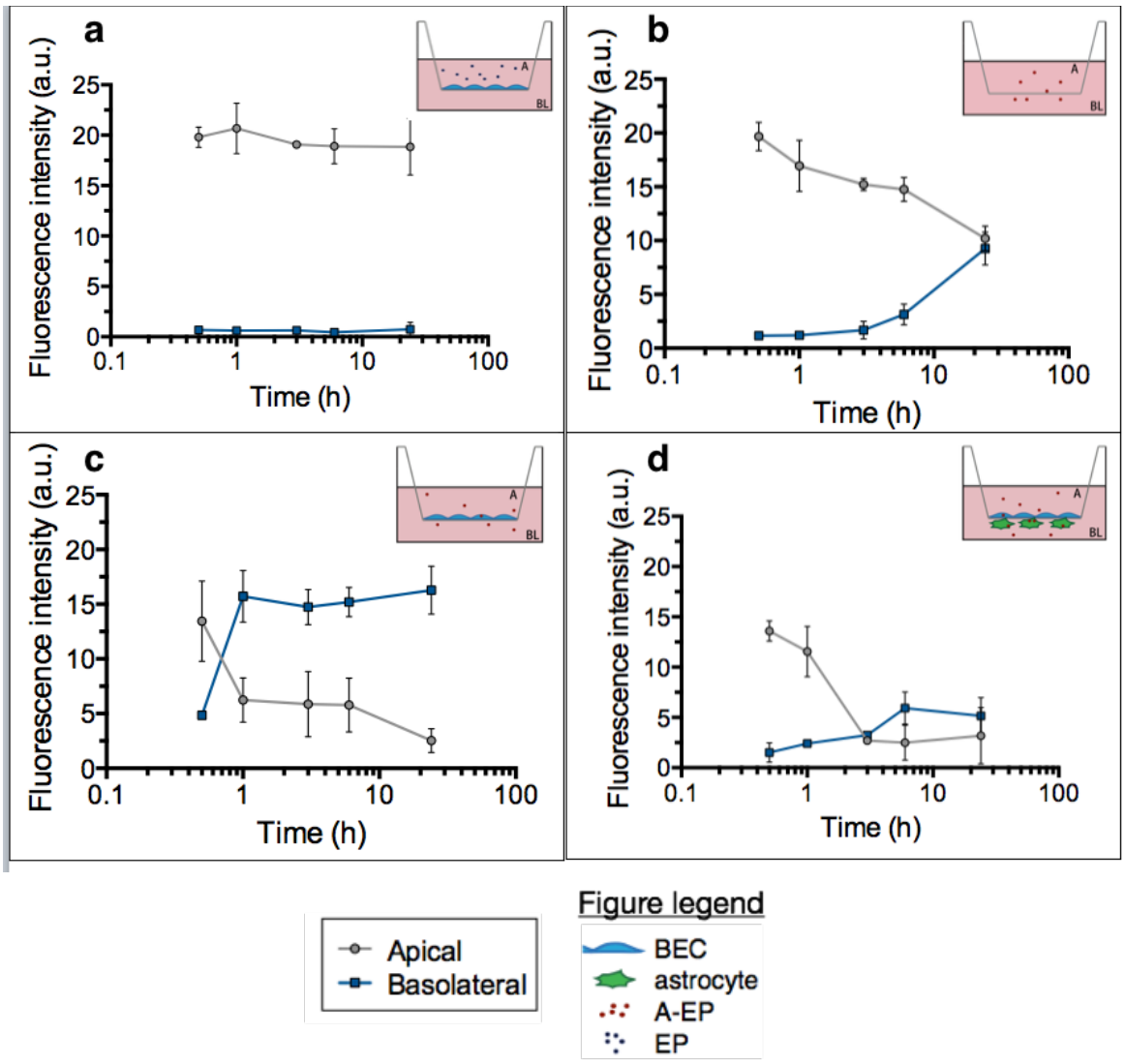

Figure 5.9. Polymersome transcytosis kinetics. Fluorescence quantification of polymersome transcytosis over time, in the presence or absence of astrocytes.

5.4.3. Visualising Polymersome Location Over Time in Transwells

The transcytosis assay of polymersome fluorescence in media over time is useful for examining the kinetics and extent of endothelial cell transcytosis, but does not discriminate between fluorescence decrease in either compartment due to polymersome presence within cells, or when passively diffusing through the 10 µm transwell membrane pores. To complement the transcytosis assay, live cell 3D confocal microscopy was used to visualise polymersomes location in the transwell. This method of acquiring serial z-stacks allows for visualising the entire length of the transwell filter, as well as any cells adhering to the filter. Figure 5.10 shows *xyz* confocal micrographs of the transwell filter reconstructed into 3D projections.

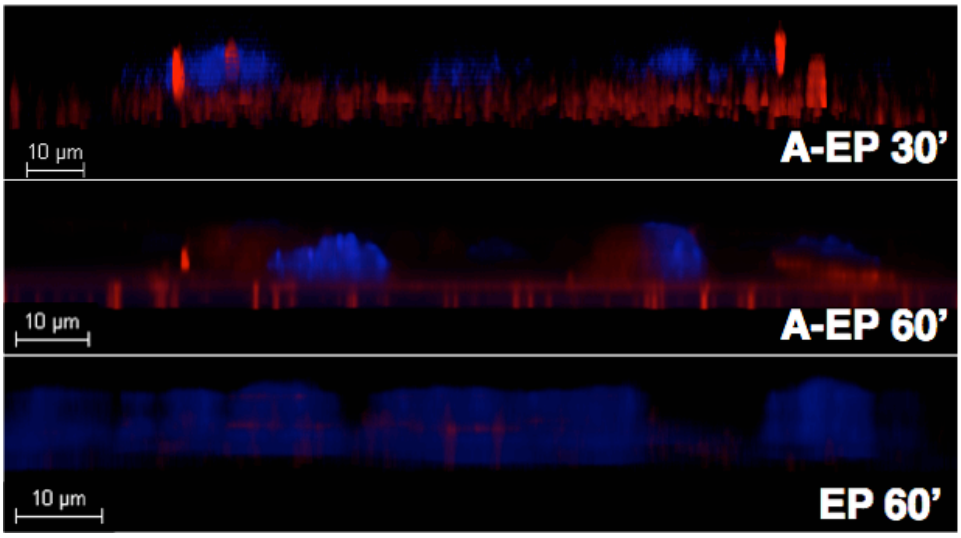

Figure 5.10. Live 3D imaging of A-EP or EP location in transwells. Confocal z-stack 3D projections of A-EP or EP distribution (red) in live bEnd.3 cells. Cell nuclei counter-stained with DAPI (blue).

Live cell imaging of A-EP polymersomes at 30 minutes showed polymersomes accumulating below the cell nuclei at the filter pore area, indicating that transcytosis was already occurring at this stage. A similar distribution of materials seen at the 60 minute time point. The EP signal was absent at 10 and 30 minutes (not shown) and very faintly detected at the cell area at 60 minutes, but not underneath the cells in the filter (figure 5.10).

To confirm that polymersome apical-to-basolateral movement occurs within 60 minutes and is the result of transcytosis rather than paracellular movement, incubation times were extended and followed by fixation and counter-staining for claudin-5 as a tight junction marker. Images acquired in the *xy* plane on the apical (top) side of the cells are shown in figure 5.11 Rapid accumulation of polymersome fluorescence was confirmed, peaking at 60 minutes. This fluorescence was very low at the examined *xy* plane at 3 and 6 hours. Polymersome fluorescence as observed after 60 minutes was predominantly intracellular, strongly indicating that the mechanism by which A-EP traverses the transwells is transcytosis as opposed to paracellular leakage due to inadequate monolayer barrier properties.

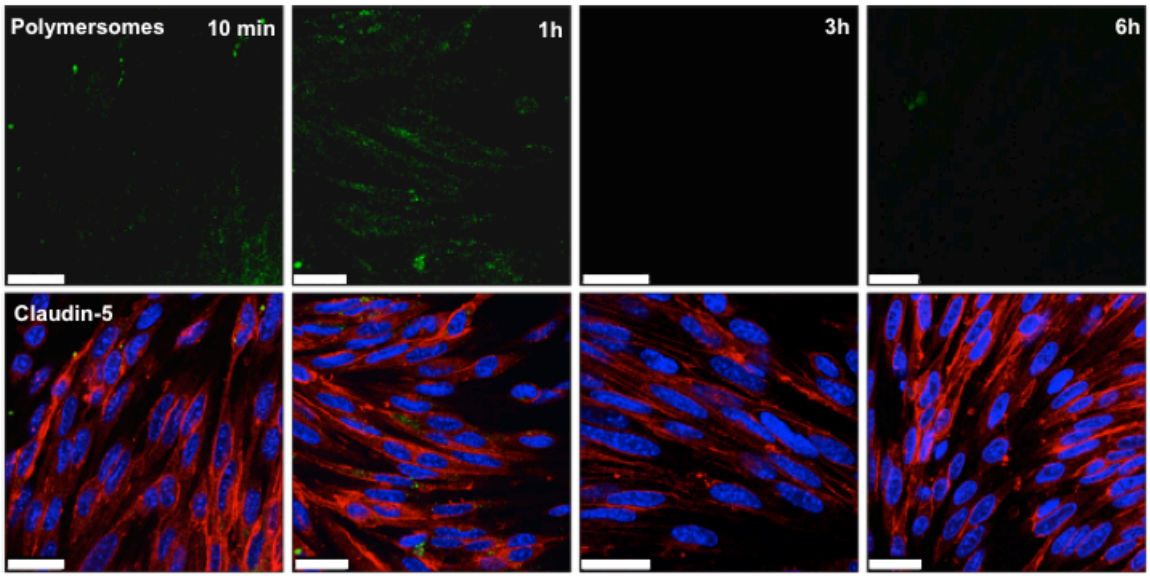

Figure 5.11. Polymersome transcytosis assessed by confocal microscopy. Confocal micrographs of polymersomes (green) in transwells, displayed from the apical side of bEnd.3 cells. Counterstained for claudin-5 (red) to mark tight junctions. Scale bar: 25 µm.

3D reconstructions of the filter and monolayers are shown in figure 5.12. Here, polymersome fluorescence can be seen inside the transwell pores from as early as 10 minutes and up to the 6 hours examined. This illustrates that the passive diffusion of polymersomes across the 10µm pores occurred significantly more slowly than the active transportation of polymersomes across brain endothelial cells. Furthermore, the method of confocal 3D imaging of the transwell filter area was shown to be a quick method for determining whether polymersome location is intracellular or within the filter pores.

5.5. Comparison of Polymersome Uptake by Endothelial Cells and Astrocytes

In order to elucidate whether the transient intracellular residence time of A-EP is unique to cells capable of transcytosis, intracellular polymersome fluorescence over time was compared between bEnd.3 and astrocytes. Figure 5.13 shows A-EP fluorescence after 0.5-6 hours in bEnd.3 or astrocyte monocultures. A moderate signal from A-EP could be observed in endothelial cells at 0.5-1h, after which the polymersomes no longer appeared to remain intracellular. By contrast, astrocytes showed modest signs of A-EP

endocytosis after 0.5 hours, with the signal intensity becoming marked at 6 hours. This indicates an ongoing internalisation of polymersomes by astrocytes, compared to a transient intracellular residence time in brain endothelial cells.

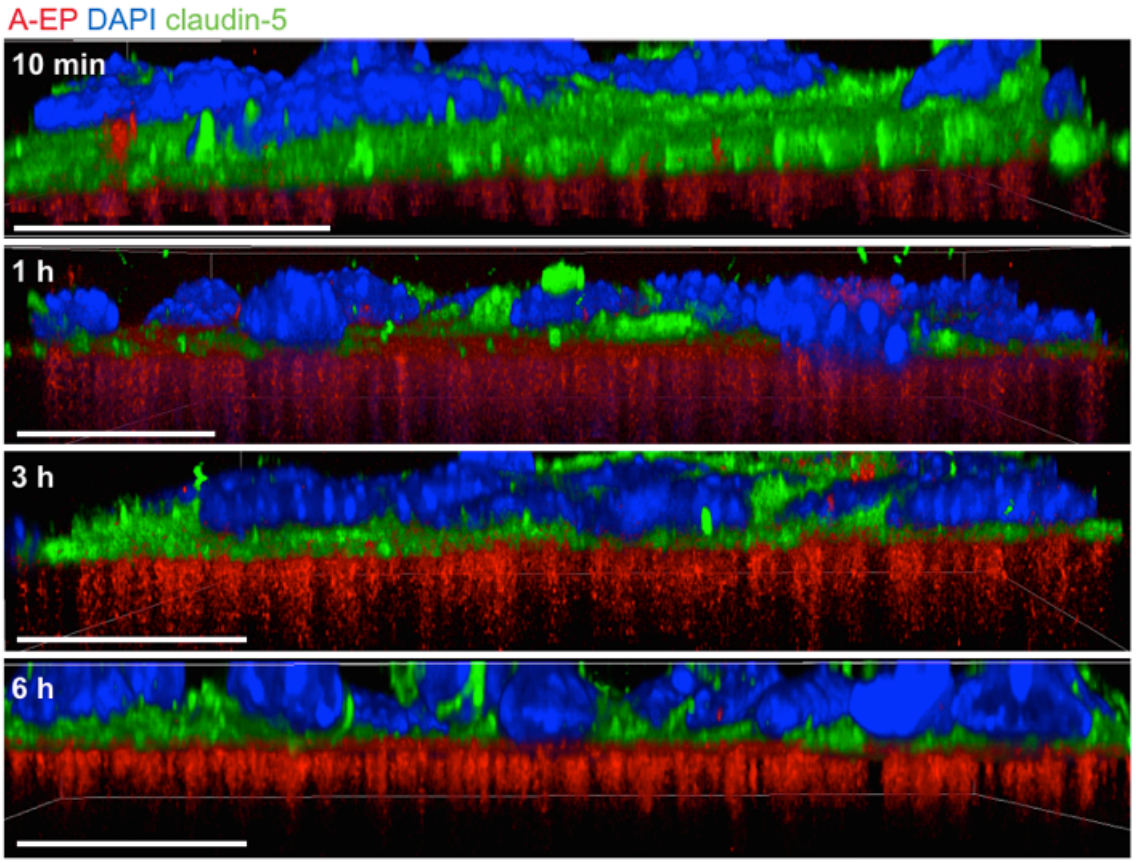

Figure 5.12. 3D projection of polymersome transcytosis. A-EP (red) transwell location over time relative to a bEnd.3 monolayer counterstained for claudin-5 (green), acquired in *xyz*. Scale bar: 25 µm.

The A-EP fluorescence intensity was quantified via ImageJ, and normalised to the Hoechst signal from nuclei. This quantification further demonstrated the difference between bEnd.3 and astrocytes, with fluorescence in the astrocytes increasing over time (figure 5.14). Polymersome fluorescence in endothelial cells was overall much lower, and decreased over time.

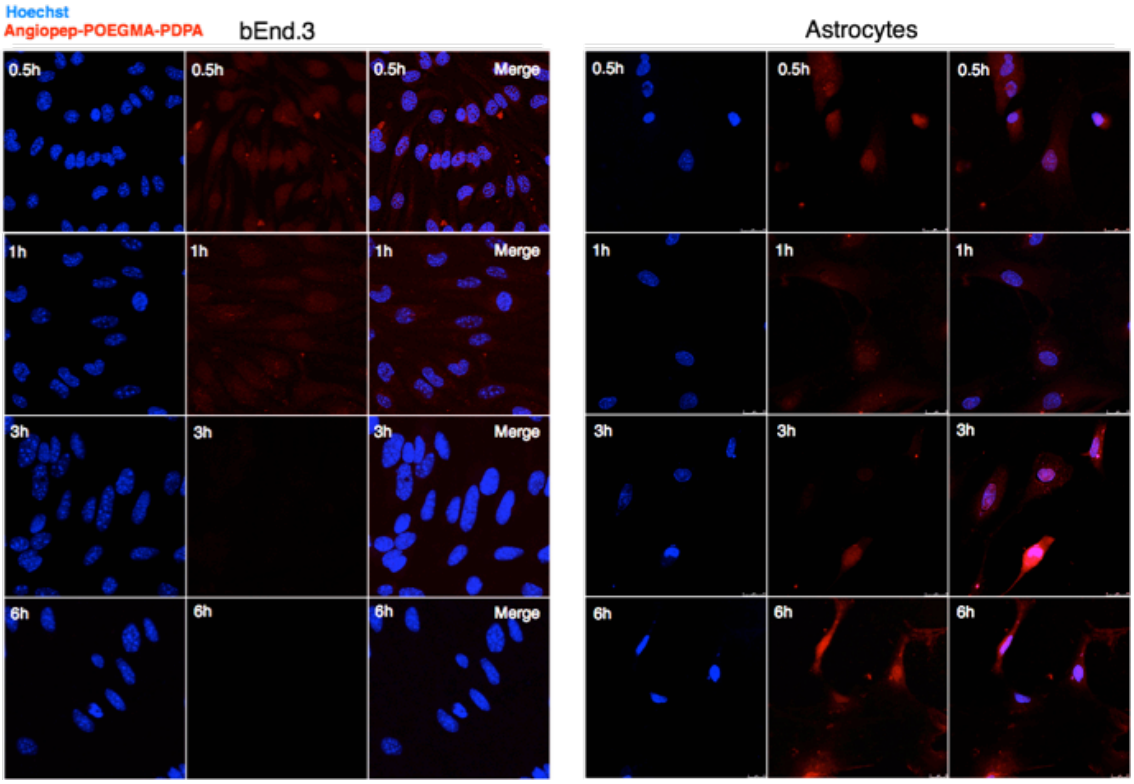

Figure 5.13. A-EP fluorescence over time in bEnd.3 and astrocyte monocultures.

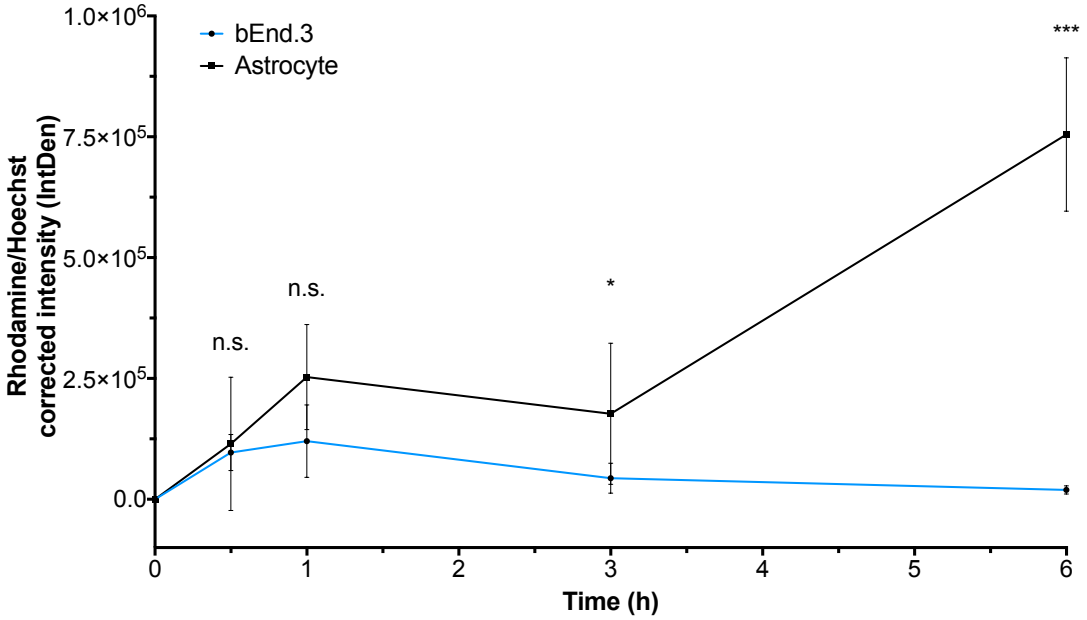

Figure 5.14. Polymersome fluorescence in different LRP-1 expressing cells of the CNS. Error bars: S.D., student's independent t-test, $p < 0.05$.

Because the overall internalisation of polymersomes was higher in astrocytes, data displayed in figure 5.14 was further normalised to the highest intensity values obtained for each group. The general trend of uptake is shown in figure 5.15. From this

normalisation it is shown more clearly that A-EP fluorescence in brain endothelial cells peaked at 1 hour in contrast to in astrocytes, where maximum internalisation was seen at 6 hours.

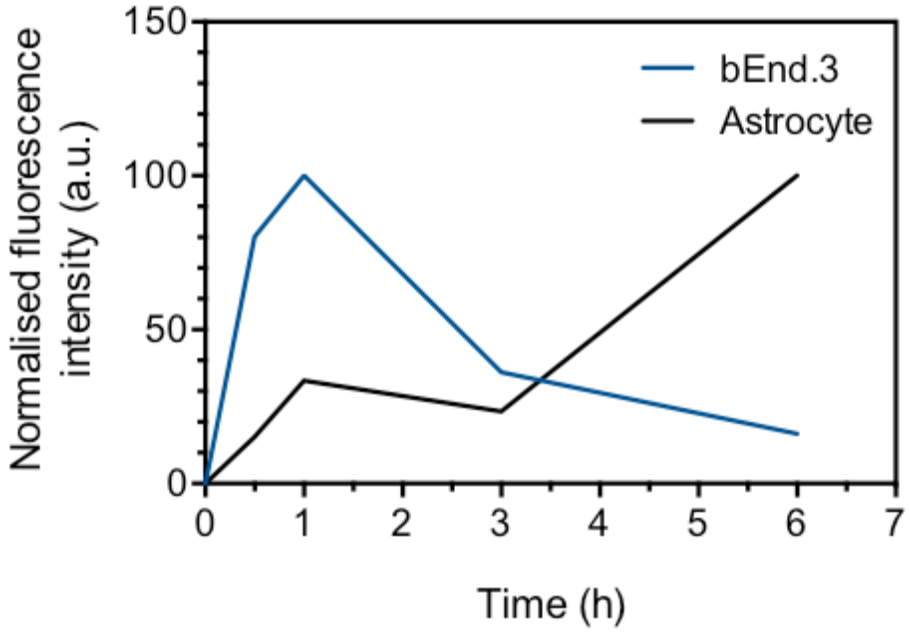

Figure 5.15. Normalisation of figure 5.14. Results normalised to the highest intensity values obtained for each group. Error bars: S.E.M.

5.6. Real Time 4D Confocal Imaging of Transcytosis at the Macroscale

To examine the timescale of apical to basolateral polymersome transcytosis as it occurs in real time, live four-dimensional (*xyz, t*) confocal videos were acquired of the transwell filter area in transwells with or without endothelial cells. Videos were captured with a 10X objective in order to observe transcytosis of a high concentration of polymersomes applied to the apical transwell compartment, observing the 'macroscale' transcytosis of a population of polymersomes. Z-stacks were acquired in resonant imaging mode on a millisecond resolution, effectively providing real time z-stack imaging or 4D imaging. Snapshots from the video can be seen in figure 5.16a, where polymersome fluorescence is visible on the basolateral side of the monolayer at the snapshot taken at 8 minutes. To obtain a more precise view of polymersome fluorescence in the transwell area, fluorescence intensity of A-EP in the *z* plane (corresponding to transwell filter depth) over time was converted into a heat map as

shown in figure 5.16b. Red corresponds to higher intensities and green to lower. Polymersome movement was slow in the control filter without cells, indicative of passive diffusion. Here, the majority of fluorescence remained within the transwell membrane itself or slightly beneath it after 30 minutes. In the bEnd.3 monolayer transwell, fluorescence had shifted from above the membrane to below it by 20 minutes. Fluorescence can be observed below the membrane in less than a few minutes from the start of the video, showing rapid transcytosis. Overall, polymersomes moved across the porous membrane faster in the presence of a bEnd.3 monolayer compared to the cell-free control, and also further away from the membrane in the same incubation time.

5.7. Transcytosis Efficiency of A-EP and Free Angiopep-2

To investigate whether transcytosis of Angiopep-2-POEGMA-PDPA occurs at rates comparable to the Angiopep-2 peptide alone, the intracellular fluorescence of A-EP (final concentration of Angiopep-2 in polymersomes: 1.75 pM) or free Angiopep-2 (1.75 pM) was compared over time in bEnd.3. Figure 5.17 shows fluorescence quantified from confocal images obtained after 10 or 60 minutes of incubation with either the peptide or polymersomes. Angiopep-2 fluorescence was low at 10 minutes, but had doubled after 60 minutes. Conversely, A-EP fluorescence started relatively high at 10 minutes and had decreased after 60 minutes. This indicates that transcytosis of Angiopep-2 is much slower than A-EP transcytosis. The decrease in A-EP fluorescence from 10 to 60 minutes indicates that ‘net’ endocytosis has already stopped and shifted to net exocytosis. Overall, it can be concluded that A-EP transcytosis is more efficient than the peptide alone.

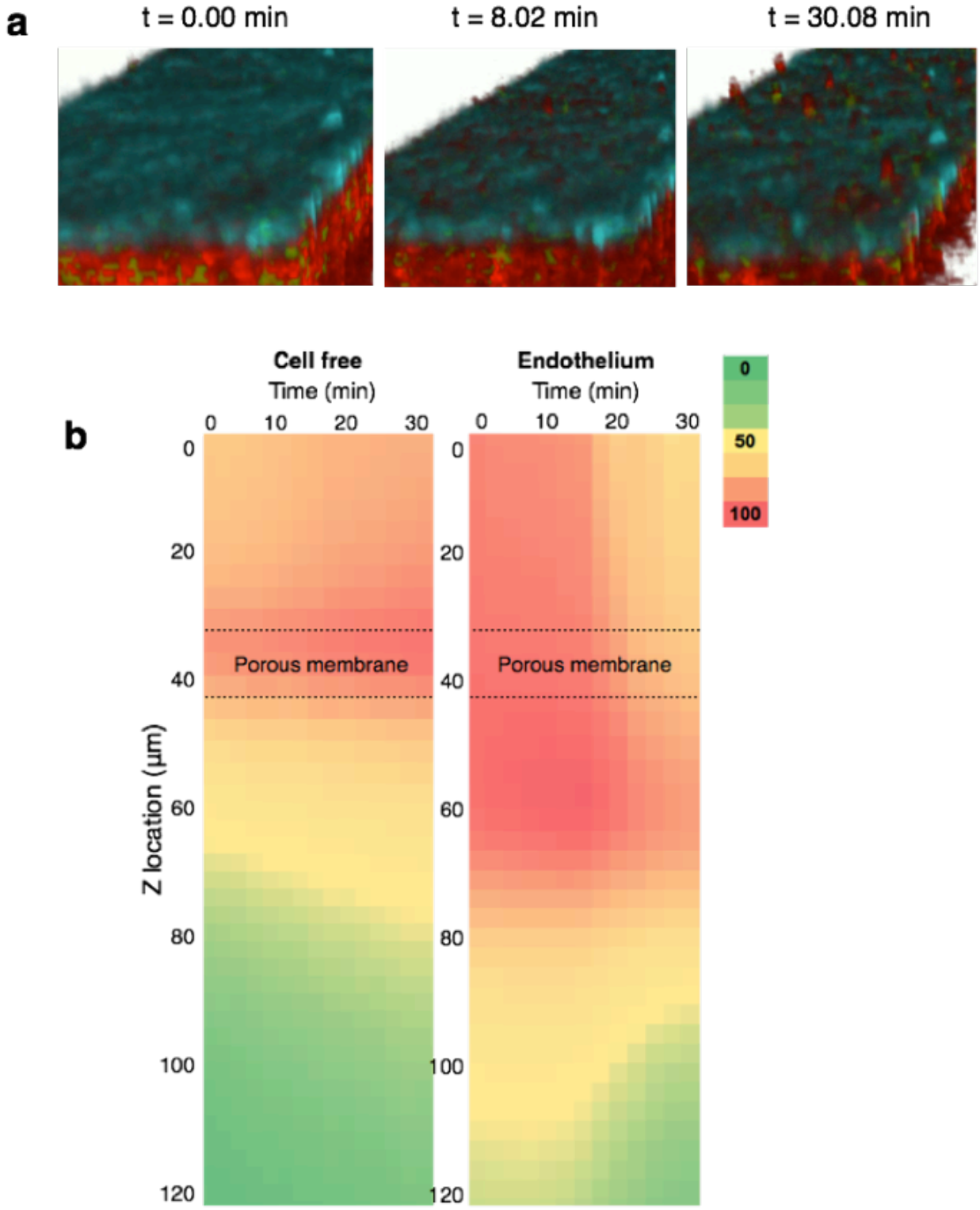

Figure 5.16. Real-time 4D confocal imaging of transcytosis. a) Snapshots from the video acquired from live cell confocal 4D imaging. **b)** Heat map of polymersome location in the extended transwell area over time, obtained through real time 4D imaging.

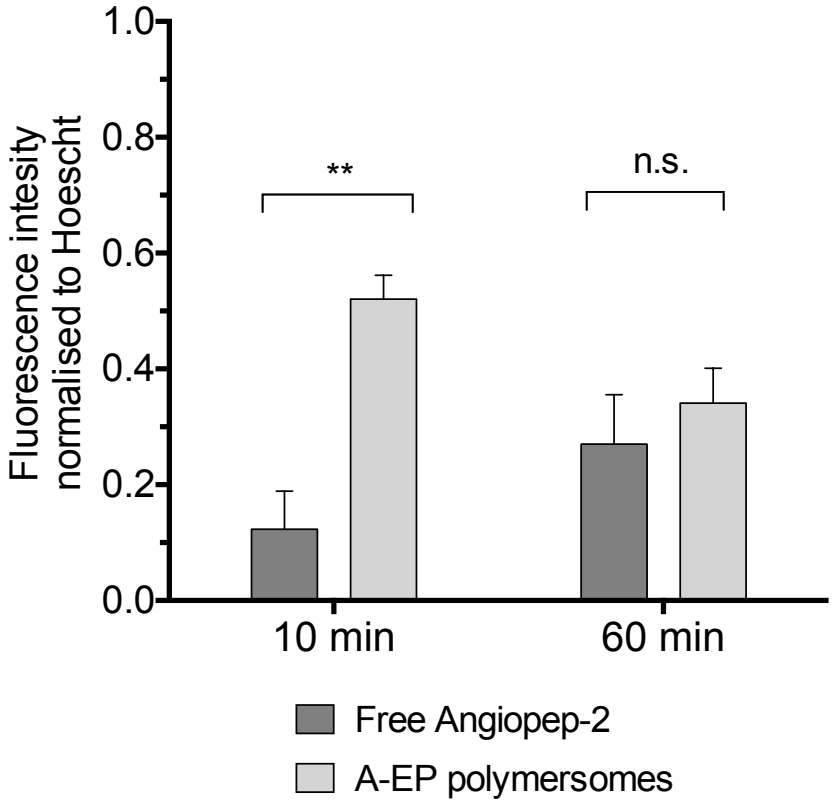

Figure 5.17. Intracellular fluorescence of A-EP compared to free Angiopep-2. Error bars: S.E.M., n=3, student's independent t-test, $p < 0.05$.

Co-incubation with polymersomes and free peptide provides an indirect way to understand whether transcytosis is more efficient of Angiopep-2 alone or when attached to polymersomes. Representative confocal images obtained at 10 and 60 minutes are displayed in figure 5.18, showing an overlap between free peptide and polymersomes.

Quantification of fluorescence of the Angiopep-2 and A-EP channels is shown in figure 5.19, alongside that obtained from incubating peptide or polymersomes only (figure 5.17) for comparison. After 10 minutes of co-incubation, A-EP fluorescence is of similar intensity as Angiopep-2, and much lower than that of A-EP after 10 minutes with no competing ligand. The free peptide fluorescence remains similar to levels without competition. On the contrary, A-EP fluorescence at 10 minutes has decreased drastically when co-incubated with free peptide than without competition. This shows

that Angiopep-2 and A-EP compete for LRP-1 binding and endocytosis, which is expected, but also that the free peptide is more likely to inhibit polymersome internalisation than vice versa at 10 minutes. When co-incubated, the intensity of A-EP and Angiopep-2 are both markedly higher at 60 minutes compared to when they are added without competition. However, competing A-EP shows a biphasic shift in behaviour compared to the A-EP only control: decreased endocytosis at 10 minutes, and increased intracellular residence i.e. decreased exocytosis at 60 minutes. The biased inhibition of A-EP transcytosis rather than Angiopep-2 may be due to a more rapid or efficient endocytosis, intracellular trafficking and exocytosis pathway occurring for A-EP than for Angiopep-2.

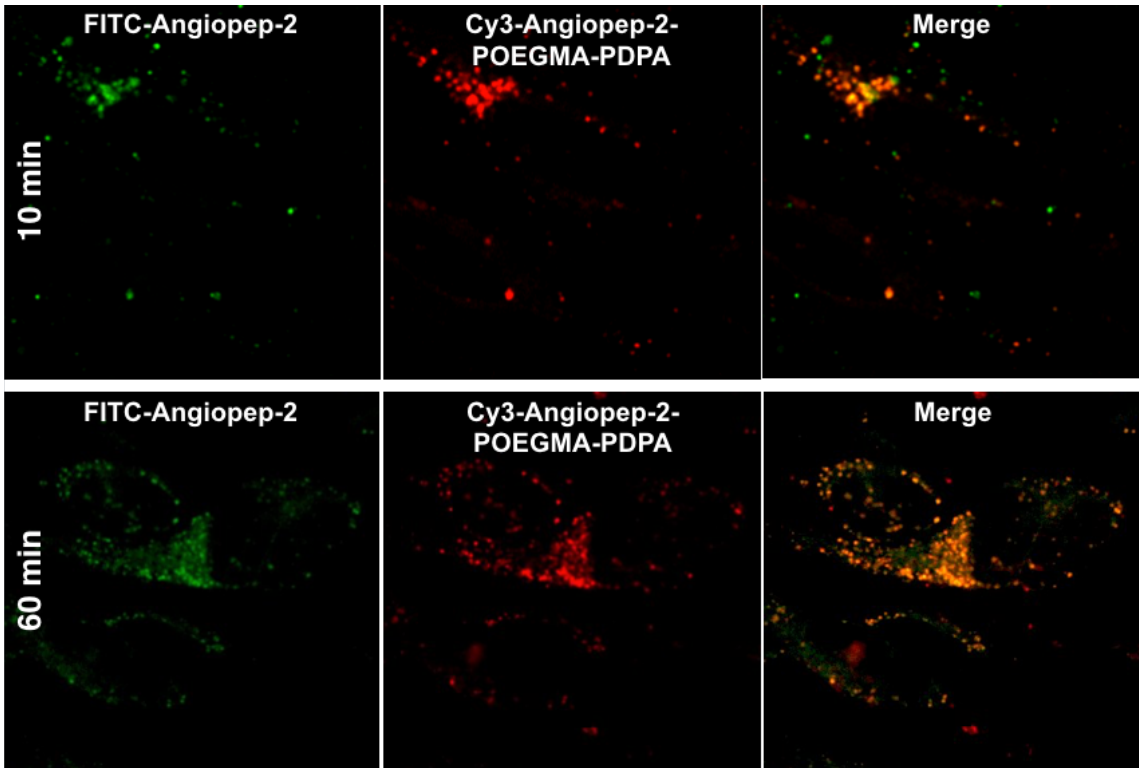

Figure 5.18. **Confocal images of A-EP and Angiopep-2 co-incubated in bEnd.3.**

The biased enhanced transcytosis of A-EP compared to Angiopep-2 cannot be due to differences in a concentration-dependent response as the same molarity of Angiopep-2 (1.75 pM) was used between the peptide and in polymersomes. Other factors must be

modulating transcytosis efficiency, such as the density of Angiopep-2 in the polymer brush.

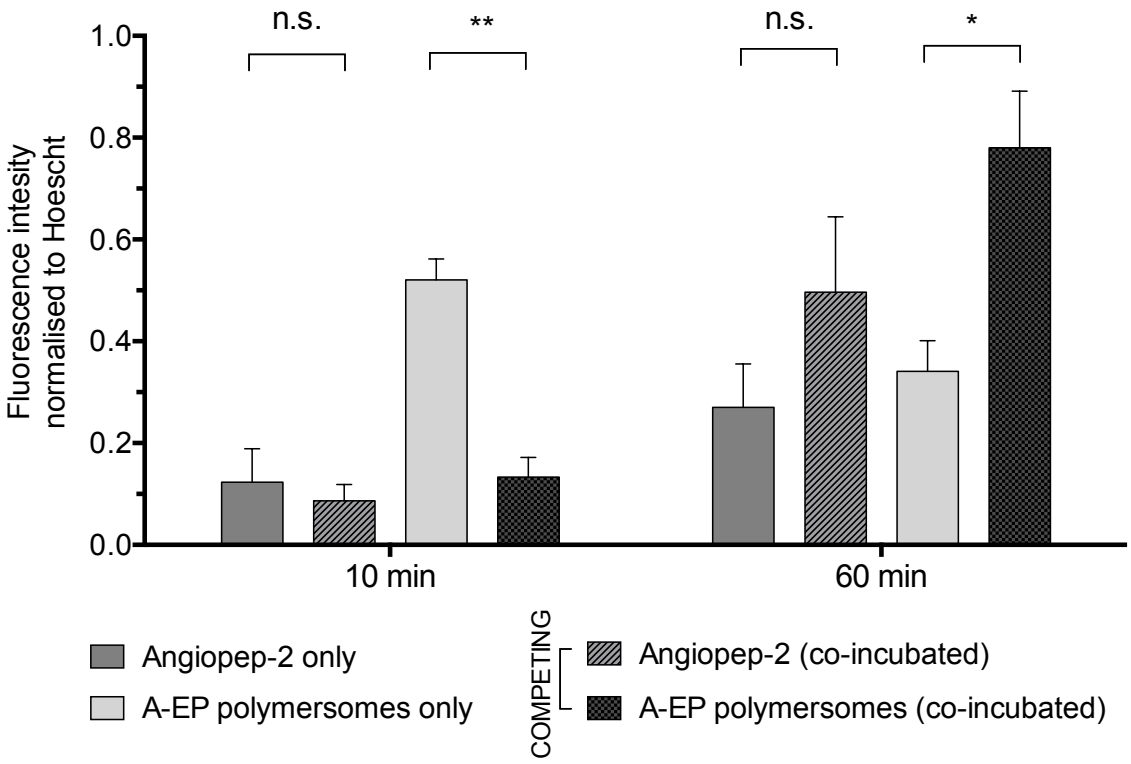

Figure 5.19. **Quantification of Angiopep-2 and A-EP fluorescence when co-incubated.** Comparison of intracellular fluorescence intensity in bEnd.3 of Angiopep-2 unconjugated or when attached to polymersomes. n=3, error bars: S.E.M, student's independent t-test, *p<0.05.

5.8. Improving Transcytosis Efficiency by Tuning Angiopep-2 Ligand Density

Ligand-receptor interactions (and subsequent receptor-mediated internalisation) are determined by a number of factors, including ligand density. Work by Tsourkas et al. demonstrated an intermediate optimal ligand density for cell-targeting nanoparticles (Elias, Poloukhtine et al. 2013). Similarly, the number of OX26 antibodies per immunoliposome was determined to be around 30 to achieve optimal CNS delivery via the transferrin receptor (Huwyler, Wu et al. 1996). The number of Angiopep-2 ligands per POEGMA-PDPA polymersome were thus calculated, and the transcytosis

efficiencies of polymersomes with increasing ligand densities were determined in a transcytosis assay.

5.8.1. Calculations of Number of Angiopep-2 Ligands per Polymersome

Through calculating the number of polymers in the membrane (N_{agg}) of a POEGMA-PDPA vesicle of the radius ***r***, it is possible to derive the number of Angiopep-2 ligands (N_{Ligand}) per polymersome. For Methodology and full calculations, refer to section 3.10 of chapter 3. For an average 80nm vesicle of $POEGMA_{25}$-$PDPA_{114}$ as used in this project, the number of Angiopep-2 peptides per vesicle are given in table 5.1:

Molar % of Angiopep-2-POEGMA-PDPA	N_{Ligand} per 80nm vesicle
0	0
1	13
2	26
3	40
4	53
5	66
6	79

Table 5.1. Calculations of N_{Ligand} with increasing molarity of A-EP.

5.8.2. Transcytosis Efficiency as a Function of N_{Ligand}

Measuring the apical and basolateral concentrations of a ligand over time provides an estimate of the transcytosis efficiency, i.e. the percentage of total ligand present in the basolateral compartment after a given incubation time. The transcytosis efficiency of polymersomes as a function of number of Angiopep-2 ligands was quantified in a transwell assay. Figure 5.20 shows transcytosis efficiency of A-EP polymersomes after 60 minutes as a function of increasing Angiopep-2 in the polymer brush (denoted $A\text{-}EP_x$ for number of Angiopep-2 ligands). POEGMA-PDPA polymersomes without Angiopep-2

did not migrate to the basolateral compartment, whilst A-EP$_{13}$ had a transcytosis efficiency of 72±8% (n=3) of total polymersome fluorescence intensity present in the basolateral compartment. Increasing ligand density to 26 caused the highest transcytosis efficiency of 93±6% (n=3) after 60 minutes. Values rapidly declined at the use of Angiopep-2 above A-EP$_{26}$, with a slight increasing trend from A-EP$_{40}$ to A-EP$_{79}$. Overall, these results are consistent with the hypothesis that ligand density is optimal for cell uptake in an intermediate range, with 26 Angiopep-2 per 80nm polymersome inducing the highest amount of transcytosis at 60 minutes.

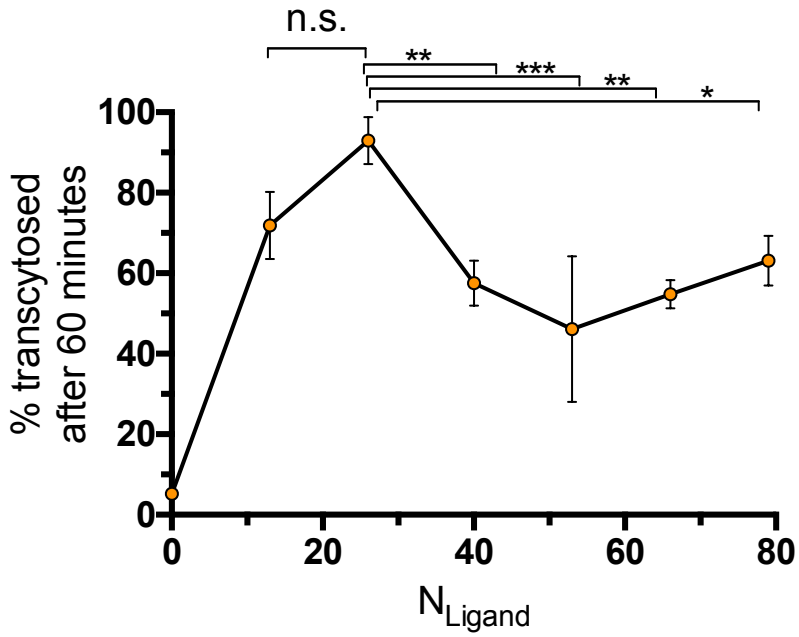

Figure 5.20. **Transcytosis efficiency after 60 minutes as a function of Angiopep-2 ligand functionalisation.** 0 is POEGMA-PDPA without Angiopep-2. Statistical analysis: ordinary one-way ANOVA. Error bars: S.E.M. *p <0.05.

A caveat of measuring transcytosis efficiency as the apical-to-basolateral transfer of materials over time is the bilateral expression of LRP-1 at the apical and basolateral BEC plasma membrane. In order to account for the potential basolateral-to-apical transcytosis of Angiopep-2-POEGMA-PDPA, the transwell assay was repeated to explore whether the transcytosis trends observed change over time. Polymersome fluorescence in the basolateral compartment measured over 24 hours is displayed in

figure 5.21. In addition to displaying the highest transcytosis efficiency after 60 minutes (figure 5.20), A-EP$_{26}$ also showed depletion from the basolateral compartment at later times, indicating polymersomes have shifted either to the transwell pores or recycled to the apical compartment. A-EP$_{13-53}$ formulations all showed a decreasing presence in the basolateral compartment over time, indicating recycling to the apical compartment. This effect was not observed in A-EP$_{66}$ to A-EP$_{79}$, where transcytosis has plateaued after 6 hours in both cases. This effect persisted at 24 hours, which may be due to complete bilateral saturation of LRP-1.

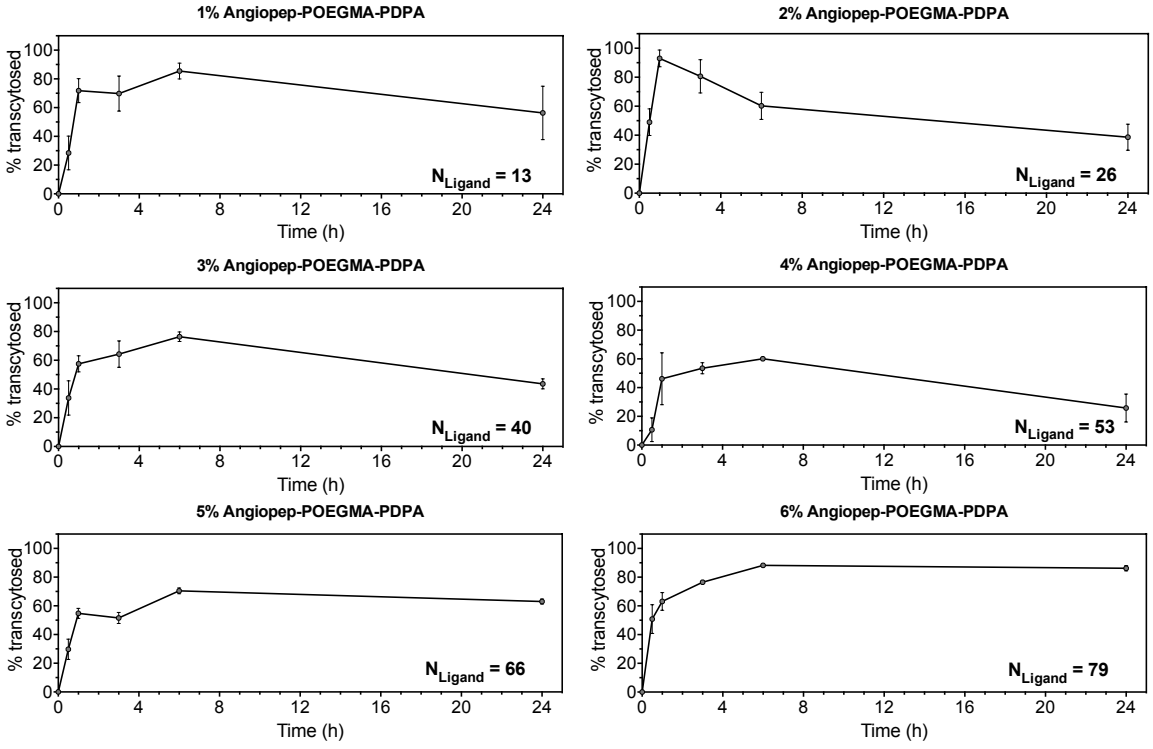

Figure 5.21. Transcytosis over 24 hours as a function of N_{Ligand}. n=3, error bar: S.E.M.

5.9. Discussion

The bEnd.3 *in vitro* blood-brain barrier model used herein provided some blood-brain barrier characteristics sufficient for experiments elucidating simplistic interactions between Angiopep-2-polymersomes and endothelial cells. The model expressed the correct set of tight junction protein markers, but had a lower immunoreactivity than expected with some protein expression also seen in the cytoplasm as opposed to along

the plasma membrane. However, TEER values were higher than reported in literature for bEnd.3 cells. The absence of transcytosis of non-targeting POEGMA-PDPA further reinforces a restrictive monolayer. The addition of pericytes raised the average TEER values, indicating an enhancement of the BBB phenotype. However, there is still a large gap between *in vitro* and *in vivo* TEER values, and the low amount of FITC-dextran as well as POEGMA-PDPA diffusion in the permeability assay seems to indicate a low amount of paracellular leakage. Overall, although the bEnd.3 BBB model has shortcomings, it is in this case an adequate model to use for probing transcytosis.

An advantage of using an *in vitro* model is the methods available to probe cell-polymersome interactions, such as 4D confocal resonant imaging where z-stacks of the transwell filter membrane can be obtained on a millisecond scale. The real time imaging of polymersome movement through a cell-free or BEC transwell illuminated the drastic difference in speed between active transportation and random diffusion of polymersomes across the filter pores. This finding was supported by other kinetics experiments, such as the transwell assays with FITC-dextran as a control. It is unclear why fluorescence intensity increases rapidly underneath the filter, as polymersome access across the filter is limited by diffusion. The relatively high intensity underneath the filter in the heatmap may be an artifact of the normalisation calculations by the confocal software. Nevertheless, A-EP increase within the z stacks corresponding to the cells showed a trend of increased movement across the bEnd.3 monolayer compared to the cell-free control. This is consistent with the idea that transcytosis is a rapid process and contrasts passive diffusion.

The low availability of antibodies to the extracellular domain of LRP-1 complicates assessing the interaction of the ligand binding domains to polymersomes. In an unstimulated state, antibody immunofluorescence against the intracellular domain of the antibody is diffuse within the cytoplasm. However, when bEnd.3 were incubated

with A-EP, the distribution of LRP-1_{ICD} became punctate and heavily based around the plasma membrane. It is highly likely that the intracellular domain of LRP-1 contains the spatial cue to transcytosis. Indeed, when LRP-1 is internalised the extracellular domain is shed into the extracellular space. Further work is required to obtain the receptor recycling rates, and to elucidate the relative contributions of domains to transcytosis.

Variation of Angiopep-2 density showed a bell-shaped distribution of transcytosis efficiencies. The ability to control ligand density confers a huge advantage when adjusting targeting to *in vivo*. Increasing the amount of targeting peptide does not equate to a higher transcytosis rate and may result in vastly different ligand-receptor interactions compared to lower ligand density.

Importantly, the kinetics of A-EP internalisation by bEnd.3 cells differ from that of non-transcytosing cells, i.e. astrocytes in this case. Uptake by endothelial cells displayed a much lower fluorescence compared to astrocytes. Furthermore, endothelial cell fluorescence peaked at 30-60 minutes and was nearly absent at 3-6 hours, whereas astrocyte fluorescence gradually increased over time. This difference highlights the differential internalisation behaviour by astrocytes and endothelial cells, with endocytosis by astrocytes being a significantly slower process than transcytosis.

Work within this section has utilised a 3D model of brain endothelial cells to confirm that transcytosis of Angiopep-POEGMA-PDPA polymersomes is mediated by LRP-1 and that it occurs within 10-15 minutes on the macroscale, as evidenced by polymersome fluorescence in the transwell filter pores. A-EP remained associated with LRP-1 for longer periods of time, which may be due to LRP-1 remaining at the opposing plasma membrane. Future work should examine LRP-1 receptor recycling rate to obtain a clearer view of the bidirectional transcytosis occurring at the BBB, and its effect of net cargo movement.

Chapter 6.

RESULTS AND DISCUSSION III

Elucidating Blood Brain Barrier Transcytosis Mechanisms

6.1. Introduction

Work presented in this section was undertaken with the aim to advance understanding of the cellular processes mediating transcytosis in brain endothelial cells. A combination of qualitative and quantitative confocal microscopy was used in conjunction with antibodies or small molecule inhibitors against proteins of interest. Here Angiopep-2-conjugated polymersomes had a dual role: contributing to the general understanding of how transcytosis works at the blood brain barrier, but also more specifically how A-EP polymersomes might traverse the barrier for drug delivery. Knowledge of the latter is useful for bridging the gap into clinical translation.

6.1.1. Small Molecule Modulators of Endocytosis

There are a number of pharmacological small molecule drugs available which inhibit specific protein mediators of endocytosis. These can be applied to explore mechanisms of transcytosis. A frequently used method to investigate the role of a protein is to genetically modify the cell to overexpress or underexpress the gene encoding the protein of interest. However, attempts to transfect brain endothelial cells often result in the recession of barrier-like properties and cellular stress (Zhang, Mitin et al. 2009, Abbott 2016). On the other hand, small molecule inhibitors are more practical to use as they immediately cause inhibition, allowing the short-term use before the onset of detrimental effects. Therefore, small molecule inhibitors are more convenient than genetic modification of the target.

6.2. Role of Caveolae in Transcytosis

Ultrastructural studies alone are insufficient to identify the nature of intracellular vesicles carrying cargo in transcytosis. Because caveolae are frequently implicated as the 'primary' mediators of transcytosis in pulmonary microvasculature, the colocalisation of polymersomes with caveolar protein caveolin-1 was examined in bEnd.3. In an unstimulated state, caveolin expression can be seen at the plasma membrane along the cells (figure 6.1).

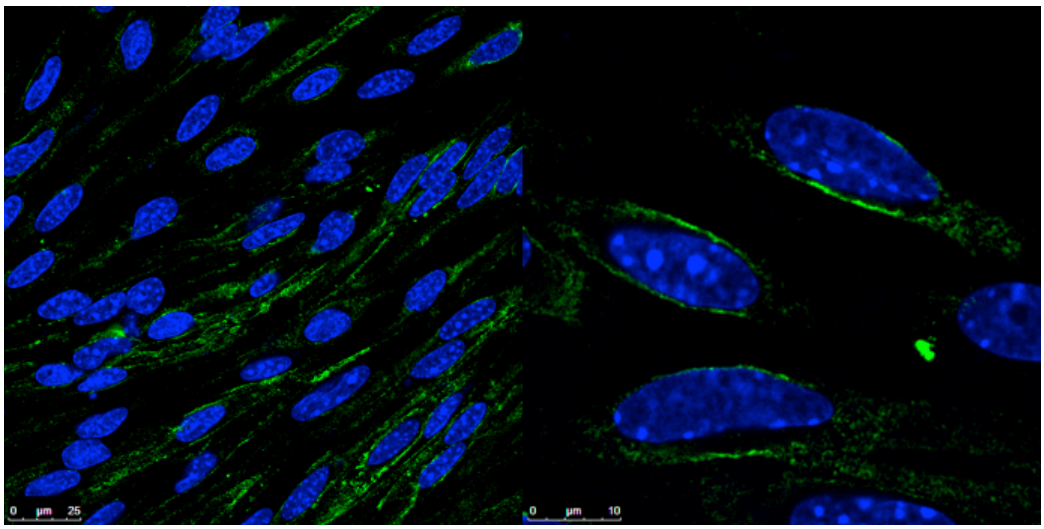

Figure 6.1. Expression of caveolin-1 by bEnd.3 cells. Cav-1 (green), DAPI (blue): nuclei.

Next, A-EP polymersome fluorescence was tracked in brain endothelial cells, obtaining colocalisation profiles with caveolin-1. Partial overlap was observed initially at 10 minutes of incubation as visualised from on top of the cells (figure 6.2). However, 3D z-stack projections (figure 6.3) show no apparent colocalisation at 10 minutes, and furthermore the appearance of A-EP in pores at this time. A few cytoplasmic puncta with fluorescence overlap were observed at 60 minutes (figure 6.4). However, Pearson's correlation coefficient were low at 0.2±0.11 (n=3) and -0.02±0.04 (n=3), at 10 and 60 minutes respectively (figure 6.5). Overall, these findings fail to show a role caveolae as essential structures for apical to basolateral transcytosis, particularly as a higher colocalisation would have been expected at around 10 minutes when the majority of transcytosis is occurring.

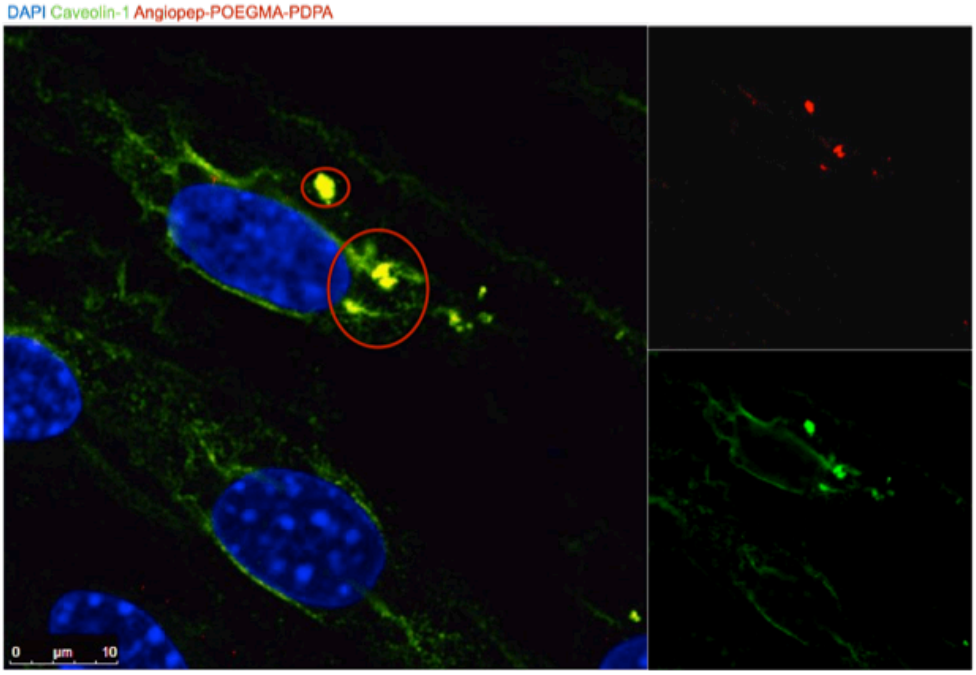

Figure 6.2. Polymersome colocalisation with Cav-1 after 10 minutes. A-EP (red) 10 minutes after addition to bEnd.3 cells, counterstained for caveolin-1 (green) and nuclei (blue).

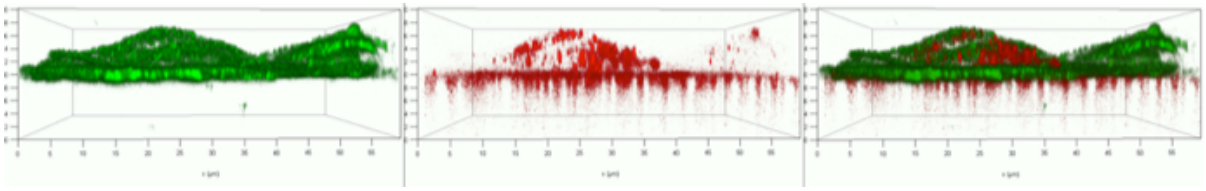

Figure 6.3. 3D projection of caveolin-1 and A-EP location in bEnd.3 cells after 10 minutes. Cav1 (green) and A-EP (red).

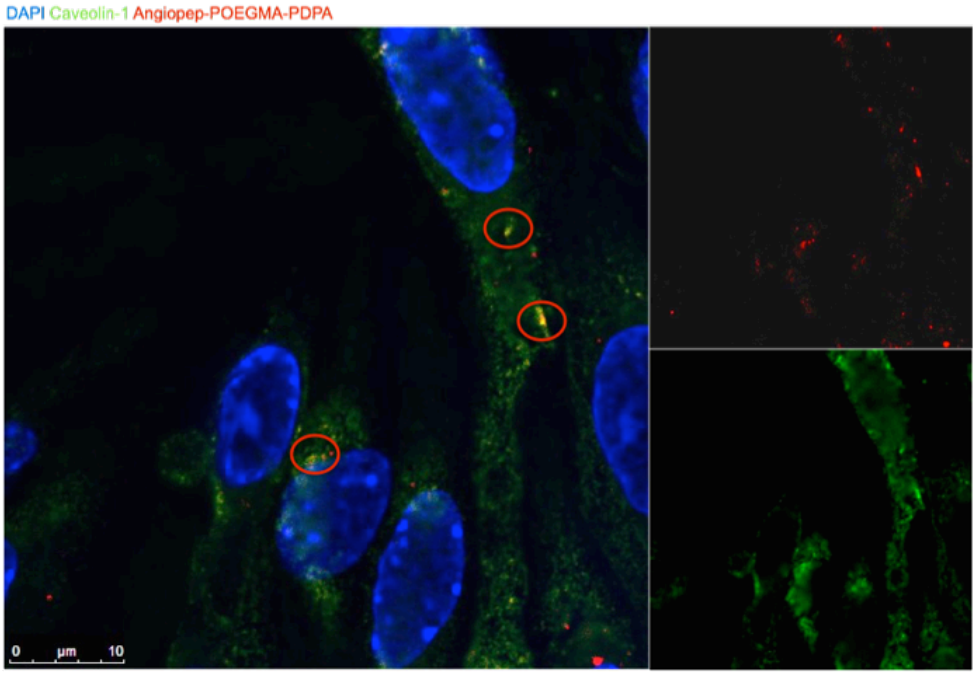

Figure 6.4. A-EP colocalisation with cav-1 after 60 minutes in bEnd.3. A-EP (red), cav-1 (green) and DAPI (blue). Areas of colocalisation are highlighted in red circles.

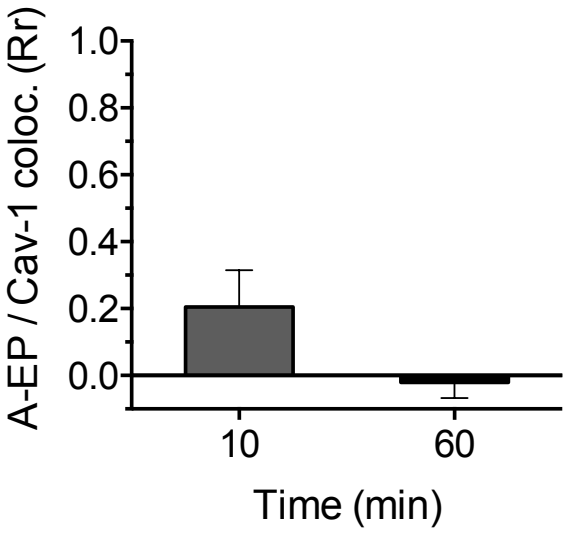

Figure 6.5. Quantification of colocalisation of caveolin-1 and A-EP polymersomes. n=3, error bars: s.d.

6.3. Disruption of Membrane Lipid Rafts with Methyl-β-Cyclodextrin

Caveolae are dependent on cholesterol-enriched lipid rafts in the plasma membrane, and depletion of cholesterol with agents such as methyl-β-cyclodextrin (CD) causes the disruption of caveolae (Le and Nabi 2003). However, depletion of cholesterol also inhibits formation of clathrin-coated structures (Rodal, Skretting et al. 1999). If extraction of cholesterol from the bEnd.3 plasma membrane causes inhibition of transcytosis in addition to disappearance of Cav-1 immunoreactivity, it could indicate that caveolae mediate transcytosis of A-EP. CD was used to deplete cholesterol from either the apical or basolateral plasma membrane by adding the agent to the apical or basolateral compartment of the transwell. TEER values were assessed in order to ensure that tight junction integrity and monolayer tightness remained intact after treatment, and showed no significant difference after treatment on either polarity of plasma membrane as shown in figure 6.6. Next, amount of cholesterol shed into the cell media was quantified via a fluorescence assay. This was done in serum free cell media in order to avoid false positives by cholesterol from FBS-supplemented media. Addition of CD to the basolateral transwell compartment caused a 4-fold increase in free cholesterol in basolateral media, as well as a 2-fold increase in free cholesterol into the apical media (figure 6.7). These effects were different when CD was added to

the apical side of the cells, resulting in a less than 2-fold increase in cholesterol into the apical media and approximately 3.5-fold increase into the basolateral media. In both cases cholesterol depletion was more efficient in the basolateral plasma membrane.

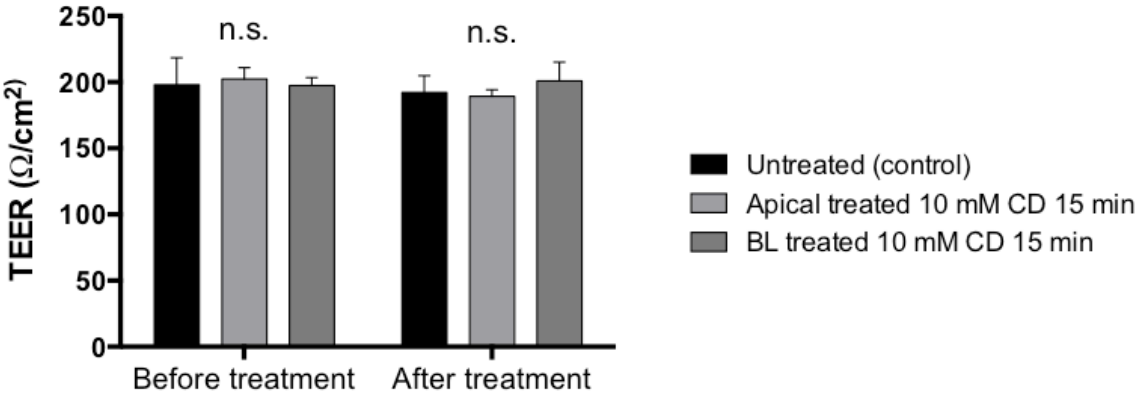

Figure 6.6. TEER values of a bEnd.3 monolayer before and after CD treatment. Student's independent t-test, $p<0.05$, n=5.

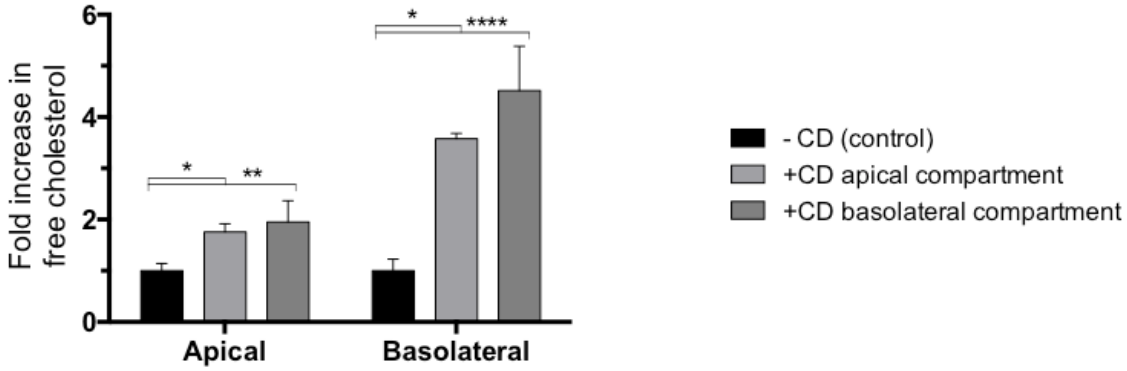

Figure 6.7. Cholesterol release into media after depletion from the plasma membrane by CD. Student's independent t-test, $p<0.05$, n=5.

Next, cells depleted of cholesterol either in the apical or basolateral plasma membrane were incubated with A-EP polymersomes for 60 minutes, fixed and counter-stained for cav-1. Surprisingly, cells stained positive for caveolin-1 even after disruption of caveolae by cholesterol depletion, with the protein appearing uniformly distributed along the entire plasma membrane (figure 6.8. Many cells positive for polymersomes

had assumed a different morphology to control cells, rounding up towards the centre rather than their normal thin elongated shapes. Overall, the cells were larger and several showed signs of blebbing, regardless of which side CD was added to. However, because the TEER values were at control levels after one hour of CD incubation, cells were still viable. Strikingly, the polymersome signal reached near saturation in many cells when CD was added to the basolateral side. This effect was not seen when CD was added at the apical side, consistent with the higher amount of cholesterol depletion in the basolateral membrane as quantified by the cholesterol quantitation assay. When CD was added to the basolateral compartment, many cells were completely saturated with polymersomes.

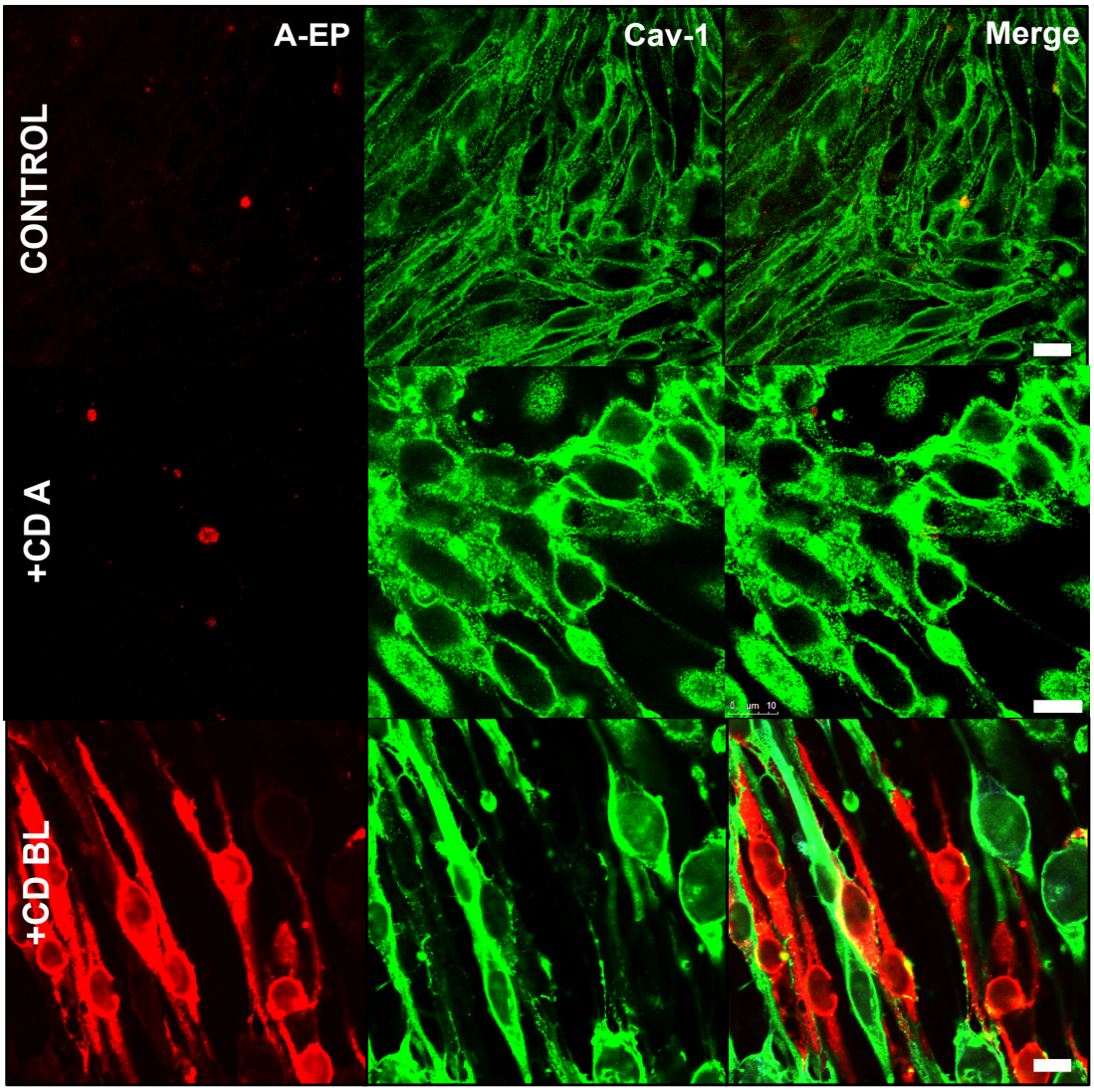

Figure 6.8. Confocal images of A-EP in cholesterol depleted bEnd.3. Intracellular location of A-EP (red) in basolateral membrane cholesterol-depleted bEnd.3 cells counterstained for caveolin-1 (green). Scale bar: 5 µm.

Figure 6.9 shows another image obtained after basolateral plasma membrane cholesterol depletion, counter-stained for caveolin-1. Interestingly, the cells positive for polymersomes have a high degree of colocalisation between caveolae and A-EP. This is markedly enhanced compared to control cells, where caveolin-1 and A-EP hardly colocalise (figures 6.2, 6.4).

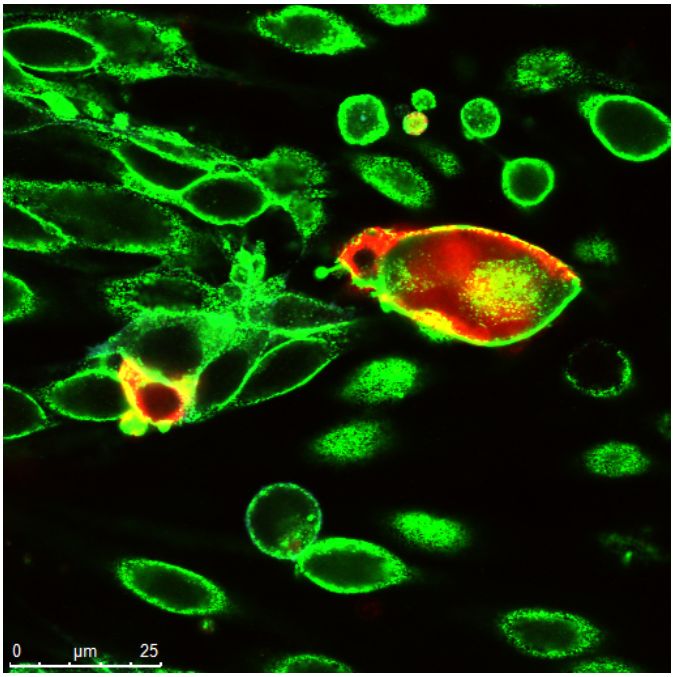

Figure 6.9. bEnd.3 swelling with polymersomes after cholesterol depletion. Cav-1 (green) and A-EP (red) in bEnd.3 depleted of cholesterol on the basolateral side.

In summary, depletion of cholesterol from the basolateral but not apical plasma membrane resulted in cells maintaining their ability to internalise A-EP polymersomes, but unable to exocytose materials. As a result cells positive for polymersomes swelled up drastically. These data suggest that cholesterol is required for exocytosis but not endocytosis of A-EP.

6.4. Role of Clathrin

Because data indicated that caveolae are not involved in A-EP transcytosis, the colocalisation of clathrin with A-EP was investigated. High magnification confocal images were obtained of A-EP in bEnd.3 cells with an antibody against the heavy chain

of clathrin, counterstained with phalloidin to visualise the cytoskeleton. A-EP fluorescence after 60 minutes is closely associated with clathrin (figure 6.10). Every A-EP puncta appears associated with a heavy chain of clathrin. However, this data is qualitative and is thus only an indication that clathrin is involved in the transcytosis of A-EP.

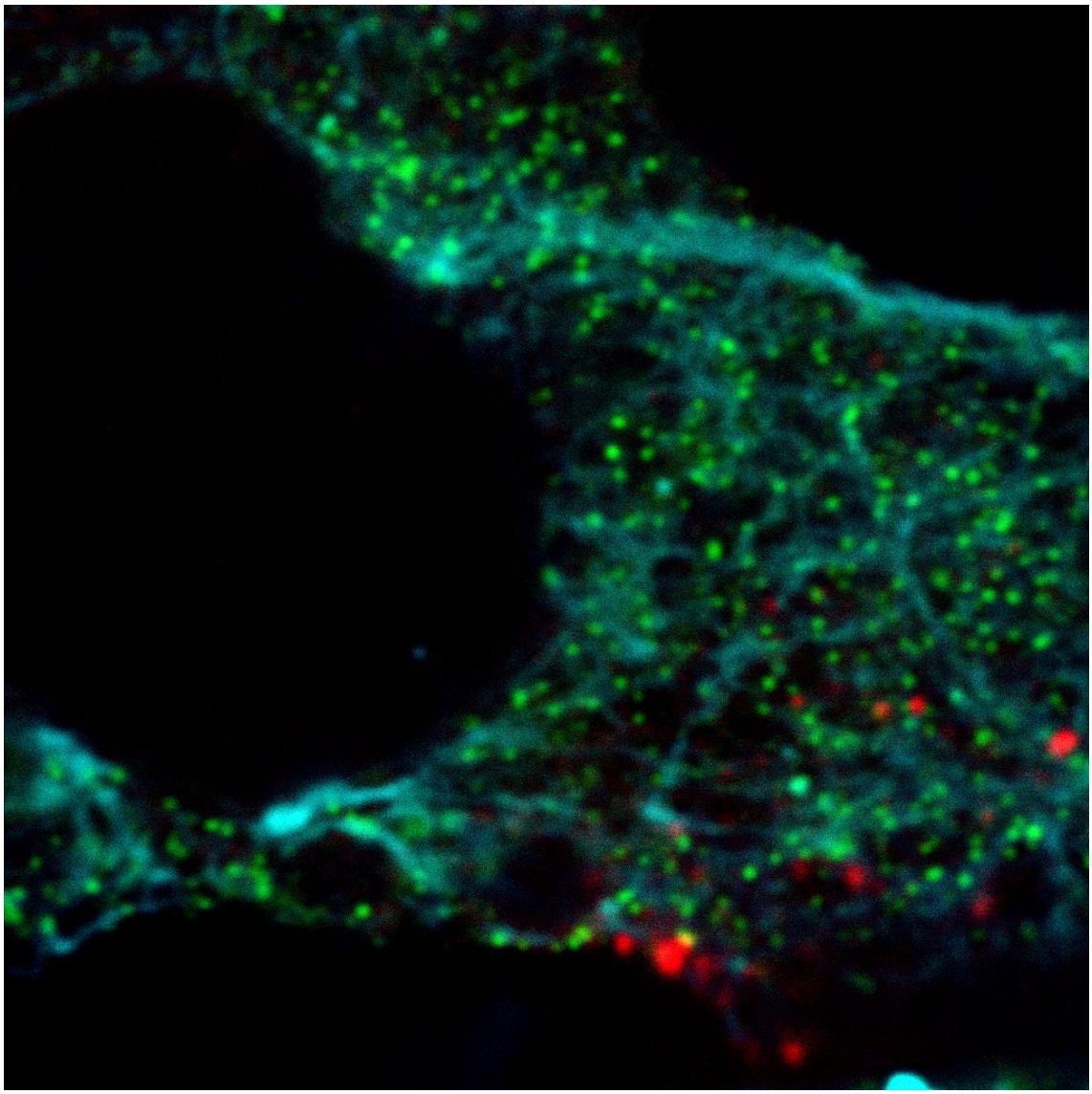

Figure 6.10. A-EP association with clathrin after 60 minutes. A-EP (red), phalloidin (cyan) and clathrin heavy chain (green).

6.5. Role of Actin in Transcytosis

Transcytosis assays combined with 3D confocal microscopy consistently indicated the appearance of A-EP inside the filter pores within 10 minutes after the start of incubation. Cytoskeletal motor proteins can quickly transport cargo from one side of a

cell to another, and were therefore of particular interest for their potential involvement in transcytosis. A study reported the caveolae-dependent endocytosis of the virus SV40 to occur through caveolar recruitment of actin and dynamin, causing temporary destabilisation of the actin stress fibres and formation of actin 'tails' (Pelkmans, Puntener et al. 2002). Subsequently, the role of actin in brain endothelial cell transcytosis was investigated.

The organisation of the actin cytoskeleton in a bEnd.3 monolayer is shown in figure 6.11. The image was acquired close to the bottom of the cells where they attach to the filter, and stress fibres are pronounced.

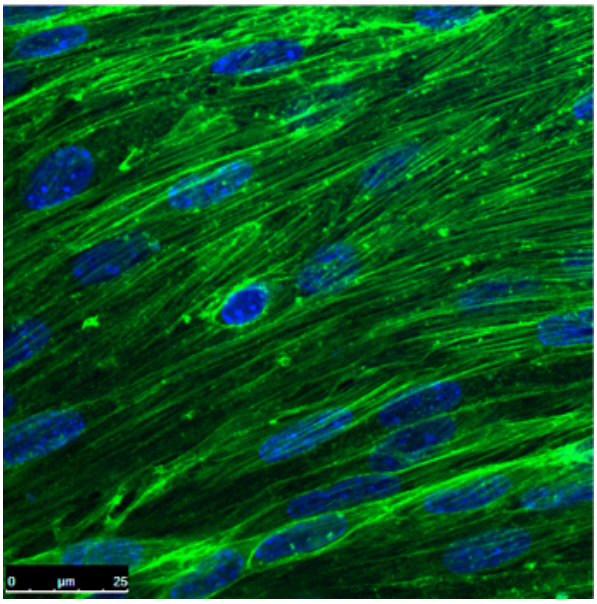

Figure 6.11. Actin cytoskeleton of bEnd.3. Phalloidin (green), nuclei: DAPI.

The organisation of the actin cytoskeleton was investigated in fixed bEnd.3 incubated with Cy5-labelled A-EP, stained with phalloidin-488 for F-actin. After five minutes there was a large overlap in fluorescence from the phalloidin and A-EP. The red/green correlation coefficient was quantified at 10, 30 and 60 minutes of incubation (figure 6.12). Confocal images of A-EP in bEnd.3 counter-stained for phalloidin are displayed in figure 6.13, with a magnification of an area of interest (arrow).

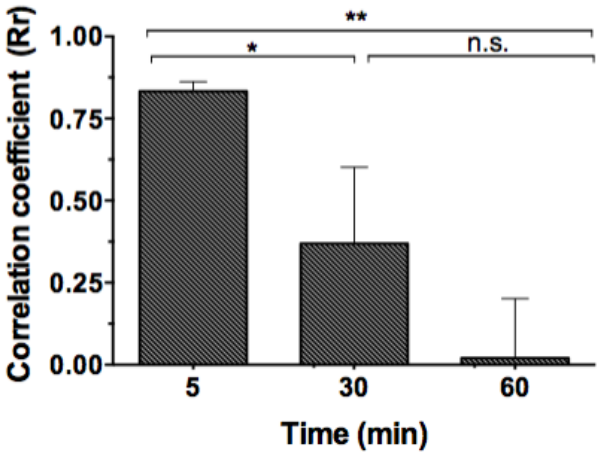

Figure 6.12. Correlation coefficient values of phalloidin and A-EP. n=3, error bars: s.d., student's independent t-test, p<0.05.

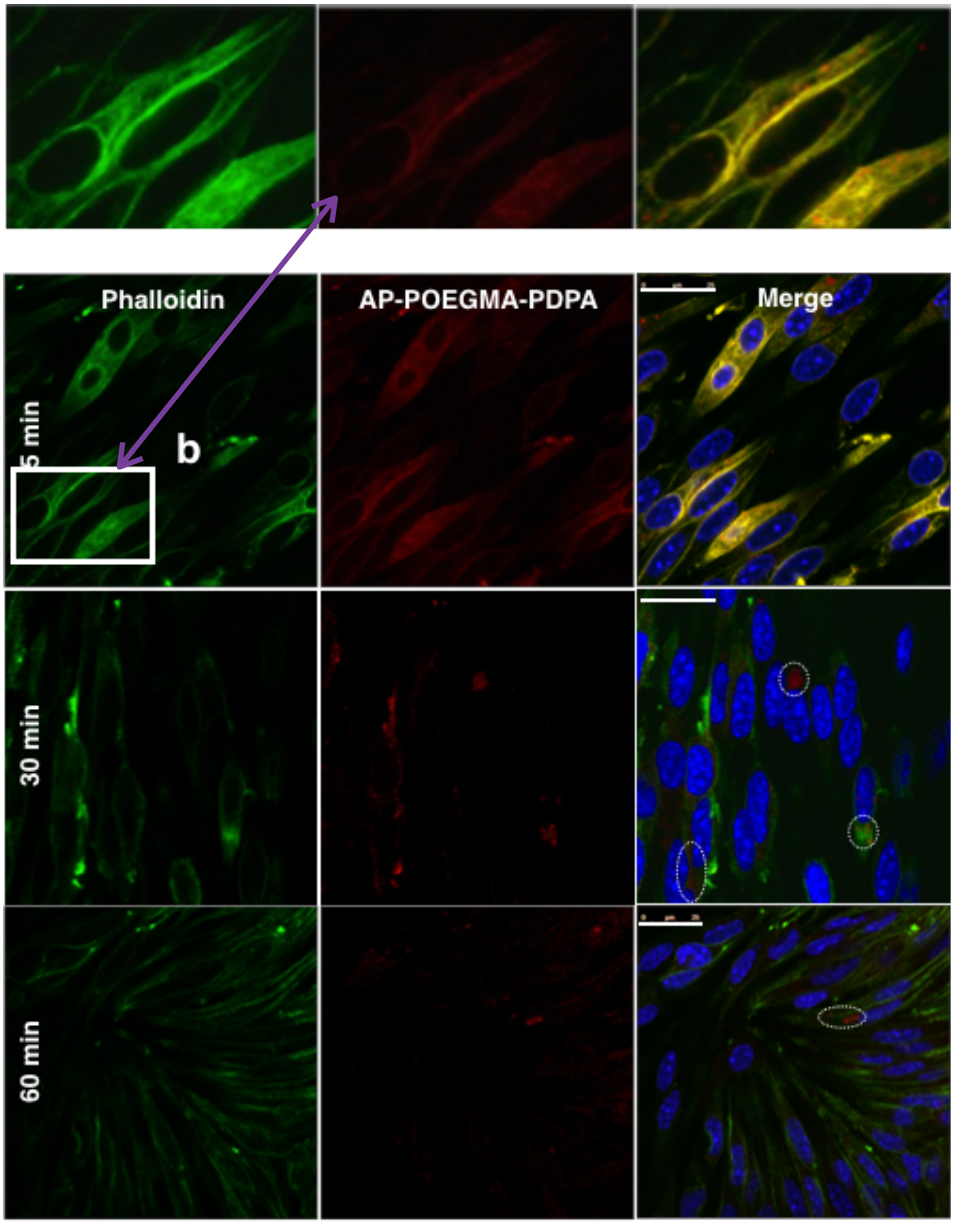

Figure 6.13. **Phalloidin and A-EP fluorescence in bEnd.3 cells over time.** Some polymersome clusters are indicated (ellipses).

From this experiment actin appears to have a role in transporting polymersomes from the apical to basolateral membrane within the first few minutes of endocytosis. The loss of colocalisation between actin and A-EP has occurred already at 30 minutes, but is pronounced after 60 minutes. However, the loss of colocalisation is independent of the vastly decreased concentration of polymersomes at 30 and 60 minutes. Future experiments should ideally utilise actin inhibitors to observe whether A-EP transcytosis inhibited. However, such inhibitors are often highly toxic to cells.

6.6. Role of Dynamin in Transcytosis

Both caveolar and clathrin-mediated endocytosis requires dynamin GTPase for the scission of an elongated membrane neck into a discrete intracellular vesicle. Therefore regardless of what kind of coat the vesicle bears, inhibition of dynamin should impair exocytosis of polymersomes. The role of dynamin in transcytosis was investigated using Dynasore, a cell permeable small molecule inhibitor of dynamin (Macia, Ehrlich et al. 2006). Cells were pre-incubated with Dynasore for 30 minutes before adding A-EP onto the monolayer and performing confocal live cell z-stack imaging. Pre-incubation with Dynasore caused polymersomes to form large aggregates on top of the cells (figure 6.14). A reconstructed z-stack shows the faint presence of A-EP underneath the monolayer, but with the majority of polymersomes closely associated with the cell surface. The inhibition of endocytosis was reversible, as addition of A-EP after washing out the Dynasore resulted in a higher fluorescence in the filter pores. The fluorescence intensity across all acquired z-stacks was quantified, and is displayed in figure 6.15 as a function of distance from the pores. This strongly indicates that dynamin is required for internalisation of A-EP in transcytosis.

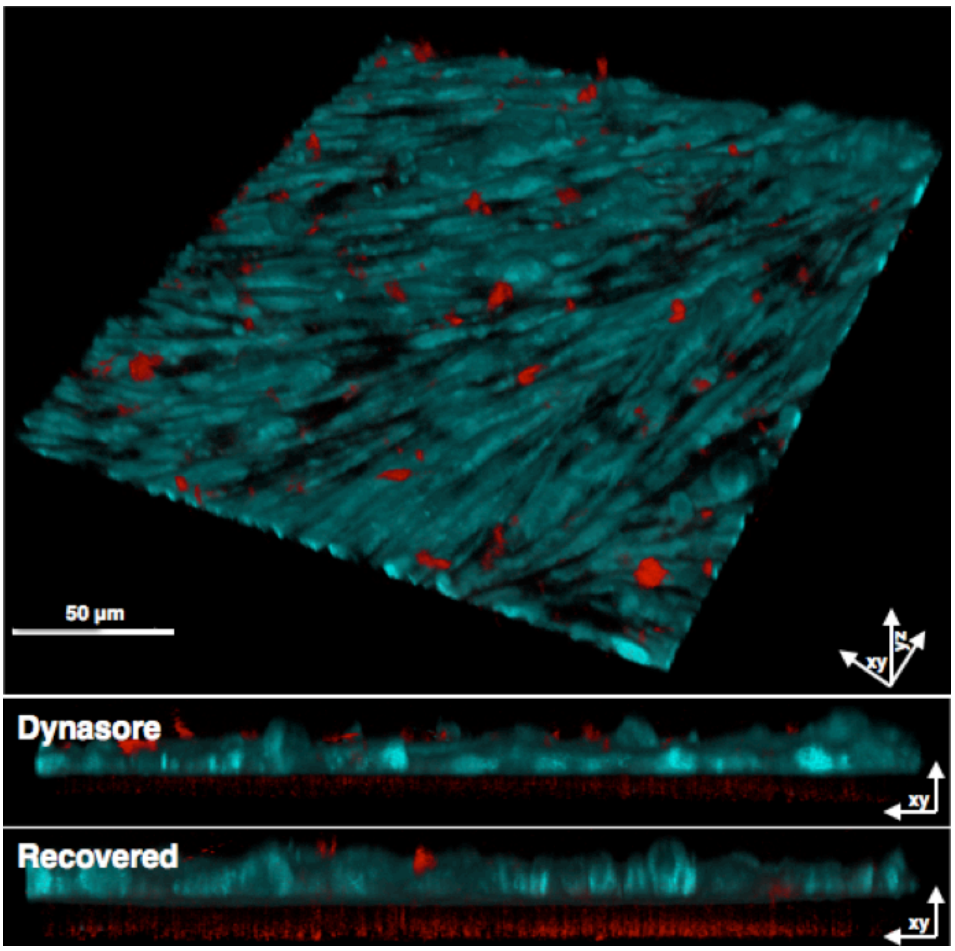

Figure 6.14. Treatment with dynasore inhibits internalisation and transcytosis of A-EP polymersomes. Confocal micrographs of live cells before and after Dynasore treatment.

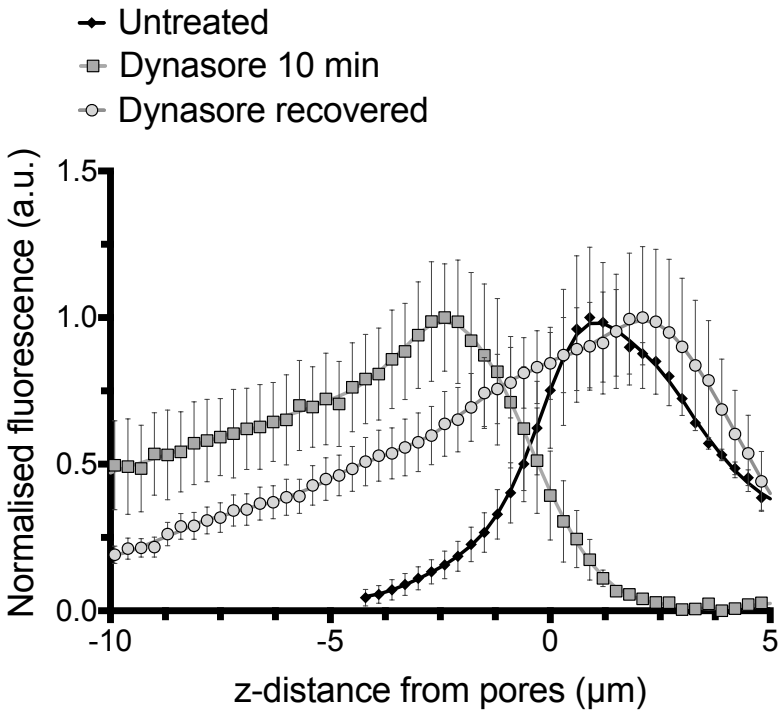

Figure 6.15. Quantification of polymersome z-stack fluorescence before and after treatment with Dynasore. 0 marks the beginning of pores, negative values above the filter and positive values within the filter. n=3, error bars: S.D.

6.7. Intracellular Transport

Clathrin-mediated endocytosis is the most common endocytosis to occur, resulting in intracellular cargo sorting through a series of endosomal compartments increasingly acidic in pH (McMahon and Boucrot 2011). Endosomes at different stages of this pathway have their own distinct protein and lipid composition, and can be distinguished as such. The intracellular fate of A-EP polymersomes was probed by using antibodies against different Rab GTPases marking certain stages of the endosomal pathway: Rab5 for early endosomes, Rab7 for early/late endosomes, Rab11 for recycling endosomes, and lysosomal associated membrane protein 1 (LAMP1) for lysosomes. Incubation times of 15, 60 and 120 minutes were chosen in order to account for the long times intracellular sorting can take (Canton and Battaglia 2012). Consistent with the hypothesis of a different non-endosomal pathway operating in brain endothelial cell transcytosis, no colocalisation was observed between A-EP polymersomes and any of the endo/lysosomal markers at any of the times examined (figure 6.16). In order to ensure that the lack of colocalisation was not because the A-EP signal was relatively low, z-stacks were acquired of the entire transwell membrane after 15 minutes of incubation and constructed into 3D projections (figure 6.17). The majority of polymersomes were present in the transwell membrane pores at this time in addition to minor intracellular presence, indicating that transcytosis of the majority of the material had already occurred at this time. Quantification with Pearson's correlation coefficient was trending towards negative, (figure 6.18) i.e. polymersomes were excluded from the Rab-positive compartments. In summary, A-EP transcytosis does not seem to involve the 'traditional' intracellular sorting through acidifying endosomal compartments.

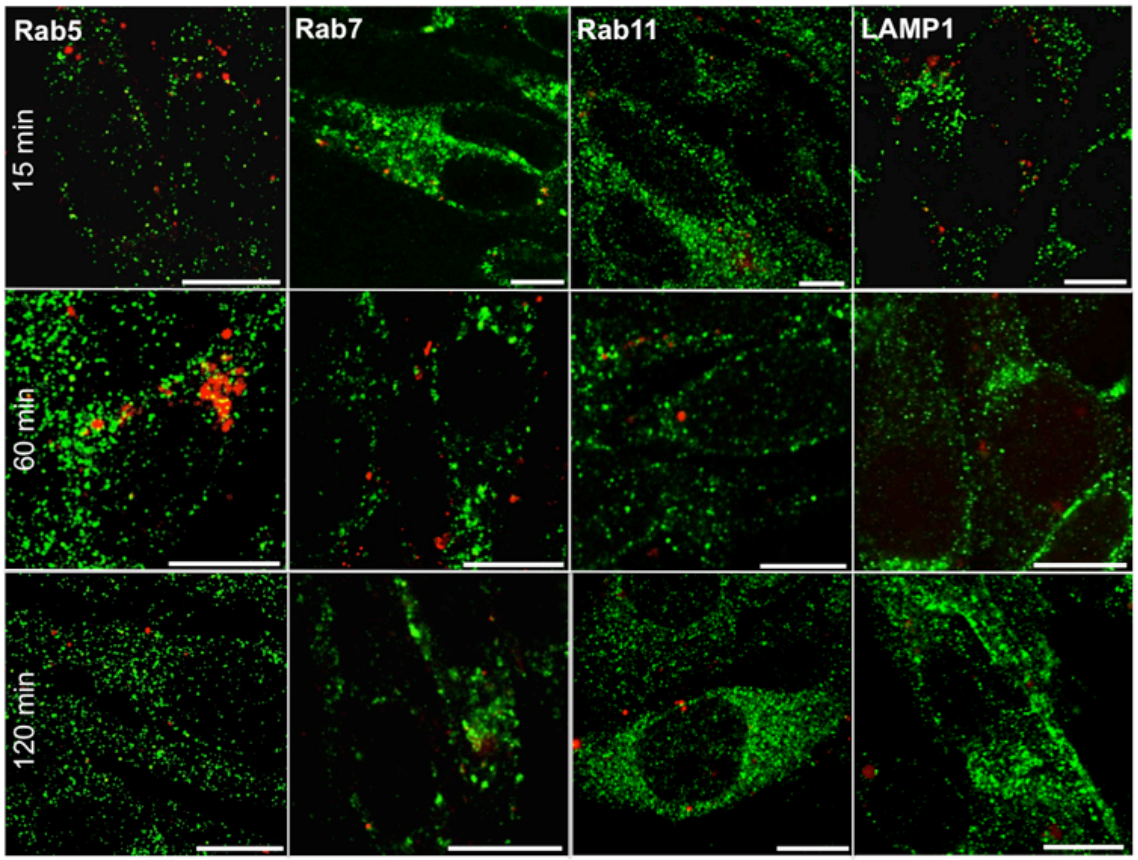

Figure 6.16. A-EP does not associate with common endosomal organelles. Colocalisation of A-EP polymersomes (red) with markers of endosomal and lysosomal pathways (green). Scale bar: 10 µm.

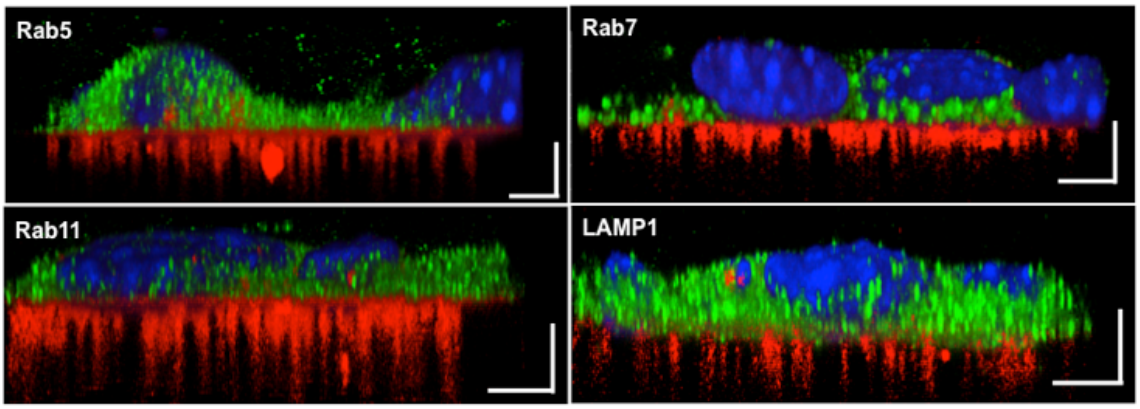

Figure 6.17. 3D projections of A-EP and endosomal markers in the transwell after 15 minutes. A-EP (red), counterstained for endo/lysosomal markers (green) and DAPI for cell nuclei (blue). Scale bar is 5 µm in the *xy* and *yz* direction.

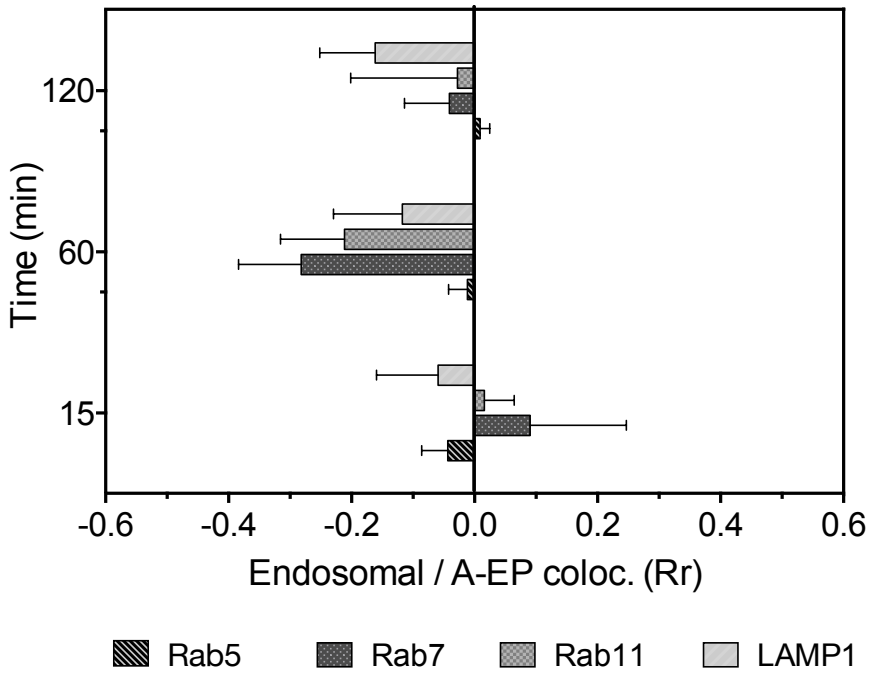

Figure 6.18. Quantification of A-EP colocalisation with endosomal markers. Rr, Pearson's correlation coefficient.

6.7.1. Fate of IgG-Alexa488 in Polymersomes Crossing the BBB *In Vitro*

Exclusion of trafficking via acidifying organelles is particularly important to transcytosis of A-EP because of the pH sensitive property of the PDPA polymer block, causing disassembly at a pH below ~6.4. To confirm that polymersomes do not disassemble during transcytosis, fluorescent IgG-Alexa488 was encapsulated as cargo into A-EP via electroporation. Figure 6.19 shows confocal micrographs of A-EP with IgG-Alexa488 in live bEnd.3 (a) or astrocytes (c) after 60 minutes. A 3D rendering of A-EP colocalisation with IgG is shown in figure 6.19b, where cargo fluorescence had the same morphology and size as the polymersomes. On the contrary, in astrocytes the IgG-Alexa488 signal (figure 6.19c) had dispersed from A-EP. The correlation coefficient (Rr) given in figure 6.20 was 0.74±0.09 in bEnd.3 and 0.23±0.09 in astrocytes (n=3, S.D.). These data show that A-EP is transcytosed by endothelial cells in a non-acidifying pathway, retaining integrity to carry cargo from one side of the cell to the other. In contrast, in astrocytes A-EP undergoes endocytosis and reaches the acidic pH to cause polymersome disassembly, releasing cargo.

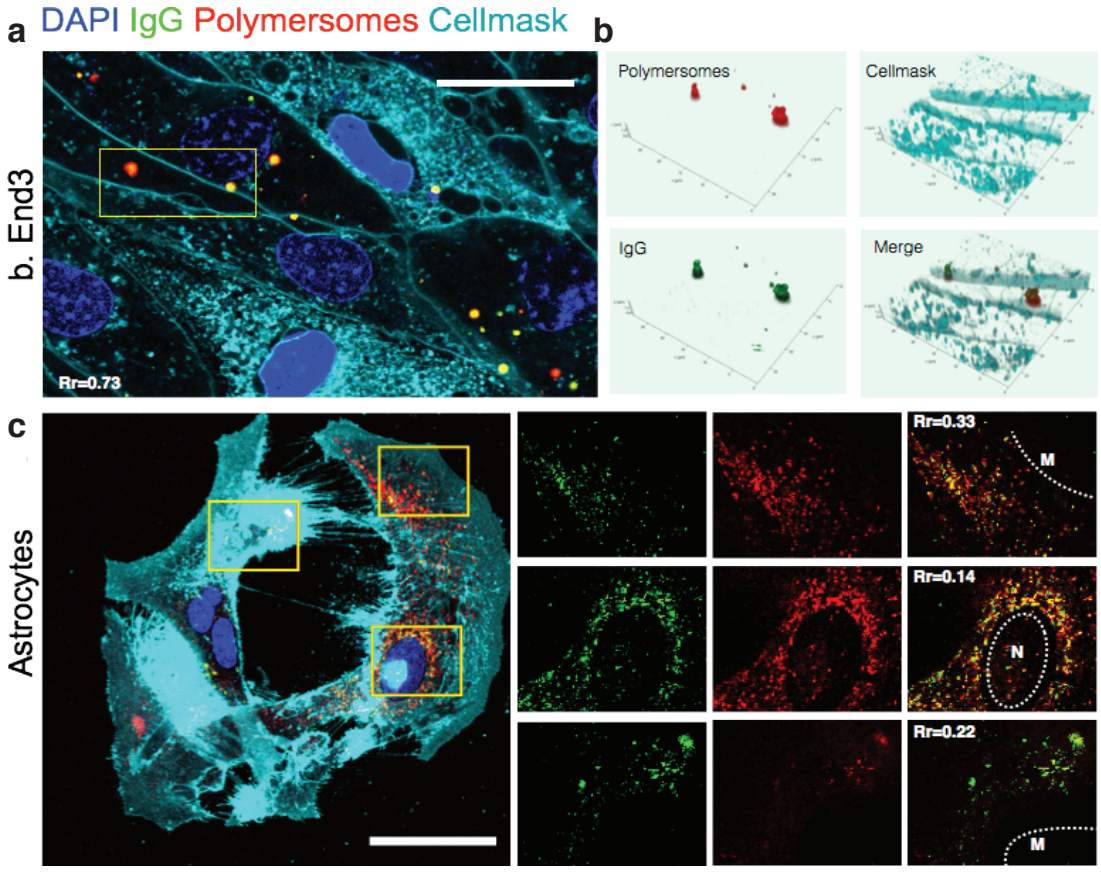

Figure 6.19. Confocal tracking of fluorescently labelled cargo in bEnd.3 or astrocytes. A-EP (red) colocalisation with encapsulated IgG-Alexa488 (green) after 60 minutes. Cells are counterstained for nuclei with DAPI (blue) and plasma membrane marker CellMask (cyan). Rr: Pearson's correlation coefficient. N, nucleus, M, membrane. Scale bar: 15 µm.

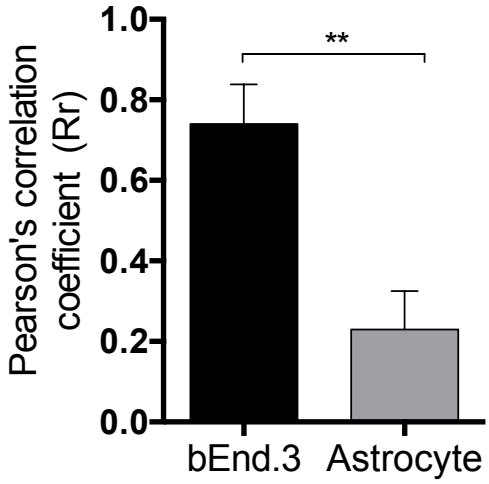

Figure 6.20. Correlation coefficient of A-EP and IgG-Alexa488 in bEnd.3 or astrocytes after 60 minutes. n=3, student's independent t-test, $p<0.05$. Error bars: S.D.

6.8. Exocytosis: Role of the SNARE Complex

Next, the role of cellular machinery involved in exocytosis was examined. N-ethylmaleimide soluble factor (NSF) is a SNARE complex component with known roles in pulmonary endothelial cell transcytosis (Predescu, Predescu et al. 2001). N-ethylmaleimide (NEM) is a small molecule inhibitor for NSF (Söllner, Whiteheart et al. 1993). It was hypothesised that inhibition with NEM would cause inhibition of exocytosis but not endocytosis, making cells swell up in a morphology similar to that observed when depleting cholesterol from the basolateral plasma membrane (figure 6.9). 3D live confocal imaging of A-EP transcytosis was performed in cells pre-incubated with NEM (figure 6.21), counter-stained with CellMask to visualise the plasma membrane. NEM caused the complete inhibition of transcytosis, with polymersomes remaining on top of the cells unable to enter. To get a quantitative understanding of polymersome location in the transwell filter, polymersome fluorescence intensity was obtained for every z-slice obtained of the extended transwell filter. Fluorescence underneath the cells was negligible after NEM treatment (figure 6.22), further indicating that no transcytosis was occurring.

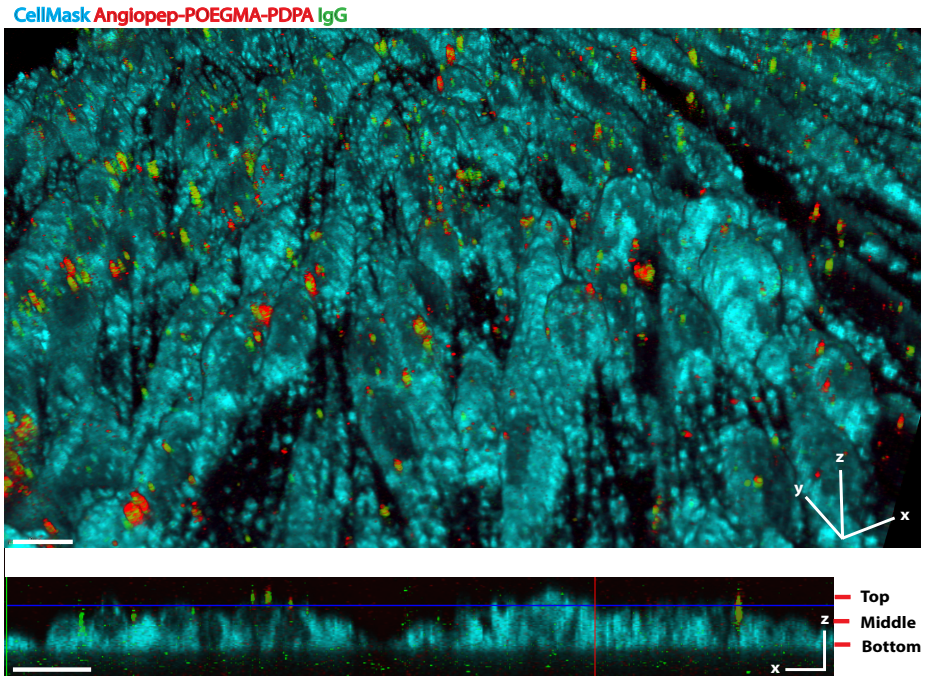

Figure 6.21. N-ethylmaleimide effect on transcytosis of A-EP in bEnd.3. Live cell confocal imaging of A-EP (red) with IgG-Alexa488 (green), cell membranes stained with CellMask (cyan) Scale bar: 5 μm.

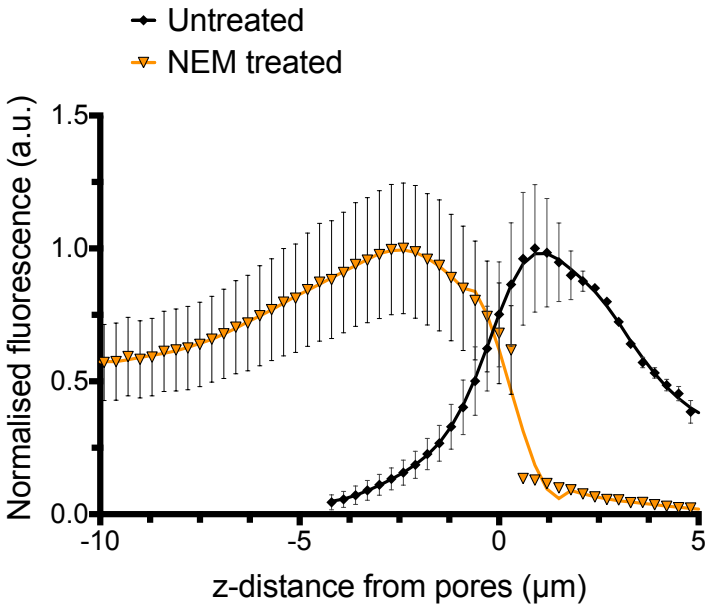

Figure 6.22. Quantification of polymersome fluorescence in NEM treated cells versus control. 0 marks the beginning of pores, negative values above the filter and positive values within the filter. n=3, error bars: S.D. Control shared with figure 6.15.

6.9. Ultrastructural Studies of Transcytosis in bEnd.3 Cells

Finally, electron microscopy was applied to investigate the transcytosis of A-EP through bEnd.3 cells. In order to do so, IgG labelled with 6nm gold nanoparticles (AuNPs) were used as an electron dense contrast agent encapsulated into A-EP via electroporation. For the morphology and size distributions of A-EP with AuNPs as assessed by DLS and TEM, refer to section 4.6.1 of chapter 4.

bEnd.3 monolayers on transwell filters were incubated with AuNP-loaded A-EP for 60 minutes before fixation and processing for sectioning. Single section micrographs of cells 1 hour after incubation are displayed in figures 6.23 and 6.24. In both of these figures several electron dense clusters corresponding well to the size of A-EP (96±19 nm, n=9) are present in the cytoplasm, as marked. Note the close proximity of these clusters to each other at the bottom of figure 6.23. The clustering of polymersomes to certain parts of the cell is consistent with the formation of channels or pores to facilitate rapid transcytosis. Furthermore, a putative tubular structure is indicated in figure 6.24 and can be seen better in the contrast enhanced magnification in figure 6.25. Similarly,

in figure 6.26 a series of apparently closed vesicles align into a straight line. These ultrastructural studies indicate that transcytosis of A-EP may occur through the alignment of intracellular vesicles into ‘tubular’ networks. However, these sections are two-dimensional, and proof of elusive transendothelial channels cannot be given without reconstructions of electron micrographs obtained in successive serial sections.

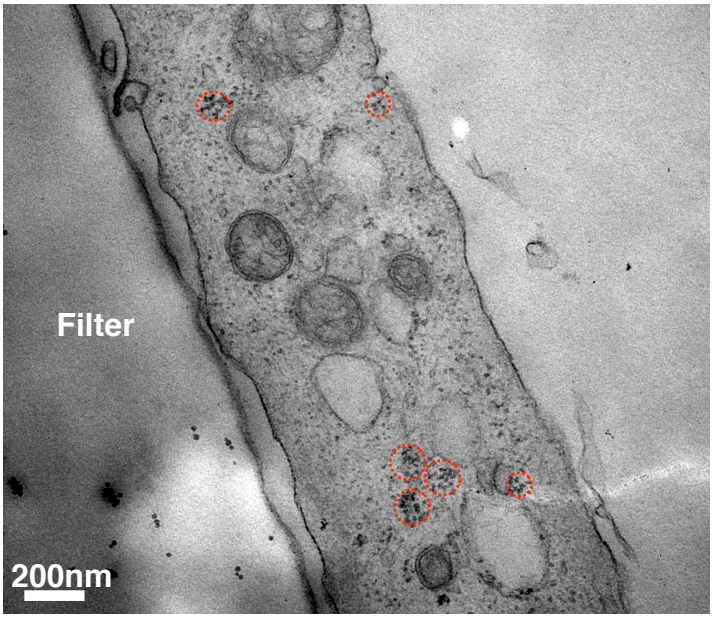

Figure 6.23. AuNP clusters (circled) in bEnd.3 after 60 minutes.

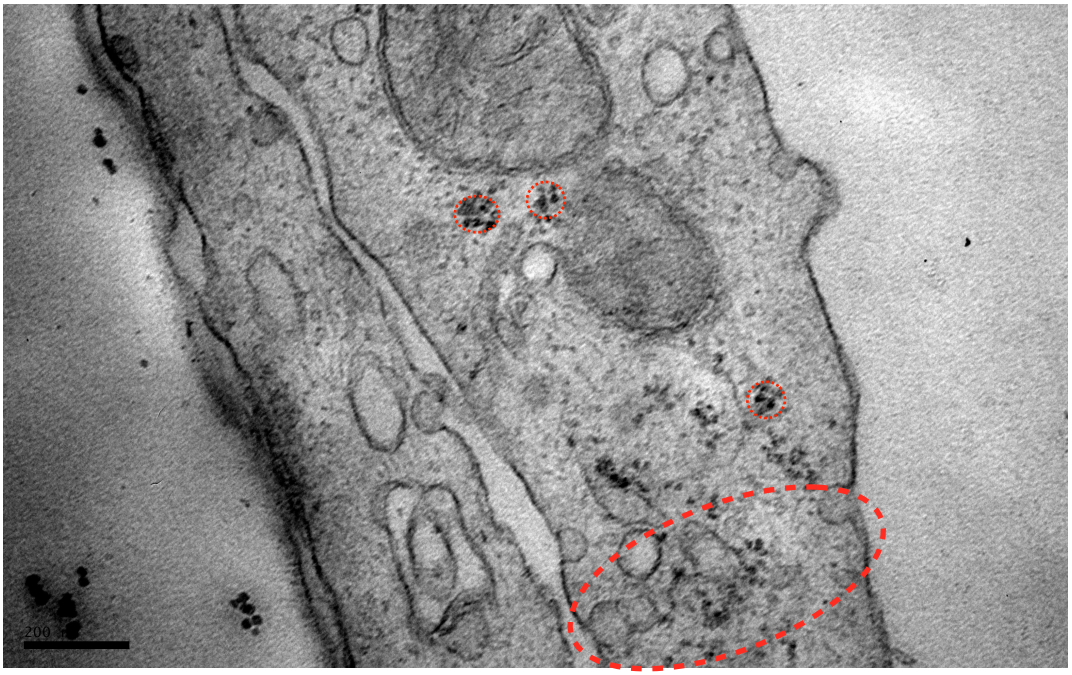

Figure 6.24. An indicated putative transendothelial channel. AuNP clusters in bEnd.3 cells after 60 minutes (ellipse).

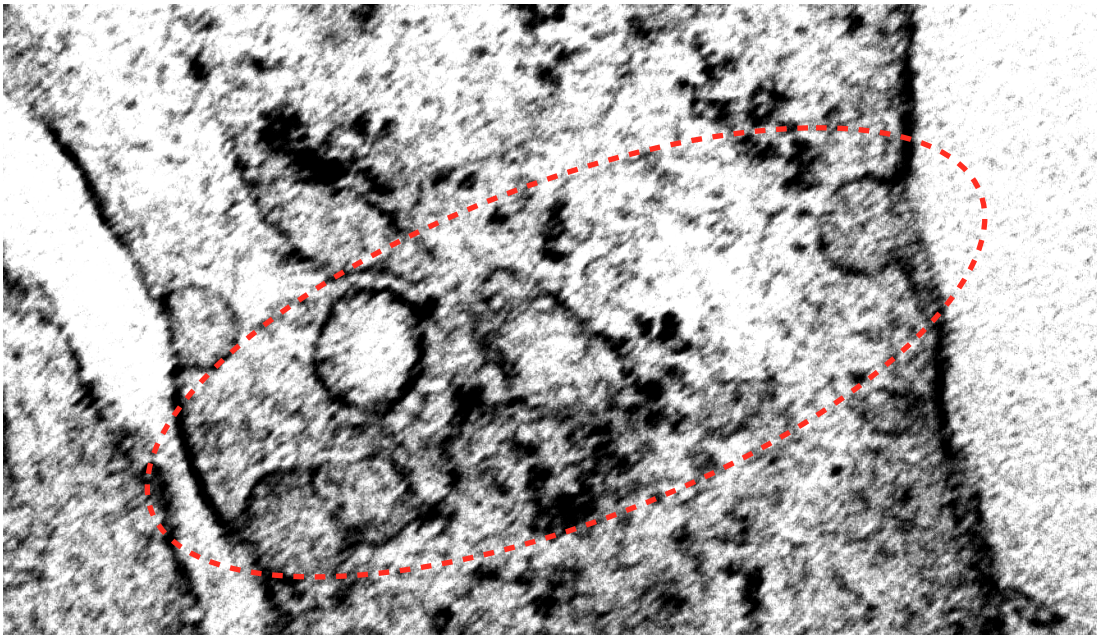

Figure 6.25. Magnification of the marked area of figure 6.24. Contrast enhanced to better illustrate the channel.

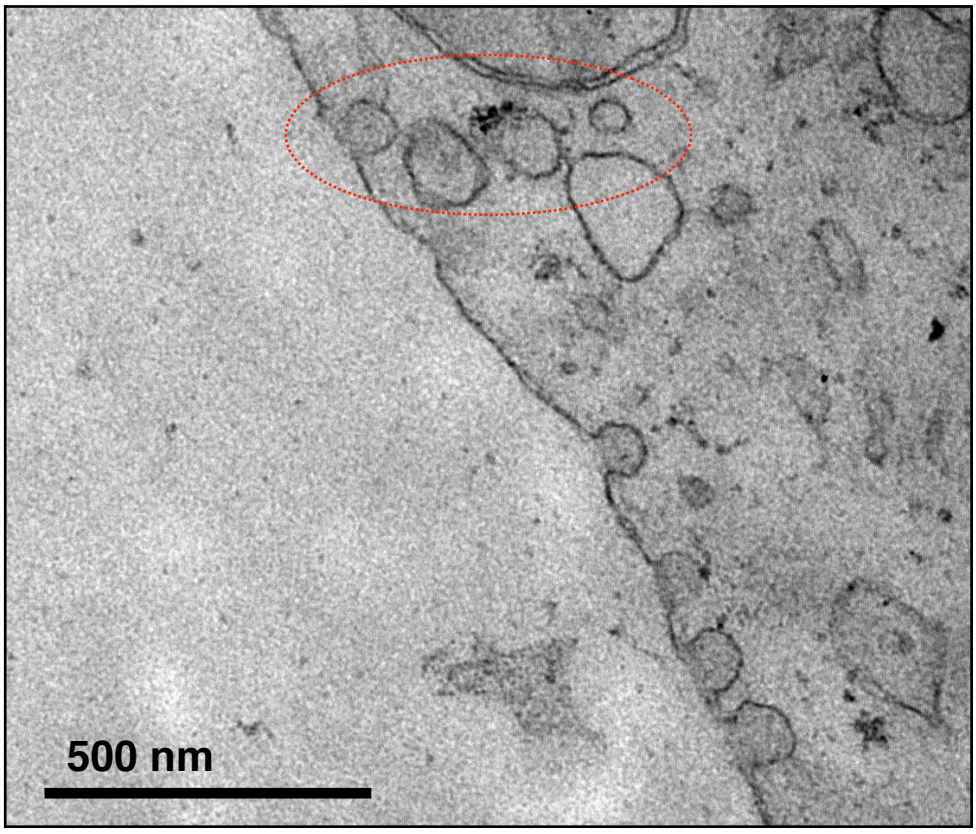

Figure 6.26. A series of aligned intracellular vesicles. bEnd.3 cells, incubated with AuNP-loaded polymersomes for 60 minutes.

6.10. Discussion and Proposed Mechanism

Little is known about how receptor-mediated transcytosis occurs at the brain endothelium. In this section, a 3D model of brain endothelial cells was used to track the fate of fluorescently labelled Angiopep-2-POEGMA-PDPA during the different stages of LRP-1-mediated transcytosis. Discussion regarding LRP-1 binding and clustering events can be found in chapter 5. Actin and dynamin appeared to be a conserved mechanism of initiating internalisation, consistent with reports of an essential role for dynamin in transcytosis in pulmonary endothelial cells (Predescu, Predescu et al. 2001). The initial colocalisation of actin with A-EP is consistent with a role of actin in apical-to-basolateral transfer: addition of the actin disrupting agent Cytochalasin D impaired internalisation from the apical but not basolateral plasma membrane in polarised epithelial cell lines MDCK and Caco-2 (Gottlieb, Ivanov et al. 1993, Jackman, Shurety et al. 1994).

Previous work investigating transcytosis in endothelial cells have frequently implicated caveolae as the main vesicular structures mediating transcytosis. However, the majority of these studies have been performed in endothelial cells of other origins than the brain microvasculature. Brain endothelial cells are known to express a different phenotype to peripheral cells, including a much lower density of vesicles in the membrane (Coomber and Stewart 1985). Immunoreactivity of caveolin-1 in bEnd.3 was mostly localised along the plasma membrane, but some cytoplasmic staining was also observed. These findings are surprising considering that caveolae are relatively rare structures in brain endothelial cells compared to peripheral endothelial cells, but may be due to the bEnd.3 model not achieving a full degree of BBB differentiation as shown by the tight junction markers. Nevertheless, confocal tracking of LRP-1 targeting A-EP polymersomes showed poor colocalisation with caveolin-1, reinforcing the hypothesis of differential roles for caveolae in peripheral and brain endothelial cells. Caveolin-1 immunofluorescence increased upon removal of cholesterol from the membrane, which

would explain the sudden colocalisation between caveolin-1 and A-EP. Furthermore, the depletion of cholesterol from the apical membrane did not inhibit transcytosis. This indicates that caveolae do not mediate transcytosis, as the removal of these cholesterol-dependent structures from the apical membrane should have inhibited transcytosis. On the other hand, some colocalisation between A-EP and the heavy chain of clathrin was observed. Nevertheless, no definite answer has been obtained regarding the nature of the vesicles mediating transcytosis in brain endothelial cells.

Immunocytochemistry of markers for various endosomal organelles confirmed that polymersomes internalised by endothelial cells do not interact with the acidifying membrane-bound trafficking compartments part of 'canonical' endocytosis. These findings are consistent with reports of cargo taking around 15 minutes to reach the first trafficking stage of early endosomes (Tjelle, Brech et al. 1996), whereas live confocal imaging of transcytosis showed that A-EP had already started appearing in the pores beneath the endothelial cell monolayer at 15 minutes. The timing of the canonical endosomal trafficking pathway is inconsistent with the kinetics presented herein, further discounting the possibility of a canonical endo-lysosomal pathway operating in brain endothelial cell transcytosis. Tracking the fate of cargo encapsulated into pH sensitive polymersomes revealed that these drug delivery vehicles enter and exit brain endothelial cells without releasing its cargo. This effect was not observed in astrocytes, where cargo was released due to the acidic endosomal pH encountered upon endocytosis. Taken together, these findings are significant as they discount the possibility of a canonical endocytosis pathway being conserved in transcytosis at brain endothelial cells, and further show that transcytosis by these cells is unlikely to be mediated by previously implicated caveolae. Taking into account the very thin apical-to-basolateral span of brain endothelial cells, it is concluded that the endosomal sorting system is a separate mechanism at the BBB reserved for cargo destined for the endothelial cells.

Surprisingly, inhibiting the SNARE complex member NSF completely stopped transcytosis before internalisation had occurred. Because the SNARE complex mediates membrane fusion, it is possible that transcytosis may not consist of discrete events of membrane fission and fusion of vesicular membrane as previously thought. Alternatively, transcytosis may cause the membrane to re-organise in an elongated tubular manner, ending with simultaneous scission and fusion events at the opposing sides mediated by dynamin and a SNARE complex, respectively. This hypothesis is supported by the requirement of cholesterol for the exocytosis stage. Work by Jahn et al. identified clustering of SNAREs into lipid rafts in the plasma membrane in a cholesterol-dependent manner, where depletion of cholesterol significantly impaired exocytosis (Lang, Bruns et al. 2001). It is possible that inhibited apical-to-basolateral transcytosis due to cholesterol depletion could be due to failure of SNAREs in the basolateral membrane to cluster and thus failure to mediate fusion of the vesicular and target membrane.

The shape of internalised transcytosis vesicles has traditionally been assumed to be vesicular, particularly due to electron microscopy morphological studies of endothelial cells (Ghitescu, Fixman et al. 1986). However, structural EM has overwhelmingly been investigating single sections of cells or tissue. Bundgaard et al. reconstructed 3D projections from serial section electron micrographs of hagfish brain endothelial cells, where the intracellular membranes arising from transcytosis were rarely single vesicles, but instead part of large multidimensional dendritic networks or ‘tubes’ (Bundgaard, Frøkjaer-Jensen et al. 1979). The deformation of the plasma membrane into a ‘tube’ connecting the apical and basolateral membranes via the shortest distance certainly seems an efficient mechanism to quickly transfer macromolecular nutrients across the BBB. The electron microscopy results from this section are somewhat consistent with this hypothesis, but cannot be taken for definite without serial 3D images to explore

whether the putative tubes observed in bEnd.3 transcytosis are real structures or artifacts.

A summarising cartoon of the proposed mechanism for brain endothelial cell transcytosis is depicted in figure 6.27. Confocal microscopy showed transcytosis to be dynamin-dependent with a likely role for actin in the initial transportation stage, but without a clear role for caveolae unlike previously implicated in reports. More surprisingly, brain endothelial transcytosis occurred without the acidification associated with endosomal trafficking organelles. Finally a role for the SNARE complex was implicated in brain endothelial cell transcytosis, which was disrupted by cholesterol depletion and also inhibition of NSF. These findings shed some light onto the mechanisms of LRP-1-mediated transcytosis.

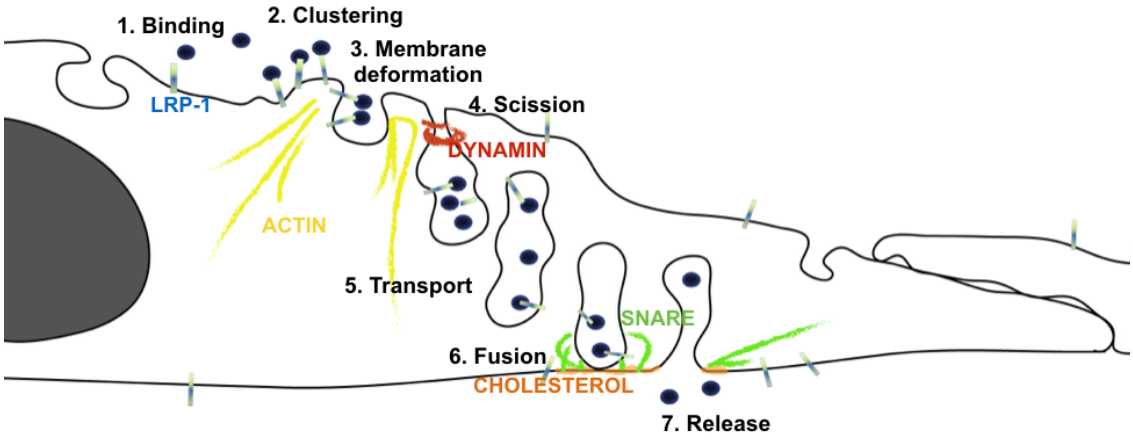

Figure 6.27. Summary of proposed transcytosis mechanism of A-EP at the BBB.

Chapter 7.

RESULTS AND DISCUSSION IV

In Vivo Validation and Applications for Polymersomes Targeting the Brain

7.1. Introduction

Work presented in this section was undertaken with the aim to validate use of A-EP as a CNS drug delivery vehicle. The first part is dedicated to obtain injected dose (%ID) values, in order to allow comparison of A-EP with other CNS drug delivery vehicles reported in literature. A technique was used to separate capillaries from the brain parenchyma to minimise false positives of transcytosis in which polymersomes are stuck within capillaries. Immunohistochemistry was used as a qualitative means to investigate polymersome distribution in the rat brain. The second part of the section aimed to explore therapeutic avenues using A-EP as a drug delivery vehicle *in vivo*. The di-peptide carnosine was encapsulated into A-EP and delivered intravenously in mice, and effects of carnosine neuroprotectant in stroke was investigated in mouse models of stroke.

7.1.1. *In Situ* Brain Perfusion

Even successful CNS drug delivery vehicles face the issue of a low delivery to the brain. For example, for OX26 %ID lies between 0.2-0.3% (Friden, Olson et al. 1996). This can be problematic for quantification of uptake into the brain, if enough dilution occurs to cause the signal from the material to fall below detection threshold. Furthermore, full body biodistribution studies inevitably cause the uptake of material into other organs, where they may be eliminated or retained without reaching the target. One way to circumvent these issues to investigate CNS uptake, and the subsequent distribution of materials within the parenchyma, is to use *in situ brain*

perfusion (ISP). This method involves surgical intervention to connect a perfusion apparatus to the carotid arteries, bypassing the rest of circulation and directly supplying the brain with a plasma-like perfusate containing the material of interest (Takasato, Rapoport et al. 1984). The setup is illustrated in figure 7.1. While ISP does not give accurate pharmacokinetics, it is useful for enhancing uptake into the CNS to quantifiable levels. ISP is especially advantageous if the aim is to look at where fluorescently or radiolabelled material becomes distributed within the brain.

Because the cerebellum receives a different blood supply (i.e. the vertebral artery), it is not perfused via ISP. The cerebellum is thus removed at the end of the experiment and not part of subsequent homogenisation or quantification.

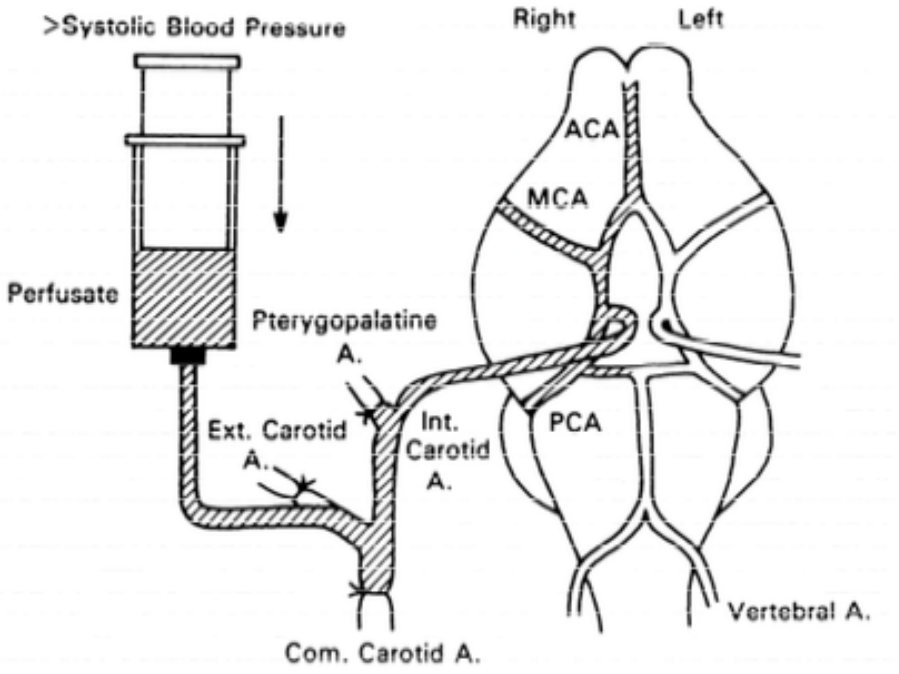

Figure 7.1. Setup of *in situ* perfusion. (Takasato, Rapoport et al. 1984)

7.1.2. Capillary Depletion Technique

In situ brain perfusion is often coupled with a capillary depletion technique. This involves homogenisation of the brain at the end of perfusion time, and separation of the

brain parenchyma from the capillaries through centrifugation (Triguero, Buciak et al. 1990). Dextran is added to the homogenate in the sample preparation process, and acts as a separating phase between parenchyma and capillaries, as the latter sediments into a pellet during centrifugation. This technique is useful to eliminate false positives in assessing cerebrovascular transfer of a material to the CNS, in the event of a CNS delivery vehicle remaining stuck within the capillaries instead of completing transcytosis.

7.2 Pilot Immunohistochemistry

After the preparation of polymersomes, it was important to establish whether it is feasible to quantify A-EP polymersome fluorescence from rat brain homogenates after perfusion. *In vitro,* A-EP consistently entered the transwell filter pore area underneath endothelial cells within 10-15 minutes. Therefore, similar times were hypothesised for transcytosis *in vivo*. ISP was performed with fluorescently labelled A-EP with perfusion times between 5 and 20 minutes. At the end of the perfusion times, the syringe pump supplying the plasma was allowed to run for another 60 seconds in order to 'flush' out unbound polymersomes from the capillaries. Half of the cerebrum was used for homogenisation and quantification, and the other half sectioned for fluorescence microscopy in order to visually confirm polymersome fluorescence inside the brain.

Figure 7.2 shows immunohistochemistry of three of the pilot study mice with A-EP perfusion times of 7 minutes, 15 minutes and 20 minutes, respectively. A-EP fluorescence was observed in the cerebral cortex at the earliest perfusion time of 7 minutes. Fluorescence at this time was closely associated with nuclei, indicating a predominantly intracellular location. Similar fluorescence distribution was seen in the 20 minute perfused sample. Sections from the 15 minute perfused mouse had a large amount of fluorescence in capillaries, but also visibly some intracellular fluorescence in areas both proximal and distal from the supplying vessels. Furthermore, a choroid

plexus section was obtained from the 15 minute perfused rat and contained a large amount of A-EP. It is unclear whether A-EP is undergoing transcytosis by the choroid plexus epithelial cells, or whether they had simply been internalised.

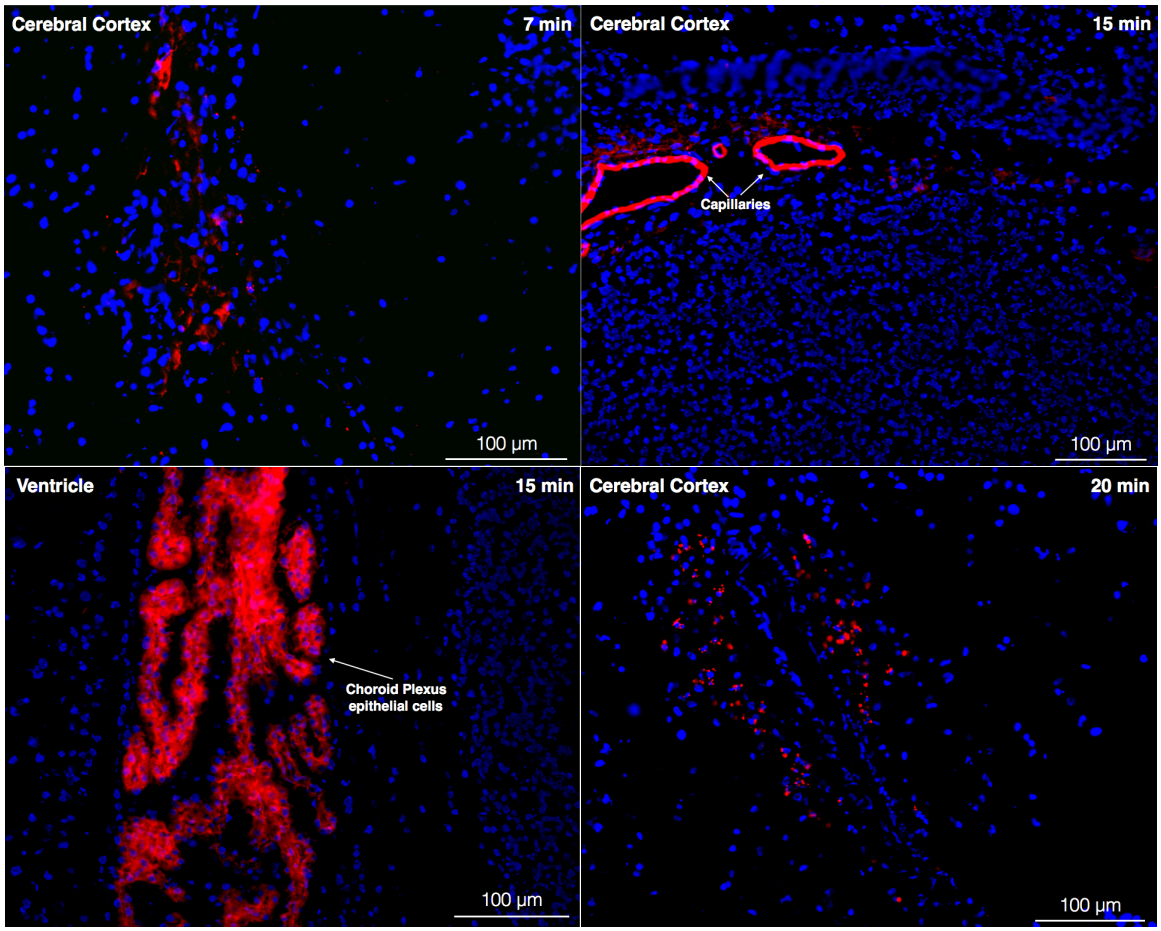

Figure 7.2. Rat brain fluorescence of A-EP after *in situ* perfusion. A-EP (red), nuclei: DAPI (blue). Perfusion times given on the top right corner of images.

7.3. Quantification of Polymersome Uptake into the Rat Brain

Fluorescence of the capillary fraction and capillary depleted (corresponding to the parenchyma) was measured in rats perfused with Cy3-labelled A-EP (n=6) or EP (n=6) for 10 minutes, as displayed in figure 7.3. After 10 minutes of perfusion and one minute of flushing the capillaries, the % injected dose per gram of brain tissue in the parenchyma was 3.3±2.0 for EP and 8.2±2.6 for A-EP. In the capillary depleted fraction, %ID/g was 2.7±1.8 for EP and 4.1±2.1 for A-EP. More than 8% of the injected dose of A-EP was present in the parenchyma after 10 minutes, which is a considerably high

value. However, some presence of non-targeting EP was also detected. It is not known whether this is because of a false positive, whether the BBB integrity has been affected, or whether POEGMA-PDPA polymersomes do interact with cells. Fluorescence in capillaries was not significantly different between A-EP and EP, both around 3-4% of the injected dose. At 10 minutes, this is a reasonable amount to expect inside endothelial cells for A-EP as some transcytosis is likely still occurring.

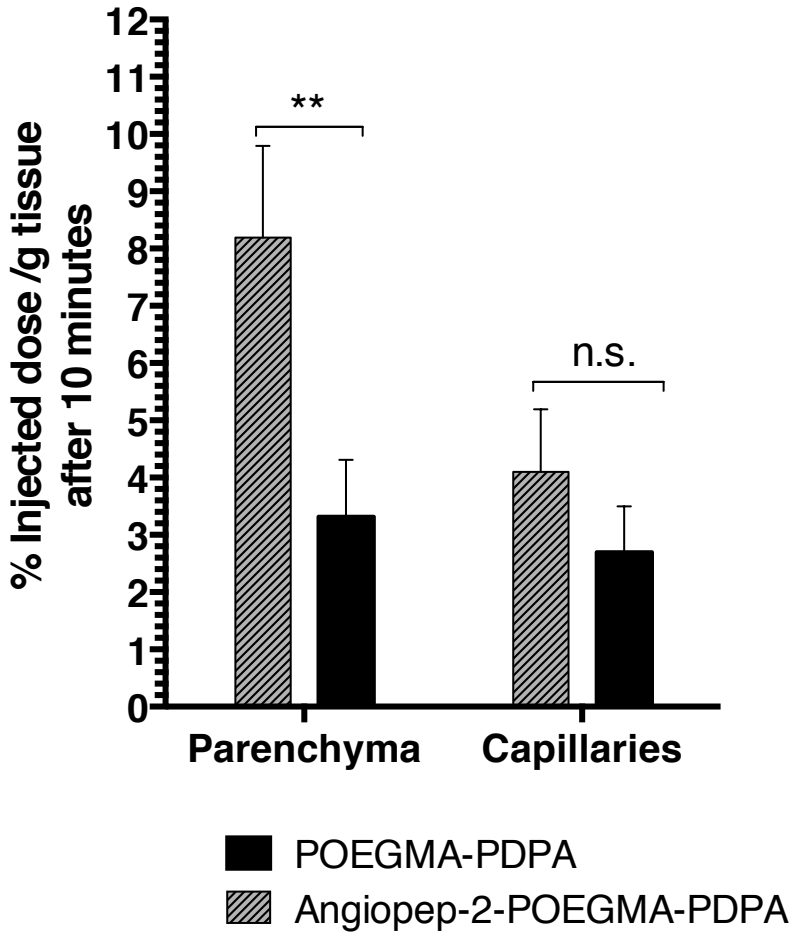

Figure 7.3. Fluorescence quantification of A-EP uptake into the brain parenchyma *in vivo*. One-way ANOVA, $p<0.05$. n=6 for A-EP and n=6 for EP. Error bars: S.E.M.

7.4. Immunohistochemistry to Investigate Polymersome Distribution in Rat Brain

Next, the location of A-EP in perfused rat brains was examined via immunohistochemistry. Previous studies showed uptake of intravenously injected A-EP

into the hippocampus and choroid plexus of mice (Tian, Nyberg et al. 2015). Furthermore, initial rat brain immunofluorescence studies (figure 7.2) located A-EP fluorescence to the choroid plexus and cortex. As a result, these three areas were chosen for investigation in this experiment, with sections of the corpus callosum chosen to be the area most proximal to a ventricle. Brains perfused with Cy3-labelled A-EP for 10, 30 or 60 minutes were compared to a sham perfused control. Sections were counter-stained for the blood vessel marker CD34 in order to distinguish between polymersomes inside capillaries and polymersomes which had migrated further out in the parenchyma (Pusztaszeri, Seelentag et al. 2006). Images obtained at a 5X magnification are shown for the cerebral cortex (figure 7.4), hippocampus (figure 7.5), and corpus callosum (figure 7.6).

It is difficult to observe polymersome fluorescence at 5X, but images obtained at this magnification provide a good orientation and overview of the area of interest. At the cerebral cortex and corpus callosum, A-EP fluorescence can be seen in a few scattered areas between 10 and 60 minutes. Images obtained from the hippocampus show higher red channel fluorescence, although the large red area in the 30 minute section is possibly an artifact from the staining procedure. However, polymersomes can be seen faintly surrounding hippocampal blood vessels at 60 minutes.

Images obtained at 20X give a better view of polymersome fluorescence. In the hippocampus (figure 7.7), polymersomes had migrated within the parenchyma but were still closely associated with blood vessels. At 30 minutes, some polymersome fluorescence was observed further away from vessels and also located close to nuclei. This migration was more pronounced after 60 minutes of perfusion, where many cells have internalised polymersomes and fluorescence was mostly in the perinuclear area.

Figure 7.8 shows the distribution of A-EP in the cortex at 20X magnification. Although some polymersomes were closely associated with a major vessel, there was fluorescence coming from a distal area and appeared to be intracellular. Fluorescence was radiating from the vessels at 30 minutes, and at 60 minutes there was a diffuse and background-like signal. A-EP was seen both in perinuclear areas and close to vessels. The least amount of fluorescence was observed in the corpus callosum, as displayed in figure 7.9, where only a few red puncta could be seen. However, A-EP was seen in the choroid plexus at 10 minutes, a magnification of which is seen in figure 7.10. This is consistent with the observations made of A-EP presence in the choroid plexus from 15 minute perfusion (figure 7.2). However, in this case fluorescence is more associated with blood vessels than the epithelial cells. At 10 minutes, polymersomes may still be migrating across the blood-brain barrier.

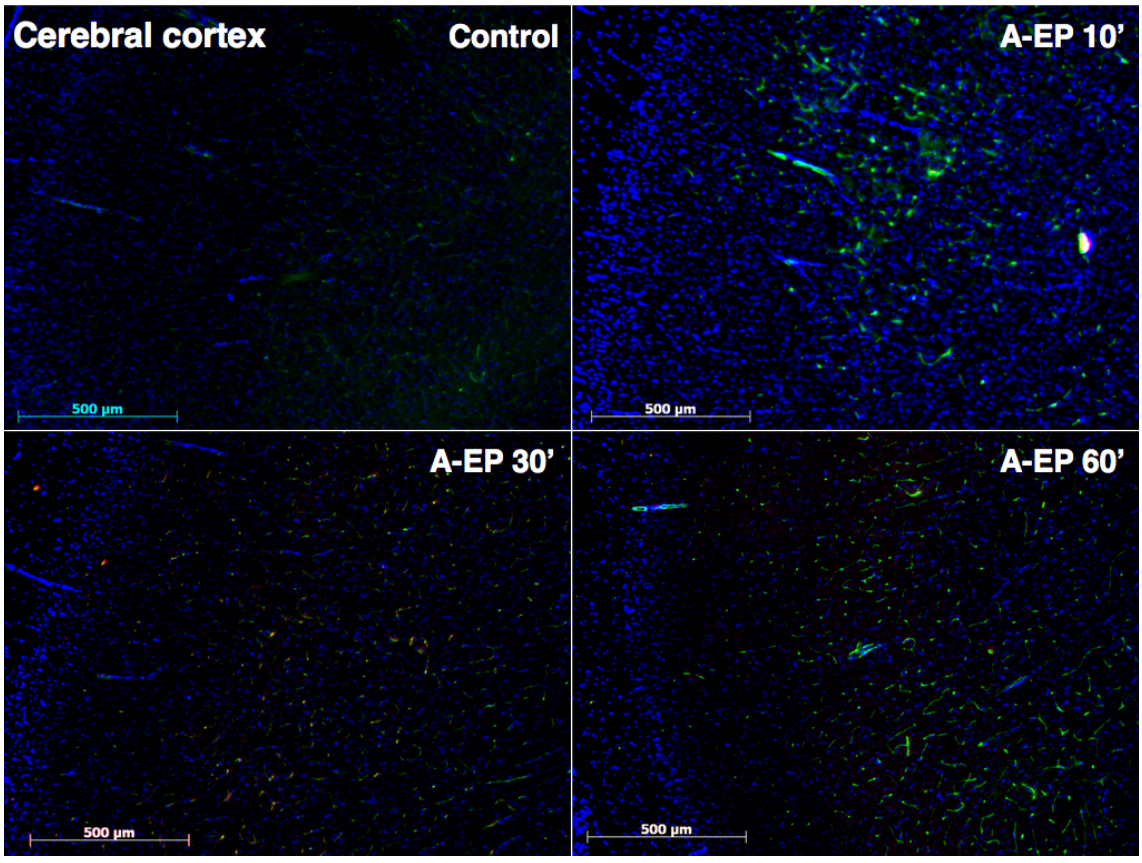

Figure 7.4. A-EP distribution in cerebral cortex, 5X magnification. A-EP (red), counter-stained for CD34 (green) and DAPI (blue).

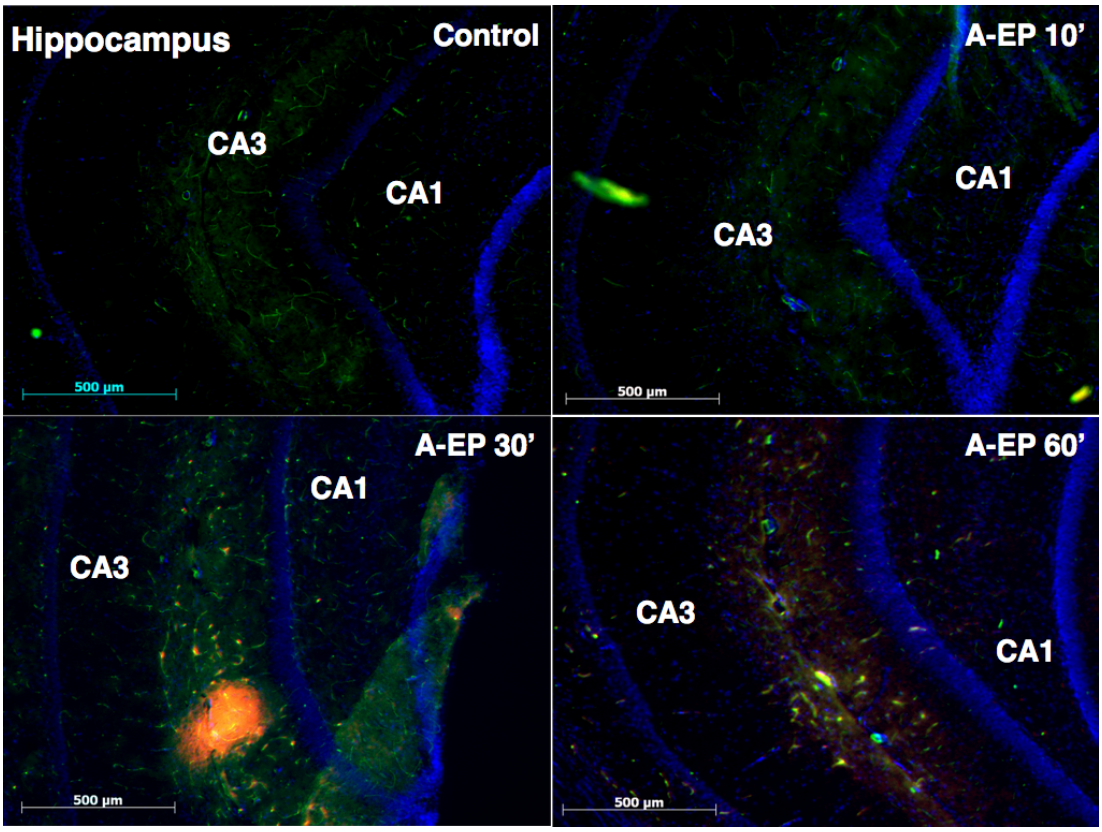

Figure 7.5. A-EP distribution in hippocampus, 5X magnification. A-EP (red), counter-stained for CD34 (green) and DAPI (blue).

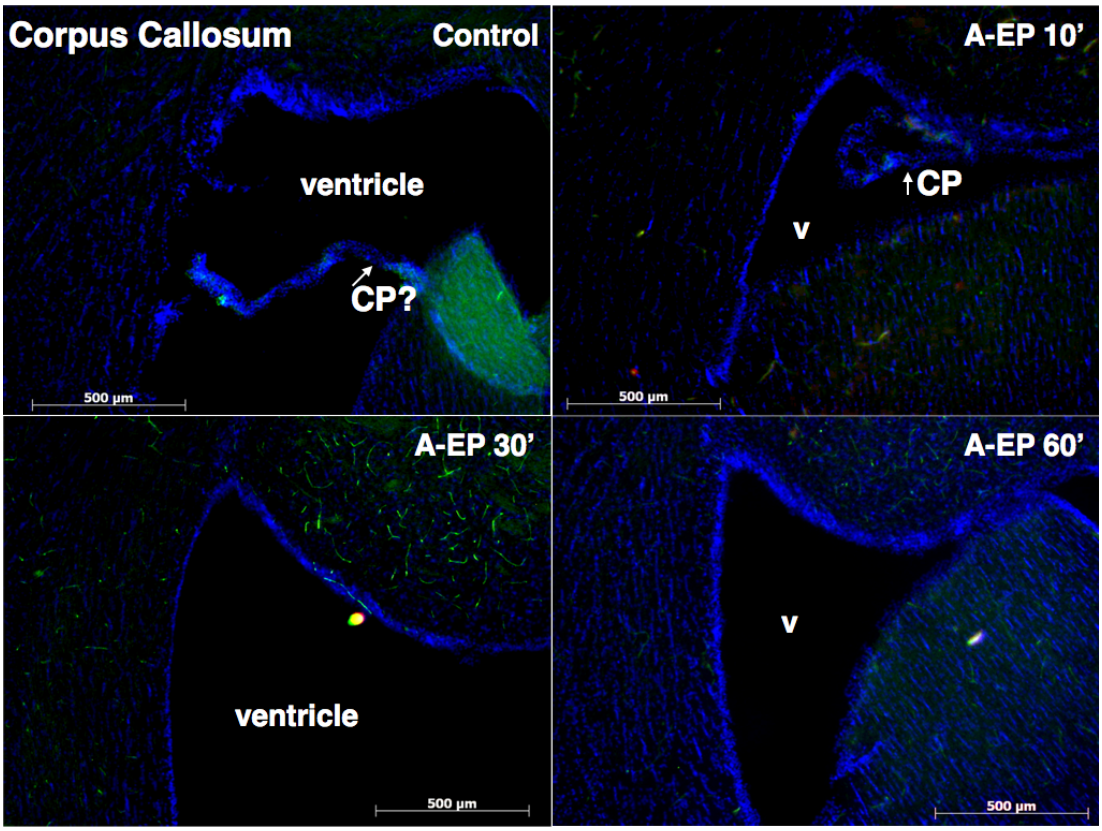

Figure 7.6. A-EP distribution in corpus callosum, 5X magnification. A-EP (red), counter-stained for CD34 (green) and DAPI (blue). CP: choroid plexus.

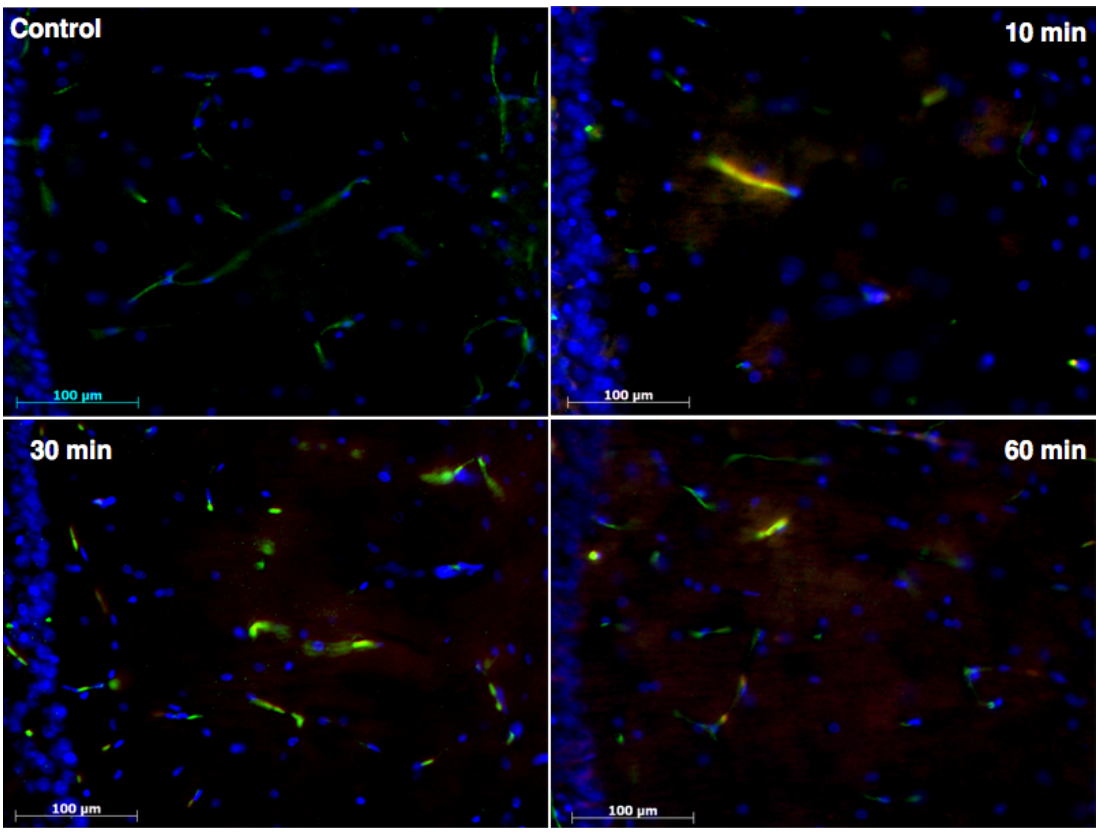

Figure 7.7. A-EP distribution in hippocampus, 20X magnification. A-EP (red), counter-stained for CD34 (green) and DAPI (blue).

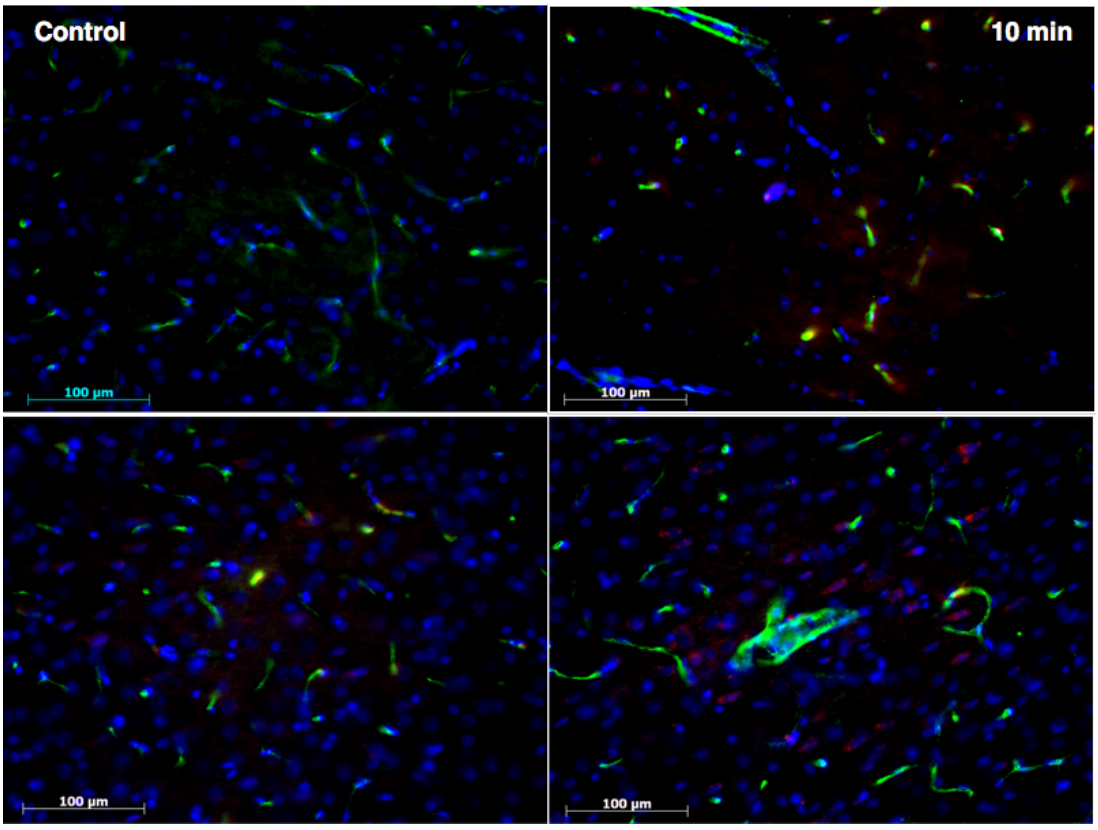

Figure 7.8. A-EP distribution in cortex, 20X magnification. A-EP (red), counter-stained for CD34 (green) and DAPI (blue).

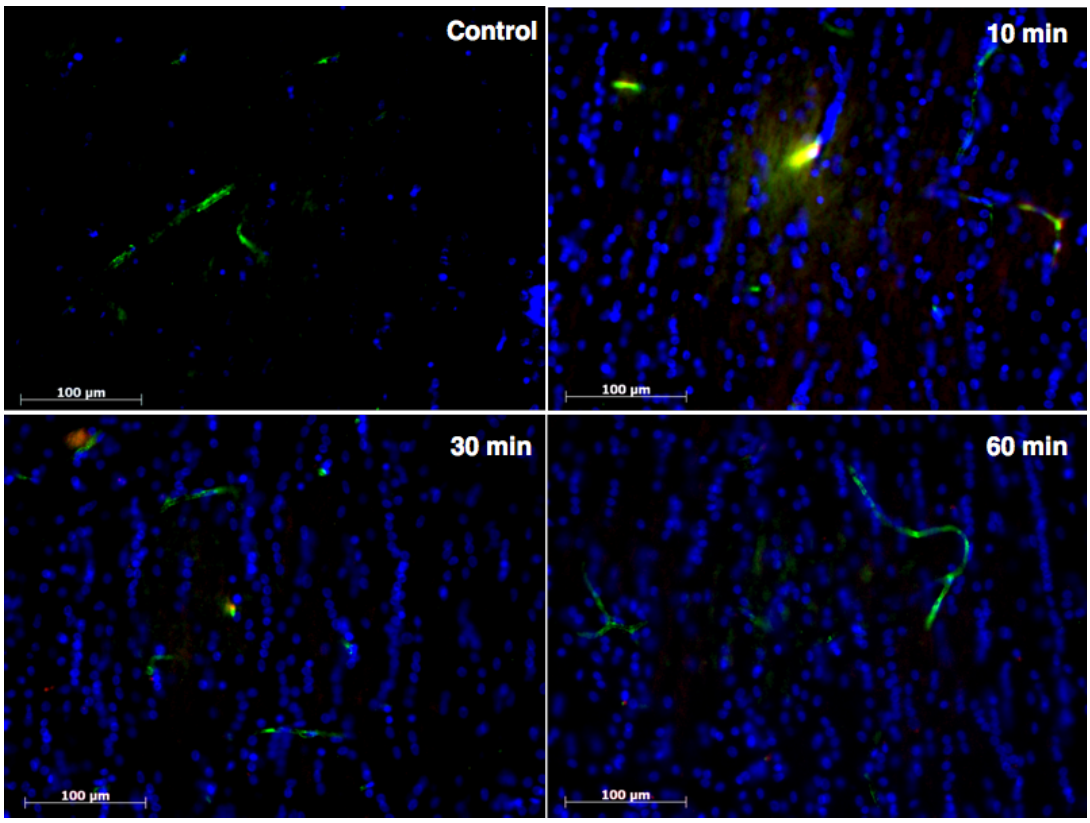

Figure 7.9. A-EP distribution in corpus callosum, 20X magnification. A-EP (red), counter-stained for CD34 (green) and DAPI (blue).

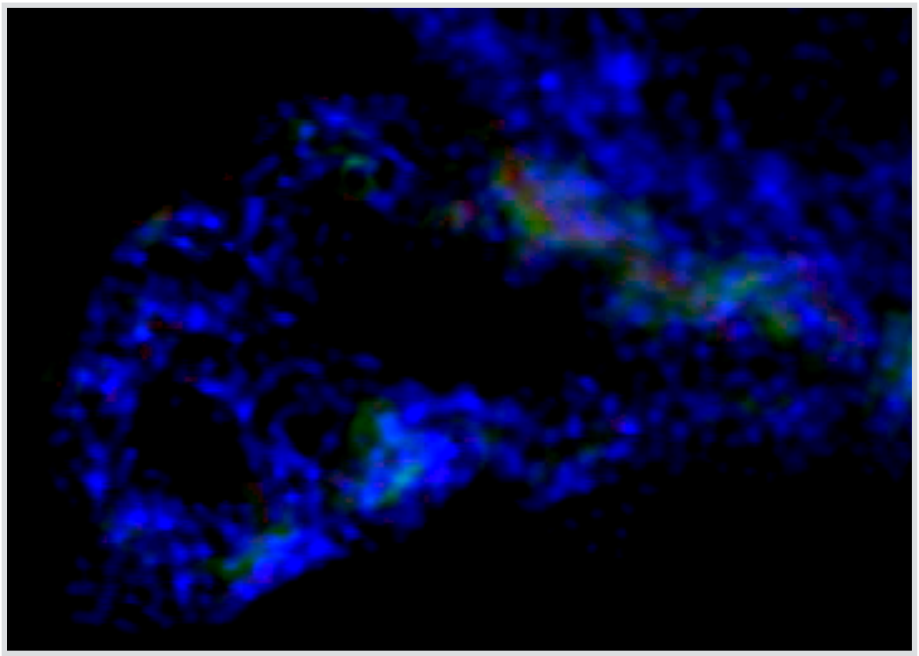

Figure 7.10. Magnification of A-EP at 10 minutes in the choroid plexus. A-EP fluorescence (red) can be seen in close association with CD34 positive blood vessels (green).

7.5. Application: Polymersomes with Carnosine for Neuroprotection in Stroke

7.5.1. Background

The high mortality rate and lack of treatment options available for stroke has been discussed in Section 1.1.2 of chapter 1. Recent research suggests that anti-oxidants can provide neuroprotectant benefits in rodent models of stroke (Majid 2014). One way to assess efficacy of novel stroke therapeutics in rodents is to measure the effect of the therapeutic on the total infarct area, i.e. the area of dead tissue resulting from ischaemia. Ischaemic stroke can be reproduced in mice using the transient middle cerebral artery occlusion (tMCAO) technique. It involves surgical arterial occlusion through a clamp, and can either be focal (i.e. localised to a specific area) or general.

Carnosine is a dipeptide with antioxidant properties (Bellia, Vecchio et al. 2011). Pre-clinical studies have shown neuroprotective effects of carnosine in animal models of stroke. However, the dosages required to obtain therapeutic effects in rats were in the range of 1000-2000 mg/kg, which may be too high to be a feasible dose to use in clinical settings (Bae, Serfozo et al. 2013). It was hypothesised that the delivery of carnosine encapsulated within Angiopep-2-POEGMA-PDPA would be able achieve the same effects at a much lower dosage rate, due to the targeting peptide and due to encapsulation of carnosine protecting it from premature degradation. Refer to section 4.6.2 of chapter 4 for the encapsulation of carnosine into A-EP.

7.5.2. Effect of Carnosine on Infarct Area

Previous studies investigating the neuroprotectant effect of carnosine injected 1000 mg/kg of the peptide in rats. Stroke volume was assessed in tMCAO rats pre-treated with 1000 mg/carnosine, empty A-EP (vehicle) or A-EP containing 1 mg/ml carnosine. Because the maximum allowed intravenous injection volume in rats is 1 ml, the dose roughly converts to 0.25 mg/kg in a 250 g rat. The infarct area of saline treated rats was 53.5 ± 24 mm^3 (n=10) (figure 7.11). In the A-EP vehicle treated rats, the area was

59 ± 22 mm^3 (n=14). Treatment with 1000 mg/kg carnosine dissolved in saline resulted in a reduction in the infarct area to an average of 36 ± 27 mm^3 (n=10). In rats pre-treated with carnosine encapsulated in A-EP, the stroke area was 34 ± 28 mm^3 (n=10). Free carnosine and A-EP carnosine both significantly reduced the infarct area against that of A-EP vehicle treated rats, but not saline treated. However, the standard deviations obtained were high and the n number per group should be increased to obtain more accurate results.

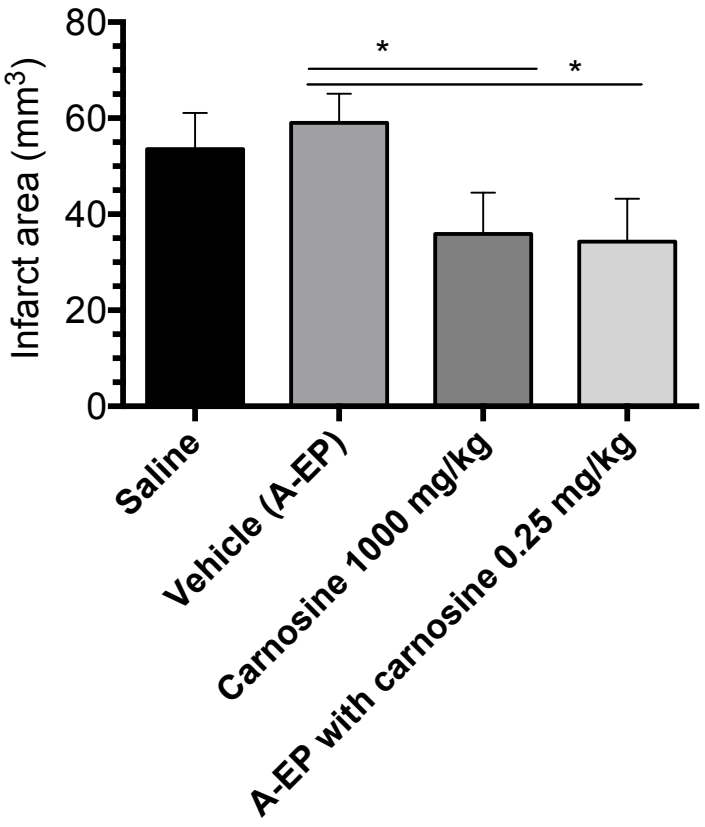

Figure 7.11. Infarct area in rat brains after pre-treatment with A-EP-carnosine, free carnosine, or vehicle. Error bars: S.E.M. Student's independent t-test, *p<0.05.

7.6. Discussion

The *in vivo* quantification of fluorescently labelled polymersomes was possible due to the high molarity of label in the polymersome membrane. The slight uptake of POEGMA-PDPA polymersomes in both capillary fractions and parenchyma may either

be a false positive, background fluorescence, or due to compromised blood-brain barrier integrity. However, A-EP fluorescence in the parenchyma was more than 8% of total fluorescence only 10 minutes after injection. This injected dose value is much higher than previously reported in literature, e.g. 3-4% for HIR and 0.2-0.3% for OX26. The high uptake can also be attributed to *in situ* perfusion, bypassing degradation and uptake by the rest of the body.

Immunohistochemistry of A-EP perfused rats showed the uptake into the hippocampus and cerebral cortex. Polymersome uptake into the hippocampus is consistent with A-EP uptake into hippocampus in mice following intravenous administration.(Tian, Nyberg et al. 2015) Furthermore, the presence of A-EP in the choroid plexus after 15 minutes is interesting. It is unclear whether this is because choroid plexus take up a large amount of A-EP through endocytosis, or whether it is an elimination route.

A-EP containing carnosine were injected at 1 mg/ml. And yet, the intravenous injection of A-EP with carnosine into mouse models of stroke resulted in the same amount of infarct area reduction that 1000 mg/kg free carnosine did. However, the values were not statistically significant to the saline perfused control, but only to the A-EP vehicle. The n number should be increased as *in vivo* results tend to display huge variation. An important next step would be validation in other stroke models. A caveat of animal models of stroke is that they are predominantly rodent based, and the methods used for models differ.

Chapter 8.
Discussion and Future Directions

Understanding how the barriers protecting the CNS work and how their transport and regulation systems work is key to enable drug delivery to the CNS beyond small molecules with a narrow range of physicochemical properties. The cellular mechanisms involved in macromolecular transport at the blood-brain barrier are poorly understood. Further work is required to give a comprehensive overview brain endothelial cell transcytosis, from ligand-receptor binding to membrane trafficking and exocytosis. Understanding BEC transcytosis is important both from a disease point of view and to use smart materials exploiting this system to deliver drugs past the blood-brain barrier.

In vitro models of the blood-brain barrier are useful for investigating fundamental brain endothelial cell properties. Work presented in this thesis has characterised the interaction of bEnd.3 cells and polymersomes mostly in a monoculture setting. The bEnd.3 model used fell short on expression of tight junction proteins, but did obtain higher TEER values than average. Future work may include the addition of pericytes to enhance barrier properties more closely mimic the BBB. Furthermore, ideally work should be compared between a cell line and primary endothelial cells, which is likely to have a different expression pattern of tight junction proteins, receptors and transporters.

The nature of the intracellular vesicles mediating transcytosis in brain endothelial cells is still to be confirmed, but data failed to find an involvement of acidifying endosomal compartments in bEnd.3 transcytosis. This is consistent with the hypothesis that brain endothelial cells may reserve such organelles for ‘traditional’ endocytosis, i.e. where cargo is destined to remain within the endothelial cells. The hypothesis that

transendothelial channels may form to enhance transcytosis is controversial, because the putative presence of an open channel between two environments negates the presence of tight junctions and would entail a low TEER. However, the hypothesis may be partially true in that some networks of vesicles closed off from the plasma membrane may form, as observed by Bundgaard and colleagues. Data indicated that caveolae were not the vesicles involved in A-EP transcytosis, whereas clathrin appeared in close proximity to A-EP at the time examined. Furthermore, electron microscopy studies indicated that the transendothelial vesicular network hypothesis may be true for brain endothelial cells, but further work needs to utilise serial 3D reconstructions of sections to gain context of these vesicles.

Modifying Angiopep-2 ligand density drastically altered transcytosis rates, providing a simple future tool for increasing uptake into the CNS. However, the relative contributions of receptor saturation, basolateral-to-apical recycling and ligand-receptor affinity in LRP-1 transcytosis kinetics remain to be elucidated. It is unclear why A-EP transcytosis reached saturation in some of the kinetics studies, i.e. no net apical-to-basolateral or basolateral-to-apical transcytosis was occurring. It is possible that LRP-1 recycling occurs more slowly than previously expected, or that transcytosis is a polarised event. Future work should investigate ligand-receptor interactions and receptor recycling rates, in order to fine-tune receptor binding and transcytosis efficiency for use of pH sensitive polymersomes in CNS drug delivery *in vivo*. Future work should also investigate the integrity of A-EP after transcytosis, e.g. by characterising size before and after a transwell assay, as to explore whether polymersome physicochemical properties change and as a result modify interactions with the endothelial monolayer.

The uptake of Angiopep-2-polymersomes into the rat brain reached an impressive 8% only 10 minutes after injection. However, the high dose could partly be attributed to

administration via *in situ* perfusion. Further experiments should be performed with intravenous injection to obtain a comparable injected dose value to other nanocarriers reported in literature. Additionally, endeavours to further characterise A-EP protein corona formation would be useful as this may affect uptake significantly.

Overall, results presented within this thesis have shown that polymersomes with a blood-brain barrier targeting mechanism can be used as CNS drug delivery vehicles. The very same targeting mechanism facilitates transcytosis by brain endothelial cells, followed by endocytosis by LRP-1-expressing cells of the CNS where cargo is released. Because polymersomes can encapsulate hydrophobic or hydrophilic cargo even of macromolecular nature, there is a wide range of potential therapeutics that polymersomes could deliver to the CNS. Thus, A-EP polymersomes are a promising CNS drug delivery system which exploits transcytosis at the blood-brain barrier to obtain widespread delivery.

COLLABORATION ACKNOWLEDGEMENT

The following acknowledgement concerns section 7.5, entitled 'application: carnosine as a neuroprotectant in stroke'. This application was undertaken as part of a collaboration, with roles distributed as follows: the author (S.N.) prepared polymersomes, performed optimisation of the encapsulation of protein, and did the physicochemical characterisation. *In vivo* experiments and analysis of the resulting data (figure 7.14) was performed by Dr Ok-Nam Bae (Hanyang University, Republic of Korea) and Prof Arshad Majid (University of Sheffield, U.K.)

Bibliography

Abbott, N. J. (2005). "Dynamics of CNS barriers: evolution, differentiation, and modulation." Cell Mol Neurobiol **25**(1): 5-23.

Abbott, N. J. (2016). Personal Correspondence.

Abbott, N. J., A. A. K. Patabendige, D. E. M. Dolman, S. R. Yusof and D. J. Begley (2010). Structure and function of the blood-brain barrier. **37:** 13-25.

Abbott, N. J., L. Rönnbäck and E. Hansson (2006). "Astrocyte-endothelial interactions at the blood-brain barrier." Nature reviews. Neuroscience **7**: 41-53.

Abulrob, A., H. Sprong, P. Van Bergen En Henegouwen and D. Stanimirovic (2005). "The blood-brain barrier transmigrating single domain antibody: Mechanisms of transport and antigenic epitopes in human brain endothelial cells." Journal of Neurochemistry **95**(4): 1201-1214.

Adamson, P., S. Etienne, P. O. Couraud, V. Calder and J. Greenwood (1999). "Lymphocyte migration through brain endothelial cell monolayers involves signaling through endothelial ICAM-1 via a rho-dependent pathway." J Immunol **162**(5): 2964-2973.

Agrawal, S., P. Anderson, M. Durbeej, N. Van Rooijen, F. Ivars, G. Opdenakker and L. M. Sorokin (2006). "Dystroglycan is selectively cleaved at the parenchymal basement membrane at sites of leukocyte extravasation in experimental autoimmune encephalomyelitis." Journal of Cell Biology **173**(2): 1007-1019.

Ajay, G. W. Bemis and M. A. Murcko (1999). "Designing libraries with CNS activity." Journal of Medicinal Chemistry **42**(24): 4942-4951.

Akinc, A. and G. Battaglia (2013). "Exploiting endocytosis for nanomedicines." Cold Spring Harb Perspect Biol **5**(11).

Allen, T. M. and L. G. Cleland (1980). "Serum-induced leakage of liposome contents." Biochim Biophys Acta **597**(2): 418-426.

Alswieleh, A. M., N. Cheng, I. Canton, B. Ustbas, X. Xue, V. Ladmiral, S. Xia, R. E. Ducker, O. El Zubir, M. L. Cartron, C. N. Hunter, G. J. Leggett and S. P. Armes (2014). "Zwitterionic poly(amino acid methacrylate) brushes." J Am Chem Soc **136**(26): 9404-9413.

Armulik, A., G. Genove, M. Mae, M. H. Nisancioglu, E. Wallgard, C. Niaudet, L. He, J. Norlin, P. Lindblom, K. Strittmatter, B. R. Johansson and C. Betsholtz (2010). "Pericytes regulate the blood-brain barrier." Nature **468**(7323): 557-561.

Azizi, P. M., R. E. Zyla, S. Guan, C. Wang, J. Liu, S. S. Bolz, B. Heit, A. Klip and W. L. Lee (2015). "Clathrin-dependent entry and vesicle-mediated exocytosis define insulin transcytosis across microvascular endothelial cells." Mol Biol Cell **26**(4): 740-750.

Bae, O. N., K. Serfozo, S. H. Baek, K. Y. Lee, A. Dorrance, W. Rumbeiha, S. D. Fitzgerald, M. U. Farooq, B. Naravelta, A. Bhatt and A. Majid (2013). "Safety and efficacy evaluation of carnosine, an endogenous neuroprotective agent for ischemic stroke." Stroke **44**(1): 205-212.

Balasubramanian, N., D. W. Scott, J. D. Castle, J. E. Casanova and M. A. Schwartz (2007). "Arf6 and microtubules in adhesion-dependent trafficking of lipid rafts." Nat Cell Biol **9**(12): 1381-1391.

Battaglia, G. and A. J. Ryan (2005). "Bilayers and interdigitation in block copolymer vesicles." J Am Chem Soc **127**(24): 8757-8764.

Battaglia, G., A. J. Ryan and S. Tomas (2006). "Polymeric vesicle permeability: A facile chemical assay." Langmuir : the ACS journal of surfaces and colloids **22**(11): 4910-4913.

Beisiegel, U., W. Weber, G. Ihrke, J. Herz and K. K. Stanley (1989). "The LDL-receptor-related protein, LRP, is an apolipoprotein E-binding protein." Nature **341**(6238): 162-164.

Bellia, F., G. Vecchio, S. Cuzzocrea, V. Calabrese and E. Rizzarelli (2011). "Neuroprotective features of carnosine in oxidative driven diseases." Mol Aspects Med **32**(4-6): 258-266.

Bickerton, G. R., G. V. Paolini, J. Besnard, S. Muresan and A. L. Hopkins (2012). "Quantifying the chemical beauty of drugs." Nat Chem **4**(2): 90-98.
Bien-Ly, N., Y. J. Yu, D. Bumbaca, J. Elstrott, C. A. Boswell, Y. Zhang, W. Luk, Y. Lu, M. S. Dennis, R. M. Weimer, I. Chung and R. J. Watts (2014). "Transferrin receptor (TfR) trafficking determines brain uptake of TfR antibody affinity variants." The Journal of experimental medicine **211**(2): 233-244.
Bolton, S. J., D. C. Anthony and V. H. Perry (1998). "Loss of the tight junction proteins occludin and zonula occludens-1 from cerebral vascular endothelium during neutrophil-induced blood-brain barrier breakdown in vivo." Neuroscience **86**(4): 1245-1257.
Boockvar, J. A., A. J. Tsiouris, C. P. Hofstetter, I. Kovanlikaya, S. Fralin, K. Kesavabhotla, S. M. Seedial, S. C. Pannullo, T. H. Schwartz, P. Stieg, R. D. Zimmerman, J. Knopman, R. J. Scheff, P. Christos, S. Vallabhajosula and H. A. Riina (2011). "Safety and maximum tolerated dose of superselective intraarterial cerebral infusion of bevacizumab after osmotic blood-brain barrier disruption for recurrent malignant glioma. Clinical article." J Neurosurg **114**(3): 624-632.
Bottaro, D. P., S. Bonner-Weir and G. L. King (1989). "Insulin receptor recycling in vascular endothelial cells. Regulation by insulin and phorbol ester." J Biol Chem **264**(10): 5916-5923.
Brightman, M. W. and T. S. Reese (1969). "Junctions between intimately apposed cell membranes in the vertebrate brain." The Journal of cell biology **40**(3): 648-677.
Brodsky, F. M., C. Y. Chen, C. Knuehl, M. C. Towler and D. E. Wakeham (2001). "Biological basket weaving: formation and function of clathrin-coated vesicles." Annual review of cell and developmental biology **17**: 517-568.
Brown, P. D., S. L. Davies, T. Speake and I. D. Millar (2004). Molecular mechanisms of cerebrospinal fluid production. **129:** 957-970.
Brown, R. C., A. P. Morris and R. G. O'Neil (2007). "Tight junction protein expression and barrier properties of immortalized mouse brain microvessel endothelial cells." Brain research **1130**(1): 17-30.
Bu, G., E. A. Maksymovitch, H. Geuze and A. L. Schwartz (1994). "Subcellular localization and endocytic function of low density lipoprotein receptor-related protein in human glioblastoma cells." The Journal of biological chemistry **269**(47): 29874-29882.
Bu, G., E. A. Maksymovitch, J. M. Nerbonne and A. L. Schwartz (1994). "Expression and function of the low density lipoprotein receptor-related protein (LRP) in mammalian central neurons." The Journal of biological chemistry **269**(28): 18521-18528.
Bucci, C., R. G. Parton, I. H. Mather, H. Stunnenberg, K. Simons, B. Hoflack and M. Zerial (1992). "The small GTPase rab5 functions as a regulatory factor in the early endocytic pathway." Cell **70**(5): 715-728.
Bundgaard, M., J. Frøkjaer-Jensen and C. Crone (1979). "Endothelial plasmalemmal vesicles as elements in a system of branching invaginations from the cell surface." Proceedings of the National Academy of Sciences of the United States of America **76**(12): 6439-6442.
Canton, I. and G. Battaglia (2012). "Endocytosis at the nanoscale." Chem Soc Rev **41**(7): 2718-2739.
Carlson, C., S. M. Hussain, A. M. Schrand, L. K. Braydich-Stolle, K. L. Hess, R. L. Jones and J. J. Schlager (2008). "Unique cellular interaction of silver nanoparticles: size-dependent generation of reactive oxygen species." J Phys Chem B **112**(43): 13608-13619.
Carman, C. V. (2009). "Mechanisms for transcellular diapedesis: probing and pathfinding by 'invadosome-like protrusions'." J Cell Sci **122**(Pt 17): 3025-3035.
Carman, C. V. and T. A. Springer (2004). "A transmigratory cup in leukocyte diapedesis both through individual vascular endothelial cells and between them." J Cell Biol **167**(2): 377-388.
Chames, P., M. Van Regenmortel, E. Weiss and D. Baty (2009). "Therapeutic antibodies: successes, limitations and hopes for the future." Br J Pharmacol **157**(2): 220-233.

Chappell, D. A., G. L. Fry, M. A. Waknitz, P. H. Iverius, S. E. Williams and D. K. Strickland (1992). "The low density lipoprotein receptor-related protein/alpha 2-macroglobulin receptor binds and mediates catabolism of bovine milk lipoprotein lipase." The Journal of biological chemistry **267**(36): 25764-25767.
Chen, W., F. Meng, R. Cheng and Z. Zhong (2010). "pH-Sensitive degradable polymersomes for triggered release of anticancer drugs: A comparative study with micelles." Journal of Controlled Release **142**: 40-46.
Cheng, Y., Q. Dai, R. A. Morshed, X. Fan, M. L. Wegscheid, D. A. Wainwright, Y. Han, L. Zhang, B. Auffinger, A. L. Tobias, E. Rincon, B. Thaci, A. U. Ahmed, P. C. Warnke, C. He and M. S. Lesniak (2014). "Blood-brain barrier permeable gold nanoparticles: an efficient delivery platform for enhanced malignant glioma therapy and imaging." Small **10**(24): 5137-5150.
Cho, J., S. H. Lee, J. H. Seo, H. S. Kim, J. G. Ahn, S. S. Kim, S. V. Yim, D. K. Song and S. S. Cho (2002). "Increased expression of phosphatase and tensin homolog in reactive astrogliosis following intracerebroventricular kainic acid injection in mouse hippocampus." Neurosci Lett **334**(2): 131-134.
Cifelli, A., M. Arridge, P. Jezzard, M. M. Esiri, J. Palace and P. M. Matthews (2002). "Thalamic neurodegeneration in multiple sclerosis." Annals of Neurology **52**(5): 650-653.
Coker, G. T., D. Studelska, S. Harmon, W. Burke, apos and K. L. Malley (1990). "Analysis of tyrosine hydroxylase and insulin transcripts in human neuroendocrine tissues." Molecular Brain Research **8**: 93-98.
Comas-Herrera, A., R. Wittenberg, L. Pickard and M. Knapp (2007). "Cognitive impairment in older people: Future demand for long-term care services and the associated costs." International Journal of Geriatric Psychiatry **22**(10): 1037-1045.
Coomber, B. L. and P. A. Stewart (1985). "Morphometric analysis of CNS microvascular endothelium." Microvasc Res **30**(1): 99-115.
Coomber, B. L. and P. A. Stewart (1986). "Three-dimensional reconstruction of vesicles in endothelium of blood-brain barrier versus highly permeable microvessels." Anat Rec **215**(3): 256-261.
Couper, K. N., T. Barnes, J. C. Hafalla, V. Combes, B. Ryffel, T. Secher, G. E. Grau, E. M. Riley and J. B. de Souza (2010). "Parasite-derived plasma microparticles contribute significantly to malaria infection-induced inflammation through potent macrophage stimulation." PLoS Pathog **6**(1): e1000744.
Crone, C. and S. P. Olesen (1982). "Electrical resistance of brain microvascular endothelium." Brain Research **241**(1): 49-55.
Cummings, J. L., T. Morstorf and K. Zhong (2014). "Alzheimer's disease drug-development pipeline: few candidates, frequent failures." Alzheimers Res Ther **6**(4): 37.
Daneman, R., L. Zhou, A. A. Kebede and B. A. Barres (2010). "Pericytes are required for blood-brain barrier integrity during embryogenesis." Nature **468**(7323): 562-566.
Dauchy, S., F. Dutheil, R. J. Weaver, F. Chassoux, C. Daumas-Duport, P. O. Couraud, J. M. Scherrmann, I. De Waziers and X. Declèves (2008). "ABC transporters, cytochromes P450 and their main transcription factors: Expression at the human blood-brain barrier." Journal of Neurochemistry **107**(6): 1518-1528.
Deane, R., S. Du Yan, R. K. Submamaryan, B. LaRue, S. Jovanovic, E. Hogg, D. Welch, L. Manness, C. Lin, J. Yu, H. Zhu, J. Ghiso, B. Frangione, A. Stern, A. M. Schmidt, D. L. Armstrong, B. Arnold, B. Liliensiek, P. Nawroth, F. Hofman, M. Kindy, D. Stern and B. Zlokovic (2003). "RAGE mediates amyloid-beta peptide transport across the blood-brain barrier and accumulation in brain." Nat Med **9**(7): 907-913.
Deane, R., Z. Wu, A. Sagare, J. Davis, S. Du Yan, K. Hamm, F. Xu, M. Parisi, B. LaRue, H. W. Hu, P. Spijkers, H. Guo, X. Song, P. J. Lenting, W. E. Van Nostrand and B. V. Zlokovic (2004). "LRP/amyloid beta-peptide interaction mediates differential brain efflux of Abeta isoforms." Neuron **43**(3): 333-344.
Demeule, M., J. C. Currie, Y. Bertrand, C. Che, T. Nguyen, A. Regina, R. Gabathuler, J. P. Castaigne and R. Beliveau (2008). "Involvement of the low-density lipoprotein

receptor-related protein in the transcytosis of the brain delivery vector angiopep-2." Journal of neurochemistry **106**(4): 1534-1544.
Demeule, M., A. Regina, C. Che, J. Poirier, T. Nguyen, R. Gabathuler, J. P. Castaigne and R. Beliveau (2008). "Identification and design of peptides as a new drug delivery system for the brain." The Journal of pharmacology and experimental therapeutics **324**(3): 1064-1072.
Derfus, A. M., W. C. W. Chan and S. N. Bhatia (2004). "Probing the Cytotoxicity of Semiconductor Quantum Dots." Nano Letters **4**(1): 11-18.
Dickson, P. W., A. R. Aldred, P. D. Marley, D. Bannister and G. Schreiber (1986). "Rat choroid plexus specializes in the synthesis and the secretion of transthyretin (prealbumin). Regulation of transthyretin synthesis in choroid plexus is independent from that in liver." J Biol Chem **261**(8): 3475-3478.
Dieu, L. H., D. Wu, C. G. Palivan, V. Balasubramanian and J. Huwyler (2014). "Polymersomes conjugated to 83-14 monoclonal antibodies: in vitro targeting of brain capillary endothelial cells." Eur J Pharm Biopharm **88**(2): 316-324.
Discher, D. E. and A. Eisenberg (2002). "Polymer vesicles." Science **297**(5583): 967-973.
Drab, M., P. Verkade, M. Elger, M. Kasper, M. Lohn, B. Lauterbach, J. Menne, C. Lindschau, F. Mende, F. C. Luft, A. Schedl, H. Haller and T. V. Kurzchalia (2001). "Loss of caveolae, vascular dysfunction, and pulmonary defects in caveolin-1 gene-disrupted mice." Science (New York, N.Y.) **293**: 2449-2452.
Dulubova, I., M. Khvotchev, S. Liu, I. Huryeva, T. C. Südhof and J. Rizo (2007). "Munc18-1 binds directly to the neuronal SNARE complex." Proceedings of the National Academy of Sciences of the United States of America **104**(8): 2697-2702.
Dutheil, F., A. Jacob, S. Dauchy, P. Beaune, J.-M. Scherrmann, X. Declèves and M.-A. Loriot (2010). "ABC transporters and cytochromes P450 in the human central nervous system: influence on brain pharmacokinetics and contribution to neurodegenerative disorders." Expert opinion on drug metabolism & toxicology **6**(10): 1161-1174.
Ebrahimi, C. M., J. W. Kern, T. R. Sheen, M. A. Ebrahimi-Fardooee, N. M. van Sorge, O. Schneewind and K. S. Doran (2009). "Penetration of the blood-brain barrier by Bacillus anthracis requires the pXO1-encoded BslA protein." J Bacteriol **191**(23): 7165-7173.
Ehrlich, M., W. Boll, A. Van Oijen, R. Hariharan, K. Chandran, M. L. Nibert and T. Kirchhausen (2004). "Endocytosis by random initiation and stabilization of clathrin-coated pits." Cell **118**: 591-605.
Ehrlich, P. (1908) "Nobel Lecture: Partial Cell Functions."
Elias, D. R., A. Poloukhtine, V. Popik and A. Tsourkas (2013). "Effect of ligand density, receptor density, and nanoparticle size on cell targeting." Nanomedicine: Nanotechnology, Biology, and Medicine **9**(2): 194-201.
Ellens, N. P., I. Kobelevskiy, A. Chau, A. C. Waspe, R. M. Staruch, R. Chopra and K. Hynynen (2015). "The targeting accuracy of a preclinical MRI-guided focused ultrasound system." Med Phys **42**(1): 430-439.
Fawcett, D. W. (1965). "Surface Specializations of Absorbing Cells." J Histochem Cytochem **13**: 75-91.
Ferri, C. P., M. Prince, C. Brayne, H. Brodaty, L. Fratiglioni, M. Ganguli, K. Hall, K. Hasegawa, H. Hendrie, Y. Huang, A. Jorm, C. Mathers, P. R. Menezes, E. Rimmer and M. Scazufca (2005). Global prevalence of dementia: A Delphi consensus study. **366:** 2112-2117.
Fishman, J. B., J. B. Rubin, J. V. Handrahan, J. R. Connor and R. E. Fine (1987). "Receptor-mediated transcytosis of transferrin across the blood-brain barrier." Journal of neuroscience research **18**: 299-304.
Frank, P. G., S. E. Woodman, D. S. Park and M. P. Lisanti (2003). Caveolin, caveolae, and endothelial cell function. **23:** 1161-1168.
Friden, P. M., T. S. Olson, R. Obar, L. R. Walus and S. D. Putney (1996). "Characterization, receptor mapping and blood-brain barrier transcytosis of antibodies

to the human transferrin receptor." The Journal of pharmacology and experimental therapeutics **278**(3): 1491-1498.
Frijns, C. J., L. J. Kappelle, J. van Gijn, H. K. Nieuwenhuis, J. J. Sixma and R. Fijnheer (1997). "Soluble adhesion molecules reflect endothelial cell activation in ischemic stroke and in carotid atherosclerosis." Stroke **28**(11): 2214-2218.
Fu, J., A. P. Naren, X. Gao, G. U. Ahmmed and A. B. Malik (2005). "Protease-activated receptor-1 activation of endothelial cells induces protein kinase Calpha-dependent phosphorylation of syntaxin 4 and Munc18c: role in signaling p-selectin expression." J Biol Chem **280**(5): 3178-3184.
Fuentealba, R. A., Q. Liu, J. Zhang, T. Kanekiyo, X. Hu, J. M. Lee, M. J. Ladu and G. Bu (2010). "Low-density lipoprotein receptor-related protein 1 (LRP1) mediates neuronal Aβ42 uptake and lysosomal trafficking." PLoS ONE **5**(7).
Fung, L. K., M. Shin, B. Tyler and H. Brem (1996). "Chemotherapeutic Drugs Released from Polymers: Distribution of 1, 3-bis (2-chloroethyl)-l-nitrosourea in the Rat Brain." Pharmaceutical ….
Gabbott, P. L. and M. G. Stewart (1987). "Distribution of neurons and glia in the visual cortex (area 17) of the adult albino rat: a quantitative description." Neuroscience **21**(3): 833-845.
Gage, G. J., D. R. Kipke and W. Shain (2012). "Whole animal perfusion fixation for rodents." J Vis Exp(65).
Gagliardini, E., S. Conti, A. Benigni, G. Remuzzi and A. Remuzzi (2010). "Imaging of the porous ultrastructure of the glomerular epithelial filtration slit." J Am Soc Nephrol **21**(12): 2081-2089.
Gao, X., Y. Cui, R. M. Levenson, L. W. Chung and S. Nie (2004). "In vivo cancer targeting and imaging with semiconductor quantum dots." Nat Biotechnol **22**(8): 969-976.
Gao, X. and L. Huang (1995). "Cationic liposome-mediated gene transfer." Gene therapy **2**: 710-722.
Gao, X., J. Qian, S. Zheng, Y. Changyi, J. Zhang, S. Ju, J. Zhu and C. Li (2014). "Overcoming the blood-brain barrier for delivering drugs into the brain by using adenosine receptor nanoagonist." ACS Nano **8**(4): 3678-3689.
Ghitescu, L., A. Fixman, M. Simionescu and N. Simionescu (1986). "Specific binding sites for albumin restricted to plasmalemmal vesicles of continuous capillary endothelium: Receptor-mediated transcytosis." Journal of Cell Biology **102**(4): 1304-1311.
Ghose, A. K., V. N. Viswanadhan and J. J. Wendoloski (1999). "A knowledge-based approach in designing combinatorial or medicinal chemistry libraries for drug discovery. 1. A qualitative and quantitative characterization of known drug databases." J Comb Chem **1**(1): 55-68.
Goldmann, E. (1909). "Die äussere und Sekretion des gesunden und kranken Organismus im Lichte der "vitalen Färbung"." Beitr Klin Chirurz. **64**: 192-265.
Goldmann, E. (1913). "Vital färbung am Zentralnervensystem." Abh Preuss Akad Wiss Phys-Math **1**: 1-60.
Gosk, S., C. Vermehren, G. Storm and T. Moos (2004). "Targeting anti-transferrin receptor antibody (OX26) and OX26-conjugated liposomes to brain capillary endothelial cells using in situ perfusion." Journal of cerebral blood flow and metabolism : official journal of the International Society of Cerebral Blood Flow and Metabolism **24**(11): 1193-1204.
Goto, J. J. and R. E. Tanzi (2002). "The role of the low-density lipoprotein receptor-related protein (LRP1) in Alzheimer's A beta generation: development of a cell-based model system." J Mol Neurosci **19**(1-2): 37-41.
Gottlieb, T. A., I. E. Ivanov, M. Adesnik and D. D. Sabatini (1993). "Actin microfilaments play a critical role in endocytosis at the apical but not the basolateral surface of polarized epithelial cells." J Cell Biol **120**(3): 695-710.
Gould, G. W. and J. Lippincott-Schwartz (2009). "New roles for endosomes: from vesicular carriers to multi-purpose platforms." Nat Rev Mol Cell Biol **10**(4): 287-292.

Grassin-Delyle, S., A. Buenestado, E. Naline, C. Faisy, S. Blouquit-Laye, L. J. Couderc, M. Le Guen, M. Fischler and P. Devillier (2012). "Intranasal drug delivery: an efficient and non-invasive route for systemic administration: focus on opioids." Pharmacol Ther **134**(3): 366-379.
Greenwood, J., S. J. Heasman, J. I. Alvarez, A. Prat, R. Lyck and B. Engelhardt (2011). "Review: Leucocyte-endothelial cell crosstalk at the blood-brain barrier: A prerequisite for successful immune cell entry to the brain." Neuropathology and Applied Neurobiology **37**(1): 24-39.
Gref, R., Y. Minamitake, M. T. Peracchia, V. Trubetskoy, V. Torchilin and R. Langer (1994). "Biodegradable long-circulating polymeric nanospheres." Science **263**(5153): 1600-1603.
Gromnicova, R., H. A. Davies, P. Sreekanthreddy, I. A. Romero, T. Lund, I. M. Roitt, J. B. Phillips and D. K. Male (2013). "Glucose-coated gold nanoparticles transfer across human brain endothelium and enter astrocytes in vitro." PLoS One **8**(12): e81043.
Guerin, C., A. Olivi, J. D. Weingart, H. C. Lawson and H. Brem (2004). "Recent advances in brain tumor therapy: local intracerebral drug delivery by polymers." Invest New Drugs **22**(1): 27-37.
Hall, W. A., N. D. Doolittle, M. Daman, P. K. Bruns, L. Muldoon, D. Fortin and E. A. Neuwelt (2006). "Osmotic blood-brain barrier disruption chemotherapy for diffuse pontine gliomas." J Neurooncol **77**(3): 279-284.
Hanig, J. P., J. M. Morrison, Jr. and S. Krop (1972). "Ethanol enhancement of blood-brain barrier permeability to catecholamines in chicks." Eur J Pharmacol **18**(1): 79-82.
Hawkins, B. T. and T. P. Davis (2005). "The blood-brain barrier/neurovascular unit in health and disease." Pharmacological reviews **57**: 173-185.
Hediger, M. A., B. Clemencon, R. E. Burrier and E. A. Bruford (2013). "The ABCs of membrane transporters in health and disease (SLC series): introduction." Mol Aspects Med **34**(2-3): 95-107.
Henley, J. R., E. W. Krueger, B. J. Oswald and M. A. McNiven (1998). "Dynamin-mediated internalization of caveolae." The Journal of cell biology **141**: 85-99.
Herve, F., N. Ghinea and J. M. Scherrmann (2008). "CNS delivery via adsorptive transcytosis." AAPS J **10**(3): 455-472.
Herz, J., U. Hamann, S. Rogne, O. Myklebost, H. Gausepohl and K. K. Stanley (1988). "Surface location and high affinity for calcium of a 500-kd liver membrane protein closely related to the LDL-receptor suggest a physiological role as lipoprotein receptor." EMBO J **7**(13): 4119-4127.
Herz, J., U. Hamann, S. Rogne, O. Myklebost, H. Gausepohl and K. K. Stanley (1988). "Surface location and high affinity for calcium of a 500-kd liver membrane protein closely related to the LDL-receptor suggest a physiological role as lipoprotein receptor." The EMBO journal **7**(13): 4119-4127.
Herz, J. and D. K. Strickland (2001). "LRP: a multifunctional scavenger and signaling receptor." J Clin Invest **108**(6): 779-784.
Hong, W. (2005). "SNAREs and traffic." Biochim Biophys Acta **1744**(3): 493-517.
Hooper, C., F. Pinteaux-Jones, V. A. H. Fry, I. G. Sevastou, D. Baker, S. J. Heales and J. M. Pocock (2009). "Differential effects of albumin on microglia and macrophages; Implications for neurodegeneration following blood-brain barrier damage." Journal of Neurochemistry **109**(3): 694-705.
Hostetler, K. Y., L. M. Stuhmiller, H. B. Lenting, H. van den Bosch and D. D. Richman (1990). "Synthesis and antiretroviral activity of phospholipid analogs of azidothymidine and other antiviral nucleosides." The Journal of biological chemistry **265**: 6112-6117.
Huettinger, M., H. Retzek, M. Hermann and H. Goldenberg (1992). "Lactoferrin specifically inhibits endocytosis of chylomicron remnants but not alpha-macroglobulin." J Biol Chem **267**(26): 18551-18557.
Huwyler, J., D. Wu and W. M. Pardridge (1996). "Brain drug delivery of small molecules using immunoliposomes." Proceedings of the National Academy of Sciences of the United States of America **93**: 14164-14169.

Iacopetta, B. J. and E. H. Morgan (1983). "The kinetics of transferrin endocytosis and iron uptake from transferrin in rabbit reticulocytes." J Biol Chem **258**(15): 9108-9115.
Iliff, J. J., M. Wang, Y. Liao, B. A. Plogg, W. Peng, G. A. Gundersen, H. Benveniste, G. E. Vates, R. Deane, S. A. Goldman, E. A. Nagelhus and M. Nedergaard (2012). A Paravascular Pathway Facilitates CSF Flow Through the Brain Parenchyma and the Clearance of Interstitial Solutes, Including Amyloid **4:** 147ra111-147ra111.
Jackman, M. R., W. Shurety, J. A. Ellis and J. P. Luzio (1994). "Inhibition of apical but not basolateral endocytosis of ricin and folate in Caco-2 cells by cytochalasin D." J Cell Sci **107 (Pt 9)**: 2547-2556.
Janigro, D. (2012). "Are you in or out? Leukocyte, ion, and neurotransmitter permeability across the epileptic blood-brain barrier." Epilepsia **53**(SUPPL. 1): 26-34.
Kaetzel, C. S., J. K. Robinson, K. R. Chintalacharuvu, J. P. Vaerman and M. E. Lamm (1991). "The polymeric immunoglobulin receptor (secretory component) mediates transport of immune complexes across epithelial cells: a local defense function for IgA." Proc Natl Acad Sci U S A **88**(19): 8796-8800.
Kageyama, T., M. Nakamura, A. Matsuo, Y. Yamasaki, Y. Takakura, M. Hashida, Y. Kanai, M. Naito, T. Tsuruo, N. Minato and S. Shimohama (2000). "The 4F2hc/LAT1 complex transports L-DOPA across the blood-brain barrier." Brain Research **879**(1-2): 115-121.
Kandel, E., J. H. Schwartz and T. M. Jessell (2012). Principles of Neural Science, McGraw-Hill.
Keep, R. F. and H. C. Jones (1990). "A morphometric study on the development of the lateral ventricle choroid plexus, choroid plexus capillaries and ventricular ependyma in the rat." Brain research. Developmental brain research **56**(1): 47-53.
Kinoshita, M., N. McDannold, F. A. Jolesz and K. Hynynen (2006). "Noninvasive localized delivery of Herceptin to the mouse brain by MRI-guided focused ultrasound-induced blood-brain barrier disruption." Proceedings of the National Academy of Sciences of the United States of America **103**(31): 11719-11723.
Klibanov, A. L., K. Maruyama, A. M. Beckerleg, V. P. Torchilin and L. Huang (1991). "Activity of amphipathic poly(ethylene glycol) 5000 to prolong the circulation time of liposomes depends on the liposome size and is unfavorable for immunoliposome binding to target." Biochimica et biophysica acta **1062**(2): 142-148.
Klingen, Y., K. K. Conzelmann and S. Finke (2008). "Double-labeled rabies virus: live tracking of enveloped virus transport." Journal of virology **82**(1): 237-245.
Kordower, J. H., S. Palfi, E. Y. Chen, S. Y. Ma, T. Sendera, E. J. Cochran, E. J. Mufson, R. Penn, C. G. Goetz and C. D. Comella (1999). "Clinicopathological findings following intraventricular glial-derived neurotrophic factor treatment in a patient with Parkinson's disease." Annals of Neurology **46**(3): 419-424.
Kotulska, M., J. Basalyga, M. B. Derylo and P. Sadowski (2010). "Metastable pores at the onset of constant-current electroporation." J Membr Biol **236**(1): 37-41.
Kounnas, M. Z., R. D. Moir, G. W. Rebeck, A. I. Bush, W. S. Argraves, R. E. Tanzi, B. T. Hyman and D. K. Strickland (1995). "LDL receptor-related protein, a multifunctional ApoE receptor, binds secreted beta-amyloid precursor protein and mediates its degradation." Cell **82**(2): 331-340.
Kristensson, K. (2011). "Microbes' roadmap to neurons." Nat Rev Neurosci **12**(6): 345-357.
Kristensson, K., M. Nygard, G. Bertini and M. Bentivoglio (2010). "African trypanosome infections of the nervous system: parasite entry and effects on sleep and synaptic functions." Prog Neurobiol **91**(2): 152-171.
Kristensson, K. and Y. Olsson (1973). "Diffusion pathways and retrograde axonal transport of protein tracers in peripheral nerves." Prog Neurobiol **1**(2): 87-109.
Kumar, P., H. Wu, J. L. McBride, K. E. Jung, M. H. Kim, B. L. Davidson, S. K. Lee, P. Shankar and N. Manjunath (2007). "Transvascular delivery of small interfering RNA to the central nervous system." Nature **448**(7149): 39-43.
Lafon, M. (2004). "Subversive neuroinvasive strategy of rabies virus." Arch Virol Suppl(18): 149-159.

Lang, T., D. Bruns, D. Wenzel, D. Riedel, P. Holroyd, C. Thiele and R. Jahn (2001). "SNAREs are concentrated in cholesterol-dependent clusters that define docking and fusion sites for exocytosis." EMBO Journal **20**(9): 2202-2213.
Le, P. U. and I. R. Nabi (2003). "Distinct caveolae-mediated endocytic pathways target the Golgi apparatus and the endoplasmic reticulum." J Cell Sci **116**(Pt 6): 1059-1071.
Lee, H. J., B. Engelhardt, J. Lesley, U. Bickel and W. M. Pardridge (2000). "Targeting rat anti-mouse transferrin receptor monoclonal antibodies through blood-brain barrier in mouse." The Journal of pharmacology and experimental therapeutics **292**(3): 1048-1052.
Lee, J. C., H. Bermudez, B. M. Discher, M. A. Sheehan, Y. Y. Won, F. S. Bates and D. E. Discher (2001). "Preparation, stability, and in vitro performance of vesicles made with diblock copolymers." Biotechnol Bioeng **73**(2): 135-145.
Li, C.-H., C. Jhan, Y.-W. Cheng, C.-H. Tsai, C.-W. Liu, C.-C. Lee, R.-M. Chen, M.-K. Shyu and J.-J. Kang (2015). "Gold nanoparticles increase endothelial paracellular permeability by altering components of endothelial tight junctions, and increase blood-brain barrier permeability in mice." Toxicological Sciences.
Li, M.-H. and P. Keller (2009). Stimuli-responsive polymer vesicles. **5:** 927-927.
Li, Y., W. Lu, M. P. Marzolo and G. Bu (2001). "Differential functions of members of the low density lipoprotein receptor family suggested by their distinct endocytosis rates." The Journal of biological chemistry **276**(21): 18000-18006.
Li, Y., M. P. Marzolo, P. van Kerkhof, G. J. Strous and G. Bu (2000). "The YXXL motif, but not the two NPXY motifs, serves as the dominant endocytosis signal for low density lipoprotein receptor-related protein." The Journal of biological chemistry **275**(22): 17187-17194.
Lillis, A. P., L. B. Van Duyn, J. E. Murphy-Ullrich and D. K. Strickland (2008). "LDL receptor-related protein 1: unique tissue-specific functions revealed by selective gene knockout studies." Physiological reviews **88**(3): 887-918.
Lipinski, C. A., F. Lombardo, B. W. Dominy and P. J. Feeney (2001). "Experimental and computational approaches to estimate solubility and permeability in drug discovery and development settings." Adv Drug Deliv Rev **46**(1-3): 3-26.
Lippmann, E. S., S. M. Azarin, J. E. Kay, R. A. Nessler, H. K. Wilson, A. Al-Ahmad, S. P. Palecek and E. V. Shusta (2012). Derivation of blood-brain barrier endothelial cells from human pluripotent stem cells. **30:** 783-791.
Lippmann, E. S., C. Weidenfeller, C. N. Svendsen and E. V. Shusta (2011). "Blood-brain barrier modeling with co-cultured neural progenitor cell-derived astrocytes and neurons." Journal of Neurochemistry **119**(3): 507-520.
Liu, N. Q., A. S. Lossinsky, W. Popik, X. Li, C. Gujuluva, B. Kriederman, J. Roberts, T. Pushkarsky, M. Bukrinsky, M. Witte, M. Weinand and M. Fiala (2002). "Human immunodeficiency virus type 1 enters brain microvascular endothelia by macropinocytosis dependent on lipid rafts and the mitogen-activated protein kinase signaling pathway." J Virol **76**(13): 6689-6700.
Lomas, H., I. Canton, S. MacNeil, J. Du, S. P. Armes, A. J. Ryan, A. L. Lewis and G. Battaglia (2007). "Biomimetic pH sensitive polymersomes for efficient DNA encapsulation and delivery." Advanced Materials **19**(23): 4238-+.
Lomas, H., M. Massignani, K. A. Abdullah, I. Canton, C. Lo Presti, S. MacNeil, J. Du, A. Blanazs, J. Madsen, S. P. Armes, A. L. Lewis and G. Battaglia (2008). "Non-cytotoxic polymer vesicles for rapid and efficient intracellular delivery." Faraday discussions **139**: 128-143,419-420.
Long, M., S. H. Huang, C. H. Wu, G. M. Shackleford and A. Jong (2012). "Lipid raft/caveolae signaling is required for Cryptococcus neoformans invasion into human brain microvascular endothelial cells." J Biomed Sci **19**: 19.
Longmire, M., P. L. Choyke and H. Kobayashi (2008). "Clearance properties of nano-sized particles and molecules as imaging agents: considerations and caveats." Nanomedicine (London, England) **3**(5): 703-717.

LoPresti, C., H. Lomas, M. Massignani, T. Smart and G. Battaglia (2009). "Polymersomes: nature inspired nanometer sized compartments." Journal of Materials Chemistry **19**(22): 3576-3590.
LoPresti, C., M. Massignani, C. Fernyhough, A. Blanazs, A. J. Ryan, J. Madsen, N. J. Warren, S. P. Armes, A. L. Lewis, S. Chirasatitsin, A. J. Engler and G. Battaglia (2011). "Controlling polymersome surface topology at the nanoscale by membrane confined polymer/polymer phase separation." ACS nano **5**(3): 1775-1784.
Loscher, W. and H. Potschka (2005). "Blood-brain barrier active efflux transporters: ATP-binding cassette gene family." NeuroRx **2**(1): 86-98.
Lynch, I., A. Salvati and K. A. Dawson (2009). "Protein-nanoparticle interactions: What does the cell see?" Nat Nano **4**(9): 546-547.
Macia, E., M. Ehrlich, R. Massol, E. Boucrot, C. Brunner and T. Kirchhausen (2006). "Dynasore, a Cell-Permeable Inhibitor of Dynamin." Developmental Cell **10**(6): 839-850.
Madsen, J., N. J. Warren, S. P. Armes and A. L. Lewis (2011). "Synthesis of rhodamine 6G-based compounds for the ATRP synthesis of fluorescently labeled biocompatible polymers." Biomacromolecules **12**: 2225-2234.
Maisner, A., J. Neufeld and H. Weingartl (2009). "Organ- and endotheliotropism of Nipah virus infections in vivo and in vitro." Thromb Haemost **102**(6): 1014-1023.
Majid, A. (2014). "Neuroprotection in stroke: past, present, and future." ISRN Neurol **2014**: 515716.
Mantuano, E., M. S. Lam and S. L. Gonias (2013). "LRP1 assembles unique co-receptor systems to initiate cell signaling in response to tissue-type plasminogen activator and myelin-associated glycoprotein." J Biol Chem **288**(47): 34009-34018.
Markou, A., C. Chiamulera, M. A. Geyer, M. Tricklebank and T. Steckler (2009). "Removing obstacles in neuroscience drug discovery: the future path for animal models." Neuropsychopharmacology **34**(1): 74-89.
Massignani, M., C. Lopresti, A. Blanazs, J. Madsen, S. P. Armes, A. L. Lewis and G. Battaglia (2009). "Controlling cellular uptake by surface chemistry, size, and surface topology at the nanoscale." Small **5**(21): 2424-2432.
McMahon, H. T. and E. Boucrot (2011). "Molecular mechanism and physiological functions of clathrin-mediated endocytosis." Nat Rev Mol Cell Biol **12**(8): 517-533.
Menei, P., J. M. Pean, V. Nerrière-Daguin, C. Jollivet, P. Brachet and J. P. Benoit (2000). "Intracerebral implantation of NGF-releasing biodegradable microspheres protects striatum against excitotoxic damage." Experimental neurology **161**(1): 259-272.
Mercer, J., M. Schelhaas and A. Helenius (2010). "Virus entry by endocytosis." Annu Rev Biochem **79**: 803-833.
Messager, L., J. Gaitzsch, L. Chierico and G. Battaglia (2014). "Novel aspects of encapsulation and delivery using polymersomes." Curr Opin Pharmacol **18**: 104-111.
Michalet, X., F. F. Pinaud, L. A. Bentolila, J. M. Tsay, S. Doose, J. J. Li, G. Sundaresan, A. M. Wu, S. S. Gambhir and S. Weiss (2005). "Quantum dots for live cells, in vivo imaging, and diagnostics." Science **307**(5709): 538-544.
Milhorat, T. H., M. K. Hammock, J. D. Fenstermacher and V. A. Levin (1971). "Cerebrospinal fluid production by the choroid plexus and brain." Science (New York, N.Y.) **173**: 330-332.
Moestrup, S. K., J. Gliemann and G. Pallesen (1992). "Distribution of the alpha 2-macroglobulin receptor/low density lipoprotein receptor-related protein in human tissues." Cell and tissue research **269**(3): 375-382.
Mohammed, A. H., E. Norrby and K. Kristensson (1993). "Viruses and behavioural changes: a review of clinical and experimental findings." Rev Neurosci **4**(3): 267-286.
Moos, T. and E. H. Morgan (2000). "Transferrin and transferrin receptor function in brain barrier systems." Cellular and molecular neurobiology **20**(1): 77-95.
Moos, T. and E. H. Morgan (2001). "Restricted transport of anti-transferrin receptor antibody (OX26) through the blood-brain barrier in the rat." Journal of Neurochemistry **79**(1): 119-129.

Muyldermans, S., T. Atarhouch, J. Saldanha, J. A. Barbosa and R. Hamers (1994). "Sequence and structure of VH domain from naturally occurring camel heavy chain immunoglobulins lacking light chains." Protein Eng **7**(9): 1129-1135.
Neumann, E., M. Schaefer-Ridder, Y. Wang and P. H. Hofschneider (1982). "Gene transfer into mouse lyoma cells by electroporation in high electric fields." The EMBO journal **1**(7): 841-845.
O'Neil, C. P., T. Suzuki, D. Demurtas, A. Finka and J. A. Hubbell (2009). "A Novel Method for the Encapsulation of Biomolecules into Polymersomes via Direct Hydration." Langmuir **25**(16): 9025-9029.
Oh, P., P. Borgström, H. Witkiewicz, Y. Li, B. J. Borgström, A. Chrastina, K. Iwata, K. R. Zinn, R. Baldwin, J. E. Testa and J. E. Schnitzer (2007). "Live dynamic imaging of caveolae pumping targeted antibody rapidly and specifically across endothelium in the lung." Nature biotechnology **25**: 327-337.
Oh, P., D. P. McIntosh and J. E. Schnitzer (1998). "Dynamin at the neck of caveolae mediates their budding to form transport vesicles by GTP-driven fission from the plasma membrane of endothelium." The Journal of cell biology **141**: 101-114.
Olesen, S. P. and C. Crone (1983). "Electrical resistance of muscle capillary endothelium." Biophysical journal **42**(1): 31-41.
Pardridge, W. M. (2001). Brain Drug Targeting: The Future of Brain Drug Development. New York, NY, Cambridge University Press.
Pardridge, W. M. (2005). "The blood-brain barrier: bottleneck in brain drug development." NeuroRx : the journal of the American Society for Experimental NeuroTherapeutics **2**(1): 3-14.
Pardridge, W. M. (2006). Molecular Trojan horses for blood-brain barrier drug delivery. **6:** 494-500.
Pardridge, W. M., J. Eisenberg and W. T. Cefalu (1985). "Absence of albumin receptor on brain capillaries in vivo or in vitro." Am J Physiol **249**(3 Pt 1): E264-267.
Pardridge, W. M., Y. S. Kang, J. L. Buciak and J. Yang (1995). "Human insulin receptor monoclonal antibody undergoes high affinity binding to human brain capillaries in vitro and rapid transcytosis through the blood-brain barrier in vivo in the primate." Pharm Res **12**(6): 807-816.
Pardridge, W. M., Y. S. Kang, J. L. Buciak and J. Yang (1995). "Human insulin receptor monoclonal antibody undergoes high affinity binding to human brain capillaries in vitro and rapid transcytosis through the blood-brain barrier in vivo in the primate." Pharmaceutical research **12**(6): 807-816.
Paris-Robidas, S., V. Emond, C. Tremblay, D. Soulet and F. Calon (2011). "In vivo labeling of brain capillary endothelial cells after intravenous injection of monoclonal antibodies targeting the transferrin receptor." Molecular pharmacology **80**(1): 32-39.
Park, T. E., B. Singh, H. Li, J. Y. Lee, S. K. Kang, Y. J. Choi and C. S. Cho (2015). "Enhanced BBB permeability of osmotically active poly(mannitol-co-PEI) modified with rabies virus glycoprotein via selective stimulation of caveolar endocytosis for RNAi therapeutics in Alzheimer's disease." Biomaterials **38**: 61-71.
Parton, R. G. (1994). "Ultrastructural localization of gangliosides; GM1 is concentrated in caveolae." J Histochem Cytochem **42**(2): 155-166.
Patabendige, A., R. A. Skinner and N. J. Abbott (2013). "Establishment of a simplified in vitro porcine blood-brain barrier model with high transendothelial electrical resistance." Brain Research **1521**: 1-15.
Pearson, R. T., N. J. Warren, A. L. Lewis, S. P. Armes and G. Battaglia (2013). "Effect of pH and Temperature on PMPC–PDPA Copolymer Self-Assembly." Macromolecules **46**(4): 1400-1407.
Pegoraro, C., D. Cecchin, L. S. Gracia, N. Warren, J. Madsen, S. P. Armes, A. Lewis, S. Macneil and G. Battaglia (2013). "Enhanced drug delivery to melanoma cells using PMPC-PDPA polymersomes." Cancer Lett **334**(2): 328-337.
Pelkmans, L., J. Kartenbeck and A. Helenius (2001). "Caveolar endocytosis of simian virus 40 reveals a new two-step vesicular-transport pathway to the ER." Nature cell biology **3**: 473-483.

Pelkmans, L., D. Puntener and A. Helenius (2002). "Local actin polymerization and dynamin recruitment in SV40-induced internalization of caveolae." Science **296**(5567): 535-539.
Peppiatt, C. M., C. Howarth, P. Mobbs and D. Attwell (2006). "Bidirectional control of CNS capillary diameter by pericytes." Nature **443**: 700-704.
Pfeffer, S. R. (2001). Rab GTPases: Specifying and deciphering organelle identity and function. **11:** 487-491.
Pflanzner, T., M. C. Janko, B. André-Dohmen, S. Reuss, S. Weggen, A. J. M. Roebroek, C. R. W. Kuhlmann and C. U. Pietrzik (2011). "LRP1 mediates bidirectional transcytosis of amyloid-β across the blood-brain barrier." Neurobiology of Aging **32**(12).
Plumb, J., S. McQuaid, M. Mirakhur and J. Kirk (2002). "Abnormal endothelial tight junctions in active lesions and normal-appearing white matter in multiple sclerosis." Brain pathology **12**(2): 154-169.
Predescu, D., R. Horvat, S. Predescu and G. E. Palade (1994). "Transcytosis in the continuous endothelium of the myocardial microvasculature is inhibited by N-ethylmaleimide." Proceedings of the National Academy of Sciences of the United States of America **91**: 3014-3018.
Predescu, S. a., D. N. Predescu and A. B. Malik (2007). "Molecular determinants of endothelial transcytosis and their role in endothelial permeability." American journal of physiology. Lung cellular and molecular physiology **293**(4): L823-842.
Predescu, S. A., D. N. Predescu and G. E. Palade (2001). "Endothelial transcytotic machinery involves supramolecular protein-lipid complexes." Molecular biology of the cell **12**: 1019-1033.
Predescu, S. A., D. N. Predescu, K. Shimizu, I. K. Klein and A. B. Malik (2005). "Cholesterol-dependent syntaxin-4 and SNAP-23 clustering regulates caveolar fusion with the endothelial plasma membrane." The Journal of biological chemistry **280**: 37130-37138.
Prencipe, M., F. Culasso, M. Rasura, A. Anzini, M. Beccia, M. Cao, F. Giubilei and C. Fieschi (1998). "Long-term prognosis after a minor stroke: 10-year mortality and major stroke recurrence rates in a hospital-based cohort." Stroke **29**(1): 126-132.
Pusztaszeri, M. P., W. Seelentag and F. T. Bosman (2006). "Immunohistochemical expression of endothelial markers CD31, CD34, von Willebrand factor, and Fli-1 in normal human tissues." J Histochem Cytochem **54**(4): 385-395.
Quinn, K. A., P. G. Grimsley, Y. P. Dai, M. Tapner, C. N. Chesterman and D. A. Owensby (1997). "Soluble low density lipoprotein receptor-related protein (LRP) circulates in human plasma." The Journal of biological chemistry **272**(38): 23946-23951.
Ranganathan, S., C. Cao, J. Catania, M. Migliorini, L. Zhang and D. K. Strickland (2011). "Molecular basis for the interaction of low density lipoprotein receptor-related protein 1 (LRP1) with integrin alphaMbeta2: identification of binding sites within alphaMbeta2 for LRP1." J Biol Chem **286**(35): 30535-30541.
Rapoport, S. I. (1970). "Effect of concentrated solutions on blood-brain barrier." Am J Physiol **219**(1): 270-274.
Reed, S. D., S. C. Cramer, D. K. Blough, K. Meyer and J. G. Jarvik (2001). "Treatment with tissue plasminogen activator and inpatient mortality rates for patients with ischemic stroke treated in community hospitals." Stroke **32**(8): 1832-1840.
Reese, T. S. and M. J. Karnovsky (1967). "Fine structural localization of a blood-brain barrier to exogenous peroxidase." J Cell Biol **34**(1): 207-217.
Roberts, R., A. Sandra, G. C. Siek, J. J. Lucas and R. E. Fine (1992). "Studies of the mechanism of iron transport across the blood-brain barrier." Ann Neurol **32 Suppl**: S43-50.
Robertson, J. D., G. Yealland, M. Avila-Olias, L. Chierico, O. Bandmann, S. a. Renshaw and G. Battaglia (2014). "pH-Sensitive Tubular Polymersomes: Formation and Applications in Cellular Delivery." ACS nano.

Rodal, S. K., G. Skretting, O. Garred, F. Vilhardt, B. van Deurs and K. Sandvig (1999). "Extraction of cholesterol with methyl-beta-cyclodextrin perturbs formation of clathrin-coated endocytic vesicles." Mol Biol Cell **10**(4): 961-974.
Rosen, C., O. Hansson, K. Blennow and H. Zetterberg (2013). "Fluid biomarkers in Alzheimer's disease - current concepts." Mol Neurodegener **8**: 20.
Saija, A., P. Princi, D. Trombetta, M. Lanza and A. De Pasquale (1997). "Changes in the permeability of the blood-brain barrier following sodium dodecyl sulphate administration in the rat." Exp Brain Res **115**(3): 546-551.
Saito, Y. and E. M. Wright (1983). "Bicarbonate transport across the frog choroid plexus and its control by cyclic nucleotides." The Journal of physiology **336**: 635-648.
Sanders, S. E., J. L. Madara, D. K. McGuirk, D. S. Gelman and S. P. Colgan (1995). "Assessment of inflammatory events in epithelial permeability: a rapid screening method using fluorescein dextrans." Epithelial cell biology **4**: 25-34.
Savjani, K. T., A. K. Gajjar and J. K. Savjani (2012). "Drug solubility: importance and enhancement techniques." ISRN Pharm **2012**: 195727.
Schinkel, A. H. and J. W. Jonker (2012). Mammalian drug efflux transporters of the ATP binding cassette (ABC) family: An overview. **64:** 138-153.
Schnitzer, J. E., P. Oh, E. Pinney and J. Allard (1994). "Filipin-sensitive caveolae-mediated transport in endothelium: reduced transcytosis, scavenger endocytosis, and capillary permeability of select macromolecules." The Journal of cell biology **127**: 1217-1232.
Schoch, S., F. Deak, A. Konigstorfer, M. Mozhayeva, Y. Sara, T. C. Sudhof and E. T. Kavalali (2001). "SNARE function analyzed in synaptobrevin/VAMP knockout mice." Science **294**(5544): 1117-1122.
Schubert, W., P. G. Frank, B. Razani, D. S. Park, C. W. Chow and M. P. Lisanti (2001). "Caveolae-deficient endothelial cells show defects in the uptake and transport of albumin in vivo." The Journal of biological chemistry **276**: 48619-48622.
Shibata, M., S. Yamada, S. R. Kumar, M. Calero, J. Bading, B. Frangione, D. M. Holtzman, C. A. Miller, D. K. Strickland, J. Ghiso and B. V. Zlokovic (2000). "Clearance of Alzheimer's amyloid-ss(1-40) peptide from brain by LDL receptor-related protein-1 at the blood-brain barrier." The Journal of clinical investigation **106**(12): 1489-1499.
Siddhartha, S., B. Tanmay, R. Arnab, S. Gajendra, P. Ramachandrarao and D. Debabrata (2007). "Characterization of enhanced antibacterial effects of novel silver nanoparticles." Nanotechnology **18**(22): 225103.
Simionescu, M., D. Popov and A. Sima (2009). "Endothelial transcytosis in health and disease." Cell and tissue research **335**(1): 27-40.
Simone, E. A., T. D. Dziubla and V. R. Muzykantov (2008). "Polymeric carriers: role of geometry in drug delivery." Expert Opin Drug Deliv **5**(12): 1283-1300.
Simons, K. and E. Ikonen (1997). "Functional rafts in cell membranes." Nature **387**(6633): 569-572.
Simons, K. and W. L. C. Vaz (2004). "Model systems, lipid rafts, and cell membranes." Annual review of biophysics and biomolecular structure **33**: 269-295.
Smart, T., H. Lomas, M. Massignani, M. V. Flores-Merino, L. R. Perez and G. Battaglia (2008). Block copolymer nanostructures. **3:** 38-46.
Smart, T. P., O. O. Mykhaylyk, A. J. Ryan and G. Battaglia (2009). "Polymersomes hydrophilic brush scaling relations." Soft Matter **5**(19): 3607-3610.
Söllner, T., S. W. Whiteheart, M. Brunner, H. Erdjument-Bromage, S. Geromanos, P. Tempst and J. E. Rothman (1993). "SNAP receptors implicated in vesicle targeting and fusion." Nature **362**(6418): 318-324.
Sönnichsen, B., S. De Renzis, E. Nielsen, J. Rietdorf and M. Zerial (2000). "Distinct membrane domains on endosomes in the recycling pathway visualized by multicolor imaging of Rab4, Rab5, and Rab11." The Journal of cell biology **149**: 901-914.
Sönnichsen, B., S. De Renzis, E. Nielsen, J. Rietdorf and M. Zerial (2000). "Distinct membrane domains on endosomes in the recycling pathway visualized by multicolor imaging of Rab4, Rab5, and Rab11." Journal of Cell Biology **149**(4): 901-913.

Stenmark, H. (2009). "Rab GTPases as coordinators of vesicle traffic." Nat Rev Mol Cell Biol **10**(8): 513-525.
Stewart, P. A. and M. J. Wiley (1981). "Developing nervous tissue induces formation of blood-brain barrier characteristics in invading endothelial cells: a study using quail--chick transplantation chimeras." Developmental biology **84**(1): 183-192.
Stojanov, K., J. V. Georgieva, R. P. Brinkhuis, J. C. Van Hest, F. P. Rutjes, R. A. J. O. Dierckx, E. F. J. De Vries and I. S. Zuhorn (2012). "In vivo biodistribution of prion- and GM1-targeted polymersomes following intravenous administration in mice." Molecular Pharmaceutics **9**(6): 1620-1627.
Stolp, H. B. and K. M. Dziegielewska (2009). "Review: Role of developmental inflammation and blood-brain barrier dysfunction in neurodevelopmental and neurodegenerative diseases." Neuropathology and Applied Neurobiology **35**(2): 132-146.
Stow, J. G. L. and L. Jennifer (2005). "Rab11 in Recycling Endosomes Regulates the Sorting and Basolateral Transport of E-Cadherin." Molecular biology of the cell **16**(1): 1-13.
Stylianopoulou, F., J. Herbert, M. B. Soares and A. Efstratiadis (1988). "Expression of the insulin-like growth factor II gene in the choroid plexus and the leptomeninges of the adult rat central nervous system." Proc Natl Acad Sci U S A **85**(1): 141-145.
Südhof, T. C. and J. E. Rothman (2009). "Membrane fusion: grappling with SNARE and SM proteins." Science (New York, N.Y.) **323**(5913): 474-477.
Sztul, E., M. Colombo, P. Stahl and R. Samanta (1993). "Control of protein traffic between distinct plasma membrane domains. Requirement for a novel 108,000 protein in the fusion of transcytotic vesicles with the apical plasma membrane." J Biol Chem **268**(3): 1876-1885.
Takano, T., G. F. Tian, W. Peng, N. Lou, W. Libionka, X. Han and M. Nedergaard (2006). "Astrocyte-mediated control of cerebral blood flow." Nat Neurosci **9**(2): 260-267.
Takasato, Y., S. I. Rapoport and Q. R. Smith (1984). "An in situ brain perfusion technique to study cerebrovascular transport in the rat." The American journal of physiology **247**: H484-H493.
Thomsen, P., K. Roepstorff, M. Stahlhut and B. van Deurs (2002). "Caveolae are highly immobile plasma membrane microdomains, which are not involved in constitutive endocytic trafficking." Molecular biology of the cell **13**: 238-250.
Tian, X. (2014). Screening Functionalised Polymersomes Targeting Transcytosis Across Blood-Brain Barrier. D. Phil., The University of Sheffield.
Tian, X., S. Nyberg, P. S. Sharp, J. Madsen, N. Daneshpour, S. P. Armes, J. Berwick, M. Azzouz, P. Shaw, N. J. Abbott and G. Battaglia (2015). "LRP-1-mediated intracellular antibody delivery to the Central Nervous System." Sci. Rep. **5**.
Tirosh, O., Y. Barenholz, J. Katzhendler and A. Priev (1998). "Hydration of polyethylene glycol-grafted liposomes." Biophys J **74**(3): 1371-1379.
Tjelle, T. E., a. Brech, L. K. Juvet, G. Griffiths and T. Berg (1996). "Isolation and characterization of early endosomes, late endosomes and terminal lysosomes: their role in protein degradation." Journal of cell science **109 (Pt 1**: 2905-2914.
Toonen, R. F., O. Kochubey, H. de Wit, A. Gulyas-Kovacs, B. Konijnenburg, J. B. Sørensen, J. Klingauf and M. Verhage (2006). "Dissecting docking and tethering of secretory vesicles at the target membrane." The EMBO journal **25**(16): 3725-3737.
Tooyama, I., T. Kawamata, H. Akiyama, H. Kimura, S. K. Moestrup, J. Gliemann, A. Matsuo and P. L. McGeer (1995). "Subcellular localization of the low density lipoprotein receptor-related protein (alpha 2-macroglobulin receptor) in human brain." Brain research **691**(1-2): 235-238.
Triguero, D., J. Buciak and W. M. Pardridge (1990). "Capillary depletion method for quantification of blood-brain barrier transport of circulating peptides and plasma proteins." Journal of Neurochemistry **54**: 1882-1888.
Tugizov, S. M., R. Herrera and J. M. Palefsky (2013). "Epstein-Barr virus transcytosis through polarized oral epithelial cells." J Virol **87**(14): 8179-8194.

Tugulu, S. and H. A. Klok (2008). "Stability and nonfouling properties of poly(poly(ethylene glycol) methacrylate) Brushes under cell culture conditions." Biomacromolecules **9**(3): 906-912.
Tuma, P. L. and A. L. Hubbard (2003). "Transcytosis: crossing cellular barriers." Physiological reviews **83**: 871-932.
Tuma, P. L., M. C. Stachniak and C. A. Collins (1993). "Activation of dynamin GTPase by acidic phospholipids and endogenous rat brain vesicles." The Journal of biological chemistry **268**: 17240-17246.
van Ginkel, F. W., J. R. McGhee, J. M. Watt, A. Campos-Torres, L. A. Parish and D. E. Briles (2003). "Pneumococcal carriage results in ganglioside-mediated olfactory tissue infection." Proc Natl Acad Sci U S A **100**(24): 14363-14367.
van Kerkhof, P., J. Lee, L. McCormick, E. Tetrault, W. Lu, M. Schoenfish, V. Oorschot, G. J. Strous, J. Klumperman and G. Bu (2005). "Sorting nexin 17 facilitates LRP recycling in the early endosome." The EMBO journal **24**(16): 2851-2861.
Veronese, F. M. and G. Pasut (2005). PEGylation, successful approach to drug delivery. **10:** 1451-1458.
Virgintino, D., D. Robertson, M. Errede, V. Benagiano, U. Tauer, L. Roncali and M. Bertossi (2002). "Expression of caveolin-1 in human brain microvessels." Neuroscience **115**(1): 145-152.
Vitelli, R., M. Santillo, D. Lattero, M. Chiariello, M. Bifulco, C. B. Bruni and C. Bucci (1997). "Role of the small GTPase RAB7 in the late endocytic pathway." Journal of Biological Chemistry **272**(7): 4391-4397.
Vogel, C. L., M. A. Cobleigh, D. Tripathy, J. C. Gutheil, L. N. Harris, L. Fehrenbacher, D. J. Slamon, M. Murphy, W. F. Novotny, M. Burchmore, S. Shak, S. J. Stewart and M. Press (2002). "Efficacy and safety of trastuzumab as a single agent in first-line treatment of HER2-overexpressing metastatic breast cancer." J Clin Oncol **20**(3): 719-726.
Vu, K., B. Weksler, I. Romero, P. O. Couraud and A. Gelli (2009). "Immortalized human brain endothelial cell line HCMEC/D3 as a model of the blood-brain barrier facilitates in vitro studies of central nervous system infection by Cryptococcus neoformans." Eukaryot Cell **8**(11): 1803-1807.
Wandinger-Ness, A. and M. Zerial (2014). "Rab proteins and the compartmentalization of the endosomal system." Cold Spring Harb Perspect Biol **6**(11): a022616.
Wang, L., L. Chierico, D. Little, N. Patikarnmonthon, Z. Yang, M. Azzouz, J. Madsen, S. P. Armes and G. Battaglia (2012). "Encapsulation of biomacromolecules within polymersomes by electroporation." Angewandte Chemie - International Edition **51**: 11122-11125.
Wang, L., L. Chierico, D. Little, N. Patikarnmonthon, Z. Yang, M. Azzouz, J. Madsen, S. P. Armes and G. Battaglia (2012). "Encapsulation of biomacromolecules within polymersomes by electroporation." Angewandte Chemie - International Edition **51**(44): 11122-11125.
Willnow, T. E., J. L. Goldstein, K. Orth, M. S. Brown and J. Herz (1992). "Low density lipoprotein receptor-related protein and gp330 bind similar ligands, including plasminogen activator-inhibitor complexes and lactoferrin, an inhibitor of chylomicron remnant clearance." Journal of Biological Chemistry **267**(36): 26172-26180.
Winkler, J., G. A. Ramirez, H. G. Kuhn, D. A. Peterson, P. A. Day-Lollini, G. R. Stewart, M. H. Tuszynski, F. H. Gage and L. J. Thal (1997). "Reversible schwann cell hyperplasia and sprouting of sensory and sympathetic neurites after intraventricular administration of nerve growth factor." Annals of Neurology **41**(1): 82-93.
Wolburg, H. and A. Lippoldt (2002). "Tight junctions of the blood-brain barrier: development, composition and regulation." Vascul Pharmacol **38**(6): 323-337.
Wolf, B. B., M. B. Lopes, S. R. VandenBerg and S. L. Gonias (1992). "Characterization and immunohistochemical localization of alpha 2-macroglobulin receptor (low-density lipoprotein receptor-related protein) in human brain." Am J Pathol **141**(1): 37-42.

Wu, D., J. G. Clement and W. M. Pardridge (1998). "Low blood-brain barrier permeability to azidothymidine (AZT), 3TC(TM), and thymidine in the rat." Brain Research **791**(1-2): 313-316.
Wu, D., J. Yang and W. M. Pardridge (1997). "Drug targeting of a peptide radiopharmaceutical through the primate blood-brain barrier in vivo with a monoclonal antibody to the human insulin receptor." J Clin Invest **100**(7): 1804-1812.
Xu, T., T. Binz, H. Niemann and E. Neher (1998). "Multiple kinetic components of exocytosis distinguished by neurotoxin sensitivity." Nature neuroscience **1**(3): 192-200.
Yamada, K., A. Kinoshita, E. Kohmura, T. Sakaguchi, J. Taguchi, K. Kataoka and T. Hayakawa (1991). "Basic fibroblast growth factor prevents thalamic degeneration after cortical infarction." Journal of cerebral blood flow and metabolism : official journal of the International Society of Cerebral Blood Flow and Metabolism **11**(3): 472-478.
Yan, Q., C. Matheson, J. Sun, M. J. Radeke, S. C. Feinstein and J. A. Miller (1994). "Distribution of intracerebral ventricularly administered neurotrophins in rat brain and its correlation with trk receptor expression." Exp Neurol **127**(1): 23-36.
Yang, T., F. D. Cui, M. K. Choi, J. W. Cho, S. J. Chung, C. K. Shim and D. D. Kim (2007). "Enhanced solubility and stability of PEGylated liposomal paclitaxel: In vitro and in vivo evaluation." International Journal of Pharmaceutics **338**: 317-326.
Yu, Y. J., Y. Zhang, M. Kenrick, K. Hoyte, W. Luk, Y. Lu, J. Atwal, J. M. Elliott, S. Prabhu, R. J. Watts and M. S. Dennis (2011). "Boosting brain uptake of a therapeutic antibody by reducing its affinity for a transcytosis target." Science translational medicine **3**(84): 84ra44-84ra44.
Zensi, A., D. Begley, C. Pontikis, C. Legros, L. Mihoreanu, S. Wagner, C. Buchel, H. von Briesen and J. Kreuter (2009). "Albumin nanoparticles targeted with Apo E enter the CNS by transcytosis and are delivered to neurones." J Control Release **137**(1): 78-86.
Zhang, H., A. Mitin and S. V. Vinogradov (2009). "Efficient transfection of blood-brain barrier endothelial cells by lipoplexes and polyplexes in the presence of nuclear targeting NLS-PEG-acridine conjugates." Bioconjug Chem **20**(1): 120-128.
Zlokovic, B. V., R. Deane, A. P. Sagare, R. D. Bell and E. A. Winkler (2010). "Low-density lipoprotein receptor-related protein-1: A serial clearance homeostatic mechanism controlling Alzheimer's amyloid ??-peptide elimination from the brain." Journal of Neurochemistry **115**(5): 1077-1089.
Zysk, G., B. K. Schneider-Wald, J. H. Hwang, L. Bejo, K. S. Kim, T. J. Mitchell, R. Hakenbeck and H. P. Heinz (2001). "Pneumolysin is the main inducer of cytotoxicity to brain microvascular endothelial cells caused by Streptococcus pneumoniae." Infection and immunity **69**(2): 845-852.